Metal Oxide Catalysts for the Valorisation of Bio-renewable Feedstocks

Hamza Sani Rabiu

March 2023

Thesis submitted in line with requirement of Cardiff University for the award degree of Doctor of Philosophy.

Acknowledgements

During my PhD, I gained a lot of knowledge and developed professionally and personally. I have many fond memories of my time at the Cardiff Catalysis Institute, which I thoroughly enjoyed. Over the past three years, coworkers have transformed into great friends, and this trend is likely to continue. Having said that, there have also been difficult times, and I owe a lot of people for their assistance and moral support during these times.

To begin, I would like to express my gratitude to PTDF and Dr Jonathan Bartley, my PhD supervisor, for providing me with the opportunity to study at such a prestigious institution. Meeting with him on a regular basis helped me stay on track and gave me the moral support and drive to succeed at Cardiff University. I would also like to thank Dr James Hayward and Dr Sankar Meenakshisundaram for their help and support in fulfilling their roles as postdoctoral supervisor and second supervisor respectively.

I would like to express my gratitude to other postdoctoral staff; namely Drs. James Carter, Mark Douthwaite, Samuel Pattisson, and Richard James. My research's planning and execution were aided by their in-depth understanding of the subject. In addition, they were always available to assist and encourage me during difficult times. I must also thank Drs Thomas Davies, Greg Shaw, and David Morgan, who gave up a lot of their own time to help me with the problems I faced in catalysts characterisation. My MSc supervisors, Professor Umar Ibrahim Gaya, who first introduced me to the exciting field of heterogeneous catalysis, deserve special recognition.

Last but not least, I'd like to express my gratitude to my family, friends and of course, my sister Saadatu, for providing me with so much emotional support and being able to talk to me through the difficult times.

Abstract

The fact that biofuels are currently not economically competitive with conventional fossil fuels is a fundamental constraint on their use. The improvement of novel chemical processes to convert biproducts from these reactions into high value-added chemicals could be one technique to lessen the financial shortfall between these two industries. First and second generations biofuels produce glycerol and 5-hydroxymethyl furfural as byproducts. This thesis investigates the possibility of producing high-value chemicals through oxidation of these bio-derived compounds with supported gold-platinum catalysts.

The first part of this thesis involves the oxidation of 5-hydromethyl furfural (HMF) with the aim of selectively producing 2,5-furandicarboxylic acid (FDCA). Initial experiments were conducted with different lanthanum based perovskite supports under basic conditions, and it was found that AuPt/$LaMnO_3$ gave the highest yield of FDCA. The AuPt/$LaMnO_3$ catalyst was then used for an investigation into the reaction conditions and it was found that the conditions had a significant effect on the product distribution. A progressive elimination study was designed to determine the optimal conditions for the formation of FDCA. The conditions mapped were temperature, O_2 pressure and base to substrate ratio. Temperature was found to increase selectivity to FDCA as it was increased. Increasing the O_2 pressure showed an increase in FDCA selectivity up to 3 bar, at which point 100% FDCA selectivity was achieved. By increasing the base to substrate ratio, FDCA selectivity increased, however, the carbon balance decreased due to the formation of byproducts (humins). The best compromise was found to be a base to substrate ratio of 1:1 which gave a reasonable carbon balance of around 94% with 100% selectivity to FDCA. This provided an insight that would later be used to help confirm the mechanism. The parameter mapping led to a series of conditions that produced a yield of 100 % FDCA. These conditions enabled the design of experiments under base free conditions to extend the catalyst modification study.

The second part of the thesis described research into the oxidation of glycerol which is a relatively complex reaction with two potential pathways leading to a variety of products. The oxidation pathway leads to the C_3 products glyceric acid and tartronic acid, with further oxidation leading to C_2 and C_1 products. The dehydration pathway leads to lactic acid, through a currently unknown mechanism. The reaction scheme sets out two challenges to solve; what conditions are optimal for a high yield of lactic acid and what is the reaction mechanism. When observing the two challenges, one begets the other. By identifying the conditions that are optimal for lactic acid production, it would then be plausible that an experiment could be designed to confirm the mechanism of lactic acid formation.

The gold platinum catalysts were also investigated for the production of lactic acid through the exchange of the B site cation on the perovskite supports. It was found that the $LaMnO_3$ support heavily favoured the oxidation pathway under similar conditions to that for the initial catalysts screening in HMF oxidation to FDCA. This was found to correlate with the oxygen adsorption capacity on the clean perovskite lattice, as perovskites with high oxygen adsorption favoured the oxidation pathway whilst low oxygen adsorption favoured the dehydration pathway. $LaCrO_3$ was found to produce a yield of up to 86 % lactic acid under the same conditions. The selective control of reaction products could ultimately lead to more economically viable biofuel production.

Glossary

BHMF	2,5-Bis(hydromethyl)furan
CA	Citric acid
CMB / C.M.B.	Carbon mass balance
DAD	Diode array detector
DFF	2,5-diformyl furan
DHA	Dihydroxy acetone
E_a	Activation Energy
EDX	Energy-dispersive X-ray spectroscopy
FA	Formic acid
FDCA	2, 5-Furandicarboxyllic acid
FFCA	5-formyl-furan-2-carboxylic acid
FWHM	Full width half maximum
GA	Glyceric acid
GLA	Glycolic acid
GLAD	Glyceraldehyde
HAADF	High-angle annular dark-field imaging
HMF	5-Hydroxymethyl-2-furfural
HMFCA	5-hydroxymethyl-furan-2-carboxylic acid
HPLC	High performance liquid chromatography
HT	Hydrotalcite

KE	Kinetic energy
LA	Lactic acid
MA	Mesoxalic acid
MEA	Maleic acid
MP-AES	Microwave plasma atomic emission spectroscopy
NC	Nanocasting
OA	Oxalic acid
PET	Polyethylene terephthalate
PGM	Platinum group metals
PSD	Particle size distribution
PVA	Polyvinyl alcohol
RDS	Rate determining step
RID	Refractive index detector
SA	Succinic acid
SEM	Scanning Electron Microscope
SBA-15	Santa Barbara amorphous 15
TA	Tartronic acid
TEM	Transmission electron microscopy
TPA	Terephthalic acid
TPD	Temperature programmed desorption

TPR	Temperature programmed reduction
XPS	X-ray photoelectron spectroscopy
XRD	X-ray diffraction

Contents

Chapter 1

Introduction

1.1 Catalysis

Catalysis is a term describing a phenomenon in which the rate and/or the outcome of the reaction is influenced by the presence of a substance known as a "catalyst" that is not consumed during the reaction and that is subsequently removed if it is not to constitute as an impurity in the final product.[1] This phenomenon was first described by a pioneering Swedish scientist J. J. Berzelius in 1836 through rigorous experiments by adding unknown substance capable of altering the rate of chemical change that itself remains unchanged throughout the reaction.[2] Even though, this concept was heavily criticized by other scientist because this phenomenon might be outside the boundaries of other chemical disciplines, the Berzelius findings remain valid and has become the field of modern catalysis.[3]

Catalysis today has been explored and utilised due to it wide range applications, many of which are fundamental in daily activities. Among these are the production of ammonia, which serves as a vital ingredient for fertilizer, by the Haber process and the contact catalytic process to produce sulphuric acid from sulphur dioxide and oxygen using a vanadium(V) oxide (V_2O_5) catalyst which is also indirectly used for fertilizer production. Another group of catalysts of interest are biological catalysts (enzymes), which control the biochemical activities of human body and is somewhat used in biomass transformation biofuels.[4]

Catalysts are categorized in two main groups, homogeneous and heterogeneous catalysts. The former offer high yield in short time under mild conditions, although, drawbacks such as waste generation, corrosion in reaction systems and recyclability. These disadvantages mean that heterogeneous catalysts, such as metals and single and mixed metal oxides, are often

used in place of homogeneous catalysts.

1.2 Heterogeneous Catalysis

Heterogeneous catalysis is a process whereby a solid phase catalyst is present and the reactants are either gases or liquids phase, and in such a manner that the solid phase can easily be removed.[5] A typical example of this phenomenon is the production of hydrogen from steam methane reforming over a Nickel (Ni) solid and/or platinum group metals (PGM) catalysts. Such solid catalysts are widely employed at all levels of the chemical value chain, although they are especially employed in the bulk chemical industry.

Traditionally, solid materials have been employed as heterogeneous catalysts since the 1800s by a founder of heterogeneous catalysis, a great German chemist Johann Wolfgang Döbereiner, who produced a flame from hydrogen gas by the action of sulfuric acid on zinc, using platinum wire as a catalyst.[6] His finding give birth to several catalytic process for industrial applications. Examples of such catalytic processes were mentioned in Section 1.1. Heterogenous catalytic processes are classified into Gas-Solid reactions (GS) and Liquid-Solid (LS)/Gas-Liquid-Solid reactions (GLS).[7]

Gas-Liquid-Solid (GLS) reactions have been employed as heterogenous catalytic processes with a Gas/Liquid as a reactant and the solid material as a catalyst for many industrial processes, for example, petrochemical industries using traditional feedstocks (crude oil) which is the source for energy and chemicals. In this process, harsh operating conditions such as high temperature and pressure are required.

Increasing demand and attention has recently been focused on the sustainability of the chemical industry, and the need for raw materials to evolve from fossil to renewable feedstocks. This change in direction necessitates the implementation of new heterogeneous catalytic process operating in a liquid-solid phase (LS)/gas-liquid-solid phase (GLS).[8] This process involves the use of sustainable raw materials, which are normally highly

functionalised, derived from biomass, that are much less volatile with lower thermal stability compared to fossil based materials.[9] The reaction conditions for biomass processes is typically milder than petrochemical GS catalytic process due to reasons mentioned above.[10,11] The development of liquid phase heterogeneous catalytic processes depends on many factors, such as catalytic activity, synthesis cost, selectivity toward target product and catalyst lifetime in the aggressive reaction environment and how long a catalyst maintains activity and selectivity.[7]

Of note, with respect to this thesis, is the transformation of biomass platform molecules into value added chemicals through liquid phase oxidation process using solid mixed metal oxide catalysts. This is one of the the grand challenges in chemistry, driven by the pressing need for climate change mitigation to devise green and sustainable technologies for the conversion of waste biomass to biofuels, commodity chemicals and new bio-based materials such as bioplastics. The recent emergence of GLS catalytic processes can produce chemical and fuels with lower greenhouse gas emissions.

1.2.1 Perovskites as Heterogeneous Catalysts

A large number of catalysts used in the chemical industry are based on mixed metal oxides.[12] The synthesis of specific customized mixed oxides with the ability to perform complex functions is one of the most important research topics in the field of heterogeneous catalysis.[13] To achieve complex catalytic reactions, multifunctional catalysts are needed with the correct solid state, surface, and morphological properties. Extensive background knowledge of solid surface chemistry from the field of heterogeneous catalysis can be perhaps usefully applied in catalyst design and engineering of new high-performance materials. This requires a wide range of cross-fertilization, combining heterogeneous catalysis and materials science in the field of physicochemical property evaluation, solid-state chemistry and synthetic pathways.[14]

Perovskite type oxides are widely studied mixed metal oxide materials because almost 90% of the metallic elements in the periodic table can be used to make the perovskite structure, that allows the perovskite material to exhibit a broad diversity of physicochemical properties. Even though, many compounds exist in perovskite structure such as carbides, halides, hydrides and nitrides, the oxides are predominantly used in heterogeneous catalysis and surface chemistry.[15]

Table 1.1 shows the cations commonly used in perovskites structures.

A-site		B-site	
Ion	Radius (A^o)	Ion	Radius (A^o)
Na^+	1.06	Li^+	0.74
K^+	1045	Cu^{2+}	0.73
Rb^+	1.61	Mg^{2+}	0.72
Ag^+	1.40	Zn^{2+}	0.75
Ca^{2+}	1.08	Ti^{3+}	0.67
Sr^{2+}	1.23	V^{3+}	0.64
Ba^{2+}	1.46	Cr^{3+}	0.62
Pb^{2+}	1.29	Mn^{3+}	0.65
La^{3+}	1.22	Fe^{3+}	0.64
Pr^{3+}	1.10	Co^{3+}	0.52
Nd^{2+}	1.09	Ni^{3+}	0.56
Bi^{3+}	1.07	Rh^{3+}	0.66
Ce^{4+}	1.02	Ti^{4+}	0.60
Th^{4+}	1.09	Mn^{4+}	0.54
		Ru^{4+}	0.62
		Pt^{4+}	0.63
		Nb^{5+}	0.64
		Ta^{5+}	0.64
		Mo^{6+}	0.60
		W^{6+}	0.60

Table 1.1 Cations commonly used in ABO_3-Type Perovskite.

The perovskite oxides can be described by the general formula ABO_3, where A and B are cations from alkali/alkaline earth metal or lanthanide metal, occupying the 12-fold coordinated cub-octahedral cage of the oxygen sub-lattice, and transition metals, surrounded by six oxygen atoms in an octahedral coordination respectively.[16–18] one of the important

properties of perovskite materials is their ability to adopt a wide range of different compositions, substituting or partially substituting either A or the B sites with other cations of the same or different valences, thereby resulting in a new general formula of $A_{1-x}A'B_{1-y}B'O_{3\pm\infty}$ to adjust its redox and surface properties.[19] Beside their composition and structure, the morphology of the perovskite oxides also has a great impact on their physicochemical properties.

Another interesting property of perovskites is their stability with respect to their mixed oxidation state, electroneutrality and different charge distribution in their crystal structure, i.e. $A^{I}B^{V}O_3$, $A^{II}B^{IV}O_3$, or $A^{III}B^{III}O_3$, as in the examples of $NaWO_3$, $SrMnO_3$, or $LaMnO_3$. Their structural stability is related to the geometrical restrictions of the octahedral and dodecahedral cavities. In an ideal structure, where the atoms bond with one another, the B cation-O radius should be a/2 (where a is the cubic unit cell parameter) and A cation-O bond distance is a/√2 that is summarised by the Goldschmidt tolerance factor, t (Equation 1.1).[20]

$$t = \frac{(r_A + r_O)}{\sqrt{2}(r_B + r_O)}$$

1.1

This equation is only applied at room temperature to the ionic radii. The cubic perovskite structures have a tolerance value of 1 in an ideal state, however, the structure can exist for a t-value ranging from 0.75 to 1.. In several cases, distortion from the cubic structure occurrs in perovskites. A naturally occurring perovskite ($CaTiO_3$) is a typical example as it would idealy be cubic, but its true symmetry was found to be orthorhombic.[21]

In general, distortion in perovskite structure can result in orthorhombic, rhombohedral, tetragonal, monoclinic, and triclinic structures. These distorted structures can be overcome at high temperature to give the ideal structure (cubic). This change can be formed in a stepwise manner leading to intermediate distorted phases.

There are many advantages of perovskite oxides for use as a heterogenous catalysts, although

high surface areas and porosity are usually important for a good catalyst. The application of perovskite oxides in heterogeneous catalysis might be more widespread if materials with well-developed porous networks and higher surface areas could be synthesised. As mentioned above, to attain the ideal perovskite structure high temperature is required, and this results in the formation of perovskite oxides with low surface area and large crystallite sizes, making them unsuitable for many catalytic applications. However, depending on the application, many different preparation methods have been used to synthesise perovskite oxide catalysts, which will be discussed in detail in the next section.

1.2.1.1 Synthesis of Perovskite Oxides

Many methods for perovskite synthesis have been successfully developed and employed. The first method was developed in the 1970s and it was called the ceramic method. Since then, efforts were made to improve the properties of perovskites for catalytic application. The main efforts have been made to improve the specific surface area and phase homogeneity of the perovskite oxide. This gave birth to many efficient preparation routes such as sol gel[15,19,22–25], complexation,[22,26–30] supercritical antisolvent precipitation[31], coprecipitation,[32] freeze/spray, explosion method,[33] ball milling,[12] hydrothermal,[18,34,35] and more recently nano-casting (with soft and hard templates) [36–40] and an electrospinning method.[41]

Of particular note with respect to this thesis, three of the above methods were chosen to prepare the perovskite oxides, hydrothermal synthesis, citrate complexing and nano-casting using hard templates. These methods can be used to combat the high crystallinity and low surface area associated with perovskites, which currently limits their widespread application as heterogeneous catalysis.

In the sections below, the different methods used for the synthesis of perovskite oxides will be described briefly, based on the state of the starting of the reactant (i.e., solids, liquids or

gases and vapour).

1.2.1.1.1 Ceramic Method

In a simple term, the ceramic method uses a direction combination of solids to yield the final product. The method requires an equimolar solid mixture and high temperature of around 1300-1500 K, a temperature that is twice the melting temperature of the solid reactants, for the solid-state reaction to occur. The advantage of this method is the reaction it is easy to perform, the availability of the reactants and no by-product formation. However, the operating temperature in this method militates against the use of reactant forming volatile species and high oxidation state species that are unstable at high temperature. Additionally, it is difficult to obtain a pure single-phase perovskite, and there is a high tendency for contamination from the container used might occur. The particle sizes of the product obtained from this method are relatively large and the specific surface area is too low, limiting the suitability of the method for catalytic applications.[42]

Babu et al.,[43] reported the use of a ceramic method for the synthesis of a $Ba_{2-x}Sr_xEuSbO_6$ perovskite by stoichiometric mixing of the respective metal precursors. The precursors were thoroughly ground in acetone and the mixture was pelleted, followed by calcination in air at 1000 ^oC for 36h. the resultant material was ground and pelletized at 5 t/cm^2 and sintered in air at 1500-1550 ^oC for 16h.

1.2.1.1.2 Hydrothermal Synthesis

Hydrothermal synthesis is well known method in the field of catalyst synthesis. The method was originally reported by German geologist Karl Emil von Schafhäutl in 1845,[44] to make a crystalline quartz material in a pressure cooker. Three years later, Robert Bunsen produced barium and strontium carbonate at 200 °C and 15 atm in a sealed glass tube using ammonium

chloride as a solvent.[44] Since then, many scientists have used hydrothermal synthesis to make crystalline materials with different structural textures. Since these early experiments, the method has been updated with Teflon lined autoclaves now used to prepare catalysts using hydrothermal synthesis.

Hydrothermal synthesis is defined as a method for the synthesis of crystals from solutions in aqueous media at elevated temperature, usually temperature above 100 °C, and a pressure greater than 100 kPa. The resultant crystals grow in an ordered manner to give control over the particle size and morphology, with a low degree of particle aggregation or agglomeration. With this method, different crystallite morphologies can be obtained from cubic to rod like structures.[45] In addition, the properties of the crystals obtained from the hydrothermal method can be tuned/improved or have new functionalities added by coating it with particles.[44,46,47] Apart from controlling the characteristics of the crystals, the method offers substantial benefits such as mild synthetic conditions, fast and flexible continuous and batch processes, large scale production etc. Additionally, hash operational condition such high calcination temperature and milling step are not always required with this method.[46]

Bernard and Durand[48] reported the use of a hydrothermal method for the synthesis of $LaMnO_3$ from lanthanum and manganese nitrate precursors using citric acid as chelating agent and ammonia as precipitating agent. The hydrothermal treatment was carried out at 150 °C for 20 h under autogenous pressures followed by calcination treatment on the dried material at different temperature, 2 °C/min for 2 h to obtain a final product.

1.2.1.1.3 Sol Gel Method

This is a method whereby a metal precursor forms a sol (usually a colloid solution of metal alkoxide) which agglomerate into chains that form a gel by heating and stirring through hydrolysis/alcoholysis process. Depending on the application, the gel is subjected to a further

drying treatment to remove the solvent (usually 110 °C for 16 h in a ventilated oven) and the dried gel is calcined to obtain the final metal oxide.[49]

Reports on this method state that the materials obtained possess excellent properties such as high surface area and phase purity for use as heterogeneous catalysts. The operation conditions used in this method are mild compared to the conventional ceramic method and that allows the operation on an industrial scale. Several reports[12,23,50–52] state the advantage of sol gel methods over conventional methods in their ability to produce single or mixed side phase from two metal in a one step process by mixing metal precursors in the correct proportion. Perovskites are a good example, where two or more metal precursors are used to synthesized them, for example Burcu et al.[25] used a sol gel method to synthesize $LaNiO_3$ catalyst for the removal of azo dyes and used lanthanum and nickel nitrates as precursors.

1.2.1.1.4 Nano-casting Method

In heterogeneous catalysis, nano-casting methods are used to synthesize nanoscale materials. The nano-casting process involve three steps, creating a template of known size and shape, filling the voids in the template with metal precursors by infiltration and subsequent processing, before removing the template from the matrix to obtain a replica structure of the template (Figure 1.1). Depending on the application, the structure of the template plays a significant role on the properties of the resultant materials, and the templates used in nano-casting methods are classified into soft and hard template.

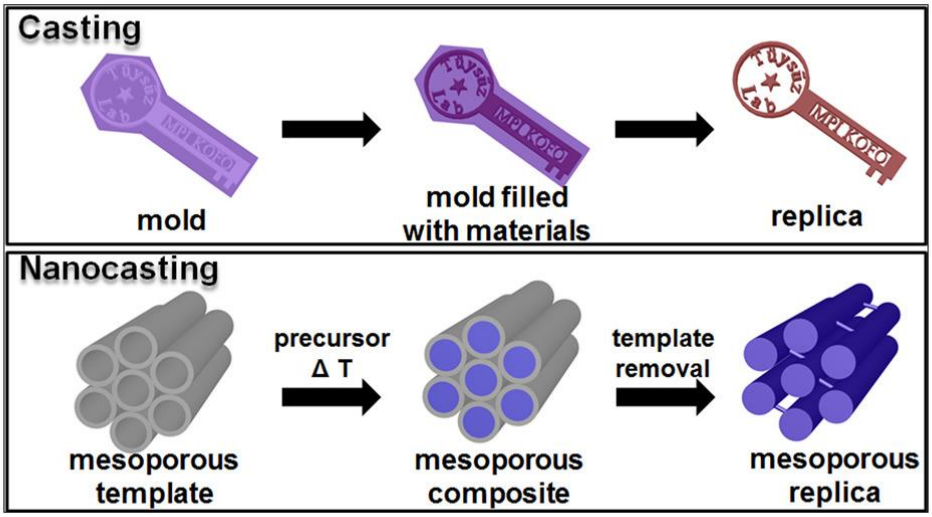

Figure 1.1 Nanocatsing technique showing the metal precursor infiltration into the template.[53]

Organic precursors species, such as surfactants that allow the formation of micelles, are often used as soft template for nano-casting methods, for example, non-ionic surfactant block copolymers (pluronic P123 and F127). Both cationic and anionic surfactants, such as alkyl trimethylammonium surfactant and hexadecane sulphonic acid respectively, are also regarded as soft templates for the synthesis of nano-porous materials via nano-casting methods. However, one should bear in mind that not all surfactants are considered as templates for nano-casting methods as the process just provides a cooperative assembling of the surfactant and inorganic phase only without replicating the surfactant structure. For instance, in the synthesis of mesoporous silica via true liquid-crystal-phase template mechanism using organic surfactant and a silica source (tetramethyl orthosilicate), the organic mesophase formed can be temporarily destroyed, for instance by the methanol during the hydrolysis of silica source. Seemingly, the templating via liquid crystals is not a true nano-casting method as it does not provide a solid framework of the replica. To understand which surfactant that can act as a soft template for nano-casting method, the liquid phase (i.e inorganic phase)

confined in the void of the surfactant most be solidified by the means of chemical process, for instance a sol gel reaction, leading to a mesostructured solid through evaporation induced self-assembly techniques. The self-assembly involves four steps, preparation of the homogeneous mixture of the inorganic precursor and the soft template in an appropriate proportion, evaporating the solvent, addition of more inorganic precursor to maximize the film filling of the template and mesostructured adjustment, and finally the thermal treatment which leads to template removal and network crystallization.

Even though the soft templates are widely used in nano-casting methods for the synthesis of mesoporous single metal oxides, its use in the synthesis of mesoporous perovskite oxides is rarely reported in the literature. This is because of the factors associated with the perovskite oxide synthesis phase purity, such as calcination treatment, has a direct negative impact on the template itself, and the homogeneity of the starting precursor which are crucial factors to attain a perovskite oxide with hundred percent phase purity. These factors limit the use of soft templating, although there are few reports in the literature that use soft templates for the synthesis of a mesoporous perovskite oxide. Brezesinki *et al*. used several soft templates such as poly(ethylene-co-butylene)-block-poly(ethylene oxide) or poly(isobutylene)-block-poly(ethylene oxide), to synthesize various perovskite oxides including $NaTaO_3$[54] and $BiFeO_3$.[55]

Despite the drawbacks associated with the use of soft template in nano-casting method, researchers still device a means to improve the process by using chelating agent (e.g citric acid) and precipitant, to synthesize mesoporous perovskite oxides. The process is improved in terms of increased homogeneity of the solution and cation dispersion during the solvent evaporation step. However, hard templating, also called repeated templating, is used to synthesize nanostructured metal oxides by a direct casting process. The method is relatively simple in contrast with the soft templating method. There are three steps involved in hard

templating method which are the formation of the template, infiltration of the metal precursor (casting step) including conversion of the precursor solution to a solid, and removal of the template using alkaline or acid solution.[40] Santa Barbara Amorphous-15 (SBA-15), Mobil Composition of Matter-41 (MCM-41) and Korea advanced Institute of Science and Technology-6 (KIT-6) are mesoporous forms of silica made via soft templating, and Carbon Mesostructured from Korea (CMK-1 and CMK-2) are commonly used as hard templates. Among these templates, SBA-15 is highly used for the synthesis of nanoporous perovskite oxides, although, because of the complex interaction between the SBA-15 and the infiltrated metal precursor species, filling the void area of the template becomes difficult in one step, and ample time is required to ensure complete metal precursor loading onto the void of the mesoporous silica.[40]

1.2.3 Application of Perovskite Oxide in Catalysis

Application of perovskite oxide depends on their crystal properties of the perovskite structure which can be structurally tuned, with numerous metals fitting the structural criteria, by the method of synthesis applied as outlined in section 1.2.1 above. One aspect that is important to the improvement of these methods is surface and bulk characterisation of the physical properties and structures of the perovskite type oxides formed. By adjusting the crystal properties of the structures, the properties of the perovskite mixed metal oxides change, and therefore should be characterised with appropriate methods. XRD, XPS, and TEM are useful tools for determining the orientation of the lattice structure, surface species, and crystal phases. The physical properties can be estimated through NH_3, CO_2 and O_2 TPD, and H_2/O_2 TPR, which can provide information on the acid-basic surface sites and redox behaviour as-well as information about the oxygen storage within the lattice structure.[13,16,56]

Of note, another condition to be fulfilled with the structural properties of perovskite oxide is

electroneutrality, i.e., the sum of charges of A and B equals the total charge of oxygen anions. This is attained by means of appropriate charge distribution of the form $A^{1+}B^{5+}O_3$, $A^{2+}B^{4+}O_3$, or $A^{3+}B^{3+}O_3$. In addition to this, partial substitution of A and B ions is allowed, thus yielding a plethora of compounds while preserving the perovskite structure. However, deficiencies of cations at the A- or B-sites or of oxygen anions are frequent, which results in defective perovskites. The nonstoichiometry in perovskites has been widely discussed in several reviews.[13,16,57] An example of perovskite oxide with ordered anion vacancies is the brownmillerite structure exhibited by $Ca_2Fe_2O_5$ and $La_2Ni_2O_5$. The former composition can be considered as an anion-deficient perovskite with one-sixth of the oxygen ions being vacant. Oxygen vacancies are ordered in alternate (001) BO_2 planes of the cubic structure such that alternate [110] rows of oxide anions are missing. Ordering of oxygen vacancies appears more complex in O-deficient $La_2Ni_2O_5$ perovskite. Since tetrahedral coordination of Ni^{2+} is unlikely, it has been suggested that oxygen vacancies ordering in $La_2Ni_2O_5$ is accommodated by means of disordered intergrowths of octahedral and square-planar layers. The review by Rao et al. covers these aspects with several examples. Until now, only a few examples with an apparent oxygen excess are known. This can be achieved by understanding of the cation vacancies at the A- and/or B-site.

Since 1960s, research into the redox capability, acid-base site and oxygen storage of perovskite has been of interest to catalysis researchers due to its tuneable nature. Due to the structure's high thermal stability, electron mobility, and redox behaviour, the use of lanthanide perovskites in automotive catalysis attracted a lot of attention at the time. However, due to the low surface area that results from treating precursors at high temperatures, perovskites were not considered industrially viable. Of recent, the use of perovskite oxides as heterogeneous catalysts has expanded because of the tuneable properties, thermal and hydrothermal stability. Perovskites have been applied to gas and solid phase

reaction at higher temperature and liquid phase reaction at mild temperatures.[38,57,58]

Of particular note, a precise knowledge of the relationships between solid-state properties and catalytic performance is crucial for the design and tailoring of efficient catalysts. In the search for these relationships, the availability of families of isostructural perovskite type oxides characterized by a great flexibility of the crystal to accommodate cation substitutions is extremely useful. There is no doubt that the structure and composition of ABO_3 model perovskites facilitate this arduous but extremely important task. By changing the A cation while keeping the B cation constant, or vice versa, a series of compounds may be synthesized with no substantial modification of the crystal structure, provided that the conditions for the lower limits of the ionic radii are met and that the relationship between the ionic radii and the tolerance factor (*t*) as defined by Goldschmidt is obeyed.

Perovskite oxides are largely used in catalytic processes due to their intrinsic properties such as redox behaviour, acid-base properties, and oxygen storage. It has been reported that catalytic activities of perovskites with ABO_3 type were determined by the A or B cation and O_2 depending on the type of the reaction. For instance, NO reduction, oxidation and decomposition reactions where perovskite catalysts have been successfully applied, the perovskite catalysts act differently by tuning the cations to achieve different properties. NO decomposition requires an oxygen deficient surface to provide a vacancy site for NO adsorption with can be achieved using $LaSrNiO_4$ with 94 % conversion achieved.[59] NO reduction, however, usually requires a reducing agent such as CO to aid conversion.[60] The dependency on the reducing agent can be mitigated by using the redox potential of the perovskite catalysts. It has been found that by altering the B site cation, that a large difference in activity is observed as the activity is based on the redox property of the B site cation.[61]

Based on a thermodynamic approach to estimate the binding energy of surface oxygen in a series of manganites, Voorhoeve et al.[62] observed that increasing activity for NO

decomposition coincides with the decreasing order of the binding energy of surface oxygen. This finding was taken as conclusive that the binding energy of oxygen determines the number of oxygen vacancies (active sites) and hence activity.[62] Another example of the influence of the binding energy between the oxygen and the lanthanide cation has been reported by Futai et al.[63] in $LnCoO_3$ (Ln) La-Dy) oxides. These authors found a correlation between the sum of the Ln-O and Co-O binding energies, reducibility, and the catalytic activity in CO oxidation. Maximum activity corresponded to $EuCoO_3$, which exhibited the lowest oxygen binding energy and was also the oxide that proved to be the easiest to reduce.

A correlation with the electronic parameters of the perovskite oxide is, however, more appropriate in superficial catalytic processes.368 In these reactions, the solid surface serves as a template providing electronic orbitals of the proper energy and symmetry for the bonding of reagents and intermediates. Sazonov et al.369 studied the oxygen equilibration

on $LaBO_3$ (B, first-row transition metal from Cr through to Ni) oxides and found the rate and activation energy of the oxygen equilibration above 500 K to be maximum for $LaMnO_3$ and $LaCoO_3$, very similar in fact to those of simple oxides of transition metals (M_2O_3). However, the temperature dependence of the rate of equilibration on AMO_3 (A is rare earth elements, La, Nd, Sm) oxides below 500 K was found to be of an identical nature to that recorded on the corresponding rare earth oxides. Thus, a distinct separation of the functions of the cations of the B-site and A-site can be seen for these perovskites, i.e., activity is determined by the cations of the transition metals at high temperature and by the rare earth ions at low temperature. These results are in agreement with those reported by Kremenic *et al.*[64] for propene and isobutene oxidation at 573 K (Figure 1.2). The twin-peak patterns in catalytic activity profiles resemble the twin-pattern which is found on going from d^0 to d^9 cations in the change in the crystal field stabilization energy caused by the change in the coordination of surface M^{3+} cations upon oxygen adsorption.370 These results suggest a close relationship

between the electronic configuration of the transition metal ion (B) and catalytic activity.

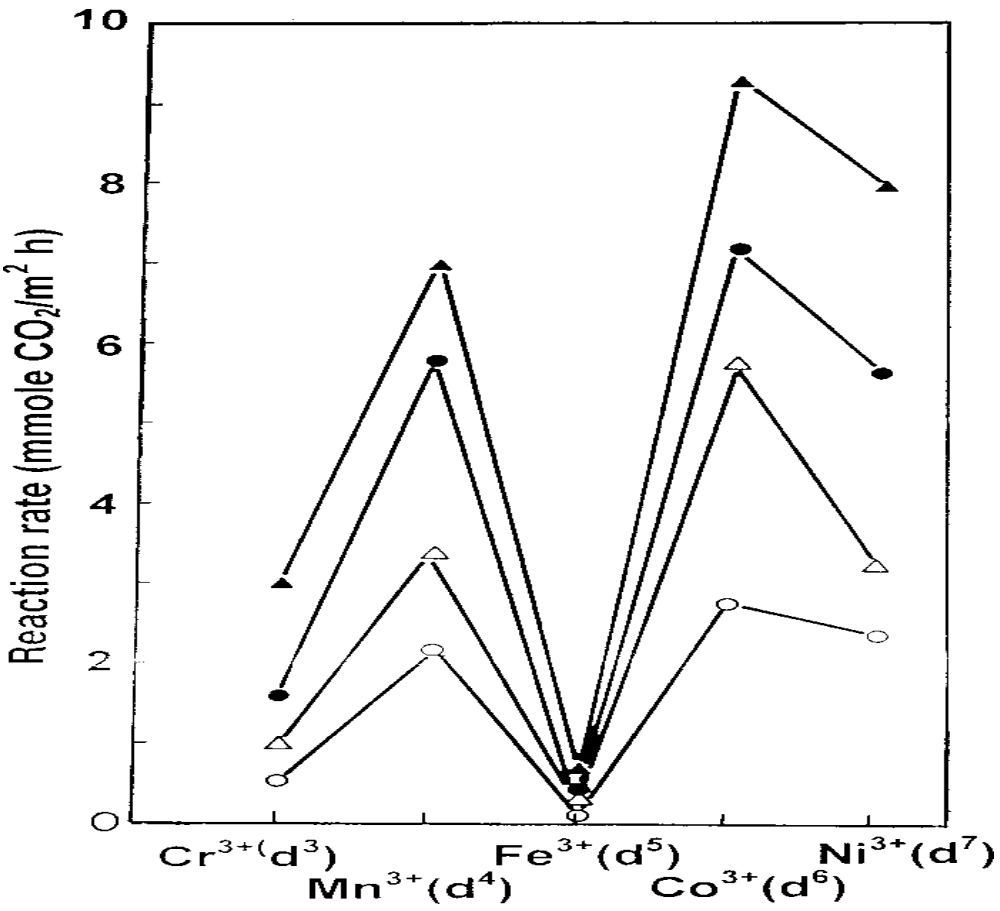

Figure 1.2 Rates of propylene (open symbols) and isobutene (filled symbols) oxidations on $LaMO_3$ oxides at 573 K. Molar ratio $HC:O_2$) 0.25:1 (circles) or 2:1 (triangles).[64]

1.3 Biomass

Biomass is a general name for materials of biological origin capable of generating renewable energy. Biofuel is a possible substitute for fossil fuel, although the debate around it concerning reliability, the high cost of the processing and structural complexity mitigate against its use in large scale energy production, its greener advantages over fossil fuels encourages its continuous industrial progress. In 2017 the International Energy Agency

(IEA) described biomass as the most important source of renewable energy.[65] The IEA also argued that the rate at which energy produced from biomass currently is way below the required level for future sustainability and urged the need to accelerate the production of bioenergy from biomass.[66] The IEA set out a target to increase the bioenergy production capacity from 2017 to 2050 spread out in three phases, that is the total energy supply increases by 6.6% by 2020 to 13.1% by 2030, eight years from now and 18.7% by 2050.[67] The Intergovernmental Panel on Climate Change (IPCC) also point out the importance of energy from biomass as it has significantly mitigated the adverse climate change if process in a right manner.[9] Most of the mitigation routes proposed by IPCC include the use of bioenergy and increased production rate to 200 EJ (exajoule) in the future. Even with this potential mitigation there are some researchers suggest that this seems a long waiting to have a positive climate impact is a problem.

1.3.1 Biomass Valorisation

Efforts continues to be made toward waste management by avoiding usage of hazardous materials such as reagents and solvents in many industries, particularly pharmaceutical and food processing companies.[65] For the past few years, emphasis has been made to substitute fossil resources with bio-renewable resources to produce commodity chemicals and fuels. Switching to biomass as a feedstock will not only be beneficial to the mitigation of environmental climate change but also provide room to produce platform chemicals and materials, in addition to biofuels which can also provide economical advantage. Also, these platform chemicals can be used as raw materials to produce bioplastics which will offer additional benefits because of their biodegradability.[65] The substitution would not be beneficial if first generation biomass is used as the feedstock because of the direct competition with the food production and consumption.[68] However, second generation biomass, such as lignocellulosic biomass, when utilized as the feedstock for bioenergy and

chemical production would be more economically viable in integrated biorefineries. This could be achieved by the valorisation of waste biomass generated in the processing of edible crops, for example, sugarcane bagasse, corn stover, orange peel etc. which indeed relates to the waste management. Food supply chain waste is indeed a new bio-renewable resource that can be used as a feedstock for biorefineries. Enormous amounts of organic waste are generated in the harvesting, processing, and use of agricultural products, including food and beverages.[69] In developed countries, additional waste is generated when food is discarded. Most of this waste goes to landfill which has a negative value and is not exactly in the spirit of "waste equals feedstock", the central tenet of the cradle-to-cradle concept.[9] The proposed second-generation bio-based economy is founded on the full utilisation of agricultural biomass to produce fuels and chemicals by employing green and sustainable development.[70]

1.3.1.1 Conversion of Secondary Generation Biomass

Global energy demand and environmental climate change concerns necessitate the utilization of biomass for energy and chemical production to reduce carbon emissions. For this purpose, the global production is estimated to be millions tonnes per annum to which of the majority are from lignocellulosic biomass (LCB) which is quite abundant in the natural world with a wide geographical distribution and can thus be explored to produce green bio-based chemicals.[71] The U.S. Department of Energy in collaboration with the U.S. Department of Agriculture have indicated that there will be a need to increase the commodities of biochemicals and bio-materials produced from biomass to 25% in 2030.[72] This target can be achieved with the use of LCB as a renewable (in term of CO_2 balance) and sustainable resource of petroleum carbon for the production of commodity chemicals. This vision moves the entire scope of the chemical industry from the prevailing petroleum refineries to LCB biorefineries which will reorient the global chemical industry and boost rural economy.[73]

Lignocellulose is much more difficult to process than first-generation renewable feedstocks – sugars, starches, and vegetable oils – but it has the advantage that it is not edible and, therefore, does not compete with food.[74] It constitutes three major polymeric components: lignin (approximately 20%), cellulose (around 40%), and hemicellulose (nearly 25%). Lignin is a three-dimensional polyaromatic (mostly phenols) biopolymer having a non-uniform structure that imparts rigidity and recalcitrance to plant cell walls. It is by volume the second largest biopolymer after cellulose and the only one composed entirely of aromatic subunits.[66]

Depending on the application, LCB needs to be processed by depolymerization and partial deoxygenation through either a thermochemical or hydrolytic process. Thermochemical processing involves pyrolysis of a mixture of charcoal and pyrolysis oil or gasification to produce syn-gas (a mixture of carbon monoxide and hydrogen), similar to syn-gas from coal gasification.[4] The syn-gas can be converted to liquid fuels or platform chemicals through well-developed technologies such as the Fischer–Tropsch process or methanol synthesis, respectively. Alternatively, the syn-gas can be used as a feedstock to produce biofuels and chemicals via microbial fermentation process.[75] However, syn-gas production from biomass is relatively expensive compared to fossil fuels produced syn-gas. Interestingly, one company, Calysta Energy, appears to have spotted the opportunity and is developing processes for the direct fermentation of methane to commodity chemicals.[76]

Conversion of LCB can also be achieved via a hydrolytic process using mineral acid at high temperatures or by enzymatic catalysts under mild conditions. However, use of mineral acid to catalyze LCB can generate salts of chloride and sulphate, and this issue can be overcome by switching to solid acid/base catalysts that give cleaner LCB conversion. In the case of enzymatic hydrolysis some form of pretreatment, such as a steam or ammonia explosion, is required to open the LCB structure and allow enzyme catalysts to have access to the targeted glycoside and ester bonds (Figure1.2).[77]. Alternatively, more added value would be obtained

by converting the lignin into chemically useful aromatic platform components, but selective conversion of this lignin remains a challenge. Some residual protein can also be formed during the conversion of LCB, and the amount is very much dependent on its source.[78] The hemicellulose, cellulose, triglycerides and proteins can be hydrolytically converted into their constituent building blocks: C_5 and C_6 monosaccharides, fatty acids plus glycerol, and amino acids, respectively.[79] The key to success in the biobased replacements with respect to petroleum-based production of chemicals is to choose the right biomass as the raw material and to use each of its components to give maximum value.

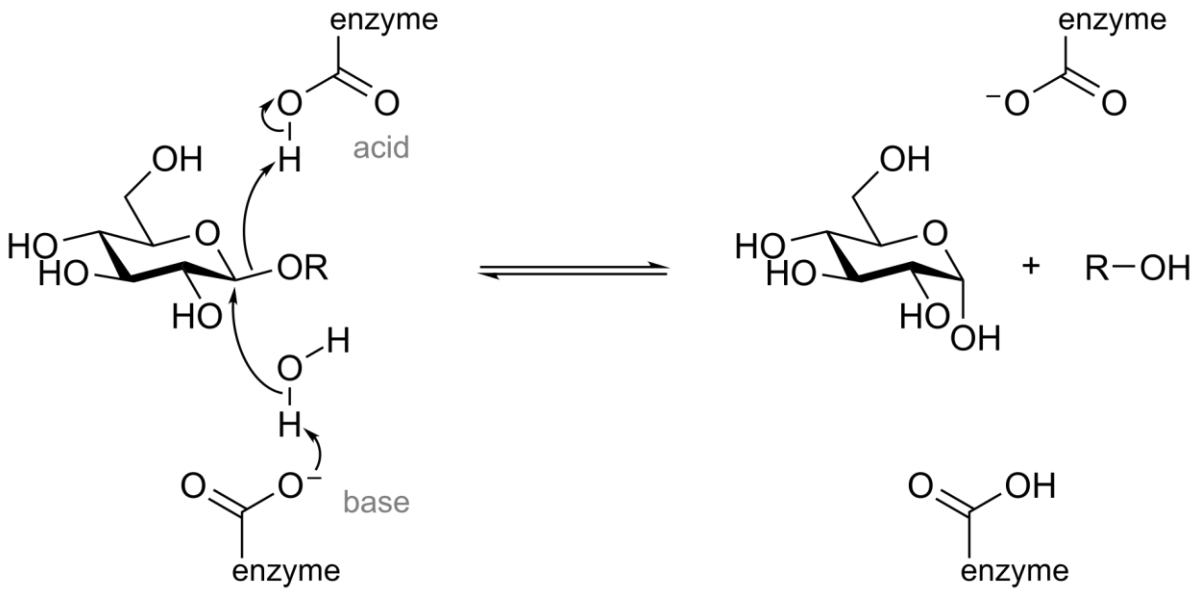

Figure 1.2: Pretreatment of lignocellulosic biomass (LCB) by enzymatic hydrolysis process.[80]

1.3.1.2 Production of Platform Chemicals from Biomass

The conversion of lignocellulosic biomass to value chemicals has been a subject of interest for decades and it can be carried out by either complete deoxygenation to petroleum hydrocarbons and further processing to commodity chemicals using established petrochemical technologies in existing reactors, or by direct conversion to oxygenates and

nitrogenates as platform chemicals. Many commodity chemicals are oxygenates that are produced in a traditional oil refinery from petroleum hydrocarbons, usually by catalytic aerobic oxidation. In contrast, the carbohydrate building blocks already contain multiple oxygen-containing functionalities. It would not seem logical, therefore, to first remove all the oxygen to generate petroleum hydrocarbons and then reintroduce oxygen functionalities by oxidation. Indeed, this forms the basis of the concept of a redox economy which maintains that it is energetically more economical to avoid, as much as possible, changes in oxidation state during a multi-step process reference to redox economy. Similarly, protein derived amino acids could be favourable building blocks for nitrogen containing molecules.

1.3.1.2.1 Conversion of Biomass Building Blocks to Hydrocarbons

There are many ways to convert biomass building blocks to petroleum hydrocarbons (Fig 1.3). One of these ways, is to produce lower alcohols (ethanol, propanol, and butanol) by fermentation and to dehydrate them to the corresponding olefins thereby providing a direct link into existing petrochemical supply chains. Indeed, it has been suggested that the optimum use of bioethanol could well be as a platform chemical rather than as a biofuel.[81] Similarly, 1-butanol is receiving attention[82,83] as a second-generation alcoholic fuel with a higher energy density and lower volatility than ethanol. Metabolic technology has been used to develop microorganisms with a recombination of two biological properties that allow them to effectively produce butanol at commercially quantities. consequently, many companies such as a DuPont/BP joint venture, Butamax Advanced Technologies, and Green Biologics are currently involved in the commercialisation of bio-1- butanol and both DuPont and later Gevo described the production of isobutanol by fermentation.[9] These two products can be readily dehydrated to 1-butene and isobutene, respectively. The availability of such bioethene and biobutene would provide a basis to produce bioproene by olefin metathesis, thus completing the C_2, C_3 and C_4 groups that forms one foundation of the petrochemical industry.

However, it would probably be more attractive to produce bio-propene from bio-isopropanol. There is currently no commercial process to these alcohols, but it is probably only a question of time before processes will be developed. Microbial production of isopropanol in a 67% yield and 143 g L^{-1} concentration after 240 h has been achieved using a metabolically engineered E. coli strain with gas stripping of the isopropanol.[84] Another C_4 petrochemical building block, butadiene, could be produced by dehydration of 1,4- or 2,3-butane diol both of which are available from fermentation of C_5 and C_6 sugars. Alternatively, butadiene, and other commodity chemicals, can be produced from bioethanol and the latter can be viewed[85] as a platform chemical in addition to being a biofuel.

Hydrocarbons can also be produced directly by fermentation, thereby avoiding the energy intensive separation of miscible lower alcohols from the aqueous medium. Enzymatic catalysis is being used to re-engineer the isoprenoid pathway or fatty acid biosynthesis, in bacteria or yeast, to directly generate hydrocarbons. In one example, Global Bioenergies is developing the direct production of isobutene by fermentation.[86] Similarly, processes for the direct production of isoprene by fermentation have been developed by Genencor and Amyris in collaboration with Goodyear and Michelin, respectively. Amyris is also commercialising the fermentative production of the sesquiterpene, β-farnesene, with genetically modified yeast. The latter is of interest as a renewable diesel fuel and a starting material in the synthesis of specialty chemicals. In a variation on this theme, the company LS9 is employing synthetic biology to reengineer fatty acid biosynthesis to produce alkanes, alkenes, alcohols and esters.[9,78]

Heterogeneous catalysis is another approach to convert biomass or its building blocks such as glucose, glycerol, etc. This can be done using aqueous phase reforming by combining solid acid and platinum group metal catalysts such as Pd or Pt, to produce a mixture of hydrogen and light alkanes. Further processing of these molecules by hydrotreatment or

dehydrocyclisation using a modified ZSM-5 zeolite catalyst, yields a mixture of gasoline, diesel and kerosene range alkanes, or the standard mixture of benzene, toluene, and xylenes respectively, that are produced in petroleum refineries. Alternatively, hydroxymethyl furfural (HMF) can be further converted to hydrocarbon fuels.

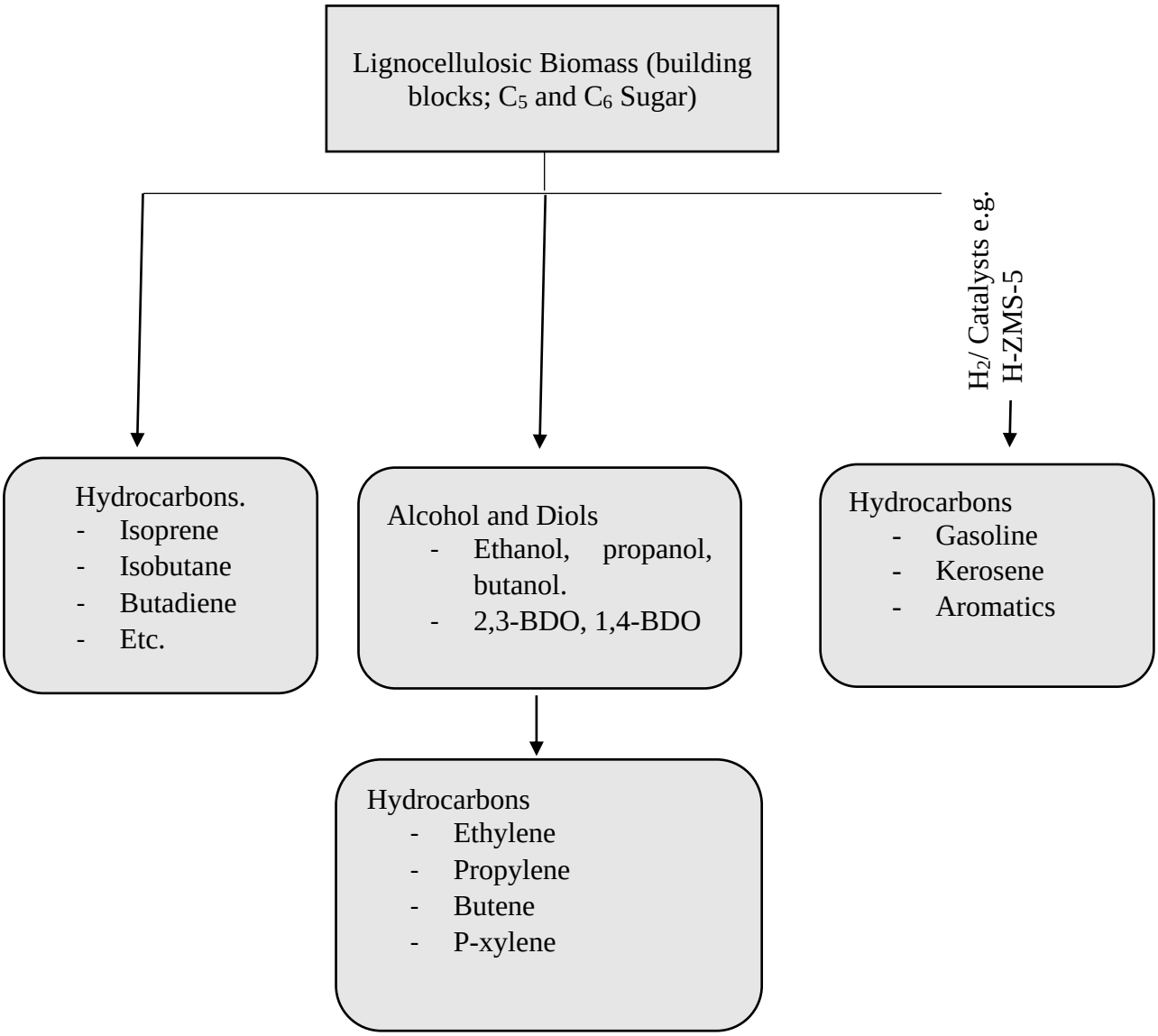

Figure 1.3 Lignocellulosic biomass to hydrocarbons platform chemicals.

1.3.1.2.2 Conversion of Biomass to Non-hydrocarbons (Oxygenates)

There are basically two interesting techniques to transform biomass into oxygen-rich molecules either by biotechnological or chemical means. These processes will be reviewed in detail under this section.

1.3.1.2.2.1 Biotechnological technology

The transformation of lignocellulosic biomass to oxygenated commodity chemicals such as short chain alcohol, diols and carboxylic acids can be achieved by biotechnological processes (Figure 1.4). Many of low chain diols are considered as commodity chemicals with many industrial applications in the production of polymers by fermentation. 1,3-propanediol for instance, is a material with a vast industrial application, the most well-known of which is the production of polyester, polytrimethylene terephthalate which in used for fibres and plastics. Similarly, 2,3-butanediol can also be produced effectively by fermentation[87] and has a variety of potential industrial applications.

Lactic acid is a first-generation biobased commodity chemical with many applications, the most important of which is probably the rapidly growing use of polylactate as a bioplastic.[88] Citric acid is another example of a commodity chemical which is produced by fermentation.[89] There are many examples of second-generation carboxylic acids which can be produced cost-effectively by fermentation. Succinic acid,[90] for example, has attracted considerable attention, because of potentially large volume applications in polyesters and polyamides. However, biotechnological approach is not the best method for the production of these chemical industrially wise because of the time and non-recyclability of enzyme involved in the process.

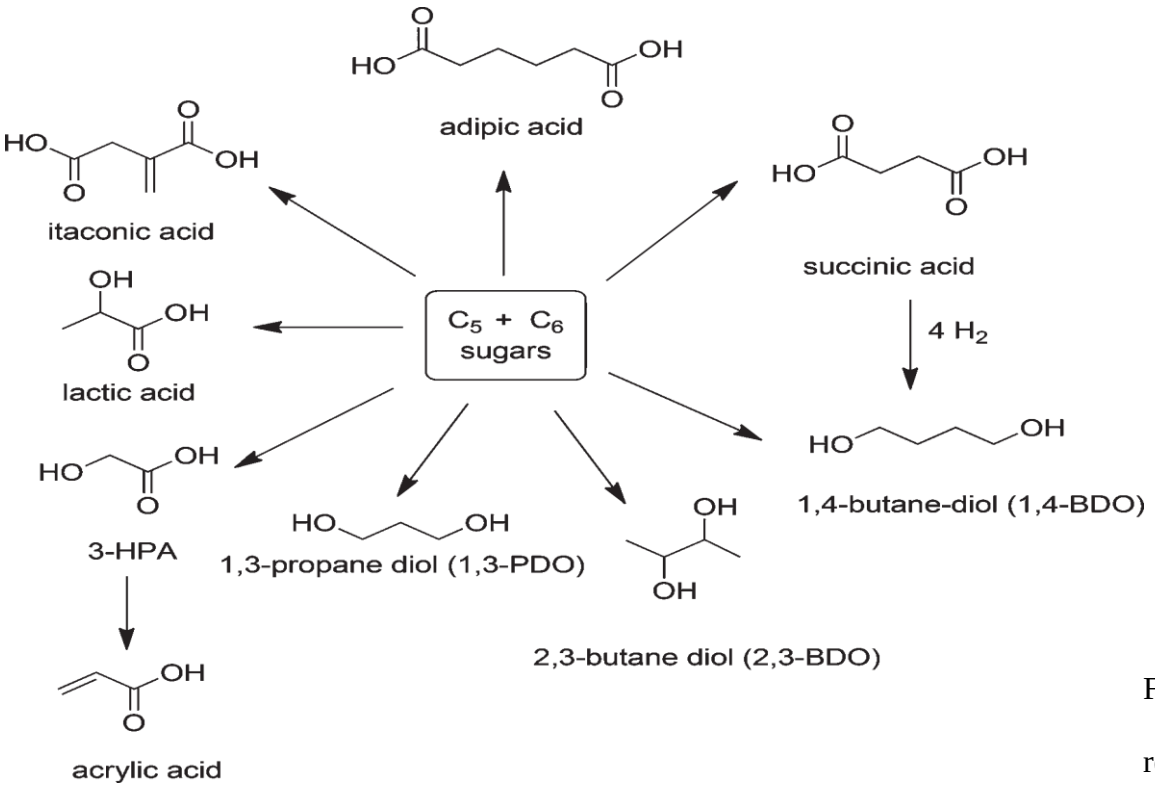

Figure 1.4 Biomass derived Sugars to some commodity chemicals

1.3.1.2.2.2 Chemical Technology

Lignocellulosic biomass derived sugars such as pentose and hexose can be transformed chemically into commodity chemical using acid-base homogeneous or heterogenous catalysts. For instance, acid catalysed hydrolysis of pentose to yield hydroxymethyl furfural (HMF) or hexose to furfural. Both products are potential platform chemicals to produce commodity chemicals. Furfural has broad applications and has been produced on an industrial scale for decades.[91,92] HMF, in contrast, has much potential[93,94] as a raw material to produce chemicals, polymers and biofuels but its production has not yet been commercialized.

1.3.1.2.2.1 HMF as a Platform Molecule

Hydroxymethyl furfural, as mentioned previously, is an oxygenated platform molecule derived from hexose sugar from lignocellulosic biomass. It possesses two functional groups

(carbonyl and hydroxyl group), which gives it enormous potential to produce commodity chemicals such as to levulinic acid (LA) and γ-valerolactone (GVL) and furan-2,5-dicarboxylic acid (FDCA), a potential building block for polyesters, depending on the treatment. One of the objectives of this project is centred toward the transforming HMF to FDCA.

1.3.1.2.2.1.1 Oxidation of HMF

Oxidation of HMF is of significant interest to both industry and academia for several reasons, including its origin, that it is highly functionalised containing hydroxyl, aldehyde, and furan ring with vast array of potential products (Figure 1.5). Utilising HMF in this way, it will accelerate the pathway towards producing HMF from biomass building blocks.

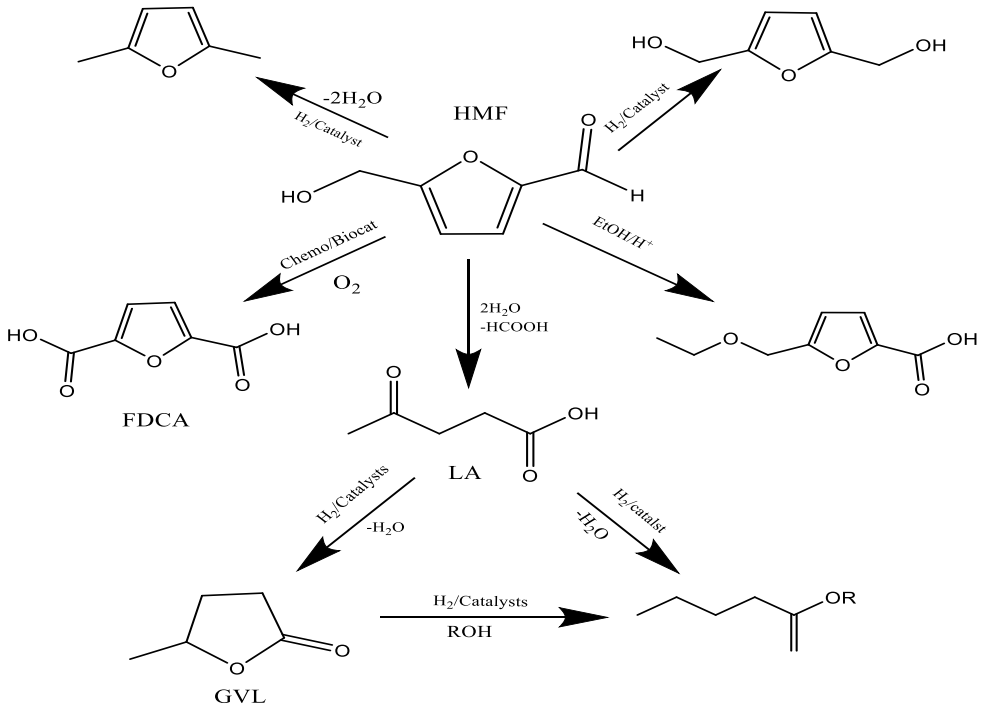

Figure 1.3 Potential products from hydroxymethyl furfural under different conditions.

Different reaction systems have been used for the oxidation of HMF with air, oxygen, or other oxidizing agents (H_2O_2, $KMnO_4$ etc.).[95] The main oxidation product is 2,5-furan dicarboxylic acid (FDCA) which as potential monomer for PTE polymer production. The chemical conversion requires harsh reaction conditions (temperature and pressure) and

additives,[96] a catalyst that has both high activity and selective towards products is of high value in this reaction. Heterogeneous catalysts have been proven to be excellent at the production of these fine chemicals.[97–100]

The oxidative production of FDCA from HMF over different heterogeneous catalysts has been studied extensively in various process environments. Mostly, the oxidation proceeds with either pure oxygen or air as an oxidizing agent; hydrogen peroxide (H_2O_2) and potassium permanganate ($KMnO_4$) have also been used but researchers mostly prefer molecular oxygen considering its higher oxidation potential, eco-friendly impact, and low cost. Different metal supported heterogeneous catalysts, such as platinum (Pt), gold (Au), ruthenium (Ru) and palladium (Pd), with good catalytic activity, recyclability, and stability, have also been developed and successfully applied in HMF oxidation to FDCA.[101] Noble metal oxides occupy the major portion of the heterogeneous catalysis scheme in the current FDCA research regime.

1.3.1.2.2.1.1 Platinum Catalysts for HMF Oxidation

Supported platinum (Pt) catalysts are more active for the oxidation of HMF when compared to other PGM catalysts.[101] When applied to HMF oxidation, carbon supported Pt catalysts (Pt/C and Pt–Pb/C) can give 81% yield of FDCA with lead (Pb)–free Pt/C and 99% with Pt–Pb/C catalyst under 1 bar O_2 pressure.[102] The detection of 2,5-hydroxymethyl furnncarboxylic acid (HMFCA) as an intermediate proves the preferred oxidation of the formyl group over the hydroxymethyl group with the lead-doped Pt catalyst. The yield increment with Pb-doping stimulated the development of bimetallic catalysts for HMF oxidation. Following this, the bismuth (Bi)-incorporated Pt catalyst (Pt–Bi/C) having a Pt–Bi molar ratio of 0.2 was developed and applied in FDCA synthesis.[103] A 29% increase in FDCA yield by Bi addition proved the improvement in the activity of the bimetallic catalyst

with identical parameters.[104] Pressure reduction negatively affected the yield and an increase in pressure did not exhibit appreciable effects.[105] As such, 1 bar oxygen pressure is the optimum pressure for the Pt/C catalyst that is easy to maintain without any potential hazard. The rapid oxidation of process intermediates, HMFCA and DFF, produces FFCA. FFCA oxidation to FDCA is the rate controlling step. Bi incorporation to produce Pt–Bi/C catalyst can stabilize the catalyst by eliminating the oxygen poisoning and Pt leaching tendency, resulting in increased catalyst life and stability.

The effects of the supports have been investigated by producing Pt–Bi/TiO_2 and Pt/TiO_2 catalysts and replacing the C support with TiO_2.[103] The TiO_2 effectively and selectively increased the FDCA yield. Reduced graphene oxides (RGOs) with their abundant surface functional groups are also promising catalyst supports and are now being applied extensively. When the support was changed to RGO (Pt/RGO), the FDCA yield was observed 84% in 24 hours, but the RGO support did not work efficiently with other noble metal catalysts such as Pd/RGO, Rh/RGO and Ru/RGO. This demonstrates the catalytic superiority of Pt over other PGMs.[106] However, an increase in the process intermediate (HMFCA) and a decrease in the final product (FDCA) was observed during the recycling experiments.

The substantial aim of low-pressure oxidation can be achieved by applying relatively cheap metal oxide-supported Pt catalysts. An exceptionally high yield (>99%) was recorded with very low oxygen pressure (0.2 bar) in alkaline medium.[107] Oxygen chemisorption on the active sites of the Pt/γ-$A1_2O_3$ catalyst negatively affected and deactivated the catalytic ability.[108] Changing the metal oxide support resolved the problem of catalyst deactivation. Pt/Zr_2O_3, Pt/C and Pt/γ-$A1_2O_3$ all performed well and Pt/TiO_2 and Pt/CeO_2 showed poor catalytic efficiency under similar conditions.[108] Bi added to form a bimetallic catalyst was found to improve the yield to 98% over Pt/ $Ce_{0.8}Bi_{0.2}O_{2-\delta}$.[109] These results suggest that non-reducible oxide (γ-$A1_2O_3$, ZrO_2, and C) supported Pt catalysts have higher catalytic

performance than reducible oxide (TiO_2 and CeO_2) supported Pt catalysts due to the low oxygen storage capacity.

Reaction kinetic studies have shown that HMF oxidation proceeds through the Pt-alkoxide intermediate.[109] Pt nanoparticles yield Pt-alkoxides by reacting with the hydroxyl groups present in HMF, substituting β-H with hydroxide ions (OH^-). Bi containing ceria accelerates the oxygen reduction due to the availability of more oxygen vacancies and the breakup of transitional peroxides.[109] This catalytic cycle continues to consume surface electrons in oxygen reduction, which demonstrates the catalytic efficiency and the Pt/$Ce_{0.8}Bi_{0.2}O_{2-\delta}$ catalyst can work efficiently even after five cycles. It has been reported that the observed yield of FDCA was 97% in the fifth cycle, which was appreciably close to the recorded yield in the first batch (98%).[109]

Alkaline medium oxidation of HMF is kinetically favourable and gives higher FDCA yield but the separation of inorganic salt and neutralization of the product solution are major problems.[110] To overcome this, base-free oxidation has been investigated.[111] The observed yield can be high enough (95%) over PVP-stabilized Pt nanoparticles (Pt/PVP) with low oxygen pressure, but long reaction time (24 hours), low feed rate (0.29 m mole), and high catalyst loading (5 moles%) are the major disadvantages of this system.[111] Hence, at this stage, the Pt/PVP catalyst is uneconomical for mass production although it has high stability and recyclability with confirmation of the green environment protocol. Platinum nanoparticles (Pt-NPs) dispersed in water have been widely employed as oxidation catalysts due to their strong oxidizing ability and diverse stability.[112] Pt-NPs-doped polymeric catalysts can not only stabilize the Pt-NPs by steric and electrostatic interactions but also boost the catalytic activity. Among the different counter anions explored so far, the Tf_2N^- anion has exhibited the highest catalytic activity, presumably because it may be displaced from the NP surface in a facile manner, generating catalytically active surface sites where the substrates

can bind and react, while simultaneously offering sufficient electronic and steric protection to stabilize the NPs during reaction.[113]

1.3.1.2.2.1.2 Gold Catalysts for HMF Oxidation

Gold (Au) was considered inactive as a catalyst for chemical processes until the pioneering work of Hutchings in 1985 bring about the discovery of its catalytic ability, a stunning breakthrough for research and development.[114] Recently, many Au catalysts were developed and applied successfully for a wide range of potential applications.[115,116] Au catalysts display encouraging performance for HMF oxidation and their catalytic efficiency is strongly influenced by supporting materials, being similar to other noble metal (Pt and Pd) catalysts.[117] Metal oxide supports play an important role and gold nanoparticles (Au-NPs) doped on CeO_2 and TiO_2 could obtain higher FDCA yield (>99%) than when supported on Fe_2O_3 and C.[118] Although the yield is superior (96%) over the Au/ CeO_2 catalyst compared to the Au/TiO_2 catalyst with higher HMF/Au ratio (640), the high oxygen pressure and activity reduction in the recycling experiments are paramount industrial barriers.[117].

The catalytic activity of Au/CeO_2 can be further improved by Bi^{3+} incorporation into the CeO_2 support nanostructure.[119] The modified catalyst not only expands O_2 activation but also increases the hydride transferability of nano-CeO_2, due to the availability of lone pair electrons (Bi^{3+}). The Bi combined catalyst, [Au/$Ce_{1-x}Bi_xO_{2-\delta}$ ($0.08 \leq x \leq 0.5$)], can increase the FDCA yield to 75% from 39% over unaided Au/CeO_2 under the same conditions.[117,119] Increased FDCA yield was observed with an increase in reaction time over Au/$Ce_{0.9}Bi_{0.1}O_{2-\delta}$ catalyst (Table 3).[119] The catalyst can be easily separated and recycled with an acceptable decrease in catalytic activity. The catalytic support dependency of Au catalysts has also been investigated by developing HY-zeolite catalysts.[120] The FDCA yield in alkaline medium is selectively high (>99%) over the Au/HY catalyst in comparison to channel-type zeolites

(ZSM-5 & H-MOR), TiO_2, $Mg(OH)_2$ and CeO_2 catalysts.[120] The efficiency enrichment is due to the uniform dispersion of Au nanoclusters in the HY zeolite super-cage structure. The developed cage structure eradicates the NP agglomeration, which thus increases the recycling efficiency and performance of the catalyst.[121] The addition of 1,3 propanediol further improves the process efficiency by suppressing the self-polymerization and humin formation over Au metal oxide catalysts.[122]

Numerous bimetallic Au catalysts with extended physicochemical properties were prepared and tested for the aerobic oxidation of HMF. These bimetallic catalysts further improved the process efficiency and catalyst stability.[123] The physicochemical properties of the developed catalyst can be altered by composition and the extent and homogeneity of mixing.[123,124] The Au–Cu/TiO2 (bimetallic) catalyst is very stable and more efficient than the Au/TiO_2 catalyst due to strong synergistic effects.[125] It not only eliminates the PVP-stabilized Au post-deposition but also accelerates the FDCA yield, reducing the rate of competitive reactions. It also improves the efficient recycling without significant agglomeration or leaching of metallic nanoparticles from the catalyst. Similar findings have also been recorded with Au–Cu/CeO_2, Au–Cu/TiO_2 and Au–Pd/AC catalysts.[126,127] Au–Pd/AC is stable but with decreased recycling efficiency. Vastly superior stability and yield were observed (99% in the fifth cycle) when the modified Au_8–Pd_2/AC catalyst was applied.[126] Hence, the deactivation of monometallic Au catalysts by the adsorption of reaction intermediates as compared to bimetallic catalysts verifies that bimetallic Au catalysts are superior in activity and stability.

Environmental concerns associated with the use of alkaline solution, salt separation, recycling and product solution neutralization have been addressed by employing base-free HMF oxidation over a hydrotalcite-supported (Au/HT) catalyst.[128] The elimination of the acid requirement for product solution neutralization caused the base-free process to be more economically competitive when compared to other alkaline medium oxidation processes. It

has been previously reported that base free processes can be performed with high FDCA yield (99%) and complete HMF conversion under low oxygen pressure. Au/MgO, Au/ Al_2O_3, Au/SiO_2 and Au/C either remain unreactive or exhibits very low reactivity, whereas Au/HT was found to have exceptional catalytic activity in a base-free environment, although the recycling performance decreases.[128] Mg^{2+} leaching from the HT support was observed due to the HT-FDCA chemical interaction, which limits the base-free conditions.[129]

The development of carbon nanotubes (CNT) supported Au–Pd catalysts (CNT–Au–Pd) substantially accelerated the base-free FDCA production.[130] The CNT–Au–Pd catalyst is more efficient when oxygen is replaced with air under moderately high pressure.[130] The CNT supported reactant adsorption with improved exposed sites and strong synergistic Au–Pd effects can contribute efficiently to the catalyst performance. Evidence of FFCA and DFF as reaction intermediates indicate the preferred oxidation of the hydroxyl group, compared to the aldehyde group, using the Au–Pd/CNT catalyst.[130] The monometallic Au/ CNT catalyst, as compared with the bimetallic Au–Pd/CNT catalyst, preferentially oxidizes the aldehyde group, producing the HFCA intermediate and conforming to the same processing scheme as over Au/CeO_2 and Au/TiO_2 catalysts in an alkaline environment.[117] Unfortunately, HMFCA initiates competitive reactions by furan ring opening and degradation.[130] The monometallic Pd/CNT and bimetallic Au–Pd/CNT catalysts propagate the reaction through identical pathways. However, Pd addition in the Au–CNT structure modifies the reaction pathway to DFF from HMFCA conversion and accelerates the FFCA to FDCA oxidation.

1.3.1.2.2.1.2 Influence of Reaction Conditions on HMF oxidation

The influence of reaction condition such as the molar ratio HMF:base, temperatures, and oxygen pressures were reported with and without the addition of homogeneous base. Davis *et*

al.[104] have compared reaction rate and product distribution over the supported metal catalyst Pd/C, Pt/C, Au/C, and Au/TiO_2. Compared to the Pd and Pt materials, the gold catalysts showed a reaction rate an order of magnitude higher under the given reaction conditions (6.9 bar O_2, room temperature). However, here, the major product was HMFCA while Pt and Pd delivered FDCA as major product. The authors reported that a higher base concentration (OH^-) and oxygen pressure was required to improve the selectivity of the gold catalysts towards the desired product FDCA.

Gorbanev *et al.*[121] reported the selective oxidation of HMF to FDCA over Au/TiO_2 at room temperature. Increasing oxygen pressure from 10 to 20 bar enhanced the yield of FDCA up to 71 % at full conversion of HMF. Here, about 4 % leaching of gold species was detected and hence a decrease of the conversion by 5 to 10 % was observed in the recycle experiments. Casanova *et al.*[117] studied differently supported gold catalysts, such as Au/TiO_2, Au/CeO_2, Au/C, and Au/FeO_2. Among the catalysts mentioned, the best results were obtained for Au/CeO_2 producing 96 % yield of FDCA at full HMF conversion. Furthermore, the recyclability of the catalyst was successful only when the oxidation reaction was performed at room temperature for 4h. During this time, all HMF was converted to HMFCA and HMF degradation was avoided and then increasing the temperature up to 130 °C was necessary to oxidize HMFCA further to FDCA. In this way the catalyst was reusable three times, otherwise the catalyst will be deactivated by blocking of active sites by HMF degradation products in the initial stage. However, a significant decrease of the FDCA yield to 81 % was observed in the 4^{th} run.

Pasini *et al.*[131] have reported the HMF oxidation of on an $Au\text{-}Cu/TiO_2$ catalyst. This bimetallic catalyst showed higher activity, better stability and resistance against poisoning compared to their monometallic counterparts, which was attributed to a strong synergistic effect. In the recycling experiments, a fast deactivation of the Au/TiO_2 catalyst was observed.

The authors stated that the monometallic catalyst had lost oxidative activity quickly and after the second run it was totally poisoned and started to polymerize rather than oxidize the reactants. In contrast, the bimetallic Au-Cu/TiO_2 catalyst was reused 5 times without losing activity but with a slight decrease of FDCA yield. Thus, the bimetallic catalyst remained catalytically active because of the presence of the second metal (copper) in the active phase.

Ait Rass *et al.*[132] have reported the selective oxidation of HMF over a Pt-Bi/C catalyst. The presence of bismuth (Bi) as promoter in the catalyst prevented the Pt catalyst from deactivation (oxygen poisoning). In addition, the group studied the nature of base by keeping the pH of the reaction solution constant. The authors stated that by using Na_2CO_3 the activity clearly increased compared to using $NaHCO_3$ while strong HMF degradation was detected when NaOH was employed.

In the absence of base the conditions and FDCA yield in the oxidation of HMF were reported in the literature. Gupta *et al.*[133] used differently supported gold catalysts, such as Au/HT, Au/Al_2O_3, Au/C and Au/SiO_2. Hydrotalcite (HT, $[Mg_{8-x}Al_x\ (OH)_{16}(CO^{2-})].nH_2O$) is considered to be a basic support and among these catalysts Au/HT delivered the highest yield of FDCA (99 %) at full conversion. Even though leaching of gold was not detected, a slight decrease of the FDCA yield was observed in consecutive runs (from 99 % in first run to 90 % in third run). Gorbanev *et al.*[134] have reported a number of catalysts based on $Ru(OH)_x$ in the TiO_2, Al_2O_3, Fe_3O_4, ZrO_2, and CeO_2. The best result was obtained using CeO_2 as support. Additionally, the catalyst was reusable. Magnesium-based carrier materials [spinel ($MgAl_2O_4$), magnesium oxide (MgO) and hydrotalcite (HT)] were also studied in the HMF oxidation by Gorbanev *et al*. High yields of FDCA were achieved with $Ru(OH)_x$ containing catalysts on HT and MgO (99 and 87 %, respectively) whereas the spinel ($MgAl_2O_4$) supported catalyst delivered only 38 % yield of FDCA after 6 h. However, compared to the

spinel material the HT and MgO catalysts turned out to be less stable due to leaching of Mg ions into the solution. Here, the authors stated that the stability of HT observed by Gupta *et al.*[133] is due to the mild reaction conditions (ambient oxygen pressure and elevated temperature).

Generally, the advantage of using metal species supported on basic materials is to produce carboxylic acids rather than their salts form, which is beneficial economically and environmental aspects.[129,133] Davis *et al.*[135] have reported oxidation steps for the selective oxidation of HMF in the presence of base on supported Pt and Au catalysts utilizing the isotopically-labeled $^{18}O_2$ and $H_2{}^{18}O$ to investigate the source of the oxygen in the products (Scheme 1.1). However, the first step involved a reversible hydration of the aldehyde group of HMF to a germinal diol via nucleophilic attack of hydroxide ions (OH^-) to the carbonyl group and then the proton will be transferred from the water to the formed alkoxy ion intermediate. The second step involved the dehydrogenation of the formed germinal diol intermediate, aided by the hydroxide ions (OH^-) adsorbed on the metal surface, to form the carboxylic acid product (5-hydroxymethyl-furan-2-carboxylic acid, HMFCA) which is present as carboxylate in alkaline solution. Here, two water molecules and two electrons were produced where the electrons are deposited on the metal surface of the catalyst. In third step, an alkoxy intermediates is formed after the deprotonation of the alcohol group by hydroxide ion. Then, the alkoxy intermediate reacts to the aldehyde, formally by loss of hydride. Two water molecules and two additional electrons were produced in the step 3. The fourth step involved a reversible hydration of the aldehyde to the germinal diol (as occurred in the step 1). In the fifth step involved the dehydrogenation of the formed germinal diol, aided by the hydroxide ion adsorbed on the metal surface catalyst, to produce the carboxylic acid (2,5-furandicarboxylic acid, FDCA), which is present as carboxylate in alkaline solution, with liberating two electrons and two water molecules. In total, six electrons were produced during

this mechanism and deposited on the metal surface of the catalyst. The results showed that $^{18}O_2$ atoms were incorporated in HMFCA and FDCA products when the oxidation is performed in $H_2{}^{18}O$. It was stated that the water employed as oxygen source. The oxygen is not involved in this mechanism because it was found that the oxygen served as electron scavenger on the metal, thereby closing the catalytic cycle.

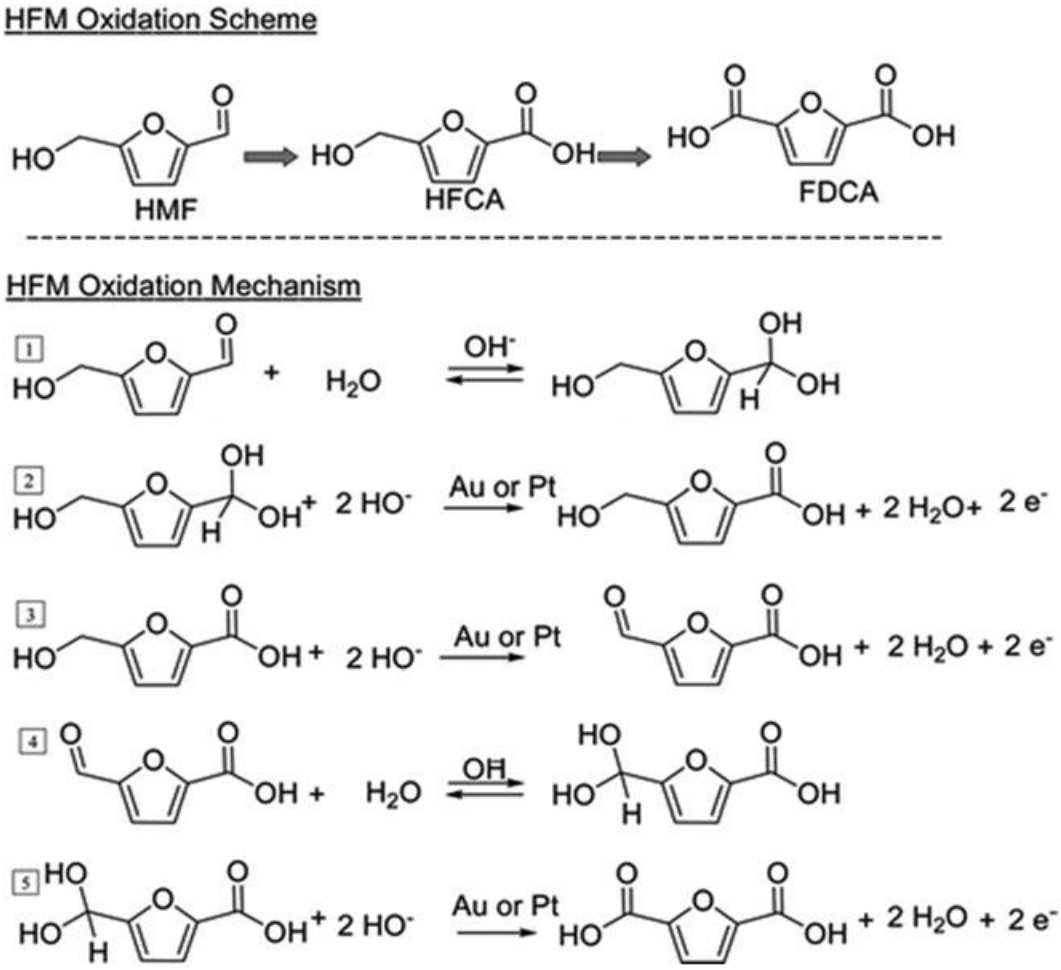

Scheme 1.1. Oxidation steps for HMF oxidation in alkaline aqueous solution on Pt or Au catalysts.[135]

1.3.1.2.2.1.2 Oxidation of Glycerol

Biodiesel is potentially used as an alternative fuel source which seems to be promising in comparison to conventional fossil fuels; with a lot of countries deciding to invest heavily into infrastructure to make it easier to make and use biofuels. Biofuels are currently not regarded as a viable alternative to fossil fuels. The production of waste chemicals demonstrates a lack of atom efficiency, which is a primary limitation of biofuels. Methods that recycle these waste chemicals for use in new applications must be developed immediately.

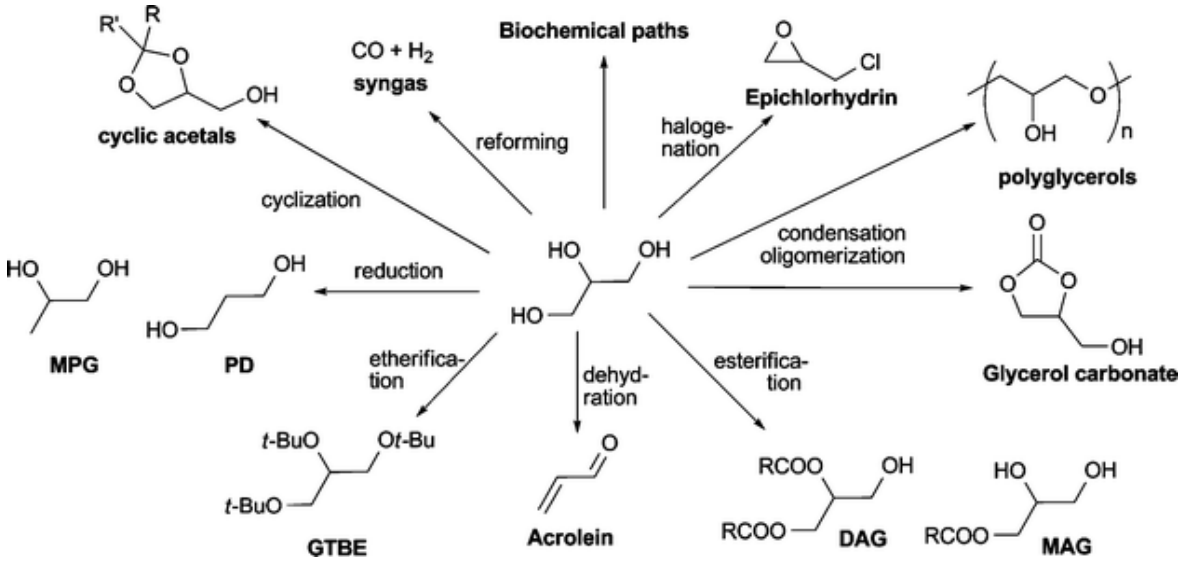

Scheme 1.2. Glycerol is considered to be a key platform chemical and can be used for the synthesis of many other compounds.[136]

Glycerol is an acyclic compound containing three hydroxyl groups in each carbon atom. Its primary industrial production comes as a biproduct of biodiesel production *via* the alcoholysis of triacylglycerol sourced predominantly from soybean or palm oils. Its three hydroxyl groups mean that it possesses excellent potential for development into other fine chemicals. The EU directive (2009/28/EC) features renewable energy targets for the countries in the EU and as a result, the industrial production of glycerol is projected to increase in the coming years. This projection has left a huge area of research for the exploitation of glycerol

as a platform chemical. Glyceric acid (GA), tartronic acid (TA), LA, dihydroxyacetone (DHA), mesoxalic acid (MA) and glycolic acid (GLA) are all fine chemicals which can be synthesised from glycerol. The selective oxidation using heterogeneous catalysts has proven to be an exceptional method in attaining these fine chemicals from glycerol.[136,137]

The first pioneering research on the catalytic oxidation of glycerol involved the use of Bi doped Pt catalysts for the production of DHA. The authors showed that the addition of Bi to a supported Pt catalyst increased the selectivity to DHA from 10% to 80%. A subsequent publication explained that the role of the Bi was to prevent over oxidation of the products. Additionally, it was proposed that the Bi ad-atoms selectively oriented the substrate on the surface to promote the oxidation of the additional hydroxyl group. Garcia *et al.*[138] confirmed this work but also revealed that high yields of GA could be achieved for the oxidation of glycerol over a 5% Pd/C catalyst. It was also determined that the experimental conditions can significantly alter the selectivity of the catalyst. Rossi and Prati and co-workers were the first to determine that supported Au catalysts in the presence of O_2 could selectively oxidise glycerol.[139] In the same publication they showed how the choice of support and the preparation method can profoundly affect the performance of the catalyst. Following on from this, Hutchings and co-workers[140] showed that Au/Graphite was an excellent catalyst for the selective oxidation of glycerol to GA. These works triggered a cascade of additional publications from both the Prati and Hutchings groups whose contributions to the use of Au in this field of research was summarised in a recent review.[137]

The preparation of bimetallic catalysts containing Au can affect both catalyst activity and selectivity. It has been reported that AuPd bimetallic catalysts can significantly enhance activity and C_3 selectivity when compared to their monometallic counterparts.[141–143] Work by Davis and co-workers[144] showed that the incorporation of Pd into Au has shown to increase the C_3 selectivity with GA being the predominant product. It is suggested that the role of Pd

is to catalyse the decomposition of H_2O_2 bi-product which is believed to be responsible for C-C cleavage and leads to the production of unfavourable C_1 and C_2 products. Furthermore, metal particle size can also have a huge impact on the performance of a catalyst for this reaction[145] which highlights the importance of the preparation method. Catalyst preparation and particle size effects have shown to be a crucial feature associated with catalytic performance in a range of other oxidation reactions; benzyl alcohol oxidation,[146] CO oxidation[147] and the epoxidation of olefins.[148]

The reaction conditions can also play a significant role in the selectivity of the catalyst. Gil *et al.*[149] reported in detail, the significant effect operation conditions can have on the selective oxidation of glycerol using Au nanoparticles supported on a range of different carbonaceous materials. It was observed that an increase in oxygen pressure slightly increased the rate of glycerol consumption but significantly enhanced the selectivity to GA for all catalysts tested. It was suggested that the increase in GA came predominantly at the expense of the sequential oxidation to TA. It was postulated that this increase in C_3 selectivity was a result of a decrease in the in-situ production of H_2O_2 which has been suggested to be responsible for some of the C-C cleavage observed in the oxidation of glycerol.[126,141,144] H_2O_2 is believed to be produced as a consequence of O_2 reduction prior to its dissociation,[150–152] with the water acting as a sacrificial oxidant toward the diatomic oxygen. It is not clear in the current literature how the H_2O_2 interacts with the substrate/products to instigate the C-C cleavage.

$O2^* + H2O^* \rightarrow OOH^* + HO^*$

$OOH^* + H2O^* \rightarrow H2O2^* + HO^*$

$HO^* + e^- \leftrightarrow HO^- + *$

Scheme 1.3. The equations highlight the role of H_2O in the activation of oxygen, with H_2O_2 being produced as a by-product. * depicts a site on the surface of the metal.

The temperature in which the reaction is conducted can also have a significant effect on the selectivity of the reaction. As with most catalytic processes increasing reaction temperature increases the rate of glycerol consumption which links back to the role of temperature in basic collision theory. A publication by Valverde and co-workers[149] reported that increasing temperature not only increased the rate of glycerol consumption, but also affected the selectivity of the reaction. With an increasing temperature, a higher selectivity of GA and oxalic acid (OA) was observed. Another study by Prati and co- workers[153] also showed that reactions occurring at 50 ºC showed greater selectivity toward GA than at 30 ºC using bimetallic Au, Pd and Pt catalysts. Valverde and co-workers[154] postulated that the reason for this was that glycolic GLA production is directly related to the presence of H_2O_2 and pointed out that previous studies investigating the production of H_2O_2 have shown that less H_2O_2 is made with increasing temperature. This is not the case as the reason the observed concentration H_2O_2 at high temperatures decreases is because it decomposes rapidly at elevated temperatures. This opinion is consistent throughout the literature as the direct synthesis of H_2O_2 from H_2 and O_2 must be carried out at temperatures close to 0 ºC to inhibit the subsequent decomposition. Other publications suggest that the formation of GLA is attributed to the oxidation of intermediate species such as DHA and glyceraldehyde (GLAD) proceeding *via* different mechanistic pathways.[141,155]

It has been well documented that the pH of the aqueous solution drastically affects the rate of glycerol oxidation and the selectivity of the products. Prati and Rossi were the first to postulate the role of NaOH in the oxidation of alcohols when Au supported catalysts were used for the oxidation of C_3 diols.[156] They suggested that the external hydroxyl group plays an integral role in the initial dehydrogenation of the alcohol group to form the carbonyl. In the absence of a sacrificial base, the cleavage of the C-H bond and subsequent H-abstraction of the hydrogen atom adjacent to the target alcohol group is difficult. This theory was later

supported by the Hutchings group.[157] Furthermore, increasing concentrations of base have shown to enhance C_3 selectivity through the base promoted decomposition of H_2O_2[141] which as discussed previously, is widely believed to be responsible for the C-C cleavage in the catalytic oxidation of glycerol. Since this work, significant contributions from Davis and co-workers[144,150,158] give a more defined and detailed description of the role of external hydroxyl groups in the oxidation of alcohols. Using density functional theory, Davis and co-workers[159] explained that surface-bound hydroxide intermediates significantly lower the energy barrier for C-H and O-H bond activation with Au nanoparticles. The formation of the initial alkoxy intermediate is also possible in solution alone, but the energy barrier for the subsequent C- H activation is significantly reduced when adsorbed hydroxyl intermediates are involved. Thus, both the OH ion and the heterogeneous catalyst have pivotal roles in the dehydrogenation of the alcohol species to form the aldehyde.

A significant amount of recent work has focussed on the oxidation of glycerol in a base free / neutral aqueous medium. For the industrialisation of such a process, the sacrificial consumption of NaOH is not favourable. Early work suggested that supported platinum catalysts displayed great promise with particle size proving an essential attribute for activity.[160] Further work and by Brett *et al.*[161] involved the preparation of supported AuPt alloys. These alloys were found to display high activities in a base free environment. In addition, this publication highlighted the importance of support selection, which appears to have a significant impact on a given catalysts activity under base-free conditions. An additional contribution from Tongsakul *et al.*[162] suggested that the incorporation of Au into Pt changes the electronic and geometric nature of the Pt, hereby promoting its catalytic activity. Further work from Villa *et al.*[163] suggested that under base free conditions basic supports promote activity but also enhance C-C cleavage with acidity promoting the selectivity to C3 products. It was stated that the performance of these acidic supported catalyst was not

dependent on the type of acidic site, but the quantity.

1.4 Aim of Sthe Thesis

The aim of this thesis is the continuing investigation into synthesizing and testing of gold-platinum nanoparticle catalysys on different lanthanum-based perovskite oxides for the valorisation of bio renewable feedstocks with following objectives.

- To synthesize the catalyst supports using hydrothermal and nano-casting (hard templating) routes.
- To characterize the catalyst supports by XRD, SEM, BET, TPR XPS, EDX, as synthesized.
- To synthesize the hard templates SBA-15 and ordered mesoporous carbon templates.
- To characterize the templates as synthesis by XRD, SEM, EDX and BET.
- To use the templates for catalysts synthesis and characterize them by the same techniques mentioned above.
- To use the perovskite oxide ($LaMO_3$ where M = Cr, Mn, Fe, Co, Ni) as catalyst support for gold-platinum nanoparticles by sol immobilization method.
- To determine the activity of these catalysts on HMF and glycerol oxidation reaction.
- To characterize the above-mentioned catalysts by XPS, TEM, XRD, EDX and DRIFTS.

References

1. Tryuk, M. Chapter 1. Setting the scene. *Ethics Interpret.* (2016) doi:10.3726/978-3-653-05204-6/12.

2. Evans, C. D. Glycerol Oxidation ; An investigation into the control of product distribution and mechanistic pathways using novel supports for the degree of Doctor of Philosophy. (2017).

3. Dowden, D. A. Chapter 2. Catalysis. *Annu. Reports Sect. 'C' (Physical Chem.* **76**, 3 (1979).

4. Hayward, J. Supported Metal Catalysts for the Production of. (2013).

5. Murzin, D. Y. & Salmi, T. Chapter 7 - Heterogeneous Catalytic Kinetics BT - Catalytic Kinetics (Second Edition). **3**, 345–446 (2016).

6. Kauffman, B. G. B., Fichte, J. G., Wilhelm, G., Hegel, F. & Joseph, F. W. Among Its Faculty the Illustrious Philosophers. 122–128 (1999).

7. Hammond, C. Intensification studies of heterogeneous catalysts: Probing and overcoming catalyst deactivation during liquid phase operation. *Green Chem.* **19**, 2711–2728 (2017).

8. Védrine, J. C. Heterogeneous catalysis on metal oxides. *Catalysts* **7**, (2017).

9. Sheldon, R. A. Green and sustainable manufacture of chemicals from biomass: State of the art. *Green Chem.* **16**, 950–963 (2014).

10. Lanzafame, P., Temi, D. M., Perathoner, S., Spadaro, A. N. & Centi, G. Direct conversion of cellulose to glucose and valuable intermediates in mild reaction conditions over solid acid catalysts. *Catal. Today* **179**, 178–184 (2012).

11. Zhang, X., Wilson, K. & Lee, A. F. Heterogeneously Catalyzed Hydrothermal Processing of C5-C6 Sugars. *Chem. Rev.* **116**, 12328–12368 (2016).

12. Atta, N. F., Galal, A. & El-Ads, E. H. Perovskite Nanomaterials – Synthesis, Characterization, and Applications. *Perovskite Mater. - Synth. Characterisation, Prop. Appl.* (2016) doi:10.5772/61280.

13. Peña, M. A. & Fierro, J. L. G. Chemical structures and performance of perovskite oxides. *Chem. Rev.* **101**, 1981–2017 (2001).

14. Schlögl, R. Heterogeneous catalysis. *Angew. Chemie - Int. Ed.* **54**, 3465–3520 (2015).

15. Arandiyan, H. R. & Parvari, M. Studies on mixed metal oxides solid solutions as heterogeneous catalysts. *Brazilian J. Chem. Eng.* **26**, 63–74 (2009).

16. Royer, S. *et al.* Perovskites as substitutes of noble metals for heterogeneous catalysis: Dream or reality. *Chem. Rev.* **114**, 10292–10368 (2014).

17. Pirone, R. Wet A ir Oxidation of A cetovanillone over LaFeO 3 as C atalyst: A Model R eaction for L ignin Valorization. *J. Adv. Catal. Sci. Technol.* **3**, 49–62 (2016).

18. Tepech-Carrillo, L. *et al.* Preparation of Nanosized LaCoO3 through Calcination of a Hydrothermally Synthesized Precursor. *J. Nanomater.* **2016**, (2016).

19. Goldwasser, M. R. *et al.* Combined methane reforming in presence of CO2 and O2 over LaFe1-xCoxO3 mixed-oxide perovskites as catalysts precursors. *Catal. Today* **107**–**108**, 106–113 (2005).

20. Keav, S., Matam, S. K., Ferri, D. & Weidenkaff, A. Structured perovskite-based catalysts and their application as Three-Way Catalytic converters-a review. *Catalysts* **4**, 226–255 (2014).

21. Pabst, A. Crystal structure of gadolinium formate, Gd(OOCH)3. *J. Chem. Phys.* **11**, 145–149 (1943).

22. Li, J. *et al.* Fine-Tuning Surface Properties of Perovskites via Nanocompositing with Inert Oxide toward Developing Superior Catalysts for Advanced Oxidation. *Adv. Funct. Mater.* **28**, 1–12 (2018).

23. Femina, P. & Sanjay, P. LaCoO3 perovskite catalysts for the environmental application of Auto motive CO oxidation. *Res. J. Recent Sci. Res.J.Recent Sci* **1**, 178–184 (2011).

24. Chu, Y. *et al.* Efficient removal of organic and bacterial pollutants by Ag-La0.8Ca0.2Fe0.94O3-Δ perovskite via catalytic peroxymonosulfate activation. *J. Hazard. Mater.* **356**, 53–60 (2018).

25. Palas, B., Ersöz, G. & Atalay, S. Catalytic wet air oxidation of Reactive Black 5 in the presence of LaNiO3 perovskite catalyst as a green process for azo dye removal. *Chemosphere* **209**, 823–830 (2018).

26. Liu, D. J. & Krumpelt, M. Activity and structure of perovskites as diesel-reforming catalysts for solid oxide fuel cell. *Int. J. Appl. Ceram. Technol.* **2**, 301–307 (2005).

27. Lai, K. Y. & Manthiram, A. Self-Regenerating Co-Fe Nanoparticles on Perovskite Oxides as a Hydrocarbon Fuel Oxidation Catalyst in Solid Oxide Fuel Cells. *Chem. Mater.* **30**, 2515–2525 (2018).

28. Hansen, K. K., Skou, E. M., Christensen, H. & Turek, T. Perovskites as catalysts for the selective catalytic reduction of nitric oxide with propene: Relationship between solid state properties and catalytic activity. *J. Catal.* **199**, 132–140 (2001).

29. Stege, W. P., Cadús, L. E. & Barbero, B. P. La1-xCaxMnO3 perovskites as catalysts

for total oxidation of volatile organic compounds. *Catal. Today* **172**, 53–57 (2011).

30. Silva, G. R. O. *et al.* Synthesis and Characterization of LaNixCo1-xO3 Perovskites via Complex Precursor Methods. *Mater. Sci. Appl.* **01**, 39–45 (2010).

31. Evans, C. D. *et al.* The preparation of large surface area lanthanum based perovskite supports for AuPt nanoparticles: Tuning the glycerol oxidation reaction pathway by switching the perovskite B site. *Faraday Discuss.* **188**, 427–450 (2016).

32. Jin, C., Cao, X., Zhang, L., Zhang, C. & Yang, R. Preparation and electrochemical properties of urchin-like La 0.8Sr0.2MnO3 perovskite oxide as a bifunctional catalyst for oxygen reduction and oxygen evolution reaction. *J. Power Sources* **241**, 225–230 (2013).

33. Odahara, J., Miura, A., Rosero-navarro, N. C. & Tadanaga, K. Explosive Reaction for Barium Niobium Perovskite Oxynitride. 8–11 (2018) doi:10.1021/acs.inorgchem.7b02660.

34. Walton, R. I. Perovskite Oxides Prepared by Hydrothermal and Solvothermal Synthesis : A Review of Crystallisation , Chemistry , and Compositions. 9041–9069 (2020) doi:10.1002/chem.202000707.

35. Özbay, N. & Şahin, R. Z. Y. Preparation and characterization of LaMnO3 and LaNiO3 perovskite type oxides by the hydrothermal synthesis method. *AIP Conf. Proc.* **1809**, (2017).

36. Si, W., Wang, Y., Peng, Y. & Li, J. Selective Dissolution of A-Site Cations in ABO3 Perovskites: A New Path to High-Performance Catalysts. *Angew. Chemie - Int. Ed.* **54**, 7954–7957 (2015).

37. Zheng, J. *et al.* The synthesis and catalytic performances of three-dimensionally

ordered macroporous perovskite-type LaMn 1-xFe xO 3 complex oxide catalysts with different pore diameters for diesel soot combustion. *Catal. Today* **191**, 146–153 (2012).

38. Afzal, S., Quan, X. & Zhang, J. High surface area mesoporous nanocast LaMO3 (M = Mn, Fe) perovskites for efficient catalytic ozonation and an insight into probable catalytic mechanism. *Appl. Catal. B Environ.* **206**, 692–703 (2017).

39. Nair, M. M., Kaliaguine, S. & Kleitz, F. Nanocast LaNiO3 perovskites as precursors for the preparation of coke-resistant dry reforming catalysts. *ACS Catal.* **4**, 3837–3846 (2014).

40. Huang, X., Zhao, G., Wang, G. & Irvine, J. T. S. Synthesis and applications of nanoporous perovskite metal oxides. *Chem. Sci.* **9**, 3623–3637 (2018).

41. Yue, B., Hu, Q., Ji, L., Wang, Y. & Liu, J. Facile synthesis of perovskite CeMnO3 nanofibers as an anode material for high performance lithium-ion batteries. *RSC Adv.* **9**, 38271–38279 (2019).

42. Wiley, J. & Central, E. Ceramic Methods. 17–22 (2023).

43. Babu, T. G. N. & Koshy, J. Development and Dielectric Properties of Ba 2 ! x Sr x DyTaO 6 (x 1 , 0 ، , and 2) Substrates for YBa 2 Cu 3 O 7 ! Films. **528**, 522–528 (1997).

44. Review, A. Conventional and Microwave Hydrothermal Synthesis and Application of Functional Materials : A Review. (2019) doi:10.3390/ma12071177.

45. Suvaci, E. & Özel, E. Hydrothermal Synthesis. **1**, 59–68 (2021).

46. Yazdanbakhsh, M. *et al.* Microwave Synthesis of Perovskite Based High Surface Area srTio Nanoparticles : Application for Adsorption of Congo Red Dye in Water. *Ceram.*

Int. **44**, 5735–5742 (2018).

47. Ding, Y., Yu, S. H., Liu, C. & Zang, Z. A. 3D architectures of iron molybdate: Phase selective synthesis, growth mechanism, and magnetic properties. *Chem. - A Eur. J.* **13**, 746–753 (2007).

48. Bernard, C. & Durand, B. Hydrothermal synthesis of LaMnO 3 + δ : F . T . I . R . and W . A . X . S . investigations of the evolution from amorphous to crystallized powder. **9**, 2821–2826 (2004).

49. Bokov, D. *et al.* Nanomaterial by Sol-Gel Method: Synthesis and Application. *Adv. Mater. Sci. Eng.* **2021**, (2021).

50. Lian, J. *et al.* Ni Supported on LaFeO3 Perovskites for Methane Steam Reforming: On the Promotional Effects of Plasma Treatment in H2–Ar Atmosphere. *Top. Catal.* **60**, 831–842 (2017).

51. Zhang, S., Zhao, Y., Díaz-Somoano, M., Yang, J. & Zhang, J. Synergistic Mercury Removal over the CeMnO3 Perovskite Structure Oxide as a Selective Catalytic Reduction Catalyst from Coal Combustion Flue Gas. *Energy and Fuels* **32**, 11785–11795 (2018).

52. Deng, H., Lin, L. & Liu, S. Catalysis of Cu-doped Co-based perovskite-type oxide in wet oxidation of lignin to produce aromatic aldehydes. *Energy and Fuels* **24**, 4797–4802 (2010).

53. Deng, X., Chen, K. & Tüysüz, H. Protocol for the Nanocasting Method: Preparation of Ordered Mesoporous Metal Oxides. *Chem. Mater.* **29**, 40–52 (2017).

54. Brezesinski, T. & Elm, M. T. Ordered mesoporous metal oxides for electrochemical applications: correlation between structure, electrical properties and device

performance. **23**, (2021).

55. Reitz, C., Suchomski, C., Weidmann, C. & Brezesinski, T. Block Copolymer-Templated BiFeO 3 Nanoarchitectures Composed of Phase-Pure Crystallites Intermingled with a Continuous Mesoporosity : Effective Visible-Light Photocatalysts ? **4**, 414–424 (2011).

56. Zhu, J. *et al.* Perovskite oxides: Preparation, characterizations, and applications in heterogeneous catalysis. *ACS Catal.* **4**, 2917–2940 (2014).

57. Nair, M. M., Yen, H. & Kleitz, F. Nanocast mesoporous mixed metal oxides for catalytic applications. *Comptes Rendus Chim.* **17**, 641–655 (2014).

58. Evans, C. D. *et al.* The preparation of large surface area lanthanum based perovskite supports for AuPt nanoparticles: Tuning the glycerol oxidation reaction pathway by switching the perovskite B site. *Faraday Discuss.* **188**, 427–450 (2016).

59. Zhu, J., Yang, X., Xu, X. & Wei, K. Effect of strontium substitution on the activity of La2-x Sr x NiO4 (x = 0.0-1.2) in NO decomposition. *Sci. China, Ser. B Chem.* **50**, 41–46 (2007).

60. Belessi, V. C., Trikalitis, P. N., Ladavos, A. K., Bakas, T. V. & Pomonis, P. J. Structure and catalytic activity of La1 - XFeO3 system (x=0.00, 0.05, 0.10, 0.15, 0.20, 0.25, 0.35) for the NO+CO reaction. *Appl. Catal. A Gen.* **177**, 53–68 (1999).

61. Giannakas, A. E., Ladavos, A. K. & Pomonis, P. J. Preparation, characterization and investigation of catalytic activity for NO + CO reaction of LaMnO3 and LaFeO3 perovskites prepared via microemulsion method. *Appl. Catal. B Environ.* **49**, 147–158 (2004).

62. Voorhoeve, R. J. H. *Perovskite-Related Oxides as Oxidation—Reduction Catalysts*.

Advanced Materials in Catalysis (ACADEMIC PRESS, INC., 1977). doi:10.1016/b978-0-12-147450-8.50010-1.

63. Futai, M., Yonghua, C. & Louhui. Characterization of perovskite-type oxide catalysts RECoO3 by TPR. *React. Kinet. Catal. Lett.* **31**, 47–54 (1986).

64. Tejuca, N. L. G. & Catalisis, I. De. Chemisorption and Catalysis on LaMO , Oxides. 939–949 (1985).

65. Gomes, R. F. A., Mitrev, Y. N., Simeonov, S. P. & Afonso, C. A. M. Going Beyond the Limits of the Biorenewable Platform: Sodium Dithionite-Promoted Stabilization of 5-Hydroxymethylfurfural. *ChemSusChem* **11**, 1612–1616 (2018).

66. Xu, F. & Li, Y. Biomass Digestion. *Encycl. Sustain. Technol.* **3**, 197–204 (2017).

67. Ge, X. *et al. Conversion of Lignocellulosic Biomass Into Platform Chemicals for Biobased Polyurethane Application*. *Advances in Bioenergy* vol. 3 (Elsevier Inc., 2018).

68. Conference, I. S. *et al.* Catalytic Wet Air Oxidation of Lignin. 2–6 (2016).

69. Ortiz-Martínez, V. M. *et al.* Approach to biodiesel production from microalgae under supercritical conditions by the PRISMA method. *Fuel Process. Technol.* **191**, 211–222 (2019).

70. Tang, X. *et al.* In Situ Catalytic Hydrogenation of Biomass-Derived Methyl Levulinate to γ-Valerolactone in Methanol. *ChemSusChem* **8**, 1601–1607 (2015).

71. Tang, X. *et al.* Green Processing of Lignocellulosic Biomass and Its Derivatives in Deep Eutectic Solvents. 2696–2706 (2017) doi:10.1002/cssc.201700457.

72. Golecha, R. Biomass Supply Strategy for Building a Sustainable Cellulosic Biofuel

Business.

73. MINI-REVIEW H. Ohara. 2003 (2003) doi:10.1007/s00253-003-1383-7.

74. On the usage of agricultural raw materials – energy or food ? An assessment from an economics perspective. 1497–1504 (2007) doi:10.1002/biot.200700153.

75. Conversion, D., Syn, O. F. & To, G. A. S. ca. 200. 185–186 (1983).

76. Durand, A. Bioreactor designs for solid state fermentation. **13**, 113–125 (2003).

77. Kumar, P., Barrett, D. M., Delwiche, M. J. & Stroeve, P. Methods for Pretreatment of Lignocellulosic Biomass for Efficient Hydrolysis and Biofuel Production. 3713–3729 (2009).

78. Ragauskas, A. J. *et al.* Lignin valorization: Improving lignin processing in the biorefinery. *Science (80-.).* **344**, (2014).

79. Sajid, M., Zhao, X. & Liu, D. Production of 2,5-furandicarboxylic acid (FDCA) from 5-hydroxymethylfurfural (HMF): Recent progress focusing on the chemical-catalytic routes. *Green Chem.* **20**, 5427–5453 (2018).

80. Zhou, Z., Ouyang, D., Liu, D. & Zhao, X. Bioresource Technology Oxidative pretreatment of lignocellulosic biomass for enzymatic hydrolysis : Progress and challenges. *Bioresour. Technol.* **367**, 128208 (2023).

81. Rass-hansen, J., Falsig, H., Jørgensen, B. & Christensen, C. H. Bioethanol : fuel or feedstock ? **333**, 329–333 (2007).

82. Du, P. Fermentative production of butanol — the academic perspective ¨ rre. (1862) doi:10.1016/j.copbio.2011.04.010.

83. Green, E. M. Fermentative production of butanol — the industrial perspective. (2008)

doi:10.1016/j.copbio.2011.02.004.

84. Inokuma, K., Liao, J. C., Okamoto, M. & Hanai, T. Improvement of isopropanol production by metabolically engineered Escherichia coli using gas stripping. *JBIOSC* **110**, 696–701 (2010).

85. Posada, J. A. *et al.* Biore source Tec hnology Potential of bioethanol as a chemical building block for biorefineries : Preliminary sustainability assessment of 12 bioethanol-based products. *Bioresour. Technol.* **135**, 490–499 (2013).

86. Leeuwen, B. N. M. Van. Fermentative production of isobutene. 1377–1387 (2012) doi:10.1007/s00253-011-3853-7.

87. Celi, E. & Grajek, W. Biotechnological production of 2 , 3-butanediol — Current state and prospects. **27**, 715–725 (2009).

88. Of, P., Acid, L., For, A. & Applications, I. PRODUCTION OF LACTIC ACID AND POLYLACTIC. 293–316 (2022).

89. Citric, P. O. F., Acids, M. & Filamentous, I. N. AND MALIC ACIDS IN FILAMENTOUS FUNGAL. 375–398 (2022).

90. Of, P., Acid, S. & Resources, R. PRODUCTION OF SUCCINIC ACID FROM. 317–330 (2022).

91. Lange, J., Heide, E. Van Der, Buijtenen, J. Van & Price, R. Furfural — A Promising Platform for Lignocellulosic Biofuels. 150–166 (2012) doi:10.1002/cssc.201100648.

92. Dong, F. *et al.* One-step Conversion of Furfural into 2-Methyltetrahydrofuran under Mild Conditions. *ChemSusChem* **8**, 1534–1537 (2015).

93. Tong, X., Ma, Y. & Li, Y. Applied Catalysis A : General Biomass into chemicals :

Conversion of sugars to furan derivatives by catalytic processes. *"Applied Catal. A, Gen.* **385**, 1–13 (2010).

94. Putten, R. Van *et al.* Hydroxymethylfurfural , A Versatile Platform Chemical Made from Renewable Resources. (2013).

95. Wang, K. F., Liu, C. L., Sui, K. Y., Guo, C. & Liu, C. Z. Efficient Catalytic Oxidation of 5-Hydroxymethylfurfural to 2,5-Furandicarboxylic Acid by Magnetic Laccase Catalyst. *ChemBioChem* **19**, 654–659 (2018).

96. Zhang, Z., Zhen, J., Liu, B., Lv, K. & Deng, K. Selective aerobic oxidation of the biomass-derived precursor 5-hydroxymethylfurfural to 2,5-furandicarboxylic acid under mild conditions over a magnetic palladium nanocatalyst. *Green Chem.* **17**, 1308–1317 (2015).

97. Danielli Da Fonseca Ferreira, A., Dorneles De Mello, M. & Da Silva, M. A. P. Catalytic Oxidation of 5-Hydroxymethylfurfural to 2,5-Furandicarboxylic acid over Ru/Al2O3 in a Trickle-Bed Reactor. *Ind. Eng. Chem. Res.* **58**, 128–137 (2019).

98. Han, X. *et al.* N-doped carbon supported Pt catalyst for base-free oxidation of 5-hydroxymethylfurfural to 2,5-furandicarboxylic acid. *Appl. Catal. A Gen.* **526**, 1–8 (2016).

99. Li, Q. *et al.* Ruthenium supported on CoFe layered double oxide for selective hydrogenation of 5-hydroxymethylfurfural. *Mol. Catal.* **431**, 32–38 (2017).

100. Tirsoaga, A., El Fergani, M., Parvulescu, V. I. & Coman, S. M. Upgrade of 5-Hydroxymethylfurfural to Dicarboxylic Acids onto Multifunctional-Based Fe3O4@SiO2 Magnetic Catalysts. *ACS Sustain. Chem. Eng.* **6**, 14292–14301 (2018).

101. Zhang, Z. & Deng, K. Recent Advances in the Catalytic Synthesis of 2,5-

Furandicarboxylic Acid and Its Derivatives. *ACS Catal.* **5**, 6529–6544 (2015).

102. Verdeguer, P. & Gaset, N. M. A. Oxydation catalytique du HMF en acide 2 , 5-furane dicarboxylique. **85**, 327–344 (1993).

103. Ait Rass, H., Essayem, N. & Besson, M. Selective aerobic oxidation of 5-HMF into 2,5-furandicarboxylic acid with pt catalysts supported on TiO2- and ZrO2-based supports. *ChemSusChem* **8**, 1206–1217 (2015).

104. Davis, S. E., Houk, L. R., Tamargo, E. C., Datye, A. K. & Davis, R. J. Oxidation of 5-hydroxymethylfurfural over supported Pt, Pd and Au catalysts. *Catal. Today* **160**, 55–60 (2011).

105. Vuyyuru, K. R. & Strasser, P. Oxidation of biomass derived 5-hydroxymethylfurfural using heterogeneous and electrochemical catalysis. *Catal. Today* **195**, 144–154 (2012).

106. Niu, W. *et al.* Pt nanoparticles loaded on reduced graphene oxide as an effective catalyst for the direct oxidation of 5-hydroxymethylfurfural (HMF) to produce 2,5-furandicarboxylic acid (FDCA) under mild conditions. *Bull. Chem. Soc. Jpn.* **87**, 1124–1129 (2014).

107. Vinke, P., van der Poel, W. & van Bekkum, H. On the oxygen tolerance of noble metal catalysts in liquid phase alcohol oxidations the influence of the support on catalyst deactivation. *Stud. Surf. Sci. Catal.* **59**, 385–394 (1991).

108. Sahu, R. & Dhepe, P. L. Synthesis of 2,5-furandicarboxylic acid by the aerobic oxidation of 5-hydroxymethyl furfural over supported metal catalysts. *React. Kinet. Mech. Catal.* **112**, 173–187 (2014).

109. Miao, Z. *et al.* Aerobic oxidation of 5-hydroxymethylfurfural (HMF) effectively catalyzed by a Ce0.8Bi0.2O2-δ supported Pt catalyst at room temperature. *RSC Adv.* **5**,

19823–19829 (2015).

110. Motagamwala, A. H. *et al.* Toward biomass-derived renewable plastics: Production of 2,5-furandicarboxylic acid from fructose. *Sci. Adv.* **4**, 1–9 (2018).

111. Siankevich, S. *et al.* A novel platinum nanocatalyst for the oxidation of 5-Hydroxymethylfurfural into 2,5-Furandicarboxylic acid under mild conditions. *J. Catal.* **315**, 67–74 (2014).

112. Yan, N., Yuan, Y. & Dyson, P. J. Nanometallic chemistry: Deciphering nanoparticle catalysis from the perspective of organometallic chemistry and homogeneous catalysis. *Dalt. Trans.* **42**, 13294–13304 (2013).

113. Siankevich, S. *et al.* Influence of the Anion on the Oxidation of 5-Hydroxymethylfurfural by Using Ionic-Polymer-Supported Platinum Nanoparticle Catalysts. *Chempluschem* **83**, 19–23 (2018).

114. Hutchings, G. J. Vapor phase hydrochlorination of acetylene: Correlation of catalytic activity of supported metal chloride catalysts. *J. Catal.* **96**, 292–295 (1985).

115. Pan, M. *et al.* hydrogenation reactions with gold. 5002–5013 (2013) doi:10.1039/c3cs35523c.

116. Wittstock, A., Wichmann, A. & Ba, M. Nanoporous Gold as a Platform for a Building Block Catalyst. (2012).

117. Casanova, O., Iborra, S. & Corma, A. Biomass into Chemicals : Aerobic Oxidation of 5-Hydroxy- methyl-2-furfural into 2 , 5-Furandicarboxylic Acid with Gold Nanoparticle Catalysts. 1138–1144 (2009) doi:10.1002/cssc.200900137.

118. Lolli, A. *et al.* Selective oxidation of HMF via catalytic and photocatalytic processes using metal-supported catalysts. *Molecules* **23**, (2018).

119. Miao, Z. *et al.* Catalysis Science & Technology. 1314–1322 (2015) doi:10.1039/c4cy01060d.

120. Cai, J., Ma, H., Zhang, J., Song, Q. & Du, Z. Gold Nanoclusters Confined in a Supercage of Y Zeolite for Aerobic Oxidation of HMF under Mild Conditions **. 14215–14223 (2013) doi:10.1002/chem.201301735.

121. Gorbanev, Y. Y., Klitgaard, S. K., Woodley, J. M., Christensen, C. H. & Riisager, A. Gold-Catalyzed Aerobic Oxidation of 5-Hydroxymethyl- furfural in Water at Ambient Temperature. 672–675 (2009) doi:10.1002/cssc.200900059.

122. Kim, M., Su, Y., Fukuoka, A., Hensen, E. J. M. & Nakajima, K. Zuschriften Heterogeneous Catalysis Aerobic Oxidation of 5- (Hydroxymethyl) furfural Cyclic Acetal Enables Selective Furan-2 , 5-dicarboxylic Acid Formation with CeO 2 - Supported Gold Catalyst Zuschriften. **0012**, 8367–8371 (2018).

123. Wu, Y. *et al.* Sophisticated Construction of Au Islands on Pt − Ni: An Ideal Trimetallic Nanoframe Catalyst. (2014).

124. Rasul, S. *et al.* Angewandte A Highly Selective Copper – Indium Bimetallic Electrocatalyst for the Electrochemical Reduction of Aqueous CO 2 to CO **. 2146–2150 (2015) doi:10.1002/anie.201410233.

125. Pasini, T. *et al.* Green Chemistry. 2091–2099 (2011) doi:10.1039/c1gc15355b.

126. Villa, A., Schiavoni, M., Campisi, S., Veith, G. M. & Prati, L. Pd-modified Au on Carbon as an Effective and Durable Catalyst for the Direct Oxidation of HMF to 2 , 5-Furandicarboxylic Acid. **2**, 609–612 (2013).

127. Albonetti, S. *et al.* Selective oxidation of 5-hydroxymethyl-2-furfural over TiO 2 - supported gold – copper catalysts prepared from preformed nanoparticles : Effect of

Au / Cu ratio. **195**, 120–126 (2012).

128. Links, D. A. Green Chemistry. 824–827 (2011) doi:10.1039/c0gc00911c.

129. Zope, B. N., Davis, S. E. & Davis, R. J. Influence of reaction conditions on diacid formation during Au-catalyzed oxidation of glycerol and hydroxymethylfurfural. *Top. Catal.* **55**, 24–32 (2012).

130. Wan, X. *et al.* Base-free aerobic oxidation of 5-hydroxymethyl-furfural to 2,5-furandicarboxylic acid in water catalyzed by functionalized carbon nanotube-supported au-pd alloy nanoparticles. *ACS Catal.* **4**, 2175–2185 (2014).

131. Pasini, T. *et al.* Selective oxidation of 5-hydroxymethyl-2-furfural using supported gold–copper nanoparticles. *Green Chem.* **13**, 2091–2099 (2011).

132. Rass, H. A. & Essayem, N. Green Chemistry. 2240–2251 (2013) doi:10.1039/c3gc40727f.

133. Gupta, N. K., Nishimura, S., Takagaki, A. & Ebitani, K. Hydrotalcite-supported gold-nanoparticle-catalyzed highly efficient base-free aqueous oxidation of 5-hydroxymethylfurfural into 2,5-furandicarboxylic acid under atmospheric oxygen pressure. *Green Chem.* **13**, 824–827 (2011).

134. Gorbanev, Y. Y., Kegnæs, S. & Riisager, A. Selective aerobic oxidation of 5-hydroxymethylfurfural in water over solid ruthenium hydroxide catalysts with magnesium-based supports. *Catal. Letters* **141**, 1752–1760 (2011).

135. Davis, S. E., Zope, B. N. & Davis, R. J. On the mechanism of selective oxidation of 5-hydroxymethylfurfural to 2,5-furandicarboxylic acid over supported Pt and Au catalysts. *Green Chem.* **14**, 143–147 (2012).

136. Katryniok, B. *et al.* Selective catalytic oxidation of glycerol: Perspectives for high

value chemicals. *Green Chem.* **13**, 1960–1979 (2011).

137. Villa, A. *et al.* Glycerol oxidation using gold-containing catalysts. *Acc. Chem. Res.* **48**, 1403–1412 (2015).

138. Garcia, R., Besson, M. & Gallezot, P. Chemoselective catalytic oxidation of glycerol with air on platinum metals. *Appl. Catal. A, Gen.* **127**, 165–176 (1995).

139. Prati, L. & Rossi, M. Chemoselective catalytic oxidation of polyols with dioxygen on gold supported catalysts. *Stud. Surf. Sci. Catal.* **110**, 509–515 (1997).

140. Carrettin, S., McMorn, P., Johnston, P., Griffin, K. & Hutchings, G. J. Selective oxidation of glycerol to glyceric acid using a gold catalyst in aqueous sodium hydroxide. *Chem. Commun.* **7**, 696–697 (2002).

141. Dimitratos, N., Villa, A. & Prati, L. Liquid Phase Oxidation of Glycerol Using a Single Phase (Au – Pd) Alloy Supported on Activated Carbon : Effect of Reaction Conditions. 334–340 (2009) doi:10.1007/s10562-009-0192-8.

142. Prati, L., Villa, A., Campione, C. & Spontoni, P. Effect of gold addition on Pt and Pd catalysts in liquid phase oxidations. **44**, (2007).

143. Dimitratos, N. *et al.* Oxidation of glycerol using gold-palladium alloy-supported nanocrystals. *Phys. Chem. Chem. Phys.* **11**, 4952–4961 (2009).

144. Ketchie, W. C., Murayama, M. & Davis, R. J. Selective oxidation of glycerol over carbon-supported AuPd catalysts. *J. Catal.* **250**, 264–273 (2007).

145. Dimitratos, N. *et al.* Effect of particle size on monometallic and bimetallic (Au,Pd)/C on the liquid phase oxidation of glycerol. *Catal. Letters* **108**, 147–153 (2006).

146. Prati, L. *et al.* Gold catalyzed liquid phase oxidation of alcohol: The issue of

selectivity. *Faraday Discuss.* **152**, 353–365 (2011).

147. Boccuzzi, F. *et al.* Au/TiO2 nanosized samples: A catalytic, TEM, and FTIR study of the effect of calcination temperature on the CO oxidation. *J. Catal.* **202**, 256–267 (2001).

148. Hayashi, T., Tanaka, K. & Haruta, M. Selective vapor-phase epoxidation of propylene over Au/TiO2 catalysts in the presence of oxygen and hydrogen. *J. Catal.* **178**, 566–575 (1998).

149. Gil, S. *et al.* Effect of the operation conditions on the selective oxidation of glycerol with catalysts based on Au supported on carbonaceous materials. *Chem. Eng. J.* **178**, 423–435 (2011).

150. Ketchie, W. C., Murayama, M. & Davis, R. J. Promotional effect of hydroxyl on the aqueous phase oxidation of carbon monoxide and glycerol over supported Au catalysts. *Top. Catal.* **44**, 307–317 (2007).

151. Zope, B. N., Hibbitts, D. D., Neurock, M. & Davis, R. J. Reactivity of the Gold / Water Interface During Selective Oxidation Catalysis Linked references are available on JSTOR for this article : Reactivity of the Gold / Water Interface. *J. Colloid Interface Sci.* **330**, 74–78 (2019).

152. Shang, C. & Liu, Z. P. Origin and activity of gold nanoparticles as aerobic oxidation catalysts in aqueous solution. *J. Am. Chem. Soc.* **133**, 9938–9947 (2011).

153. Bianchi, C. L., Canton, P., Dimitratos, N., Porta, F. & Prati, L. Selective oxidation of glycerol with oxygen using mono and bimetallic catalysts based on Au , Pd and Pt metals. **103**, 203–212 (2005).

154. Gil, S. *et al.* Effect of the operation conditions on the selective oxidation of glycerol

with catalysts based on Au supported on carbonaceous materials. *Chem. Eng. J.* **178**, 423–435 (2011).

155. Porta, F. & Prati, L. Selective oxidation of glycerol to sodium glycerate with gold-on-carbon catalyst: An insight into reaction selectivity. *J. Catal.* **224**, 397–403 (2004).

156. Prati, L. & Rossi, M. Gold on carbon as a new catalyst for selective liquid phase oxidation of diols. *J. Catal.* **176**, 552–560 (1998).

157. Carrettin, S. *et al.* Oxidation of glycerol using supported Pt , Pd and Au catalysts. 1329–1336 (2003) doi:10.1039/b212047j.

158. Ide, M. S. & Davis, R. J. The important role of hydroxyl on oxidation catalysis by gold nanoparticles. *Acc. Chem. Res.* **47**, 825–833 (2014).

159. Zope, B. N., Hibbitts, D. D., Neurock, M. & Davis, R. J. Reactivity of the gold/water interface during selective oxidation catalysis. *Science (80-.).* **330**, 74–78 (2010).

160. Liang, D. *et al.* Glycerol oxidation with oxygen over bimetallic Pt-Bi catalysts under atmospheric pressure. *Chinese J. Catal.* **32**, 1831–1837 (2011).

161. Brett, G. L. *et al.* Selective oxidation of glycerol by highly active bimetallic catalysts at ambient temperature under base-free conditions. *Angew. Chemie - Int. Ed.* **50**, 10136–10139 (2011).

162. Tongsakul, D., Nishimura, S. & Ebitani, K. Platinum / Gold Alloy Nanoparticles-Supported Hydrotalcite Catalyst for Selective Aerobic Oxidation of Polyols in Base-Free Aqueous Solution at Room Temperature. (2013).

163. Rogers, S. M. *et al.* Tailoring Gold Nanoparticle Characteristics and the Impact on Aqueous-Phase Oxidation of Glycerol. *ACS Catal.* **5**, 4377–4384 (2015).

Chapter 2

Experimental

2.1 Material

2.1.1. Reagents

The material used throughout this project were listed below and used as received from the manufacturer.

$La(NO_3)_3 \cdot 6H_2O$	Alfa Aesar, 99%
$Mn(NO_3)_2 \cdot 4H_2O$	Honeywell, 97%
$Cr(NO_3)_2 \cdot 4H_2O$	Honeywell, 98%
$Co(NO_3)_2,9H_2O$	Sigma Aldrich, 99%
$Fe(NO_3)_2.9H_2O$	Sigma Aldrich, 98%
$Ni(NO_3)_2.4H_2O$	Sigma Aldrich, 98%
Citric Acid	Sigma Aldrich, 99%
SBA-15	Sigma Aldrich, 99%
MCM-41	Sigma Aldrich, 99%
NaOH	Sigma Aldrich, 99%
Tetraethyl orthosilicate	Sigma Aldrich, 98%
Pluronic P123	EO*20*-PO*70*EO*20*, Sigma-Aldrich
HCl	Sigma Aldrich, 37%
Ammonia	Sigma Aldrich, 35%
Sulphuric Acid	Sigma Aldrich, 95%
2,5-hydroxymethyl furfural	Sigma Aldrich, 99%
Polyvinyl alcohol	Sigma Aldrich, 99 % hydrolyzed
Sodium borohydride	Sigma Aldrich, 98 %
Glycerol	Sigma Aldrich, 98%
Ethanol	Sigma Aldrich, 98%
Propanol	Sigma Aldrich, 98%
De-ionized water	
5-hydroxylmethyl-2-furancarboxylic acid	Sigma Aldrich, 97%
5-formyl-2-furoic acid	Sigma Aldrich 95%
2,5-furandicarboxylic acid	Sigma Aldrich 97%
2,5-diformylfuran	Sigma Aldrich, 97%
Tartronic acid	Sigma Aldrich, >97%
Lactic acid	Sigma Aldrich, 85%
Glycolic acid	Sigma Aldrich, 99%
Glyceric acid	Sigma Adrich, 98%
Pyruvic acid	Sigma Aldrich, 98%
Glyceraldehyde	Sigma Aldrich, 90%
Oxalic acid	Sigma Adrich, 98%
Succinic acid	Sigma Aldrich, 99%
Meleic acid	Sigma Aldrich, 99%
Formic acid	Sigma Aldrich, 95%

2.2 Methods

2.2.1. Synthesis of Nano-casting Templates.

2.2.1.1 Santa-Barbara Amorphous-15 (SBA-15)

SBA-15 template was prepared at low HCl concentration (0.3 M) in aqueous solution using tetraethyl orthosilicate (TEOS) as the silicon source and Pluronic P123 as a structure-directing agent. These conditions allow an easy and highly reproducible preparation of high-quality SBA-15 material with high yields. In the synthesis, 13.9 g of Pluronic P123 was dissolved in 252 g of distilled water containing 7.7 g of HCl. After complete dissolution, 25 g of TEOS was added at once. The mixture was left under stirring at 35 ℃ for 24 h, and was transferred to a Teflon-lined stainless-steel autoclave for hydrothermal treatment in an oven at 100 °C for 24 h under static conditions. The solid product was filtered without washing and dried for 24 h at 110 °C. The dried solid product was finally calcined at 550 ℃ for 2 h in a flowing air furnace.

Prior to synthesis, the following precautions need to be considered to ensure excellent pore connectivity of the SBA-15.

- P123 has a glass transition temperature of 39 °C and is thick, soft substance under room temperature, which makes it difficult to precisely measure it. Prior to use P123 was kept in an oven at a temperature higher than it melting point (70-80 °C precisely) to appropriately weigh the right amount.
- A temperature between 30-40 °C is crucial for achieving high quality SBA-15 and thus the operating temperature should be maintained throughout the process.

2.2.1.2 Synthesis of Ordered Mesoporous Carbon Template.

Ordered mesoporous carbon was synthesized using P123 as carbon source and teraethyl orthosilicate as structure directing agent. A solution containing 4 g of P123 (similar treatment

mentioned in the synthesis of SBA-15 required) and 100 mL of 2 M HCl in a beaker was stirred vigorously. 9.1 mL of tetraethyl orthosilicate (TEOS) was slowly added to a solution and kept at 40 ℃ for 24 h. therefore, the mixture stands another 48 h at 100 ℃, and the resultant solid product was filtered and dried in an oven at 110 ℃ overnight. After that, the solid product was mixed with deioned water and 0.1 g of sulphuric acid and stirred for 30 min. The suspension was ultrasonicated for 5 min and pre-carbonized at 160 ^{o}C for 1 h and subsequently carbonized at 500 ℃ (1 ℃/min ramping rate) for 5 h under nitrogen atmosphere to obtain a carbon-silica composite. The silica was removed from the composite using 2 M NaOH at 100 ℃ for 24 h and the resultant carbon material was filtered, washed several times with deionized water and dried in an oven at 110 ℃ overnight.

2.2.2 Synthesis of Perovskite Oxide ($LaBO_3$)

The perovskite oxide supports ($LaMO_3$, where M = Cr, Mn, Fe, Co and Ni) were used as catalyst support for nanoparticles and synthesised by three different methods, nano-casting (using SBA-15 and carbon mesoporous templates) and the hydrothermal method. The choice of these methods heavily depends on the inherent advantages of methods, as discussed in the introduction chapter. The hydrothermal method was chosen as a potentially scalable alternative to the nano-casting method.

2.2.2.1 Synthesis by Nano-casting Method Using SBA-15

Perovskite oxides were prepared by nano-casting using SBA-15. Calculated amount of $La(NO_3)_3 \cdot 6H_2O$ and $M(NO_3)_2 \cdot 4H_2O$, respectively were dissolved in 10 ml of de-ionized water and added to a 10 ml citric acid (0.006 mol) solution making a total metal to citric acid ratio of 2:1. The mixture was added dropwise to a suspension of 1 g SBA-15 in 10 ml de-ionized water and stirred for 2 h at room temperature. The solvent evaporated at 80 ℃ for 24 h. The resultant solid material was ground to a fine powder, calcined at 500 ℃ for 2 h under

2 °C/min air. The impregnation of the precursor was repeated with a metal-citric acid ratio (1:1), followed by calcination at 700 ℃ for 2 h under 2 ℃/min air. The resultant calcined material was washed with 2 M NaOH solution to leach out the SBA-15 template and then washed with de-ionized water at room temperature. The obtained products were denoted NC(SBA-15)-$LaMO_3$.

2.2.2.2 Synthesis by Citrate Complexing Method.

Citrate complexing was adopted to prepare 2 g of $LaMnO_3$ perovskite oxide. Calculated amount of nitrates of lanthanum and manganese were dissolved in round bottom flask (100 ml capacity) containing 50 ml of de-ionized water under stirring. To the mixture, a calculated amount of citric acid was introduced when the temperature reaches 60 ℃. The system temperature was kept at 70 ℃ for 24 h, and the result solid material was collected in a evaporating dish, dried in an oven at 110 ℃ overnight. The dried solid precursor was then grounded into powder using mortar and pestle and the dried powder was calcined in a static air furnace at 700 ℃ for 2 h with a heating rate at 2 ℃/min.

2.2.2.3 Synthesis by Hydrothermal Method

Perovskite oxides were synthesized via a hydrothermal route by dissolving $La(NO_3)_3{\cdot}6H_2O$ (AlfaAeser), $M(NO_3)_2{\cdot}XH_2O$ and citric acid (Aldrich) with a stoichiometric molar ratio of 1:1:2 in 50 mL of H_2O in a 100 mL round bottom flask. The mixtures were heated to 60 °C followed by addition of ammonia solution (35%, Aldrich) in dropwise while stirring until maximum precipitation was achieved and allow it to standard for 2 h. The resultant precipitates were transferred in a Teflon-lined autoclave followed by hydrothermal treatment at 140 °C for 20 h in oven. After reaction, the resulting products were washed three times with H_2O, separated using a centrifuge (4000 rpm), and dried at 110 °C overnight. Afterward, the LaM precursors were calcined for 2 h in a static air furnace at 700 °C (heating rate 2 °C

min^{-1}) under air. The hydrothermally prepared catalyst supports were denoted as $LaMO_3$-H.

2.2.3 Catalyst Synthesis.

The method for deposition of precious metals on to the surface of the prepared perovskite materials was the sol-immobilisation preparation. Sol immobilisation provides a high dispersion of metals with a narrow particle size distribution on the surface of a catalyst and this method was chosen to ensure the differences observed were due to the role of the perovskite supports rather than the metal nanoparticles.

2.2.3.1 Sol Immobilization Preparation.

Sol immobilisation is a technique that provides a small particle size distribution of highly dispersed nanoparticles across the surface of a support material. The method involves creating a stable colloidal form of a precious metal, reducing the precious metal from its precursor form to a metallic state before depositing the resulting particles upon the surface of a support by manipulating the isoelectric point of the support until a metal surface interaction is induced resulting in good wetting of the support surface. The general procedure for sol immobilisation is detailed as follows for a 1 g catalyst.

An aqueous solution (400 mL) of $HAuCl_4$ (5 mg, 0.41 mL, 12.25 mg/ml) and H_2PtCl_6 (4.98 mg, 0.62 mL, 7.5 mg/ml) were prepared. Polyvinyl alcohol (PVA, 1 wt% aqueous solution, MW = 10 kDa) was freshly prepared and used as the stabilising agent. $NaBH_4$ (3.8 mL, 10% aqueous solution) was also freshly prepared and used as the reducing agent. To an aqueous mixture of the $HAuCl_4$ and H_2PtCl_6 in a concentration to produce 1:1 metal weight ratio, a total of 1 wt % of total metals in the prepared catalyst, the PVA solution was added (0.1 M, 1.3:1 PVA:metals ration) with vigorous stirring for 2 min. $NaBH_4$ was subsequently added such that the $NaBH_4$:total metal ratio (mol/mol) was 6.5. The resulting solution was stirred for 30 min to allow the stabilisation of the reducing colloidal particles, followed by the

addition of the perovskite material. The solution was left stirring for a further 1 h, followed by washing with distilled water and drying at 110 ˚C for 16 h.

2.2.3.2 Catalyst Modification with N-butylamine

Catalyst modification technique is a way of developing a multifunctional catalysts system by immobilizing organic base on to surface active metals. The technique involves forming the active complex on the surface of the support, annealing the surface complex under nitrogen atmosphere to a stable complex on the surface of the support. The general procedure for n-butylamine immobilisation is detailed as follows for a 1 g catalyst.

A toluene solution of n-butylamine (1 ml) was prepared in 100 ml round bottom flask with 1 g of the catalysts (1 wt% AuPt/$LaMO_3$). The mixture was refluxed for 24 h at 50 ℃. The resultant solid was filtered and washed with water, followed by drying under vacuum for 16 h. The resultant material was annealed for 2 h in air flow furnace at 200 ℃ (heating rate 10 ℃ min^{-1}) under nitrogen.

2.2.4 Catalyst Testing

The catalysts were tested in two different reactions, hydroxymethyl furfural (HMF) oxidation and glycerol oxidation. A general procedure for both reactions is detailed below.

2.2.4.1 Oxidation of Hydroxymethyl Furfural (HMF).

The HMF oxidation experiments were carried out using a Colaver reactor of 50 mL capacity, equipped with a magnetic stirrer and measurement probes for recording temperature and pressure. The reactor was charged with an aqueous solution containing 0.005 mol of HMF and 0.002 mol NaOH and varied catalyst amount (20 mg – 100 mg). The reactor was purged three times with O_2 (2 bar) and then pressurised to the desired working pressure (3 bar). The temperature was set (80 °C to 140 ℃) and the reaction mixture was stirred at 700 rpm for the

indicated reaction time (2-24 h). The initial time of the reaction (i.e., time zero) was considered when the set point temperature was reached (after ~10 min). At the end of the reaction, the reactor was cooled down to room temperature and the reaction content was centrifuged and filtered. An Agilent Infinity 1260 liquid chromatograph (HPLC-DAD) equipped with an Aminex HPX 87-H (300 mm long 7.8 mm i.d.) column using a 0.005 M H_2SO_4 solution as the mobile phase was used for this analysis. An external calibration method was employed for the identification and quantification of reactants and products using commercial samples as a reference.

Base free reactions were carried out in order to access how the base affect the substrate and the products. For these reasons, a similar procedure above was followed with the exception of NaOH base and temperature set between to 80 ℃ and 140 ℃.

2.2.4.2. Oxidation of Glycerol

Glycerol oxidation experiment was carried out using a 50 ml colaver reactor charged with an aqueous solution of glycerol (10 ml, 0.3 M in H_2O) with a NaOH base (10 mL, 1.2 M in H_2O) making it to a ratio of 4:1with substrate. A desired amount of catalyst (stated in the corresponding table caption). The reactor heater was brought up reaction temperature using a silicone oil bath feedback loop to control temperature. The round bottom flask was then sealed, pressurised to the required oxygen pressure, and purged 3 times prior to use. The oxygen inlet valve was opened to ensure oxygen pressure remains constant throughout the reaction. The reactor was then heated to temperature and the stirrer speed set to the desired speed (400 – 1000 rpm). Reaction duration varied, with periodic samples taken and analysed by high performance liquid chromatography (HPLC). HPLC analysis was fitted with UV and refractive index detectors. Reactants and products were separated using a Metacarb 67 H column. The eluent was an aqueous solution of phosphoric acid (0.01 M) at a flow rate of

0.25 ml min $^{-1}$. Each sample (0.5 ml) was diluted with eluent (4.5 ml) and products were identified by comparison with purchased samples. Quantification was achieved through an external calibration method, which allows an easy comparison between the HPLC sample response to that of target compounds.

2.2.5. Characterization Techniques

This section describes the techniques applied for the characterisation of all the supports and catalysts formed. The gases used in the different techniques were of a high-grade purity.

2.2.5.1. X-ray Diffraction (XRD)

X-ray diffraction is well known technique and was developed by Dye and Scherrer in year between 1914-1919.[1] XRD is a technique capable of determining the lattice spacing of atoms in a crystalline compound. The technique operates by measuring the elastic scattering of monochromatic X-ray light by atoms in a crystalline structure. The radiation will be scattered in all directions, and in most directions the radiation will be cancelled out by destructive interference leading to no signal. However, in certain directions the interference will instead be constructive, generating a measurable signal and as such obeys the Bragg's law (equation 2.1 and figure 2.1).

$$2d \sin \theta = n\lambda \qquad 2.1$$

where d is the spacing between the atom layer, θ is the diffraction angle, n is an integer (order of reflection), and λ is the wavelength of the incident radiation. This equation allows the lattice spacing (d) to be determined by measuring the angle of the constructive interference for X-rays exiting the crystal. The lattice spacing corresponds to specific compounds where it is possible to identify the compound's purity by their unique diffraction patterns through

comparison with a database of well-defined materials. The purity of the product is found through a semi-quantitative method by analysing the diffraction pattern of the known material and that of any residual impurities. Long range order is essential for diffraction to occur, and therefore only occurs in crystalline solids. Incomplete destructive interference of the scattering X-rays results in peak broadening relating directly to the crystallite size of the corresponding reflecting planes. This relationship is defined by the Debye-Scherrer equation (Equation 2.2).

$$D = \frac{K\lambda}{\beta \cos\theta} \qquad 2.2$$

Where D is the crystallite size in the direction perpendicular to the reflecting plane, K is a dimensional shape factor taken as 0.9, λ is the X-ray wavelength, β is the line broadening at the full width half maximum and θ is the angle between the beam and normal reflecting plane. The minimum measurement for this method is 5 nm as below this the peaks are too broad to be observed.

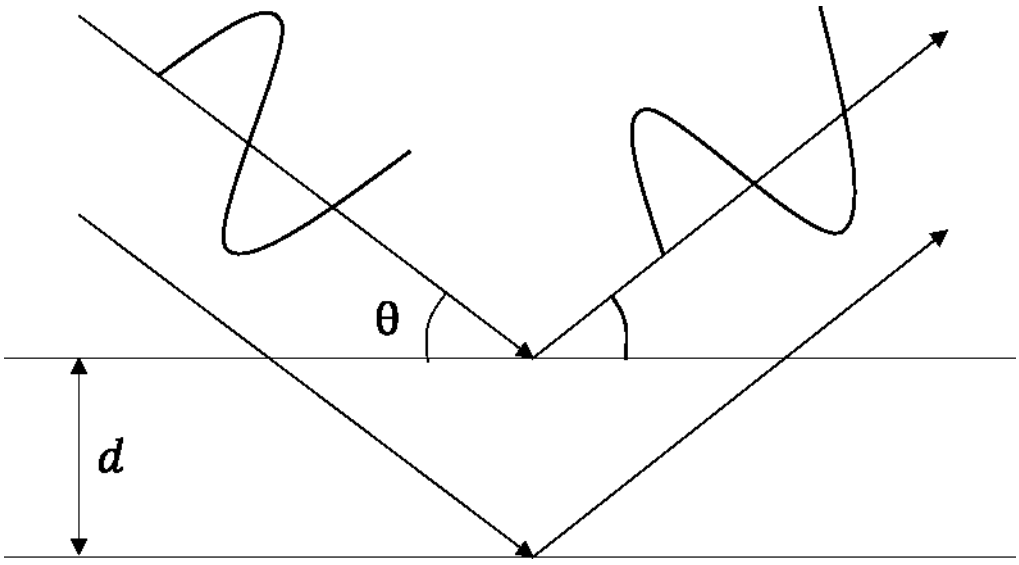

Figure 2.1. Graphic representation of the Bragg relationship showing the incident X-ray penetrating the lattice structure of the material and the resulting wave exiting the material.[2]

Powder XRD was used throughout this project to identify the compounds present in the catalysts and was carried out using a PANalytical X'pert Pro powder diffractometer with a Cu Kα source operated at 40 kV and 40 mA to obtain the data. Phase identification was performed using the X'Pert High Score data base of spectral patterns.

2.2.5.2. Brunauer, Emmett and Teller (BET) method surface area measurements

One of the crucial parameters for any given catalyst in relation to catalyst performance for many systems is the surface area, and as such the need to determine the catalyst surface area is necessary. N_2 physisorption can be used to measure surface area of a material and the general principle is based on the extended Langmuir model for monolayer molecular adsorption, which is a physical adsorption of a gas (N_2) because of relatively weak van der Waals forces of attraction between the surface of a material and the adsorbate gas. The area of gas adsorbed on a monomolecular layer of the surface of the material is then calculated which corresponds to the specific surface area.[3]

The BET analysis is carried out using multipoint measurement system and the BET adsorption isotherm equation (equation 2.3) on the result obtained. By plotting P/V (P_o – P) versus P/P_o in the BET equation should yield linear format, the gradient (C – 1)/CV_m will provide a volume of surface adsorbed gas. This value when taken under consideration along with the surface area of the adsorbate molecule, can be used to determine the surface area of the material using equation 2.4.

$$\frac{1}{\upsilon\left[\left(\frac{P_o}{P}\right)-1\right]} = \frac{C-1}{\upsilon_m C}\left(\frac{P}{P_o}\right) + \frac{1}{\upsilon_m C} \qquad 2.3$$

Where P and P_o are the equilibration and saturation pressure, υ is the volume of adsorbed gas, and υ_m is the volume of gas required to form a monolayer. C is the BET constant.

$$A_s = \left(\frac{\upsilon_m}{22414}\right) N_A \sigma \qquad 2.4$$

Where A_s is the total surface area, N_A is the Avogadro number and σ is the cross-sectional area of one nitrogen molecule.

All BET analysis measurements were performed using a Quadrasorb surface area analyser. A 5-point analysis of each material was performed with nitrogen (N_2) as the adsorbate gas. Samples were degassed at the maximum temperature (250 °C) for 2 hours prior the analysis. Surface areas calculated are recorded to the nearest 1 m^2/g due to inherent limitations of the equipment.

2.2.5.4. X-ray photoelectron spectroscopy (XPS)

X-ray photoelectron spectroscopy (XPS) is a surface-sensitive quantitative spectroscopic technique based on the photoelectric effect that can identify the elements that exist within a material or are covering its surface, as well as their chemical state, and the overall electronic structure and density of the electronic states in the material. In XPS analysis, an atom absorbs a photon of energy ($h\upsilon$) resulting in the ejection of a core or valence electron, with a specific binding energy (E_b) to be ejected at a specific kinetic energy (E_k) (equation 2.5 and figure 2.2). The binding energy of a core electron is affected by chemical bonding and changes in oxidation state of the atom which results in a chemical shift in the detected photoelectron kinetic energy. In other words, if the positive charge on the atom is increased through electron withdrawing species bound to the surface or increased oxidation state, the binding energy of the core electron is also increased.[4]

$$E_k = h\upsilon - E_b \qquad 2.5$$

$h\upsilon$ is the energy of the incoming photon, E_b the initial binding energy. Once a photoelectron has been emitted, the ionized atom must relax in some way. Relaxation of the excited ionic state to fill the core hole can lead to two final states due to spin-orbit coupling shown in equation 2.6.

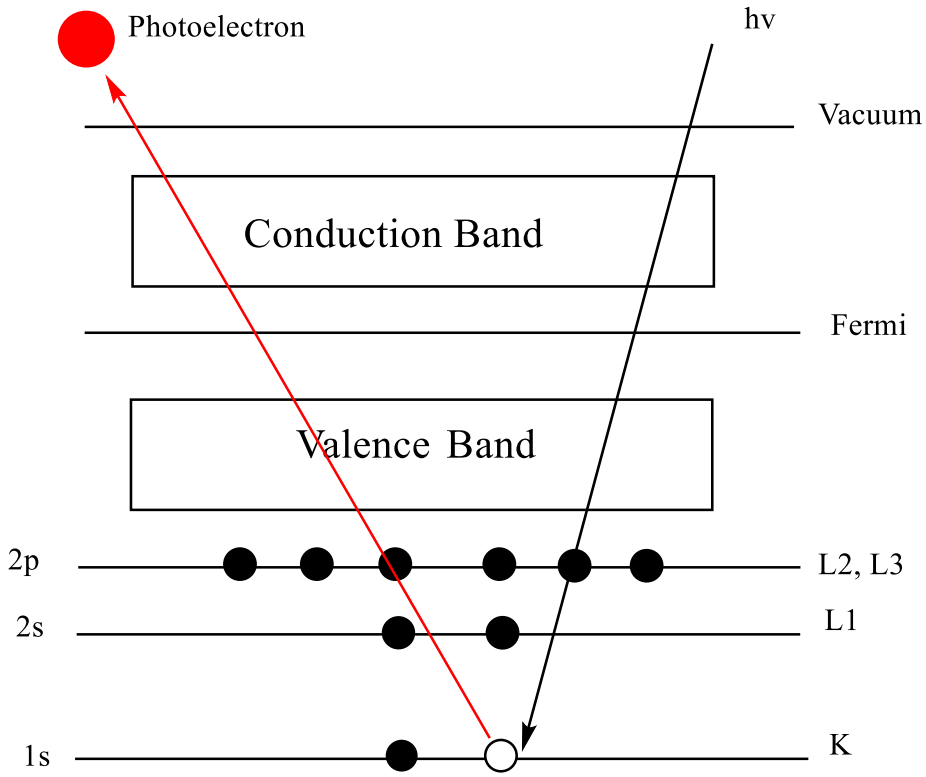

Figure 2.2. XPS process, showing photoionization of an atom by the ejection of a 1s electron.

$$j = s + l \qquad 2.6$$

For one unpaired electron, s = ±½ and the orbital angular momentum l = 0, 1, 2, 3... corresponding to s, p, d, f... orbitals. Hence for a state where l > 0 and there is one unpaired electron, a doublet peak will be observed. For example, analysis of the Zr 3d state will result in doublet peaks corresponding to $3d_{5/2}$ and $3d_{3/2}$ states.

In this project XPS measurements were performed using a Kratos Axis DLD photoelectron

spectrometer equipped with a charge neutralizer and a Mg Kα X-ray source ($h\upsilon$ = 1253.6 eV) and monochromated Al Kα ($h\upsilon$ = 1486.6 eV). Using the Mg source, high resolution spectra were recorded with an analyser pass energy of 20 eV and 67 and 80 eV for survey scans while for the monochromated Al source an analyser pass energy of 40 eV for high resolution scans and 160 eV for survey scans were employed. An X-ray power of 225 W was used.

2.2.5.4. Thermal Gravimetric Analysis (TGA)

Thermogravimetric analysis (TGA) is a quantitative technique that measures the weight loss of a sample as a function of temperature and time under different atmospheres (N_2, He/Ar or O_2) depending on the information required. In this technique the weight of the sample needs to be measured with precision for the technique to be effective.

Ideally the sample is heated to temperatures where some components of the sample will decompose into, or react to form, a different material, causing a weight change. If the original composition of the material is known, TGA can be precise enough that the species lost or gained during heating can be determined by the percentage weight change that they induce.

All samples in this project were analysed on a Seteram TGA/DTA to acquire the decomposition mass losses of catalyst precursors as outlined in the catalyst support preparation section and to obtain suitable calcination temperatures to form pure phase support materials. Sample masses were approximately 20 mg and were heated up to 800 ℃ at a ramp rate of 30 ℃ min^{-1} under 20 ml min^{-1} of flowing oxygen.

2.2.5.5. Scanning Electron Microscopy / Energy-Dispersive Xray spectroscopy

In scanning electron microscopy, a beam of electrons is discharged from an electron gun that is located at the top of the microscope. The electron beam gets focused when it passes through a series of condenser lenses and electromagnetic coils and directed on to the surface of the sample. The interaction of Primary Electrons (PE) with the surface of specimen

generates three main signals: Secondary Electrons (SE) through inelastic scattering, high energy Backscattered Electrons (BSE) and X-ray radiation. The difference between these signals originates from the difference in volume of the specimen that the primary electrons interacted with according to the energy of the primary electrons (typically between 200 eV and 30 keV). For instance, SE come from a small layer on the surface and yields the best resolution, which can be realized with a scanning electron microscope and can give information relating to the topography of samples, whereas the BSE come from deeper regions of the investigated material thus giving a lower resolution. A schematic of different the different types of electron and X-ray beams that are generated in a SEM is depicted in figure 2.3. In addition to imaging by SEM, information about the chemical composition of the material can be acquired by detection of characteristic X-ray radiations from the sample.[5]

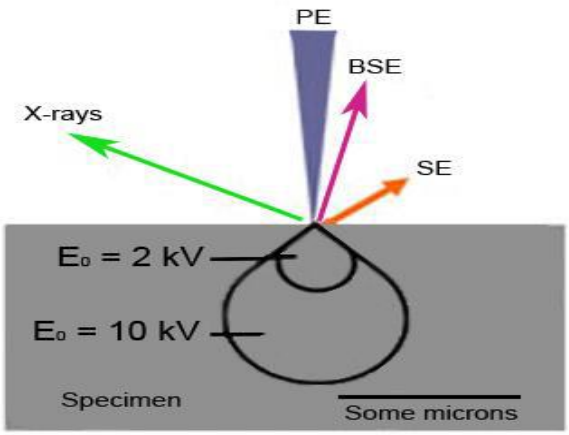

Figure 2.3. primary, secondary, and backscattered electron as well as X-ray beam generated in SEM.[6]

The analysis for both applications was performed using a Zeiss Evo-40 series Scanning Electron Microscope. The Samples were mounted on aluminium stubs using adhesive carbon tape and coated with a thin layer of gold. The gold coating provides an electrical contact over the whole specimen during analysis.

2.2.5.6. Transmission electron microscopy

Transition electron microscopy (TEM) is an extremely powerful tool for characterising material morphology. Using a high energy electron beam, an interaction between electrons and atoms within a material can be observed in order to acquire information about the crystal structure, as well as the resolution being sufficient to view nanoparticles deposited on the surface of a material. TEM operates under the same basic principle as a light microscope, utilising an electron beam instead of light (Figure 2.6). This difference is because electrons have wavelengths which are orders of magnitude lower than that of light, consequently the resolution of images observed by TEM are orders of magnitude greater than that of light microscopes. It is possible to ascertain the particle size distribution and the morphology of nanoparticles across a catalyst surface, providing information on how a catalyst works.[7]

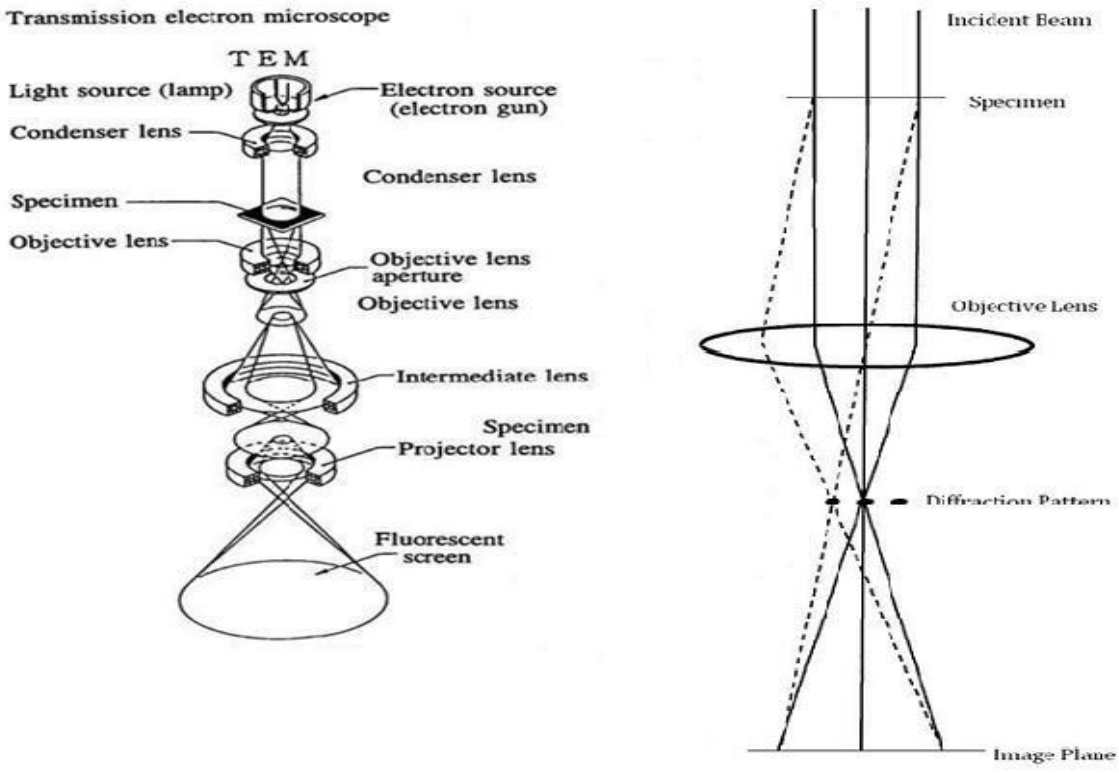

Figure 2.6. General layout of a TEM describing the path of electron beam in a TEM and ray diagram for the diffraction mechanism in TEM.[7]

The TEM analysis was carried out using a Jeol 2100 equipped with a LAB6 filament operating at 200 kV. Each sample was prepared by dispersing the powder catalyst in ethanol and dropping the suspension onto a lacey carbon film over a 300-mesh copper grid. TEM analysis was carried out by an instrument technician.

2.2.5.7. Diffuse Reflection Infrared Fourier Transform Spectroscopy (DRIFTS)

Diffuse reflectance infra-red Fourier transform spectroscopy (DRIFTS) is a surface sensitive infra-red spectroscopic technique. In DRIFTS, the infrared beam is focussed onto the sample where it can interact with the material in several different ways. The beam can be scattered or reflected from neighbouring particles in the sample, or transmitted through particles, after which the beam can be scattered or reflected once more. The absorption of infra-red radiation excites the vibrational modes of bonding moieties in molecular species. IR radiation that is not absorbed by the sample reaches a detector, and the functionalities in the sample can be identified.[8]

Titration of the surface of catalyst with probe molecules is a powerful technique for quantitative analysis of surface acidity (and basicity) of solid catalysts. NH_3, pyridine, CH_3CN, NO or CO are the most common probe molecules for characterizing the nature of acid sites using DRIFTS. In this project, pyridine and CO were the probe molecules used for acid active site of catalyst supports and coordination of nanoparticles on catalyst supports, respectively.

DRIFTS measurements were carried out on the Bruker Tensor 27 equipped with Mercury Cadmium Telluride (MCT) detector and Harrick praying mantis cell. The samples were diluted with potassium bromide (KBr) before the measurement. The samples were exposed with diluted carbon monoxide (2% in nitrogen) at flowrate of 3 mL/min for 30 min and the IR spectra were recorded under repeated sample scan measurement mode. After the

measurement, excess CO was removed by flowing the nitrogen (30 mL/min) for 1 h to record the final spectra. However, for pyridine-DRIFTS, the sample was dehydrated in a nitrogen stream (50 mL/min) at 400 °C for 1 h. For pyridine IR measurements, the dehydrated sample was cooled to 150 °C and exposed to pyridine vapor. Excess pyridine was removed at 50 °C in a N_2 stream (50 mL/min) for 1 h, and the IR spectra were recorded at 150 °C.

2.2.5.8. Temperature programmed desorption (TPD)

Temperature programmed desorption (TPD) was used to determine the acidic and basic sites on the surface of the catalysts. The procedure requires the saturation of a sample (adsorbent) with an adsorbate chemical, followed by gradual heating of the sample to observe the temperature at which desorption occurs. This allows the strength of the chemisorption to be defined, thus defining the strength of the acid/basic sites.

Theoretical models of TPD are used to interpret the TPD spectra with the goal of determining thermodynamic and kinetic parameters, which assumes that the desorption phenomenon follows a rate equation below.[9] However, in practice, the TPD analysis is conducted in a computer with temperature increased linearly with time, equation 2.8.

$$\frac{r_d}{N_s} = -\frac{d\theta_A}{dt} exp^{\left(\frac{-\varepsilon_A}{kT}\right)}\theta_A^n \qquad 2.7$$

$$T=T+\beta_H t \qquad 2.8$$

Where is the heating rate or ramp rate, T is the temperature and t is the time. r_d is the rate of desorption of species A (measured by mass spectrometry), N_S is the concentration of surface adsorption sites, θ_A is the coverage of species A on adsorption sites (fraction of sites occupied by A molecules), t is the time (the independent variable of the rate process), k_0 is a pre-exponential factor for the rate constant (depends on atomic masses and bond strengths in

species A), T is the temperature in Kelvin (K), n is the "order of the desorption reaction (the power of the rate law), ε_A (per molecule), k or k_B is the Boltzmann constant (per molecule), 1.38066 10^{-23} J K^{-1}.

Acidic sites can be identified with a basic probe molecule, in this study NH_3, whereas basic sites can be identified with the acidic species being adsorbed, in most cases CO_2. The strength of the acidic/basic sites can be quantified, as the higher the temperature at which the adsorbent is desorbed, the stronger the chemisorption with the peak areas correlating to the quantity of the adsorbate.

The acid active site can be quantified from the information on the calibration plot of area TCD signal against the amount of NH_3 in mole (which can be calculated from the ideal equation PV = nRT), and by dividing the coverage area with a response factor (slope) of the plot will provide the amount of NH_3 on the acid active and the acidity can then be found for equation 2.9.

$$Acidity\ \left(\frac{\mu mol}{g}\right) = \frac{amount\ of\ ammonia\ (\mu mol)}{catalyst\ mass\ (g)} \qquad 2.9$$

Ammonia and carbon dioxide were probe molecules used in this project to determine the active of the perovskite materials using the Automated chemisorption analyser (ChemBET Pulsar TPR/TPD) with thermal conductivity detector (TCD). The gas feed was 10% NH_3 in nitrogen, which was fed in at 150 ml min^{-1} and the temperature was increased up to 900 ℃ at a ramp rate of 10 ℃ min^{-1} after pre-treatment at 150 ℃ in He for 1.5 h. In each experiment, 50 mg of catalyst was used, which was placed in a quartz tube between two pieces of quartz wool.

2.2.5.9. Temperature programmed reduction (TPR)

Temperature programmed reduction (TPR) is a technique for determining the reducibility of a material as a function of temperature. Typically, powdered samples are placed in the elbow of the quartz analyser tube and fitted into the furnace. In TPR, diluted H_2 **(**10% H_2 in Ar) is passed over the sample and a stable baseline reading established at a low enough temperature that no reduction of the sample occurs. The temperature is then increased and at the critical temperature the H_2 reacts with the sample to form H_2O. This methodology allows different reduction processes (e.g. surface and bulk reduction of a metal oxide) to be distinguished and quantified.

TPR can provide important information regarding to the redox properties of a catalyst support.[10] Quantification of the H_2 consumption in a TPR trace can enable the calculation of the stoichiometry of the starting oxide as well as indirect information regarding the metal dispersion of a supported metal catalyst.[11]

TRP analysis was carried out on Automated chemisorption analyser (ChemBET Pulsar TPR/TPD) with thermal conductivity detector (TCD). Before the analysis, 0.1 g of the samples were pre-treated at 150 ^oC under helium flowrate of 145 mL/min for 1 hour. The pre-treated sample was exposed to 10% H_2/Ar (30 mL/min) at a temperature between 30-900 ^oC for 2.5 h.

2.2.6. Response Surface Methodology

Response surface methodology (RSM) is a statistical method for solving multivariable problems by using a reasonable experimental design method after obtaining certain data through experiments.[12] The method was introduced by George E. P. Box and K. B. Wilson in 1951. The main idea of RSM is to use a sequence of designed experiments to obtain an optimal response. RSM can be employed to maximize the production of a special substance by optimization of operational factors. Of late, for formulation optimization, the RSM, using

proper design of experiments (DoE), has become extensively used. In contrast to conventional methods, the interaction among process variables can be determined by statistical techniques.

The Box-Behnken design (BBD) method for RSM, developed by George E. P. Box and Donald Behnken in 1960, is a quadratic response surface, has been applied to approximate a response function for experimental data that cannot be described by linear functions.[13] Hence, the optimal conditions were confirmed by the BBD using RSM which showed the highest FDCA selectivity. The BBD requires three levels of each experimental factor, which are coded as −1, 0, and +1. Thus, the product selectivities were predicted using different combinations of three independent variables, as summarized in Table 2.1.

Table 2.1 Experimental design of the independent variables.

Independent variable	Factors	Range and Levels		
		+1	0	-1
Time (h)	A	24	10	3
Catalyst (mg)	B	50	30	20
Temperature (℃)	C	110	95	80

For this project, three factors were considered, namely the time (A), the catalyst amount (B), and the temperature (C). The tested conditions included reaction times of 3–24 h, catalyst amounts of 20–50 mg, and temperature of 80–110 ℃. A total of 17 experimental runs were

included outlined in Table 2.2. Data analysis was performed using Design-Expert 13 (Stat-Ease., Inc., MN, United States)

Table 2.2 Experimental designs for 17 runs

Runs	**Factors**		
	A	B	C
1	0	1	-1
2	-1	1	0
3	1	0	-1
4	-1	0	-1
5	0	-1	-1
6	1	1	0
7	0	0	0
8	0	-1	1
9	-1	-1	0
10	0	0	0
11	0	0	0
12	-1	0	1
13	1	-1	0
14	0	0	0
15	1	0	1
16	0	0	0
17	0	1	1

2.3. Reference

1. Baerlocher, C. & Mccusker, L. B. *Practical Aspects of Powder Diffraction Data Analysis*. *Advanced Zeolite Science and Applications* vol. 85 (Elsevier Masson SAS, 1994).
2. Pevelen, D. D. Le & Limited, C. Small Molecule X-Ray Crystallography , Theory and Workflow. (2010).
3. Palchoudhury, S., Baalousha, M. & Lead, J. R. *Methods for Measuring Concentration (Mass, Surface Area and Number) of Nanomaterials*. *Frontiers of Nanoscience* vol. 8 (Elsevier, 2015).
4. Li, Y. *et al.* Enhancement of Pitting Corrosion Resistance of Austenitic Stainless Steel Through Deposition of Amorphous / Nanocrystalline Oxy-nitrided Phases by Active Screen Plasma Treatment. **21**, (2018).
5. Mutzafi, M., Kaminer, I., Harari, G. & Segev, M. Non-diffracting multi-?electron vortex beams balancing their electron-electron interactions. *Nat. Commun.* **8**, 1–11 (2017).
6. Ede, J. M. Deep learning in electron microscopy. *Mach. Learn. Sci. Technol.* **2**, 153–156 (2021).
7. STOYANOV PA. *Transmission Electron Microscopes*. *Bull Acad Sci USSR Phys Ser (Columbia Tech Transl)* vol. 32 (1968).
8. Capuano, E. & van Ruth, S. M. *Infrared Spectroscopy: Applications*. *Encyclopedia of Food and Health* (Elsevier Ltd., 2015). doi:10.1016/B978-0-12-384947-2.00644-9.
9. bcsj.49.1780.pdf.
10. Fu, Q., Weber, A. & Flytzani-Stephanopoulos, M. Nanostructured Au-CeO2 catalysts for low-temperature water-gas shift. *Catal. Letters* **77**, 87–95 (2001).
11. Niemantsverdriet, J. W. Also of Interest : Spectroscopy in Catalysis Principles and

Practice of Heterogeneous Catalysis Organic Chemistry Principles and Industrial Practice. *Adsorpt. J. Int. Adsorpt. Soc.* (2003).

12. Sarabia, L. A. & Ortiz, M. C. Response Surface Methodology. Comprehensive Chemometrics. 345–390 (2009).

13. Tarjomannejad, A., Zonouz, P. R., Masoumi, M. E., Niaei, A. & Farzi, A. LaFeO3 Perovskites Obtained from Different Methods for NO + CO Reaction, Modeling and Optimization of Synthesis Process by Response Surface Methodology. *J. Inorg. Organomet. Polym. Mater.* **28**, 2012–2022 (2018).

Chapter 3

Catalyst Preparation and Characterizations

3.1 Introduction

Precious metals such as Au, Pt and Pd have been intensively studied by many research groups, however, identifying the best support materials for these platinum group metals (PGM) for oxidation reactions remains challenging.[1] CeO_2, TiO_2 and carbon have been widely studied as support materials for PGM catalysts.[2,3] Evans *et al*. have recently developed lanthanum-based perovskite oxides with different B-site cations comprising a first row transition metal (Cr, Mn, Fe, Co and Ni) as a support for Au Pt nanoparticles.[4] These catalyst supports were reported to have an influence on the product selectively for the oxidation of glycerol towards either lactic acid or glyceric acid with $LaCrO_3$ favoured dehydration route to lactic acid and $LaMnO_3$ completely hindered dehydration route and favoured oxidation route mainly to glyceric acid and tartronic acid.[4] However, the major challenge of using perovskites as a catalyst support is their high crystallinity and low surface area which need to be addressed to make them a good support material.[5,6] The problem of low surface area associated with the perovskite oxide can be addressed with advance synthetic methods such as nano-casting method using hard templating using materials such as Santa Barbara Amorphous-15 (SBA-15) and ordered mesoperous carbon (OMC), or hydrothermal synthesis methods that have been reported to yield high surface area materials.[7] Example of surface area with respect to perovskite oxide synthesized by these method are $LaMnO_3$ (119 m^2/g)[8], $LaFeO_3$ (92 m^2/g)[8], $LaCoO_3$[9], $LaNiO_3$ (150 m^2/g)[7]. Materials prepared by these methods have also been demonstrated to be excellent catalyst supports for PGM nanoparticles for many reactions.[10] Utilising these preparation methodologies would allow for the preparation of large surface area perovskite oxides. This chapter detailed the

characterization techniques use to investigates the perovskite supported gold-platinum nanoparticles in order to gained information on the selectivity of the products for the HMF and glycerol oxidation reaction in the subsequent chapters.

3.2 Result and Discussion

3.2.1 Catalyst Support

Lanthanum based perovskite oxides ($LaMO_3$) were chosen catalyst support in this project with five different B site cross the first series transition metal starting from Cr to Ni. The supports were synthesized by nano-casting method using SBA-15 template. An in-depth method for the synthesis of the SBA-15 has been described in the experimental Chapter, Section 2.2. An in-depth method for the synthesis of the SBA-15 has been described in the experimental section. To produce the specific $LaMO_3$ perovskite, an equomolar solution of lanthanum nitrate and the corresponding B site nitrate salt (1:1 ratio with La:M molar ratio) were dissolved in ethanolic solution and stirred for a period of 60 min. The resulting solution was transferred into a 100 mL round bottom flask containing a stirred suspension of SBA-15. The mixture was further stirred for another 60 min at room temperature and later raised to 80 ℃ for recrystallisation of the La:M precursor. The resultant precursor was dried and ground to a powder for calcination. The calcined material is denoted by $LaMO_3$-SiO_2 composite. The SBA-15 was removed from $LaMO_3$-SiO_2 matrix using NaOH solution (2 M) at 100 ℃ for 24 h, resulting into the final material ($LaMO_3$).

3.2.1.2. Catalyst Support Characterization

3.2.1.2.1 Thermogravimetric Analysis (TGA).

Thermogravimetric analysis was performed on the catalyst supports precursor (La:M precursor) to determine the lowest combustion/calcination temperature to yield a perovskite oxide phase. The analysis was conducted from 30 ℃ to 900 ℃, as typical calcination temperatures of perovskite oxide fall between 400 ℃ and 900 ℃ range. The TGA results (Figure 3.1) showed that there are consecutive weight losses in all the perovskite precursors with notable weigh loss in each case beginning at around 400 ℃. This can be attributed to decomposition of the metal nitrate and oxidation of the chelating agent (citric acid) present in the perovskite precursor.[6]

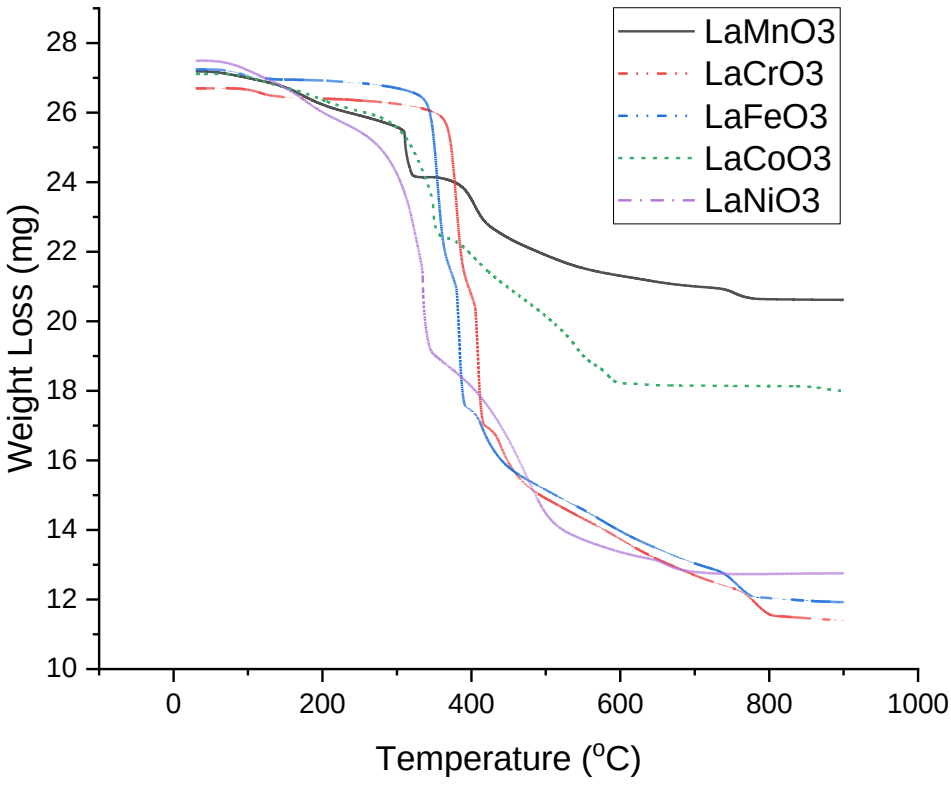

Figure 3.1 TGA plot illustrating the weight loss of the perovskite precursor.

The weight losses at higher temperature around 700 ℃ and beyond are attributed to the

transition from single metal oxide phases to the perovskite oxide phase, with the transition temperature dependant on, and controlled by, the variable oxidation states of the transition metal in the B site of the perovskite oxides.[8]

The chosen temperature for calcination for the perovskite precursors was 700 ˚C as the final weight loss event begins before this point for all the samples.

3.2.1.2.2 Powder X-ray Diffraction

The powder X-ray diffraction patterns for SBA-15, $LaMO_3$ (M is Cr, Mn, Fe, Co, Ni), $LaMO_3$-SBA-15 are shown below. For understanding, the XRD pattern of $LaMnO_3$ before and after calcination treatment was carried out are shown to understand the phase changes in each step. The powder pattern for the $LaMnO_3$ uncalcined (Figure 3.2) showed that diffraction peaks were broad and relatively low in intensity indicating that the structure was relatively not very crystalline, and that perovskite phase was not formed. The low intensity is perhaps due to chelating agent (citric acid) that was well distributed within the metal nitrates, making them amorphic rather than crystalline.[11] The phase composition in the precursor (uncalcined material) are silica (SiO_2), metal oxalates ($La_2O_2CO_3$ and trace amount of $La_2O(CO_3)_2$), perovskite ($LaMnO_3$) and single oxide (MnO_2, Mn_2O_3 and La_2O_3) revealed by the XRD (Figure 3.2).

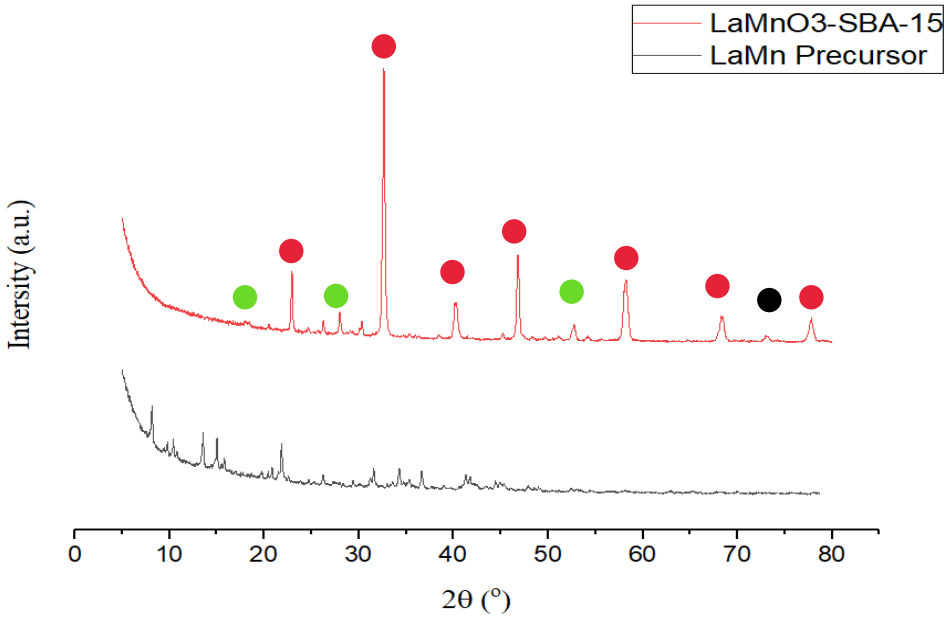

Figure 3.2 XRD patterns of $LaMnO_3$-SiO_2 composite and LaMn precursor before calcination at 700 °C. SiO_2 (green dot) and $LaMnO_3$ (red dot).

After calcination of the precursor at 700 °C (Figure 3.2) results in the formation of a thermodynamically stable metal oxide with the removal of organics and nitrates. The peaks indicating metal oxalates and nitrates were completely missing from the calcined $LaMnO_3$-SBA-15 composite. The SBA-15 was removed using 2 M NaOH followed by calcination at 450 °C and the resultant materials are shown in Figure 3.3.

In general, the XRD of the final materials ($LaMO_3$, where M is Cr, Mn, Fe, Co and Ni) was conducted and data was treated by HighScore Plus software. The semi quantitative data from each diffraction patterns showed La_2O_3 impurities except for $LaMnO_3$ and Fe_2O_3 impurity in $LaFeO_3$ (Table 3.1). This perhaps occurred due to non-stoichiometric recrystallisation of metal precursors in the SBA-15 pores resulting in a difference recrystallisation rate of the metal salt used. The calcination temperature can also have an influence on the formation of a single perovskite phase or phase segregated single oxides. High temperature is needed to

form the perovskite and the single metal oxide phase content decreases with increasing temperature. However, the surface area is drastically reduced with increasing calcination temperature (Table 3.2 and Figure 3.4) and so the temperature used is a compromise between retaining a high surface area and forming the desired perovskite.

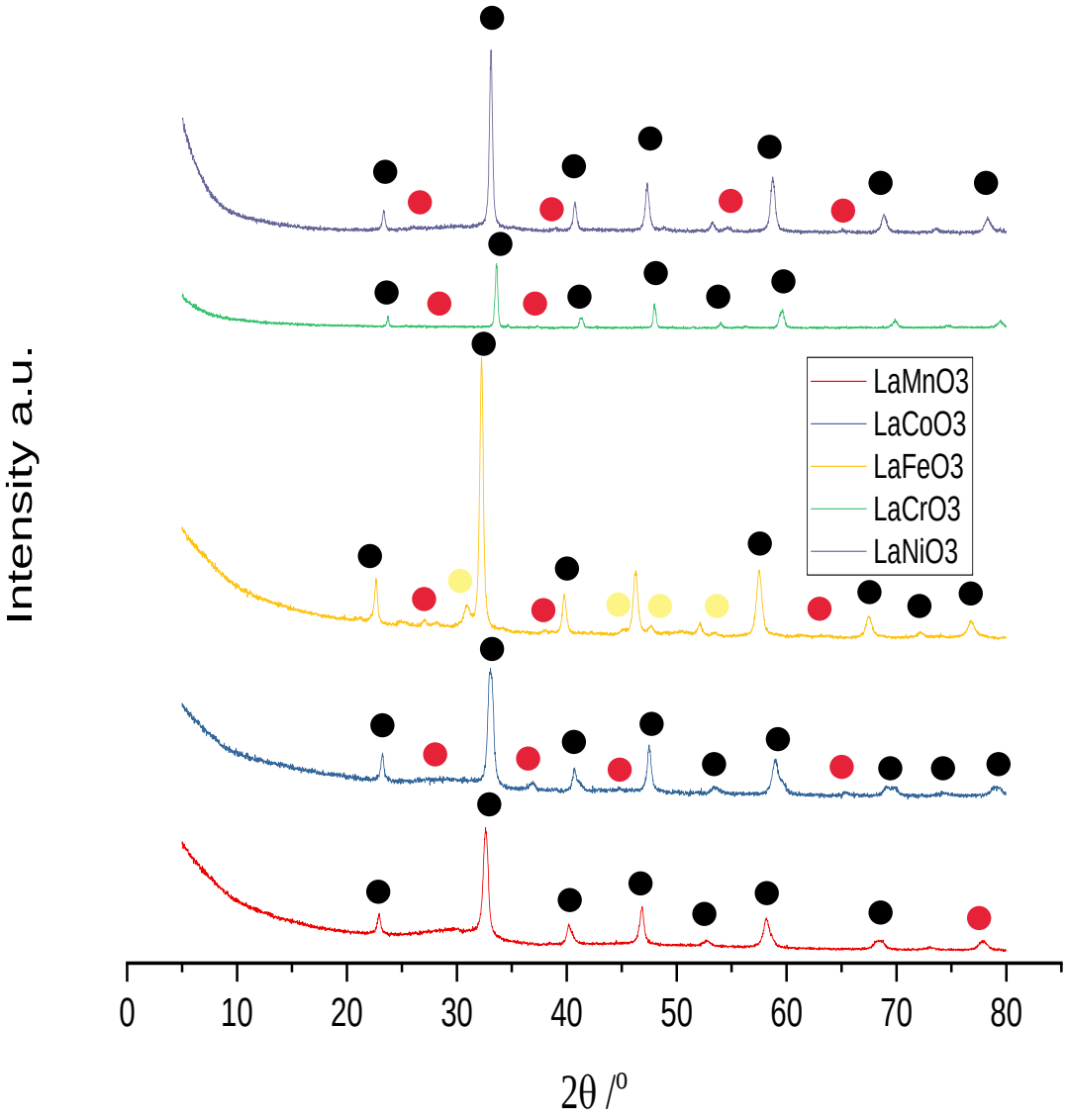

Figure 3.3 Powder X-ray diffraction patterns of the $LaMO_3$. perovskite phases (black dots) where the mixture rhombohedral, orthorhombic, and cubic phases are not differentiated); Fe_2O_3 (yellow dots) in $LaFeO_3$, La_2O_3 (red dots) in all perovskites except $LaMnO_3$.

Table 3.1 Catalyst support phase composition and crystallite size from the XRD

Catalyst Support	Phase Composition by XRD	Crystallite size (nm)
$LaMnO_3$ perovskite phase	100% $LaMnO_3$	7
$LaCoO_3$ perovskite phase	96% $LaCoO_3$ 4% La_2O_3	3
$LaFeO_3$ perovskite phase	86% $LaFeO_3$ 12% La_2O_3 2% Fe_2O_3	12
$LaCrO_3$ perovskite phase	89% $LaCrO_3$ 11% La_2O_3	5
$LaNiO_3$ perovskite phase	91% $LaNiO_3$ 9% La_2O_3	3
SBA-15 SBA-15 Uncalcined	100% SiO_2	-

The Debye-Scherrer equation relates the size of the nanoscale crystallite in a solid material to the broadening of the peak in a diffraction pattern. it was used to estimate the crystallite sizes for each of the nano-casted assisted perovskite oxides, with the resulting range being between 3 and 12 nm (Table 3.1). These crystallite sizes are relatively small in comparison to a similar perovskite material formed through other methods. Evans *et al.* obtained crystallite sizes between 6 and 22 nm using the antisolvent supercritical method for a series of $LaBO_3$ perovskite oxides.[12] The small crystallite size obtained is a result of the nano-casting preparation procedure which produces extremely small particle size that are extremely well mixed allowing for a lower calcination temperature to form the perovskite phase.

Table 3.2 Variation of calcination temperature with respective to perovskite oxide phase purity and surface area.

Calcination Temperature (°C)	Surface Area (m^2/g)	Perovskite Phase composition
600	139	$LaCrO_3$ (78%), La_2O_3 (22%)
700	105	$LaCrO_3$ (89%), La_2O_3 (11%)
800	87	$LaCrO_3$ (95%), La_2O_3 (5%)

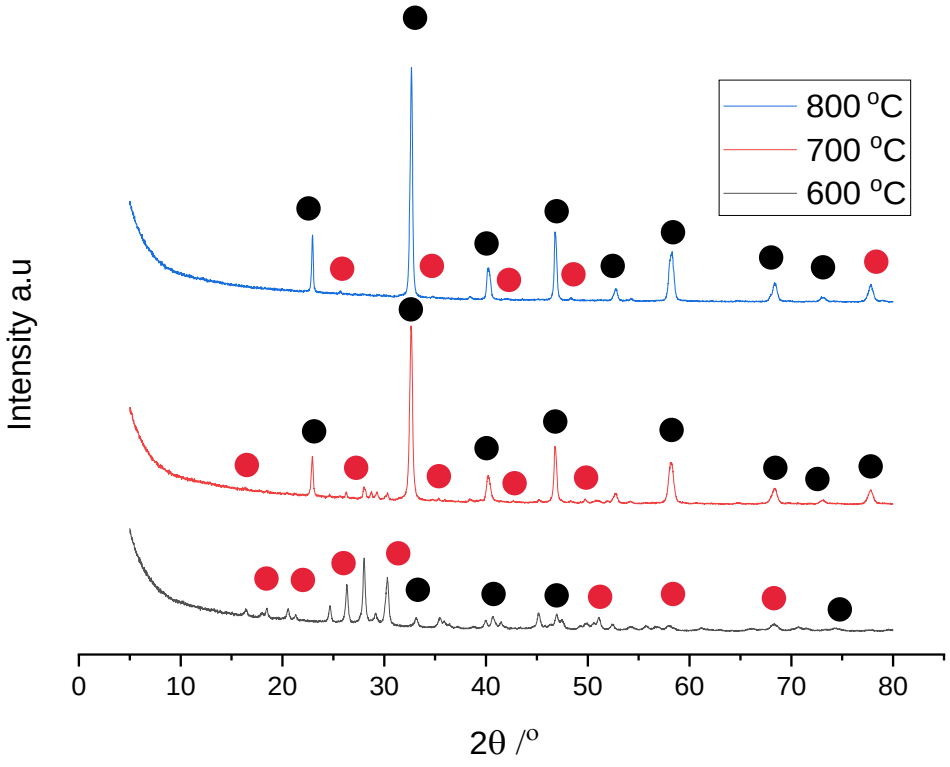

Figure 3.4 X-ray pattern for $LaCrO_3$ calcined at different temperatures. $LaCrO_3$ perovskite phase (black dots) and La_2O_3 phase (red dots)

3.2.1.2.3. BET Surface Area

The catalyst supports surface area was determined by nitrogen physisorption using the BET method are summarized in Table 3.3.

The surface area of the template (SBA-15) as synthesized was found to be 756 m^2g^{-1}, which is similar to commercial SBA-15.[13,14] As expected, the surface area of the calcined composite $LaMO_3$-SBA-15 and $LaMO_3$ after SBA-15 was removed were higher than the uncalcined counterparts, although they were, considerably lower than the SBA-15 template. The surface area of the perovskite oxides templated using SBA-15 were in the region of 68 – 156 m^2/g and arranged in ascending order $LaFeO_3$ (68 m^2 g^{-1}) > $LaMnO_3$ (95 m^2 g^{-1}) > $LaCrO_3$ (105 m^2 g^{-1}) > $LaNiO_3$ (125 m^2 g^{-1}) > $LaCoO_3$ (158 m^2 g^{-1}). These results are in good agreement with the many findings in the literature for the same perovskite oxide synthesized by the the same method $LaMnO_3$ (119 m^2/g)[8], $LaFeO_3$ (92 m^2/g)[8], $LaCoO_3$[9], $LaNiO_3$ (150 m^2/g)[7].

Table 3.3 BET surface area of the prepared materials

Catalyst Support	Surface Area (m^2/g)
$LaMnO_3$ perovskite phase	95
$LaMnO_3$-SBA-15 Calcined	587
LaMn Precursor	454
$LaCoO_3$ perovskite phase	158
$LaCoO_3$-SBA-15 Calcined	596
LaCo Precursor	488
$LaFeO_3$ perovskite phase	68
$LaFeO_3$-SBA-15 Calcined	562
LaFe Precursor	479
$LaCrO_3$ perovskite phase	105
$LaCrO_3$-SBA-15 Calcined	599
LaCr Precursor	471
$LaNiO_3$ perovskite phase	125
$LaNiO_3$-SBA-15 Calcined	599
LaNi Precursor	483
SBA-15	756
SBA-15 Uncalcined	547

Higher surface area and small crystallite size proves a larger distribution of site defects on the surface of the perovskite materials, which allows the PGM to coordinate to these defects and increases their feasibility in liquid phase system.

3.2.1.2.4. Temperature Programmed Reduction

Temperature programmed reduction (TPR) with hydrogen was performed to evaluate the reduction behaviour of the nanocasted assisted perovskite oxides. The reduction of lanthanum-based perovskite oxides has been widely studied and the TPR profile of such materials is characterised by two process, the surface and bulk reduction.[8,15,16] The temperature at which the surface and bulk reduction of perovskite oxides with structural formation of ABO_3 occurs is dependent on several factors, including the crystallite size, morphology, B-site metals as well as the concentration of defects.[1] As discussed above, the concentration of defect sites and the crystallite size are related. The H_2-TPR profile of each support is shown in Figure 3.5. In the case $LaNiO_3$ nano-assisted perovskite, the first peak was found around 385 °C which is attributed to the reduction of Ni^{3+} to Ni^{2+} in the perovskite structure. The second peak was found around 506 °C indicating a complete reduction of Ni^{2+} to Ni^0. This finding is good agreement with that of Mahesh and co-workers.[7] The authors showed the surface reduction peaks of the $LaNiO_3$ occurs below 700 ℃, which is due to oxygen mobility of $LaNiO_3$. The $LaCoO_3$ exhibited the unclear reduction peaks and is most likely related to the incomplete formation of the perovskite phase as well as the high surface area. Additionally, LaCoO3 perovskite have been reported to exhibit excellent redox properties when prepared by nanocasting strategy.[9] The $LaCoO_3$ sample shows two main reduction peaks. The low temperature peak can be assigned to the reduction of Co^{3+} to Co^{2+}, while the high temperature one is due to the reduction of Co^{2+} to metallic Co^{0+}. Meanwhile, the amount of H_2 consumed in the second reduction peak is much larger than that of the first

reduction peak, indicating the two-step reduction process. The $LaFeO_3$ reducibility profile shows four reduction temperatures at 374 °C, 430 °C, 576 °C and 724 °C. These reduction peaks were assigned to the reduction of single phase Fe_2O_3 on the surface of the perovskites from Fe^{3+} to Fe^{2+}, reduction of Fe in the perovskite structure from Fe^{4+} to Fe^{3+}, followed by Fe^{3+} to Fe^{2+}, and final reduction of Fe^{2+} to Fe^0, respectively.[17–197] For $LaMnO_3$, a peak at around 320 °C was observed that was assigned to a nonstoichiometric oxygen vacancy in the $LaMnO_3$ structure. A reduction peak at round 550 °C which was attributed to the reduction of Mn^{4+} to Mn^{3+} and a high temperature peak at around 720 °C relates to the further reduction of Mn^{3+} to Mn^{2+}. There was shoulder observed at around 640 °C which perhaps can be attributed to further reduction of some manganese in the grain boundaries.[5,19] The $LaCrO_3$ showed two reductions steps with lower reduction peak at around 370 °C which likely to be the reduction of Cr^{3+} to Cr^{2+} and higher reduction peak at around 512 °C which a subsequent reduction of Cr^{2+} to Cr metallic state.[20]

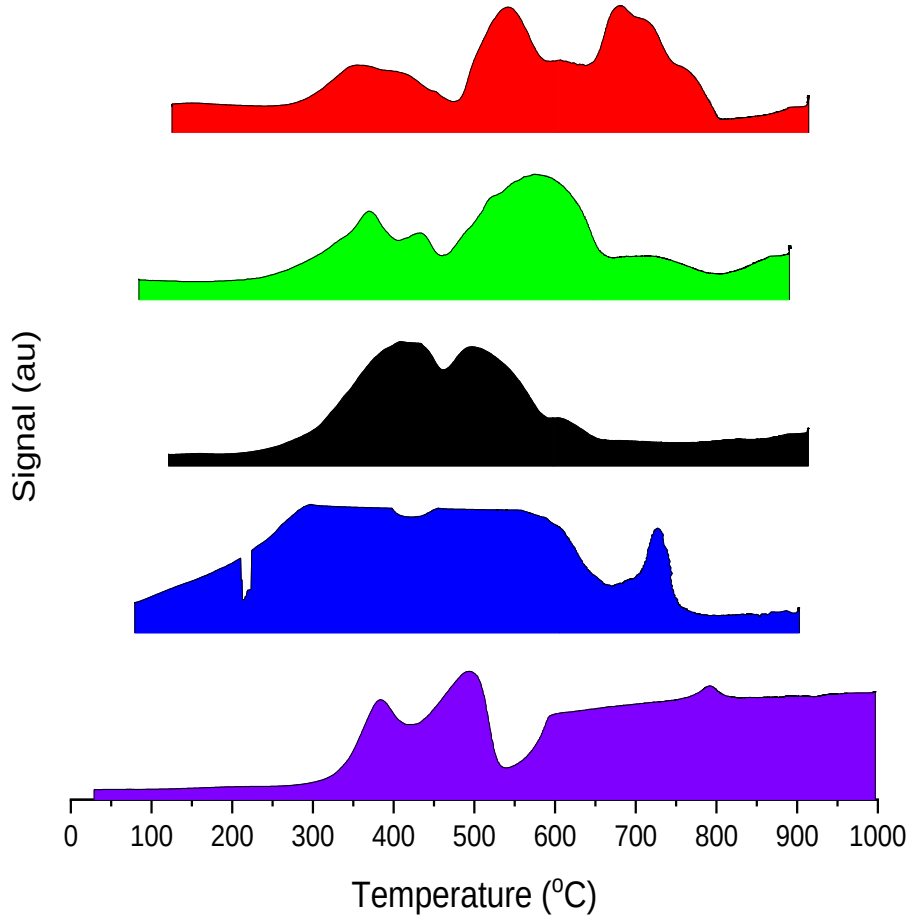

Figure 3.5 H_2-TPR plots for silica assisted perovskite oxide. $LaCrO_3$ (purple), $LaMnO_3$ (red), $LaFeO_3$ (Green), $LaCoO_3$ (Blue), $LaNiO_3$ (Black).

3.2.1.2.5. Scanning Electron Microscopy and Energy Dispersive X-ray Spectroscopy (SEM-EDS).

The template (SBA-15) and perovskite oxides after SBA-15 removal were investigated by SEM using the methods described in Section 2.2.5.5. The results can be seen in Figure 3.6. As expected, the morphological structure of SBA-15 possess a rod like shapes which is common for silica synthesized under conditions used in this work.[14,21]

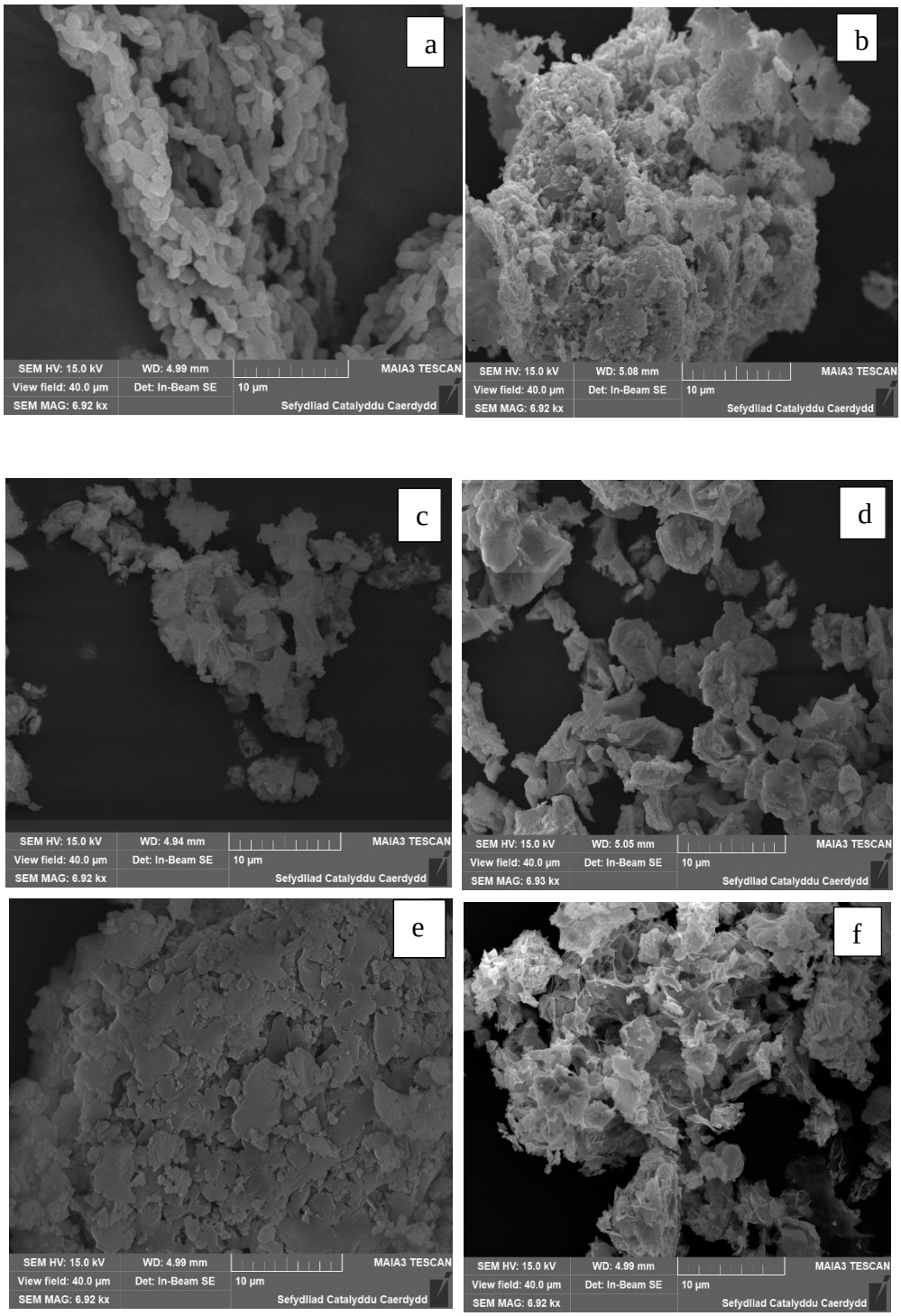

Figure 3.6. SEM images for (a) SBA-15, (b) $LaMnO_3$, (c) $LaFeO_3$ (d) $LaCoO_3$ (e) $LaCrO_3$ (f) $LaNiO_3$ at 40µm view field and 10µm magnification.

The removal of the SBA-15 does affect the shape and particles size as well as the surface area revealed by N_2 physisorption technique to a noticeable extent. The perovskite oxides have an

irregular particle size with jagged edge structure. The regular rod-like structure of the SBA-15 which was expected to replicate on the perovskite oxides was partially seen. The images indicate that, although the perovskite oxides appear rather disordered, its pore structure is quite open and accessible from the outside surface of the particles.

3.2.1.2.6 Ammonia temperature programmed desorption (NH_3-TPD)

To determine the overall number of acid sites on the perovskite oxide supports, temperature programmed desorption (TPD) was performed upon each of the samples using ammonia as a probe molecule (Figure 3.7). It has been found from previous TPD studies that lattice oxygen contained within perovskite oxides can potentially oxidise adsorbed ammonia into nitrous oxide and water.[4] This ability to oxidise the ammonia increases the complexity of the desorption profiles which lead to four potential assumptions based on desorbed species:

(1) NH_4^+ which is weakly bound to any hydroxyl groups on the surface of the perovskite,

(2) NH_3 chemisorbed to any available Lewis acidic sites,

(3) N_2O formed *via* oxidation of NH_3 with lattice oxygen and

(4) lattice oxygen desorption.

Desorption profiles for type (2) and (3) will occur with available Lewis's acid sites within the temperature range of 150 – 600 ˚C. These Lewis acid sites are present at the surface of single metal oxides due to the presence of metal cations which have an unsaturated coordination number. Desorption profiles associated with the loss of lattice oxygen (type iv) occur only with temperatures exceeding 500 ˚C.[4] This consistent with TPR profile data of $LaMnO_3$ perovskite, where oxygen vacancy destruction was observed.

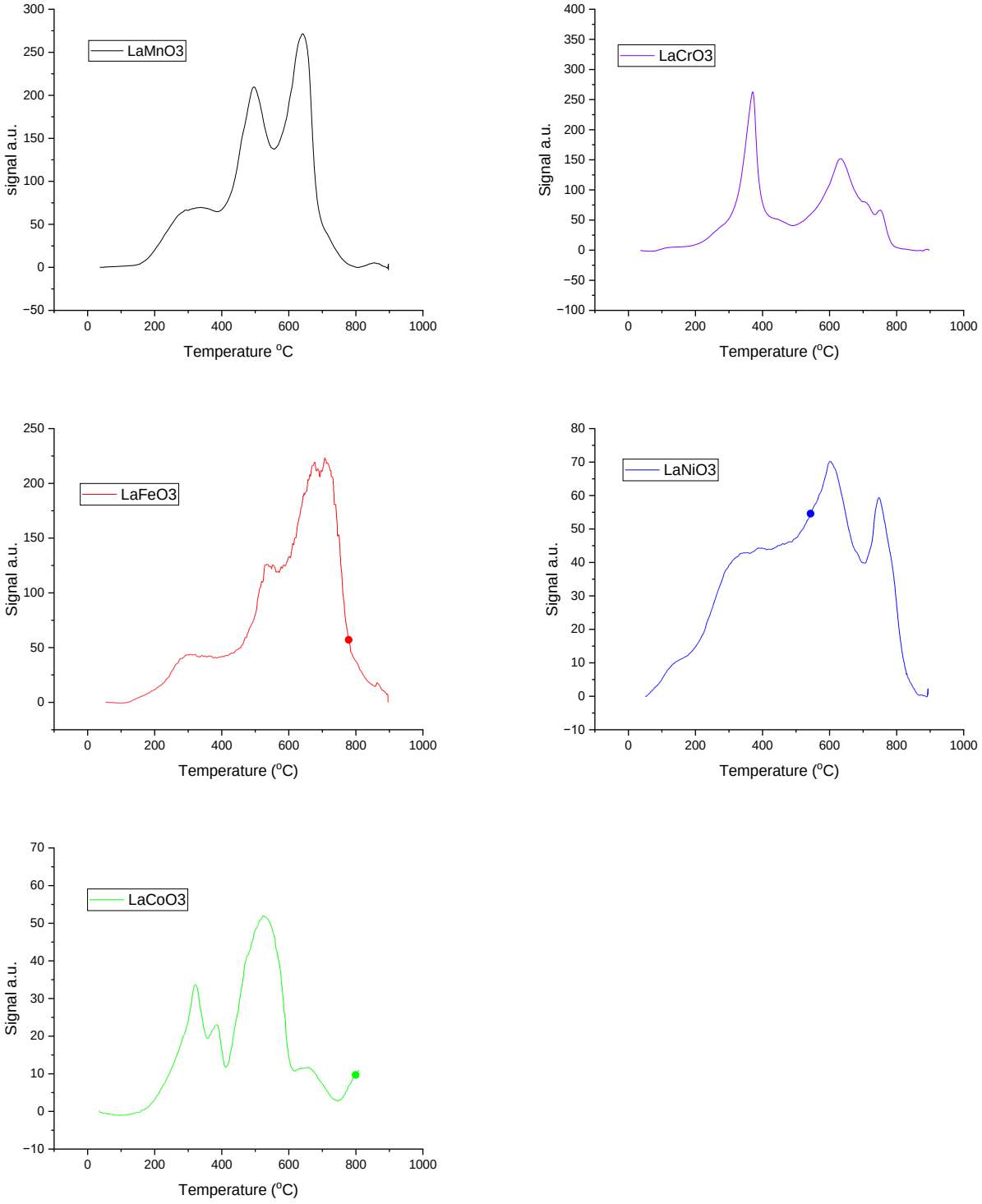

Figure 3.7 Ammonia Temperature programmed desorption profiles for the SBA-15 assisted perovskite oxide supports. $LaCrO_3$ (Purple), $LaMnO_3$ (Black), $LaFeO_3$ (Red), $LaCoO_3$ (Green) and $LaNiO_3$ (Blue).

It can be seen from the acid site analysis for all B site perovskites, that a desorption occurs between 200 – 500 ˚C, the temperature region associated with Lewis's acid sites. The results complement the XRD data (Table 3.3.), in which the single oxide impurities were found for the Fe, Co, Cr and Ni containing perovskites. Whilst the $LaFeO_3$, $LaCrO_3$, $LaCoO_3$ and $LaNiO_3$ impurities comprise mainly of La_2O_3, the $LaFeO_3$ was found to contain the spinel phase Fe_3O_4. As the $LaNiO_3$ and $LaCoO_3$ contain the lowest impurities and have very little ammonia desorption within the Lewis acid region, it can be suggested that at least a portion of the ammonia desorption can be attributed to the La_2O_3 impurities Lewis acidic nature. The XPS data (Figure 3.10b) also shows that in all the perovskite oxides, the La_2O_3 is present with the La_2O_3: perovskite phase ratio being $LaCrO_3$ > $LaFeO_3$ > $LaCoO_3$ > $LaNiO_3$ > $LaMnO_3$. Another notable feature of the desorption profiles of all the perovskite oxides is the exhibition of a desorption at high temperatures (650 – 700 ˚C), which would allude to the loss of oxygen from within the lattice of the perovskite structures.[5,8,12]

3.2.2. Catalyst Synthesis

The metals were added to the support by conventional sol immobilization method. The reason for choosing this method was because of the fact that it inherently small and well dispersed particle distribution across the surface of the support, hence providing a catalyst with the ideal properties for producing a model reaction. An aqueous solution of $HAuCl_4$ and H_2PtCl_6 were prepared at specific concentrations (10 mg ml^{-1}). Polyvinyl alcohol (PVA, 1 wt% aqueous solution, MW = 10 kDa) was freshly prepared and used as the stabilising agent. $NaBH_4$ (0.1 M aqueous solution) was also freshly prepared and used as the reducing agent. To an aqueous mixture of the HAuCl4 and H_2PtCl_6 of a concentration to produce 1:1 metal weight ratio, a total of 1 wt % of total metal in the prepared catalyst, the PVA solution was added with vigorous stirring for 2min. $NaBH_4$ was subsequently added such that the

$NaBH_4$:total metal ratio (mol/mol) was 7.5. The resulting solution was stirred for 30 min to allow the stabilisation of the reducing colloidal particles, followed by the addition of the perovskite material. The solution was left stirring for a further 1 h, followed by washing with distilled water and drying at 110 ˚C. Acidification of the support was unnecessary and would have been detrimental to the catalyst as the supports are unstable in highly acidic media.

3.2.2.1 Characterization

3.2.2.1.1. Transmission Electron Microscopy (TEM).

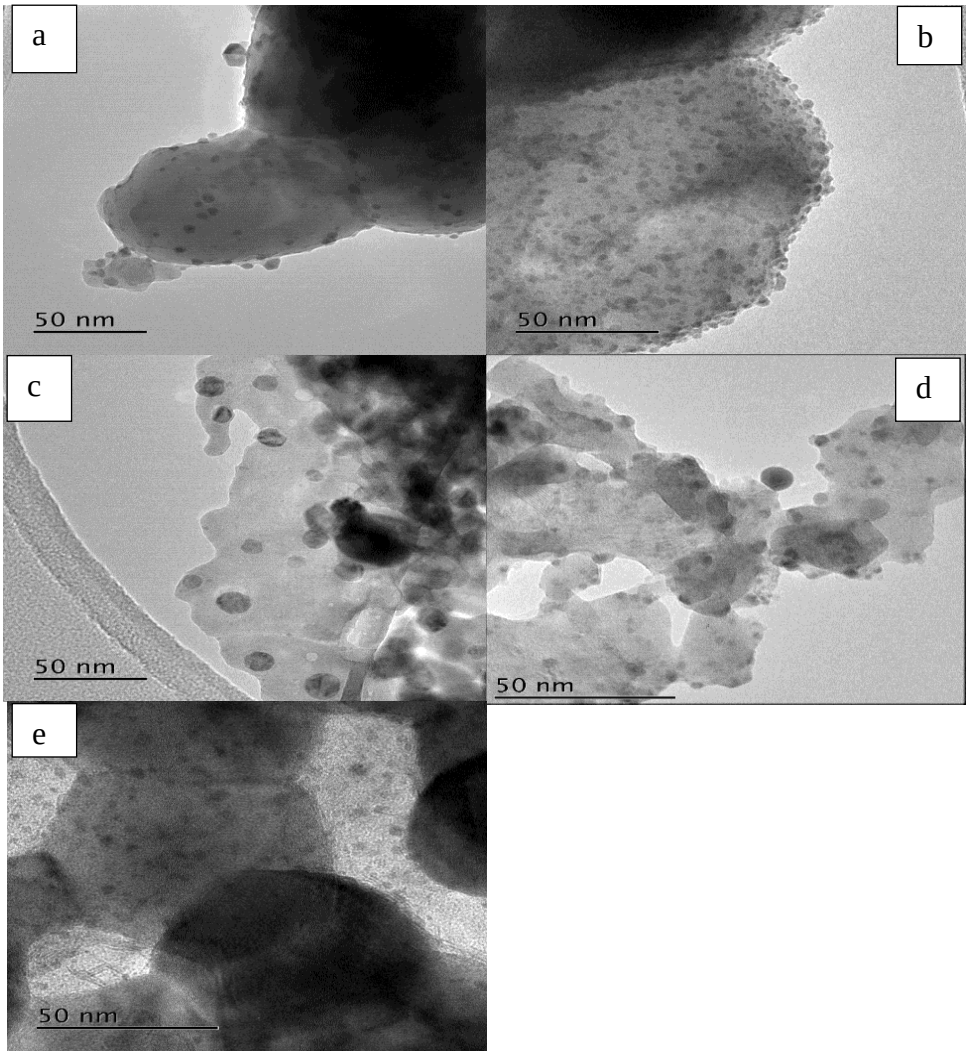

Figure 3.8 Representative transmission electron micrographs of sol-immobilisation prepared AuPt supported on the various SBA-15 assisted $LaBO_3$ perovskite oxide supports. Where, (a) $LaCoO_3$, (b) $LaCrO_3$, (c) $LaFeO_3$, (d) $LaMnO_3$, and (e) LaNiO3.

Transmission electron microscopy was conducted on each of the prepared supports with the images and particle size distribution (PSD) shown below (Figures 3.8 and 3.9). The particle size distribution (PSD) was generated from a statistically relevant number of micrographs to which a total 100 particles were counted using imageJ software. For all the perovskite oxide supports the mean particle size was found to be approximately 2 nm with a standard deviation of around 1 nm. It appears that there is no strong correlation between particle size with either the relative surface area or the specific B site element used. It is likely that the small well-defined PSD observed for these catalysts is a result of its low metal loading.[22] These results are comparable to those mentioned in literature which reports that the conventional sol-immobilisation technique generates small nanoparticles with well-defined PSD.[23] Additionally, it is evident that the particles sizes of these catalysts fall within the required region in order to be active for oxidation in liquid phase system.

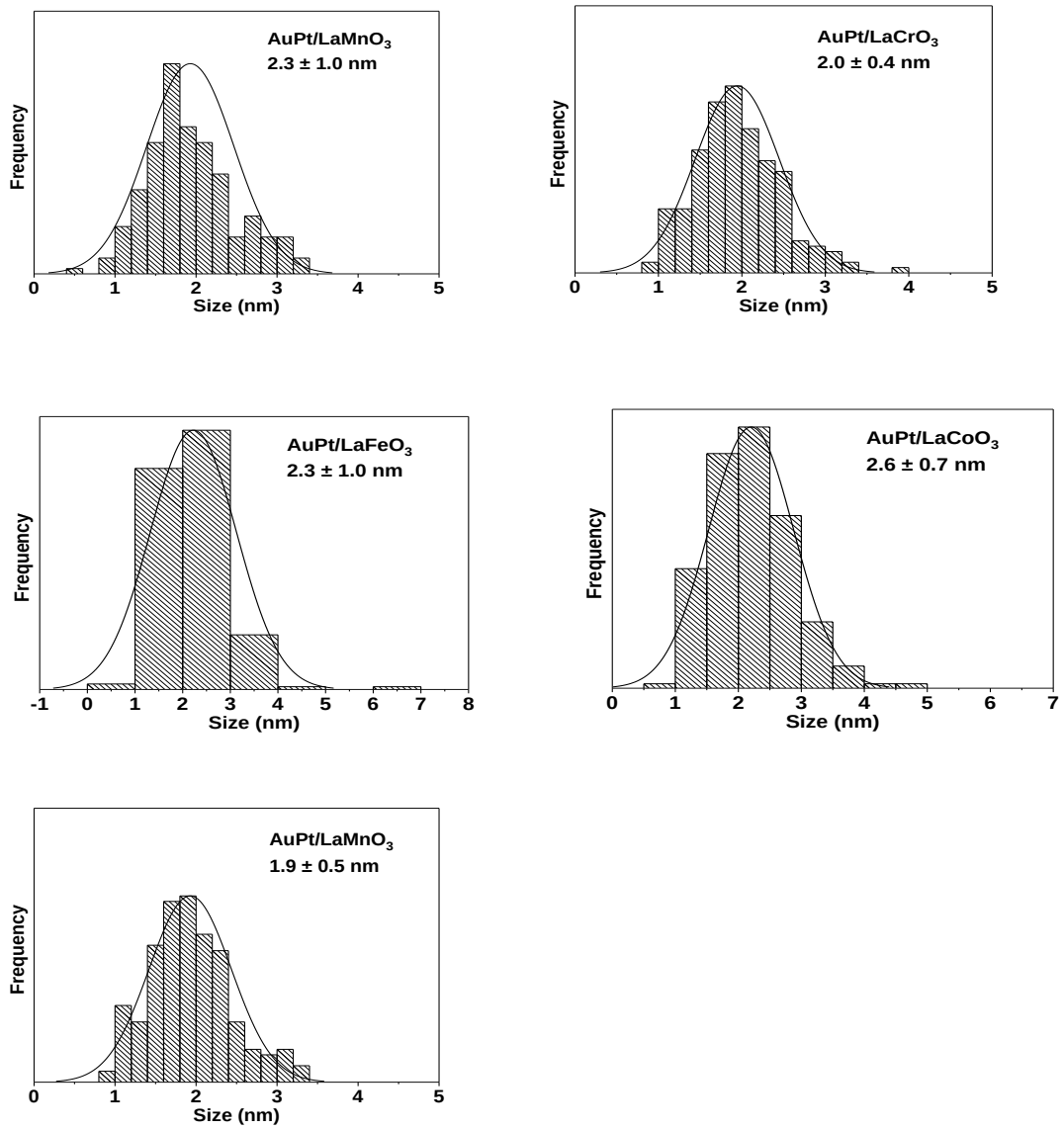

Figure 3.9 Particle size distribution histograms of AuPt supported on the different SBA-15 assisted LaBO3 perovskites.

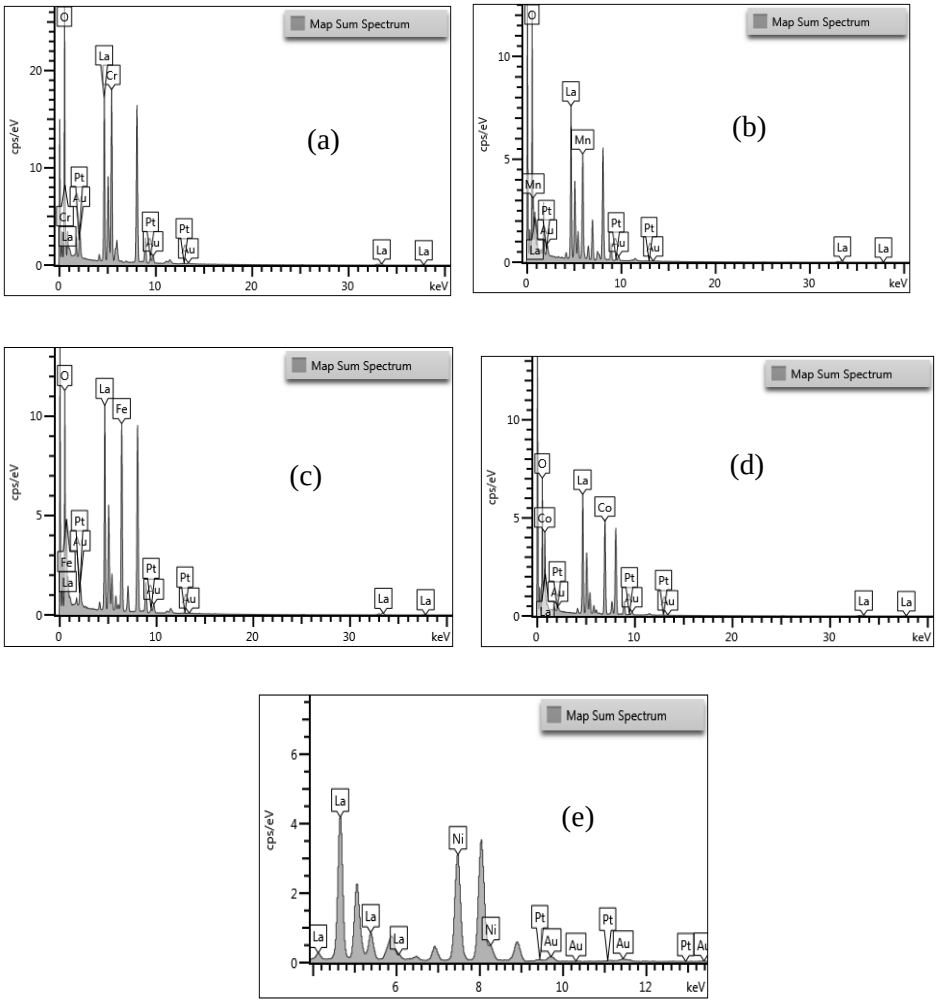

Figure 3.10a EDS spectra for AuPt supported on the various SBA-15 assisted $LaBO_3$ perovskite oxide supports. Where, (a) $LaCrO_3$, (b) $LaMnO_3$, (c) $LaFeO_3$, (d) $LaCoO_3$, and (e) $LaNiO_3$.

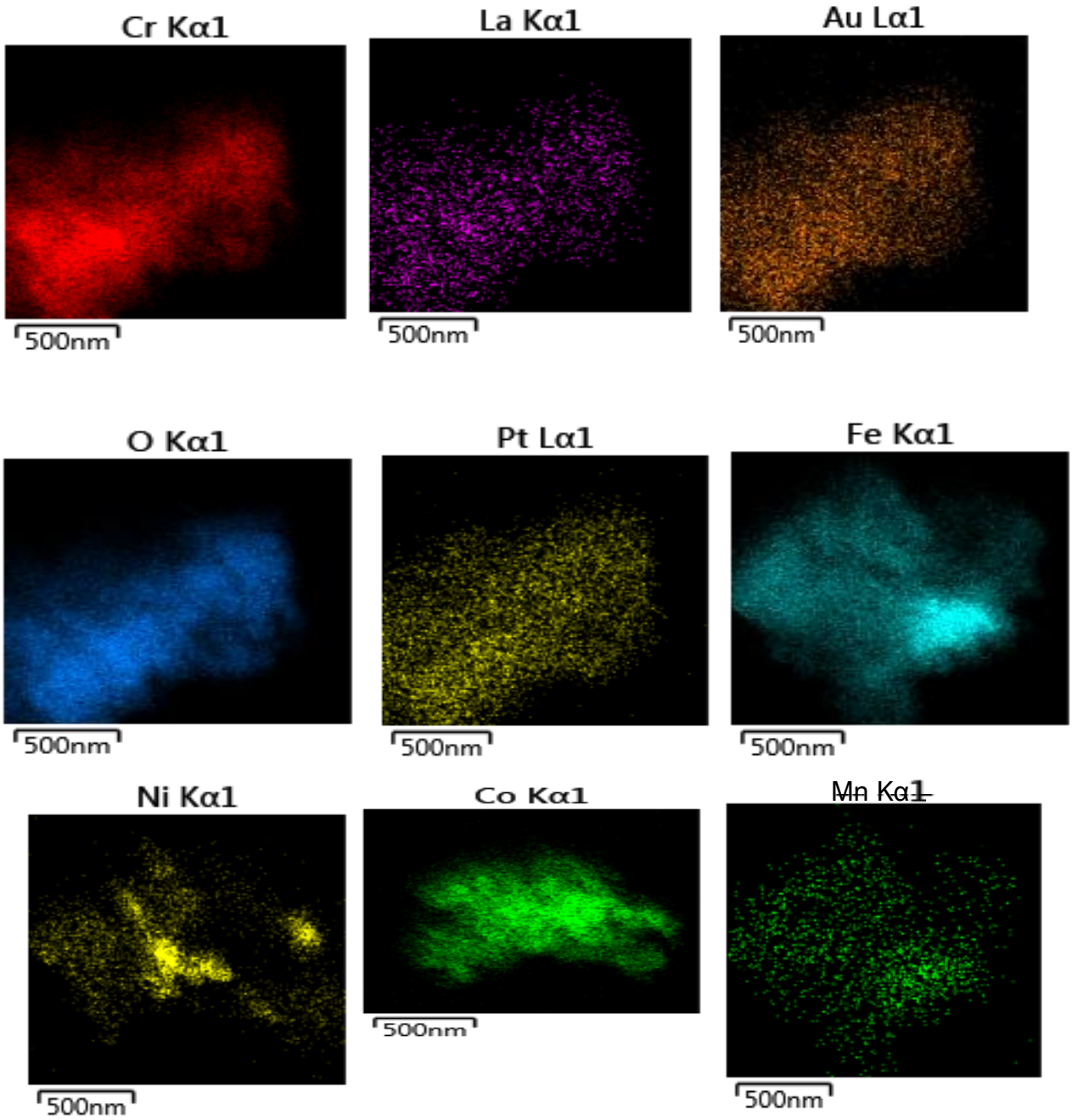

Figure 3.10b EDS Elemental mappings for AuPt supported on the various SBA-15 assisted $LaBO_3$ perovskite oxide supports.

Energy dispersive X-ray spectroscopy was employed to further investigate the nanoparticles distribution and the homogeneity of the supports. The EDS spectra and elemental mapping for each element in the catalyst is shown in Figure 3.10a and 3.10b. It was observed that in all the catalysts the Au and Pt nanoparticles were present on the surface of the perovskite supports. This demonstrates that sol immobilization method provide strong metal-support interactions as stated in the literature.[12,24,25]

3.2.2.1.2. X-ray Photoelectron Spectroscopy

The catalysts were characterized by X-ray photoelectron spectroscopy (XPS) to provide insight into oxidation state of the metal nanoparticle and the relative Au-Pt surface composition. XPS analysis of the Au and Pt $4f_{7/2}$ regions (Figure 3.11a) showed that the observed binding energies for Au and Pt were 83.2 and 70.7 eV respectively.

The binding energies associated with the Pt $4f_{7/2}$ peaks are characteristic of two different oxidation states, Pt^0 and Pt^{2+} in each perovskite oxide support. Even though, the XPS reveals the effective valence state of Pt averaged over nanocluster, Pt^{2+} species, are most likely located at the interfaced perovskite oxide supports. Therefore, changes in Pt^{2+} concentration indicates the nanoparticles-supports interface restructure at room temperature with a fraction 65 Pt^0 and 35% Pt^{2+} for 0.5 wt.% of the entire nanocluster. The Au $4f_{7/2}$ peaks are typically observed at 84.0 eV and purely metallic (Figure 3.11a). It can be seen from Table 3.4 that the surface ratio obtained for the Au and Pt varied throughout the range of perovskite oxide supports, from a minimum Au:Pt ratio of 0.8 for Co B site perovskites up to 1.5 for the Ni B site perovskites.

Table 3.4 Au and Pt bulk and surface composition for AuPt/LaBO3 catalysts analysed by MPAES and XPS.

Entry	Catalyst Support	Au and Pt content from MP-AES (wt.%)	Surface Pt^{2+}/Pt^{0} ratio from XPS	Surface $Au/Pt\&Pt^{2+}$ ratio from XPS
1	$LaCrO_3$	0.50 (Au), 0.5 (Pt)	0.40	1
2	$LaMnO_3$	0.47 (Au), 0.46 (Pt),	0.54	1.1
3	$LaFeO_3$	0.54 (Au), 0.46(Pt)	0.50	1.4
4	$LaCoO_3$	0.55 (Au), 0.50 (Pt)	0.56	0.8
5	$LaNiO_3$	0.50 (Au), 0.50(Pt)	0.67	1.5

These changes can be attributed to possible monometallic phases of the nanoparticles, a change in the composition of the alloy nanoparticles or potential formation of core-shell structures dependent on the potential interactions with the various B site cations.[26] Sol-immobilisation is also known to produce both core-shell and random alloys of AuPt nanoparticles, in which the various morphologies are well represented by the observed XPS metal ratios (*i.e.* Au:Pt ratio of 1:1 for random alloy or 0.75:1 for core-shell).[27] Using Au and Pt makes discerning the reason for the change difficult because of the structural similarities, including close atomic numbers and weights, that X-ray spectroscopy techniques find difficult to distinguish.

As shown from the XRD patterns (Figure 3.3), there are minor phases in the perovskite supports, ranging from 2-15 % according to the semi-quantitative phase analysis. The impurities can potentially influence the XPS data (Figure 3.10b), with analysis showing a noticeable surface contribution from a La species which could be reasonably assigned to that of the oxide, La_2O_3. The B site perovskites with the lowest phase purity (Fe, Co and Ni) were

found to have higher contributions of the La phases, which agrees with the data obtained through the XRD analysis.

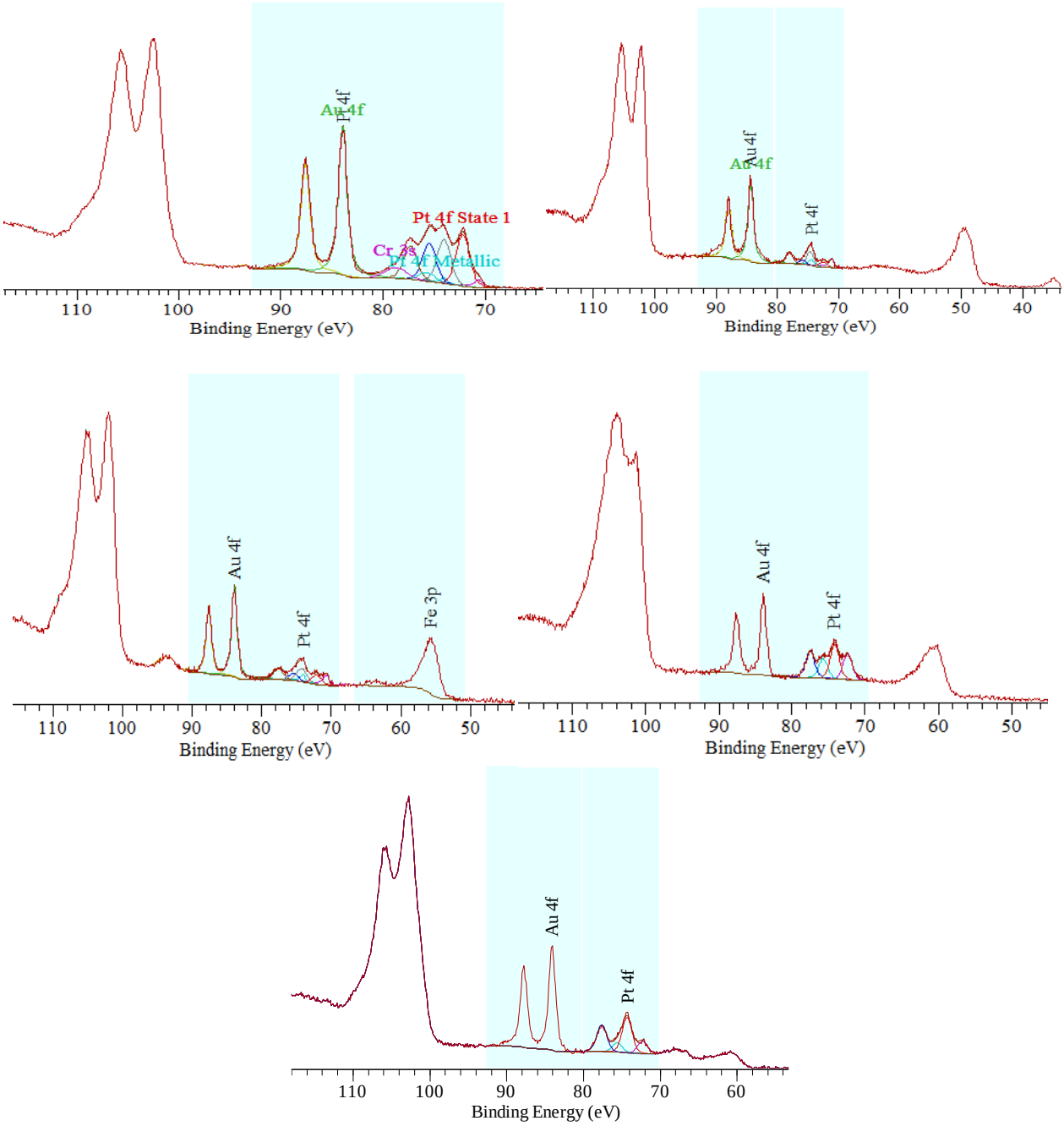

Figure 3.11(a) XPS plots of AuPt/$LaBO_3$ catalysts showing Au (4f) and Pt (4f) spectra.

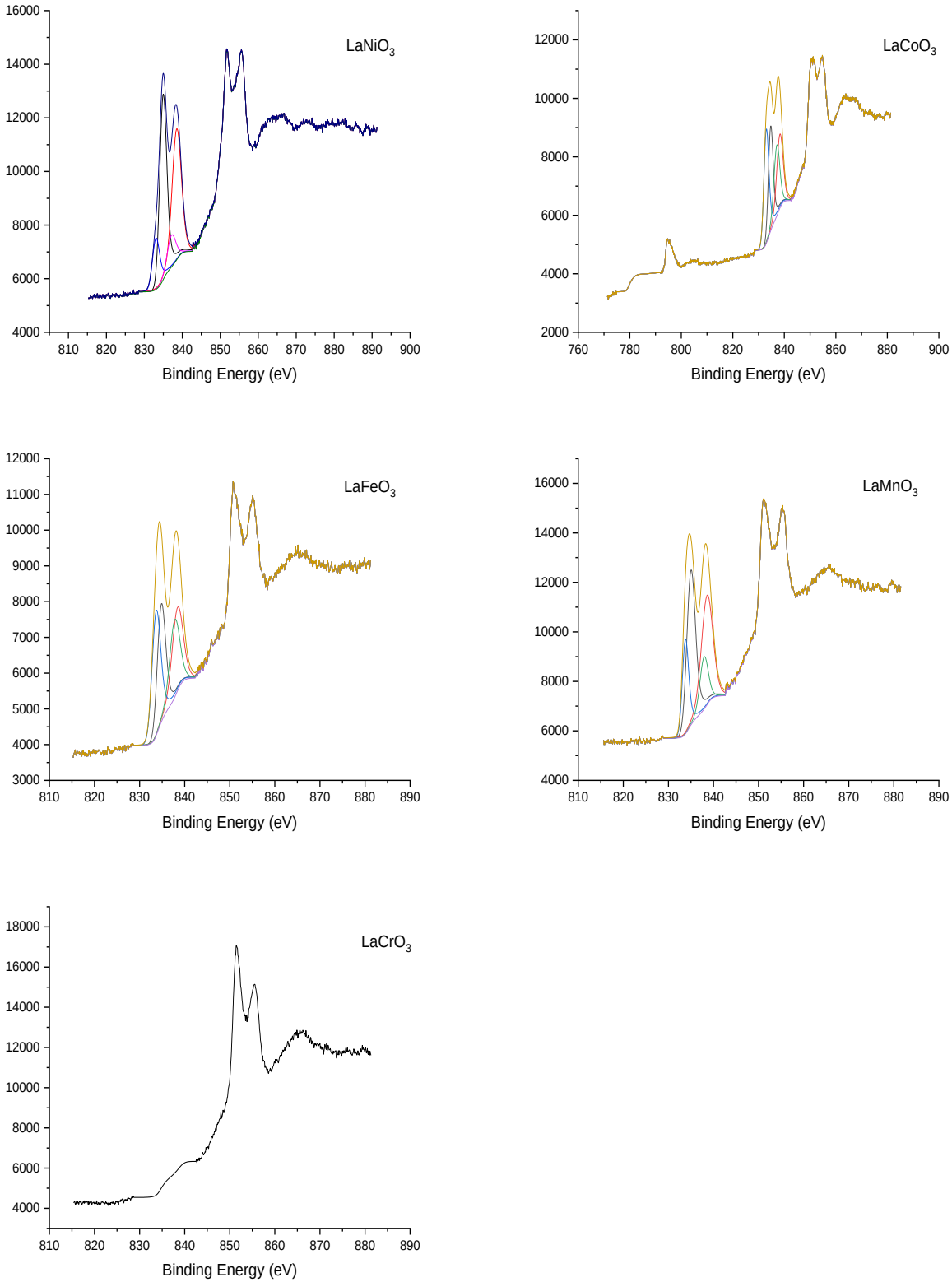

Figure 3.11(b) XPS plots of AuPt/$LaBO_3$ catalysts for La ($3d_{5/2}$) spectra. La_2O_3 (red line), $LaBO_3$ (Blue line).

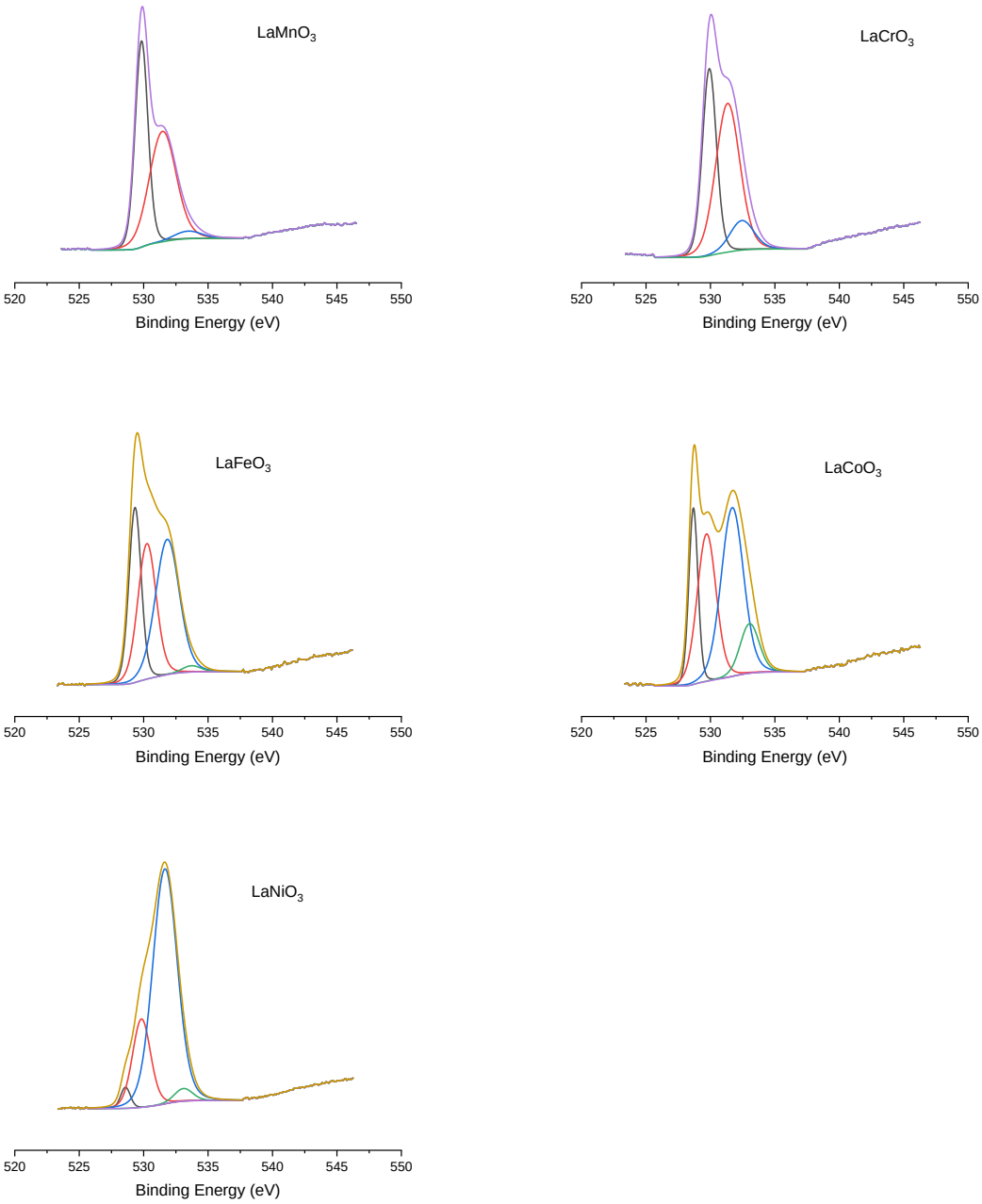

Figure 3.11 (c) XPS plots of AuPt/$LaBO_3$ catalysts for O (1s/4) spectra. O 1s from $LaBO_3$ (red line), La_2O_3 (black line), Hydroxides (blue line) and Water (green line).

The O 1s XPS spectra for the prepared perovskites are shown in Figure 3.11c, which has been categorised into four peaks with each representing a different species of oxygen. The red binding energy peak may be assigned to lattice O species. The black peak can be associated with La_2O_3, while the blue peak can be assigned to chemisorbed surface O or hydroxides

species. In particular, the green peak can be attributed to the adsorbed water species. The peaks (blue line) are assigned based on the observation that the rare earth oxides tend to be hygroscopic when exposed to atmospheric conditions.[28,29] In each perovskite support, the chemisorbed O or OH^- species correspond to the binding energy between 530 and 534 eV, while the lattice oxygen species correspond to the binding energy between 527 and 531 eV. The other two peaks in the binding energy range of 521−528 eV can be attributed to the adsorbed water species or mixed oxides.

Reference

1. Han, X. *et al.* N-doped carbon supported Pt catalyst for base-free oxidation of 5-hydroxymethylfurfural to 2,5-furandicarboxylic acid. *Appl. Catal. A Gen.* **526**, 1–8 (2016).

2. Esen, M., Akmaz, S., Koç, S. N. & Gürkaynak, M. A. The hydrogenation of 5-hydroxymethylfurfural (HMF) to 2,5-dimethylfuran (DMF) with sol–gel Ru-Co/SiO2 catalyst. *J. Sol-Gel Sci. Technol.* **91**, 664–672 (2019).

3. Li, Q. *et al.* Ruthenium supported on CoFe layered double oxide for selective hydrogenation of 5-hydroxymethylfurfural. *Mol. Catal.* **431**, 32–38 (2017).

4. Evans, C. D. *et al.* The preparation of large surface area lanthanum based perovskite supports for AuPt nanoparticles: Tuning the glycerol oxidation reaction pathway by switching the perovskite B site. *Faraday Discuss.* **188**, 427–450 (2016).

5. Chen, R. K. *et al.* The Aldolization Nature of Mn4+-Nonstoichiometric Oxygen Pair Sites of Perovskite-Type LaMnO3 in the Conversion of Ethanol. *ACS Sustain. Chem. Eng.* **6**, 11949–11958 (2018).

6. Huang, X., Zhao, G., Wang, G. & Irvine, J. T. S. Synthesis and applications of nanoporous perovskite metal oxides. *Chem. Sci.* **9**, 3623–3637 (2018).

7. Nair, M. M., Kaliaguine, S. & Kleitz, F. Nanocast LaNiO3 perovskites as precursors for the preparation of coke-resistant dry reforming catalysts. *ACS Catal.* **4**, 3837–3846 (2014).

8. Afzal, S., Quan, X. & Zhang, J. High surface area mesoporous nanocast LaMO3 (M = Mn, Fe) perovskites for efficient catalytic ozonation and an insight into probable catalytic mechanism. *Appl. Catal. B Environ.* **206**, 692–703 (2017).

9. Wang, Y. *et al.* Nanocasted Synthesis of Mesoporous LaCoO 3 Perovskite with Extremely High Surface Area and Excellent Activity in Methane Combustion. 15293–15298 (2008).

10. Russo, N., Fino, D., Saracco, G. & Specchia, V. Promotion effect of Au on perovskite catalysts for the regeneration of diesel particulate filters. *Catal. Today* **137**, 306–311 (2008).

11. Komova, O. V *et al.* The Formation of Perovskite during the Combustion of an Energy-Rich Glycine – Nitrate Precursor. 21–23 (2020).

12. Evans, C. D. *et al.* The preparation of large surface area lanthanum based perovskite supports for AuPt nanoparticles: Tuning the glycerol oxidation reaction pathway by switching the perovskite B site. *Faraday Discuss.* **188**, 427–450 (2016).

13. Camera, C. C. S. P. 产 品 规 格 书 Product Specification. 63103.

14. Deng, X., Chen, K. & Tüysüz, H. Protocol for the Nanocasting Method: Preparation of Ordered Mesoporous Metal Oxides. *Chem. Mater.* **29**, 40–52 (2017).

15. Tepech-Carrillo, L. *et al.* Preparation of Nanosized LaCoO3 through Calcination of a Hydrothermally Synthesized Precursor. *J. Nanomater.* **2016**, (2016).

16. Zhu, W. *et al.* Hierarchical Regulation of LaMnO3Dual-Pathway Strategy for Excellent Room-Temperature Organocatalytic Oxidation Performance. *Inorg. Chem.* (2022) doi:10.1021/acs.inorgchem.2c00521.

17. Tarjomannejad, A., Zonouz, P. R., Masoumi, M. E., Niaei, A. & Farzi, A. LaFeO3 Perovskites Obtained from Different Methods for NO + CO Reaction, Modeling and Optimization of Synthesis Process by Response Surface Methodology. *J. Inorg. Organomet. Polym. Mater.* **28**, 2012–2022 (2018).

18. Lian, J. *et al.* Ni Supported on LaFeO3 Perovskites for Methane Steam Reforming: On the Promotional Effects of Plasma Treatment in H2–Ar Atmosphere. *Top. Catal.* **60**, 831–842 (2017).

19. Heidinger, B., Royer, S., Alamdari, H., Giraudon, J. M. & Lamonier, J. F. Reactive grinding synthesis of LaBo3 (B: Mn, Fe) perovskite; properties for toluene total oxidation. *Catalysts* **9**, 1–18 (2019).

20. Jeon, Y. *et al.* Hollow fibers networked with perovskite nanoparticles for H 2 production from heavy oil. *Sci. Rep.* **3**, (2013).

21. Rumplecker, A., Kleitz, F., Salabas, E. L. & Schüth, F. Hard templating pathways for the synthesis of nanostructured porous Co 3O4. *Chem. Mater.* **19**, 485–496 (2007).

22. Huang, X. *et al.* Au–Pd separation enhances bimetallic catalysis of alcohol oxidation. *Nature* **603**, 271–275 (2022).

23. Douthwaite, M., Powell, N., Taylor, A., Ford, G. & López, M. Glycerol Selective Oxidation to Lactic Acid over AuPt Nanoparticles ; Enhancing Reaction Selectivity and Understanding by Support Modification. 3097–3107 (2020) doi:10.1002/cctc.202000026.

24. Villa, A. *et al.* Exploring the effect of Au/Pt ratio on glycerol oxidation in presence and absence of a base. *Catalysts* **8**, (2018).

25. Jones, D. R. *et al.* Selective Hydrogenation of Levulinic Acid Using Ru/C Catalysts Prepared by Sol-Immobilisation. *Top. Catal.* **61**, 833–843 (2018).

26. Dimitratos, N. *et al.* Solvent-free oxidation of benzyl alcohol using Au – Pd catalysts prepared by sol immobilisation. 5142–5153 (2009) doi:10.1039/b900151b.

27. Carrettin, S. *et al.* Oxidation of glycerol using supported Pt , Pd and Au catalysts. 1329–1336 (2003) doi:10.1039/b212047j.

28. De Asha, A. M., Critchley, J. T. S. & Nix, R. M. Molecular adsorption characteristics of lanthanum oxide surfaces: The interaction of water with oxide overlayers grown on Cu(111). *Surf. Sci.* **405**, 201–214 (1998).

29. Mickevičius, S. *et al.* Investigation of epitaxial LaNiO3-x thin films by high-energy XPS. *J. Alloys Compd.* **423**, 107–111 (2006).

Chapter 4

Selective Catalytic Oxidation of 5-Hydroxymethyl furfural to 2,5-furandicarboxylic Acid

4.1 Introduction

Valorisation of HMF through selective oxidation and reduction using heterogeneous catalysts to produce commodity chemicals remains a subject of interest.[1–3] Parameters such as catalyst choice, nature of the metal nanoparticles and reaction conditions need to be optimised to enhance and control the selectivity and rate of the reaction.

The application of heterogeneous catalysts for this process allows for an additional avenue to control reaction selectivity. The main oxidation product of HMF is 2,5-furandicarboxylic acid (FDCA) is a precursor to produce these green polymers, especially polyethylene 2,5-furandicarboxylate (PEF), which is a bio renewable alternative to the fossil based terephthalic acid (TPA) derived polyethylene terephthalate (PET). PEF will not only serve as a novel replacement but will also improve salient features like excellent gas barrier performance, recyclability and extended mechanical properties. Despite all the efforts and scientific research, the worldwide production of polymer for bioplastics is only a fraction of the total market supply.[4] FDCA is recorded as one of the twelve most important value-added chemicals by the United States Department of Energy because of its significant potential applications.[1] Thus, catalytic conversion of HMF to FDCA is a process with high potential and numerous catalysts have been investigated for this reaction.[5] Although metal oxide and enzyme catalysts have been studied for this reaction, precious metal catalysts showed higher catalytic performance and FDCA selectivity.[6]

It has been demonstrated that the reaction conditions can significantly influence the product selectivity and rate of the reaction. Increasing the reaction temperature has been found to

increase the FDCA selectivity.[7] However, it was suggested that this will lead to the decrease in stability of HMF at elevated temperatures. Increasing the HMF to base ratio in the reaction mixture was found to increase the rate of reaction. It was proposed that the presence of base significantly increases the initial deprotonation reaction of alcohol group on the HMF to produce the corresponding alkoxide.[8] Under strong base condition, HMF is said to undergoes side reactions involving ring opening to form products such as formic acid and levulinic acid which can lead to the formation of humins (polymers). However, it was reported that by replacing NaOH with organic base such as n-butylamine and modifying the surface of the catalysts will increases HMF stability and the possibility to tune the selectivity for other valuable products.[4] From an industrial point of view, base free oxidation is more desirable as it reduces reagent costs, removes the need for additional purification steps of FDCA and limits side product formation. There have been several publications investigating the oxidation of HMF under base free conditions CeO_2 and TiO_2 supported Ru, for instance, are able to drive this reaction under base-free conditions, with a 60% yield to FDCA after 18 h, at 140 °C. nNiO supported AuPd also reported to have high activity under base free conditions, with 95% conversion rate and 70% FDCA selectivity after 6 h at 90 °C, 10 bar.[4,5,9–12] However, it has not been possible to replicate the high rates showed under base involving reaction conditions.[13]

Based on the literature, the two fundamental areas that require further investigation; the oxidation of HMF under base free conditions; and maximising the FDCA selectivity by determining a way to supress the formation of by-products (humins). Therefore, this chapter is focussed on addressing these issues.

4.2. Aim and objectives.

4.2.1. Aim

The aim of this chapter is to investigate the role of AuPt supported on $LaBO_3$ (where B = Cr, Mn, Fe, Co or Ni) for the selective of oxidation of HMF to FDCA, in the presence of base and under base free conditions.

4.2.2. Objectives

The following were the objectives of the project in this chapter.

- To optimize the reaction conditions that help in the understanding of the performance of the 1wt% AuPt/$LaMnO_3$ catalyst.
- To investigate the oxidation of HMF under base free reaction conditions using 1wt% AuPt catalysts on perovskite supports.
- Modification of the Au Pt catalysts with tert-butylamine on the surface to develop a greater understanding of the reaction profile.
- To apply a statistical approach using response surface methodology to understand reaction variables interaction for the oxidation of HMF using 1wt% AuPt catalysts.

4.3 Result and Discussion

4.3.1 Catalyst Testing

The oxidation of HMF to FDCA was performed using the initial conditions 110 ℃, 4:1 base: substrate ratio, 3 bar oxygen pressure, 5 mmol HMF, 50 mg catalyst, and to gain an effective understanding of the reaction, a systematic approach was undertaken, altering the reaction conditions, and monitoring the effect these parameters have on the reaction. The variables investigated were reaction time, temperature, and ratio of base to HMF for batch reactions using a colaver reactor.

4.3.1.1 Catalyst Supports

Before the reaction conditions were investigated, a starting point (110 ℃, 4:1 base: substrate ratio, 3 bar oxygen pressure, 5 mmol HMF, 50 mg catalyst) that successfully produced high FDCA yield were chosen to investigate whether the perovskite oxide supports have an activity in HMF oxidation with base and without base. A blank reaction was also conducted as a comparison with no catalyst added and the result was shown in Table 4.1. From the results obtained, full conversion of HMF was achieved at 24 hours and a range of oxidation products were formed with the addition of NaOH, with poor selectivity to the main oxidation products (HMFCA, DFF, FFCA and FDCA) which is similar product distribution to that obtained with the blank experiment. Other products such as maleic acid, maleic anhydride, succunic acid and by-products (humins) were also detected. In the absence of NaOH, there is no significant conversion of the HMF over a period of 24 hours with HMFCA and FFCA the only oxidation products. This shows that any activation of the reaction will be due to the nanoparticles deposited on to the surface and the perovskite supports do not show any catalytic activity for the formation of FDCA from HMF. The small amounts of oxidation products are responsible for the non-catalytic oxidation of the carbonyl group in HMF under alkaline conditions, which is consistent with previous reports.[14,15]

Table 4.1 HMF Oxidation in the presence of $LaMO_3$ catalysts. Conditions: 5mmol HMF, 50 mg Catalyst amount, 110 ℃ **reaction temperature, 3 bar oxygen pressure, 1:4 HMF to base molar ratio, and 24 reaction time. NC= Not calculated.**

Catalyst	Base	HMF Con (%)	Selectivity (%)				CMB (%)
			HMFCA	FFCA	FDCA	Others	
$LaCrO_3$	NaOH	100	23	14	12	51	98
$LaCrO_3$	-	2	100	-	-	-	100
$LaMnO_3$	NaOH	100	27	9	20	44	91
$LaMnO_3$	-	9	78	22	-	-	100
$LaFeO_3$	NaOH	100	28	7	17	48	93
$LaFeO_3$	-	8	89	11	-	-	99
$LaCoO_3$	NaOH	100	33	12	8	47	93
$LaCoO_3$	-	8	84	16	-	-	100
$LaNiO_3$	NaOH	100	12	3	15	70	96
$LaNiO_3$	-	6	92	8	-	-	100
Blank	NaOH	99	17	27	20	NC	79

4.3.1.2 Initial Catalyst Screening

Au, Pt and mixture of both nanoparticles have been found to be highly active for HMF oxidation on a range of different catalyst supports.[1,7] For this reason, a time online study for 1% AuPt supported on $LaMO_3$ (M is Cr, Mn, Fe, Co and Ni) prepared by sol immobilization method[14] was carried out under standard reaction conditions (5 mmol HMF concentration, 110 ℃ reaction temperature, 50 mg catalyst amount, 3 bar oxygen pressure, 4:1 NaOH:HMF

molar ratio, and 1000 rpm agitation velocity).

The effect of changing the B-site element within the perovskite support catalysts was investigated, and the corresponding reaction profiles was displayed in Table 4.2. The conversion of HMF in the experiments is similar for all the catalysts and it was 100%, even at the beginning of the experiment. The $LaMnO_3$ supported catalyst showed that the selectivity towards FDCA gradually increases as the reaction proceeds with time which is a result of the sequential oxidation of HMFCA. It is thought that the formation of FDCA proceeds through the intermediate FFCA, but this product has not been observed because the step has been found to be faster when carried out in a basic reaction medium. DFF which is also a HMF oxidation product was not detected as reactions in basic medium favoured initial oxidation of aldehyde group on the HMF to HMFCA. The $LaCrO_3$ and $LaCoO_3$ catalyst support clearly showed a high HMFCA selectivity at early of the reaction which decreases over time. In each of the catalyst, no DFF product was detected meaning that the oxidation mechanism followed through the oxidation of aldehyde group on HMF ring not the alcohol group. This could be attributed to the basic nature of these perovskite support which can be seen in the TPD data in characterization section. Previously, it was reported that the oxidation of HMFCA to FFCA is the rate determining step on Au/HT. The intermediate HMFCA is oxidized to FFCA by the formation of metal alcoholate species via metal–hydride shift which was facilitated by the basicity of HT.[16]

The $LaFeO_3$ catalyst support showed that the HMFCA concentration remained unchanged after 150 mins. In contrast, the FFCA intermediate was completely oxidized to FDCA. This wasn't observed for any other perovskite supported AuPt. This observation led to the assumption that the AuPt/$LaFeO_3$ lost it capability to oxidize HMFCA completely after 150 mins. The loss of catalytic activity for the further oxidation of the HMFCA intermediate might be caused by the adsorption of the organic molecules which are formed during the

reaction on the active site of nanoparticles surface as previously reported on Au/CeO_2 and Au/TiO_2 catalysts.[17] Another possible reason was due to presence of Fe on the surface of the catalyst near the Pt and Au nanoparticles as revealed by the XRD and XPS which postulated to decease in the interaction between Pt Au metals and aldehyde group (C=O) on HMFCA as Similarly observed by Jin *et al.*,[18] in the oxidation of glycerol. The fastest formation of FDCA, connected with the highest selectivity was observed in $LaMnO_3$ support and goes in the order $LaMnO_3$ > $LaCrO_3$ > $LaNiO_3$ > $LaCoO_3$ >$LaFeO_3$. FDCA formation began almost immediately after the reaction was started. It was previously reported for Au/HT in base free HMF oxidation that the conversion of both intermediates (HMFCA and FFCA) occurred rapidly because of the basicity of the support, and hence resulting in a high yield of FDCA.[16] Another study was carried out to see whether the oxidation of HMF can be influenced by the leaching of Au and Pt species. The experiments were performed in the presence of the 1wt% $AuPt/LaFeO_3$ catalyst. The catalyst was separated from reaction mixture after 60 mins and the remaining solution was further reacted up to 180 mins. The results showed that after catalyst-removal, the amount of HMFCA, FFCA and FDCA remain unchanged (Figure 4.1). The results obtained suggest that either no Pt species leached from the catalyst, or the amount leached into reaction solution was not catalytically active anymore. The results of microwave plasma atomic emission spectroscopy analysis (MP-AES) of the final reaction mixture after 8h showed that less 2 % of total 0.5wt% of Pt was leached out into the reaction solution from the catalyst. No Au was detected in the reaction mixture.

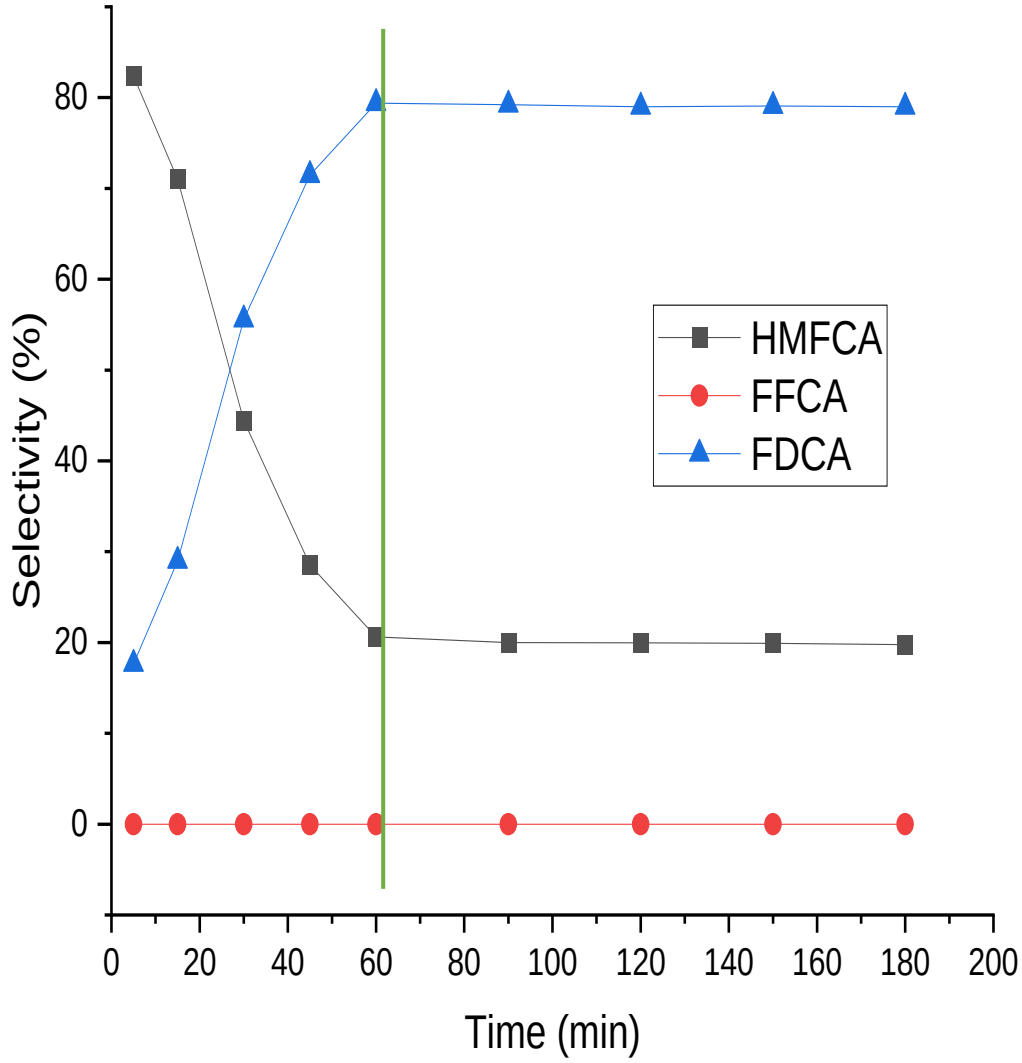

Figure 4.1. Selectivity profile of product for 1wt% AuPt/LaFeO3 within (0-60 mins) and after catalyst removal (60-180 min) in the reaction mixture. Conditions: 5 mmol HMF concentration, 4:1 NaOH:HMF molar ratio, 3 bar oxygen pressure, 110 °C reaction temperature, 50 mg catalyst amount and 1000 rpm agitation velocity.

Table 4.2 Effect of switching B-site element on conversion and selectivity profile using 1wt% AuPt/$LaMO_3$ catalyst. Conditions: 5 mmol HMF, 110 °C reaction temperature, 3 bar oxygen pressure, 50 mg catalyst amount and 1000 rpm agitation velocity.

B-site Element	Time (min)	Selectivity (%)			Carbon Balance (%)
		HMFCA	FFCA	FDCA	
Cr	30	42	1	57	99
	60	24	0	76	89
	90	10	0	90	85
	120	4	0	96	81
	150	0	0	100	84
	180	0	0	100	79
Mn	30	13	0	87	96
	60	4	0	96	89
	90	0	0	100	75
	120	0	1	100	71
	150	0	0	100	68
	180	0	0	100	62
Fe	30	17	1	82	98
	60	11	0	89	96
	90	9	0	91	93
	120	7	0	93	93
	150	6	0	94	84
	180	6	0	94	72
Co	30	74	0	26	95
	60	48	0	52	96
	90	48	0	52	83
	120	20	0	80	76
	150	11	0	89	71
	180	3	0	97	69
Ni	30	28	1	72	95
	60	16	0	84	96
	90	10	0	90	85
	120	4	0	96	79
	150	3	0	97	79
	180	1	0	99	75

4.3.1.3 Experiment on the Effect of Reaction Conditions

The conditions used for initial catalysts screening on different perovskite support provide a good example of how the reaction is sensitive to environmental conditions in which it occurs. In order to develop a greater understanding on how the experimental conditions effect the performance of the $AuPt/LaMO_3$ catalysts, parameter mapping experiments need to be conducted using the catalyst that showed high FDCA selectivity.

4.3.1.3.1. Effect of Reaction Temperature.

Temperature is vital parameter for the HMF oxidation reaction. Therefore, as the reaction temperature has such a profound effect, it was reasoned that it should be the first variable to be studied with the results shown in Table 4.3 below. At 50 °C HMFCA was the major product. These results indicate that on $AuPt/LaMnO_3$ catalyst the aldehyde group of HMF is more easily oxidized than the alcohol group in the presence of base as observed previously for Au based catalysts.[14,17,19] Raising the temperature to 80 °C, FDCA was formed as a major product with a high selectivity. Below 90 °C, the rate of the oxidation of HMFCA to FFCA is slower than the rate of the oxidation of FFCA to FDCA. This behaviour was also observed for Au based catalysts where oxidation of HMFCA to FFCA was considered as rate determining step in HMF oxidation.[17] The highest yield of FDCA of 99 % was obtained at 140 °C. In all cases, full conversion of HMF was observed at the initial rate except for 50 °C where full HMF conversion takes 120 min as shown in Figure 4.2. No C-C cleavage products was observed in the absence of catalyst were detected in the effect of temperature, however, HMF degradation products were detected which is because of the base addition that caused the degradation of the substrate to humins.

Table 4.3 Effect of temperature on selectivity profile of the products using sol immobilized 1wt% AuPt/$LaMnO_3$. Conditions; 5 mmol HMF, 50 mg catalyst, 3 bar oxygen pressure, 4:1 NaOH : HMF ratio, stirring rate of 1000 rpm.

Temperature (°C)	Time (min)	Selectivity (%)		
		HMFCA	FFCA	FDCA
50	30	91	6	3
	60	86	4	10
	90	79	1	10
	120	73	0	27
	150	68	0	32
	180	61	0	39
80	30	47	4	49
	60	31	0	69
	90	19	0	81
	120	9	0	91
	150	4	0	96
	180	1	0	99
110	30	13	0	87
	60	4	0	96
	90	1	0	99
	120	0	0	100
	150	0	0	100
	180	0	0	100
140	30	2	0	98
	60	0	0	100
	90	0	0	100
	120	0	0	100
	150	0	0	100
	180	0	0	100

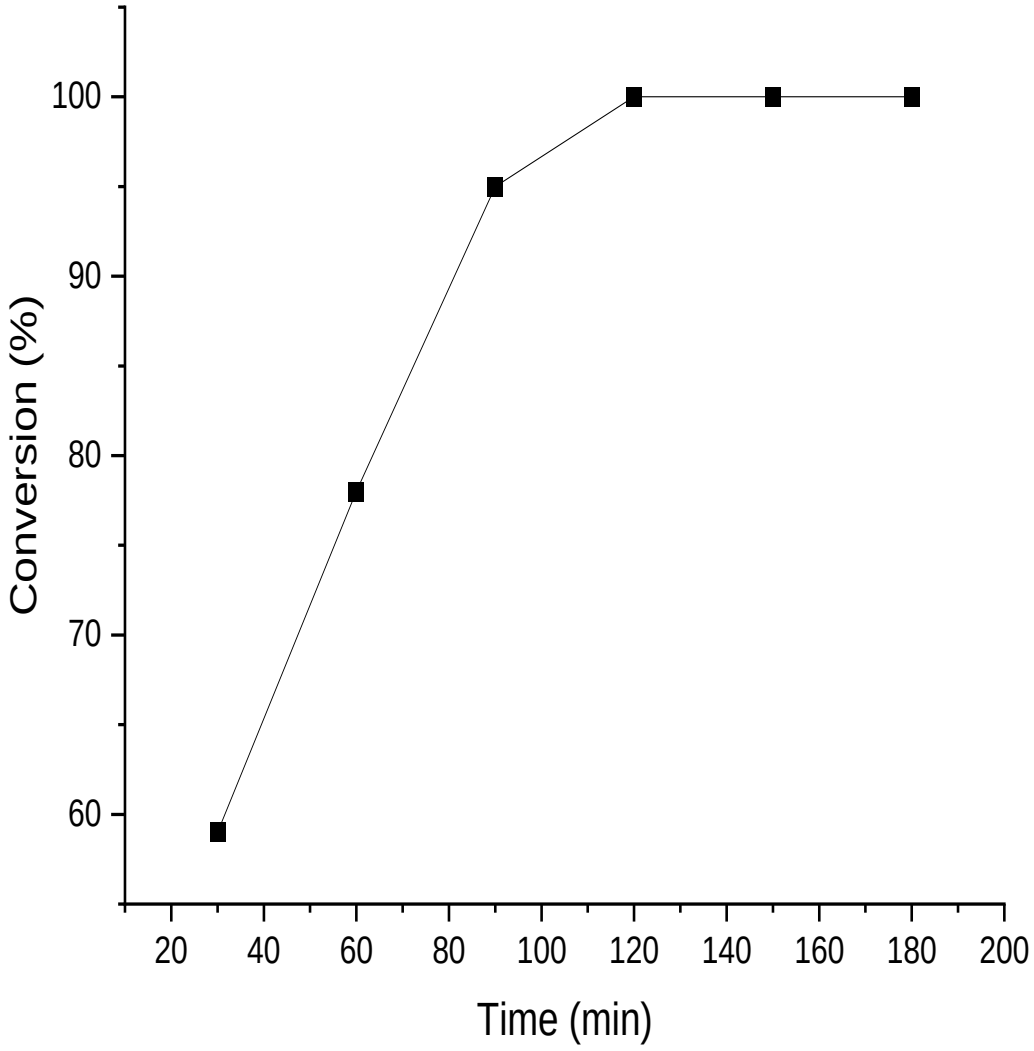

Figure 4.2 HMF conversion time online for 50°C reaction temperature for the 1wt% AuPt/$LaMnO_3$ catalyst.

From these results it can be concluded that a higher temperature clearly favours FDCA production and is needed to fully convert HMFCA and FFCA which is crucial when attempting to selectively produce FDCA, therefore the temperature carried forward for further reactions will be set at 110 °C.

4.3.1.3.2 Effect of Oxygen Pressure

Oxygen is also a vital parameter in HMF oxidation reaction and plays a significant role in product selectivity. The effect of oxygen pressure on the system involves several key mechanisms which are complicated further by mass transfer limitations.[20] These can limit the mobility of oxygen molecules from the gas phase to the catalyst interface, meaning that there are certain drawbacks associated to the used of pressure beyond the boundary limit of reactor, as going beyond the pressure capacity of the reactor will leads to the mass transfer limitations which could affect chemical interactions by oxygen pressure. Therefore, the effect of oxygen pressure on HMF conversion and products yield was studied with oxygen pressure varied from 1 to 4 bar while other parameters were kept constant, and the results shown in Figure 4.3.

The conversion of HMF for the oxygen pressure experiment conducted under the standard reaction conditions (110 ℃ reaction temperature, 5 mmol HMF, 50 mg catalyst a, 4:1 NaOH to HMF molar ratio and 1000 rpm) was always 100%, therefore the conversion data is omitted for clarity. HMFCA and FDCA were the only oxidation products observed in all experiments. FFCA an intermediate product was not detected, and this confirmed the temperature study results that FFCA to FDCA is the fastest elementary step in this reaction. HFMCA is initially the major product at lower oxygen pressure (1 to 2 bar) but then decreases with time as it is further oxidised to FDCA. Above 2 bar oxygen pressure, FDCA was found to be the major product with close to 100% yield after 90 minutes. It should be noted that increasing the pressure further, does not increase the rate of FDCA formation which remains relatively stable beyond 3 bar, indicating that the oxygen pressure does not influence the reaction but rather served as an electron scavenger. It noted that the carbon balance decreases 68% with increased reaction time (Figure 4.4). However, at lower reaction time there was negligible effect on carbon balance. This effect is attributed to the formation

of unwanted side products.

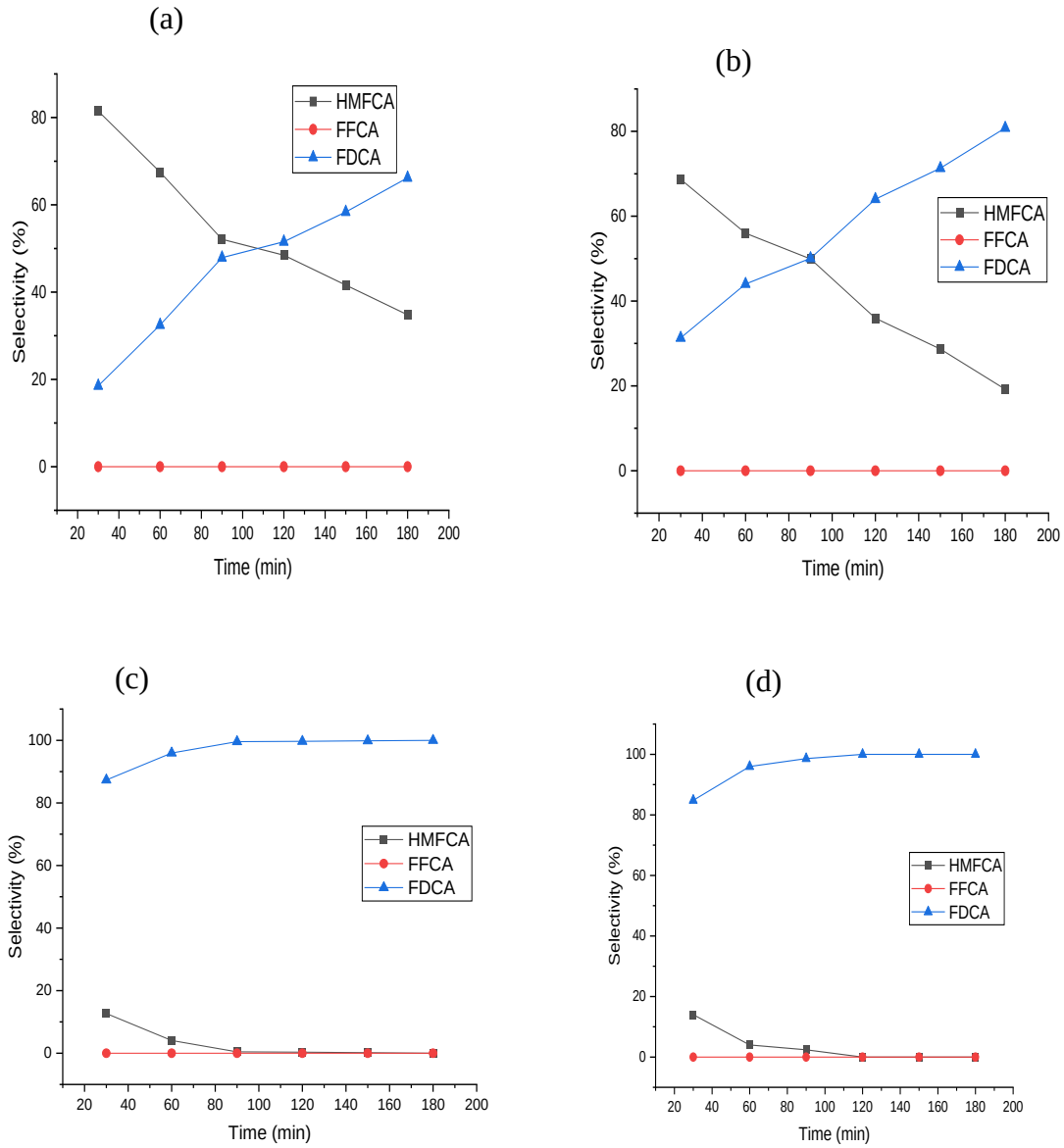

Figure 4.3 Effect of oxygen pressure on selectivity profile of the products using sol immobilized 1wt% AuPt/LaMnO$_3$. Conditions; 5 mmol HMF, 50 mg catalysts amount, 180 min reaction time, 110 ℃ reaction temperature, 4:1 NaOH: HMF ratio and 1000 rpm. (a) 1 bar (b) 2 bar (c) 3 bar (d) 4 bar.

The presented results show that the catalytic performance of the AuPt/$LaMnO_3$ in HMF oxidations depends on oxygen pressure (which changes the dissolved oxygen content in the water phase). In this study no catalyst deactivation was detected at the optimum oxygen pressure of 3 bar. It has previously been reported that Pt catalysts seem to be sensitive to high oxygen content and can deactivate with time, although Au catalyst are not reported to deactivate under high oxygen pressure in strong basic solutions.[11,14,17]

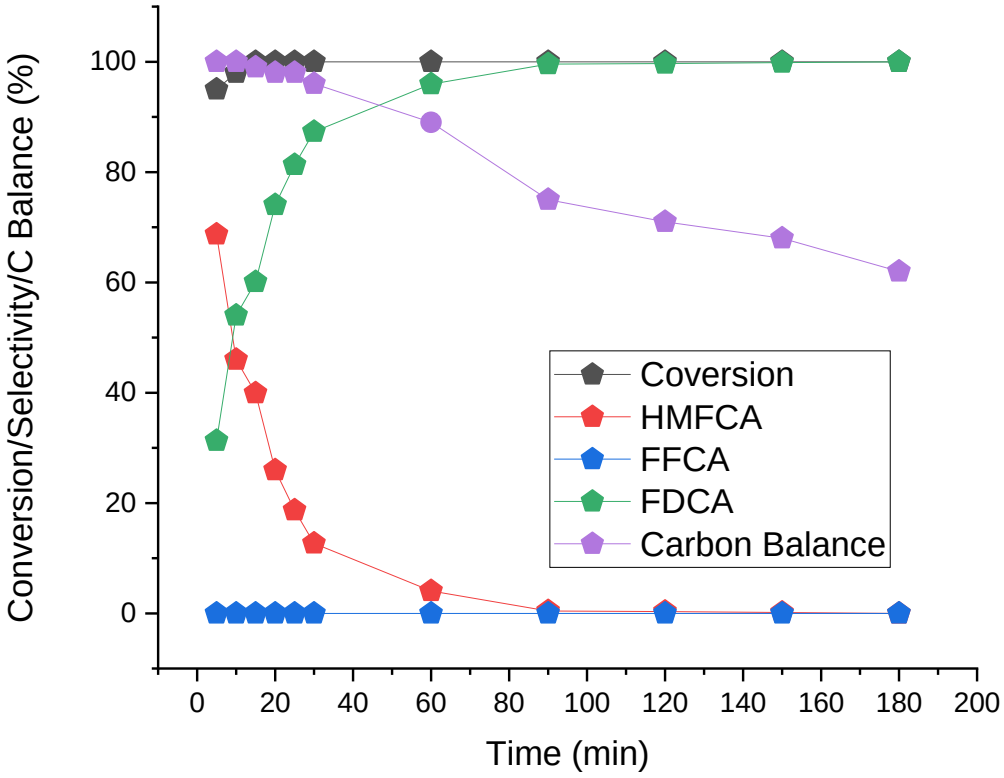

Figure 4.4 showing carbon balance for HMF oxidation using 1% AuPt/$LaMnO_3$ at 3 bar oxygen pressure.

4.3.1.3.3 Effect of NaOH to HMF Molar Ratio.

As stated in the literature, addition of base has been shown to produce significant changes to the selectivity profile for HMF oxidation. This is because the hydroxide anion acts as a promoter within the reaction system as highlighted in the introduction section. To investigate the impact of the base, different NaOH: HMF molar ratios were explored using the previously established reaction conditions.

The conversion of HMF remains relatively low for base free experiments, as can be seen in Table 4.4. As stated in the literature, base free reactions are energy demanding processes, showing that the hydroxide anion is required to promote the reaction.[20,21] The selectivity profile (Table 4.4) displays a few notable trends as the base concentration is increased. Firstly, the selectivity towards FDCA increases dramatically, which illustrates how significant the role the hydroxide anion interaction is for the formation of FDCA. Schade *et al*. reported that increasing the basicity of the solution improved desorption of FDCA from the catalyst surface.[22] In other words, increasing the solubility of FDCA prevents the precipitation of the product onto catalyst surfaces. Secondly, it is noted that the carbon balance decreases as the base ratio increased from 1 to 4 equivalents. This is attributed to the formation of humin through polymerization of competing base catalysed Cannizzaro product.[23] As the base : HMF ratio is increased, the rate of conversion of HMFCA and FFCA to FDCA is faster, (Figure 4.5).

Table 4.4 Effect of NaOH to HMF molar ratio on conversion and selectivity profile using 1wt% AuPt/$LaMnO_3$ catalyst. Conditions: 5 mmol HMF, 110 °C reaction temperature, 3 bar oxygen pressure, 50 mg catalyst and 1000 rpm agitation velocity.

Molar ratio	Time (min)	Conversion (%)	Selectivity (%)				Carbon Balance (%)
			HMFCA	DFF	FFCA	FDCA	
0	30	3	19	71	0	0	100
	60	8	22	78	0	0	99
	90	14	24	74	2	0	100
	120	18	28	61	3	0	101
	150	24	43	47	10	0	100
	180	31	54	37	13	0	100
1:1	30	45	48	0	28	23	100
	60	78	45	0	20	35	99
	90	91	26	0	6	68	98
	120	95	10	0	1	89	95
	150	99	1	0	0	99	95
	180	100	0	0	0	100	96
2:1	30	49	37	0	10	53	98
	60	86	31	0	9	60	96
	90	91	12	0	7	81	93
	120	99	5	0	2	93	93
	150	100	0	0	0	100	84
	180	100	0	0	0	100	72
3:1	30	89	8	0	0	73	95
	60	98	6	0	0	94	96
	90	99	3	0	0	97	83
	120	100	1	0	0	99	76
	150	100	0	0	0	100	71
	180	100	0	0	0	100	69
4:1	30	100	13	0	0	93	96
	60	100	4	0	0	96	89
	90	100	0	0	0	100	75
	120	100	0	0	0	100	71
	150	100	0	0	0	100	68
	180	100	0	0	0	100	62

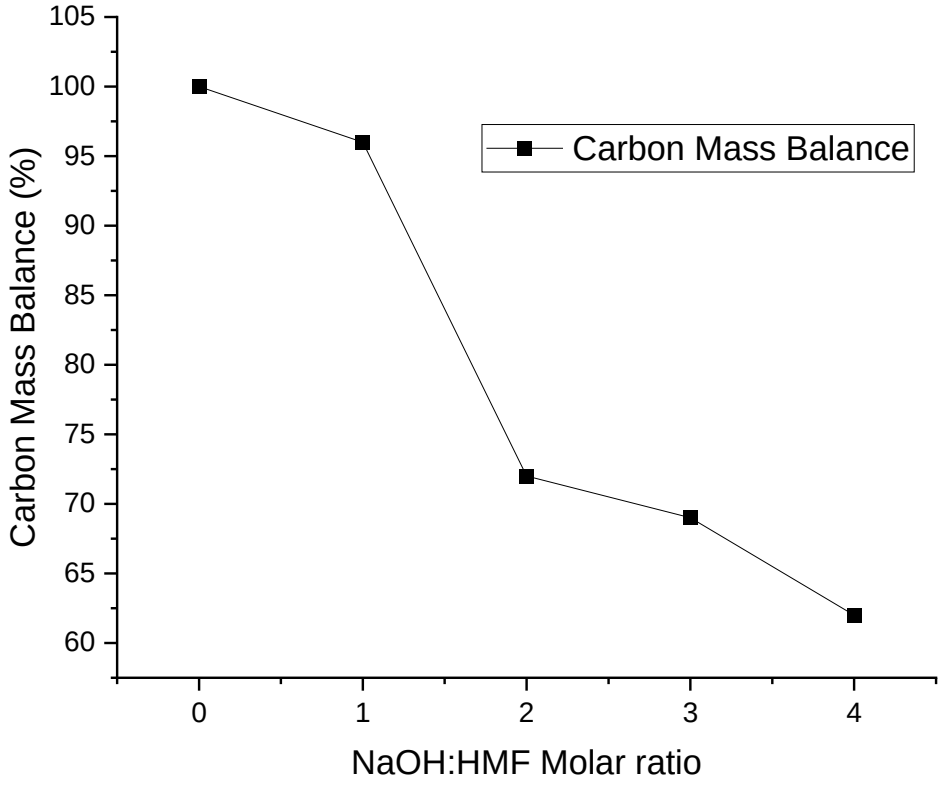

Figure 4.5 Showing the effect of NaOH equivalents on carbon balance at t = 180 mins

The mechanism for the formation of FDCA is a long-debating subject, and therefore the role of base in the formation of FDCA is unclear and will be addressed along with the mechanism later in this chapter. A factor that has been established, however, is that base has been shown to promote the dehydration pathway of hydroxyl group.[24] One hypothesis is that in alkaline medium, the aldehyde side group present in the HMF molecule is rapidly oxidized to the geminal diol through reversible nucleophilic addition. The nucleophilic addition of OH^- to carbonyl radicals and the simultaneous proton transfer from water molecules produces unstable intermediates, hence, followed by geminal diol dehydrogenation which is promoted by the adsorbed OH^- on the catalyst surface results in the formation of COOH, and the aldehyde functional group on HMF is successfully oxidized to carboxylic acid (Figure 4.6).[20]

Regardless of the catalyst used the oxidation of alcoholic group on the HMF requires base to initiate the deprotonation of the alcohol group thereby forming alkoxy intermediates which is further oxidised to FFCA and FDCA.[20,24] From the base free experiment (Table 4.4) it can be seen that, although the conversion is relatively low, the selectivity to HMFCA and DFF intermediates is high. As the reaction proceeds the selectivity to HMFCA increases over time as DFF selectivity decreases, which suggests that at longer time, the equilibrium that exists between HMFCA and DFF shifts in favour of HMFCA. The absence of further oxidation products with high DFF selectivity suggests that the formation of FFCA and FDCA occurs *via* the oxidation of aldehyde group of the HMF rather than alcohol group.

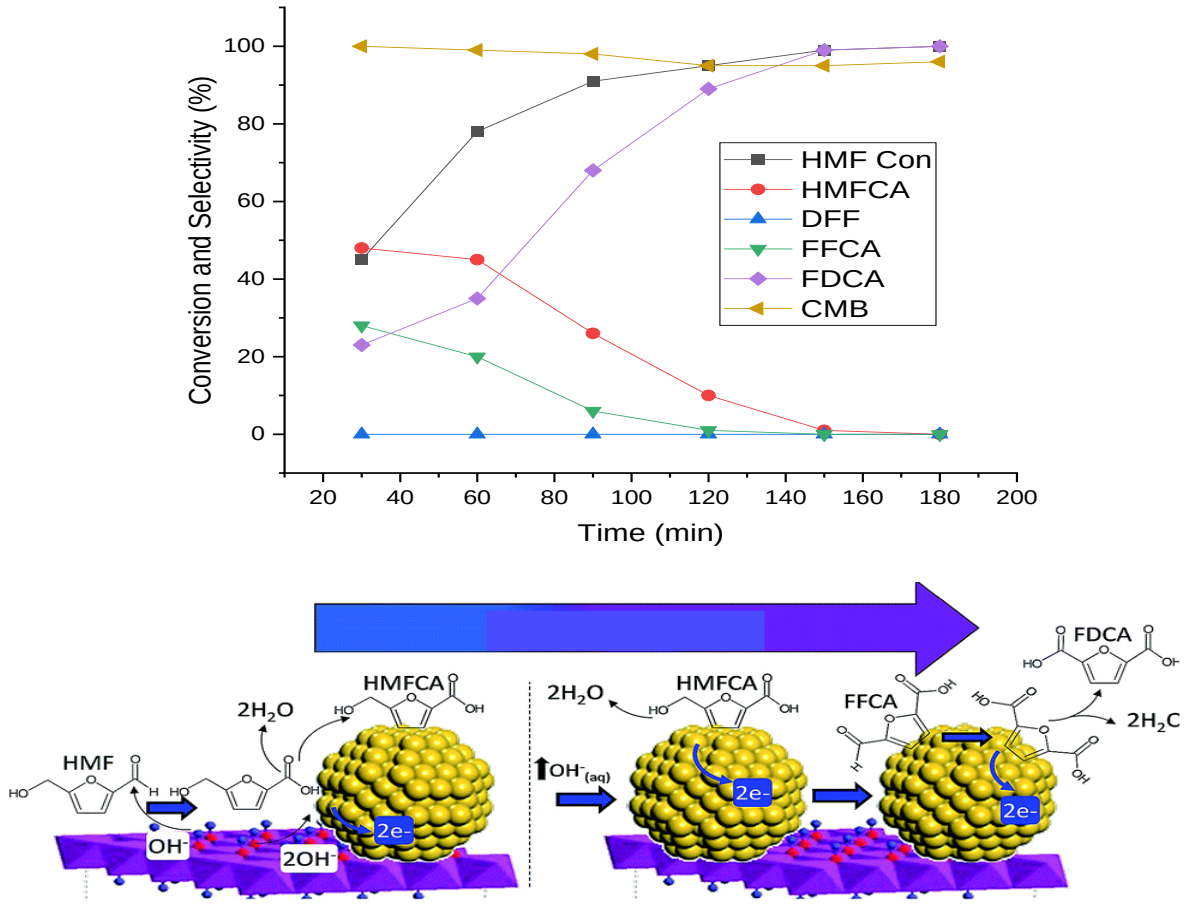

Figure 4.6 Showing the mechanism of HMF oxidation using AuPt/LaMnO3 catalyst at 1:1 NaOH:HMF ration.[24]

As a base concentration is required to optimise the production of FDCA, the competing base catalysed Cannizzaro reaction between intermediate products occurred at higher base ratio, as such the base to substrate ratio selected to facilitate higher FDCA yield is 1:1.

4.3.2 Oxidation of HMF under Base Free Condition using 1wt% AuPt/$LaMO_3$ Catalysts.

4.3.2.1 Effect of the support

It was recently reported that a high yield of FDCA (≥ 99) was obtained by the oxidation of HMF in base free aqueous solution on an Au/HT (Hydrotalcite) catalyst under an ambient oxygen pressure at 90 °C.[16] However, in this study, the HMF oxidation was performed in base free reaction medium under 110 ℃ reaction temperature, 5 mmol HMF concentration, 24 h hour reaction time, 3 bar oxygen pressure, 50 mg catalyst amount and 1000 rpm agitation velocity, to obtain information about the behaviour of the perovskite support in base free solution.

Table 4.5 HMF conversion and selectivity profile for the base free reaction using 1wt% AuPt/$LaBO_3$ catalysts. Conditions: 5 mmol HMF, 110 ℃ reaction temperature, 3 bar oxygen pressure, 50 mg catalyst amount and 1000 rpm agitation velocity.

B-site Element	Time (hours)	Conversion (%)	Selectivity (%)				Carbon Balance (%)
			HMFCA	DFF	FFCA	FDCA	
Cr	3	13	17	**32**	36	15	101
	6	15	18	0	63	18	99
	12	19	16	0	52	32	100
	24	21	12	0	41	47	100
Mn	3	42	37	59	4	0	100
	6	51	56	41	0	4	100
	12	56	15	27	0	58	99
	24	63	2	0	24	74	99
Fe	3	29	12	75	13	0	100
	6	38	6	17	36	41	100
	12	48	4	0	38	58	101
	24	58	1	0	27	72	99
Co	3	6	26	0	50	24	100
	6	35	5	0	37	59	100
	12	45	4	0	31	64	99
	24	55	3	0	19	78	98
Ni	2	27	6	0	41	48	100
	6	46	12	0	0	88	99
	12	64	6	0	0	94	100
	24	71	4	0	0	96	97

Table 4.5 shows the results for the time online for 24 hours reaction time. The data clearly shows that the rate of disappearance of the HMF increases with increased reaction time with the best catalyst support arranged in the following increasing order $LaCrO_3$ → $LaCoO_3$ → $LaFeO_3$ → $LaMnO_3$ → $LaNiO_3$. The highest conversion of HMF was observed with $LaNiO_3$

among other perovskite support, and this performance was attributed to the highest basicity of the material among the rest of the perovskite support. It can also be seen that no DFF intermediate was detected with AuPt supported on $LaNiO_3$ and $LaCoO_3$ meaning that the mechanism favours the oxidation of aldehyde group on the HMF rather than alcohol group. This reaction pathway was observed with all experiment when base was added to the reaction mixture, proving that the $LaNiO_3$ and $LaCoO_3$ were more basic in nature. As seen in the ammonia TPD data, these two-perovskite support have lesser acid active site than the other perovskite supports justifying the reason why DFF was missing in the build-up for the FDCA yield. It can be noted that DFF and HMFCA intermediates were present with AuPt supported on $LaCrO_3$, $LaMnO_3$ and $LaFeO_3$, and DFF found to be predominant intermediate at the early stage of the reaction but start to decrease over time. HMFCA increases over time with decrease DFF in these perovskite supports. This phenonium is similar those many catalysts with either neutral or amphoteric support materials.[4,5,10,25] The FDCA selectivity increases for each of the catalysts over time with lowest yield recorded in AuPt/$LaCrO_3$ catalyst and highest yield observed with AuPt/$LaNiO_3$ catalysts.

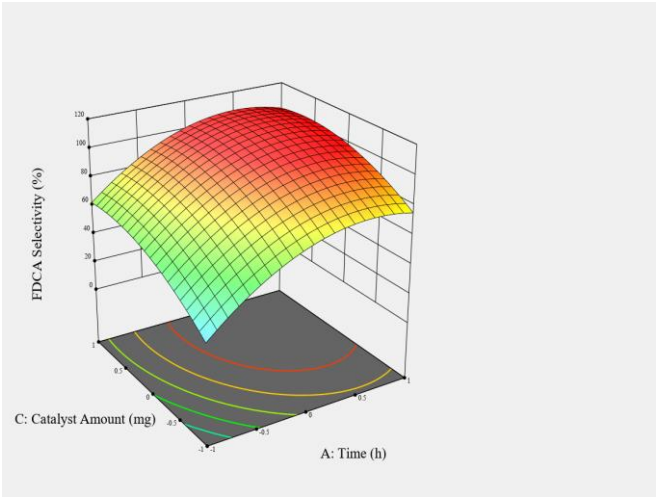

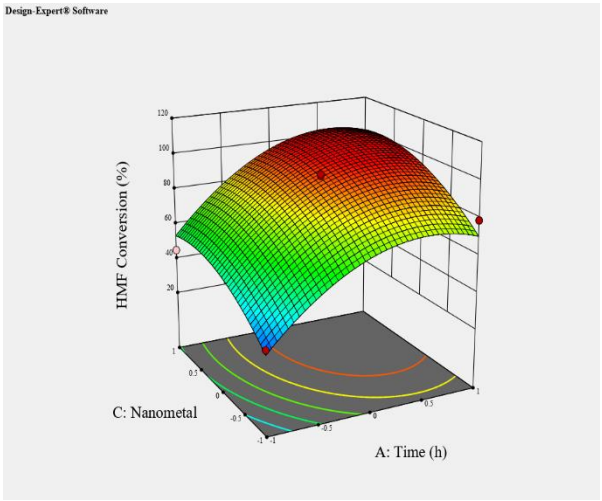

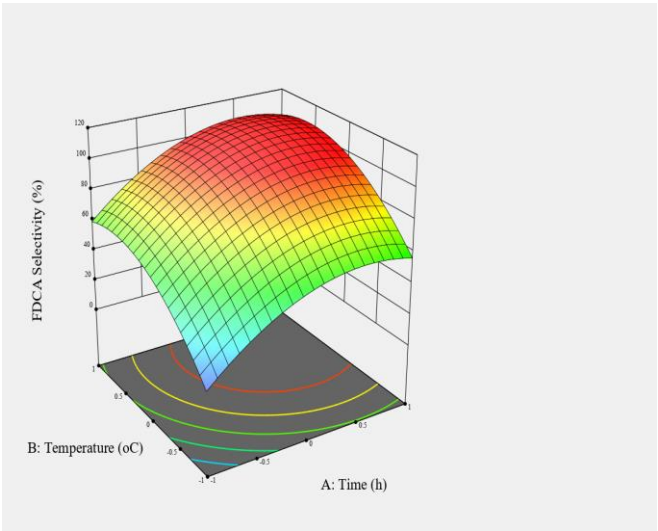

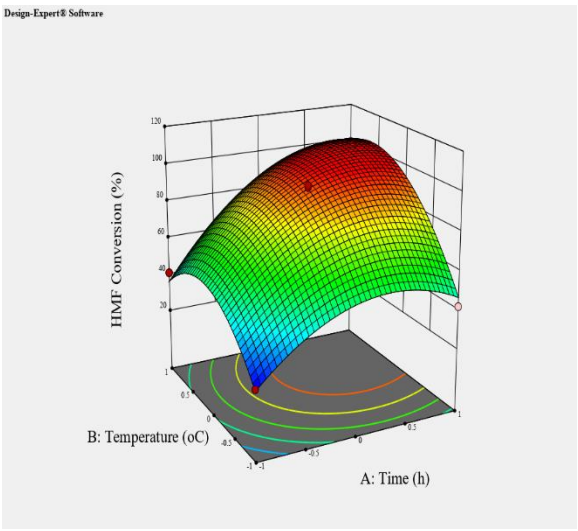

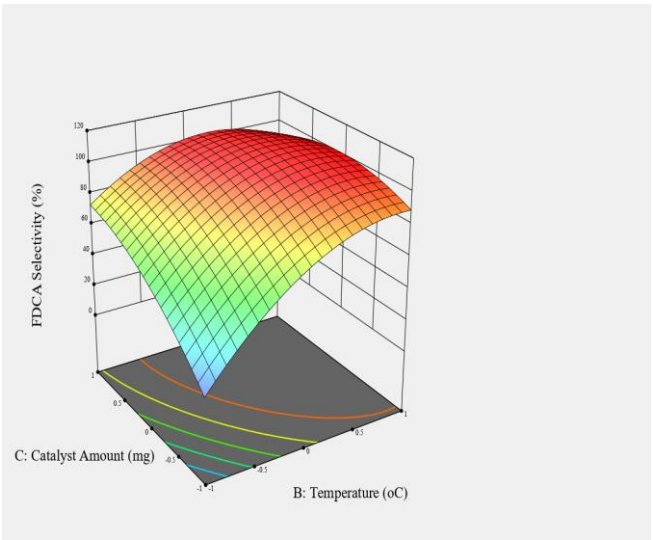

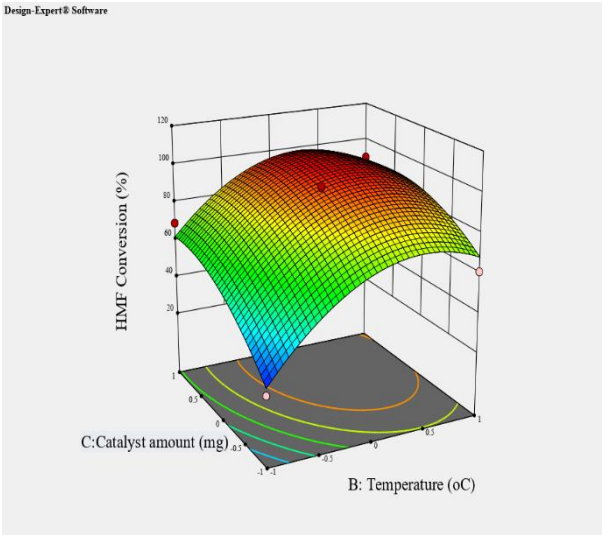

Figure 4.7 Response surface plots for HMF conversion and FDCA selectivity: (a) Catalyst amount vs time (b) Temperature vs Time (c) Catalyst amount vs temperature

Because the $LaNiO_3$ supported AuPt nanoparticles showed the best catalytic performances in base free system, the temporal evaluation of the reaction mixture on these materials was studied in detail by statistical approach using response surface methodology (RSM). Figure 4.7 shows plots of HMF conversion and FDCA selectivity versus binary reaction variables (temperature, catalyst amount and time) for the 1wt% AuPt/$LaNiO_3$ catalysts. The Box-Behnken design (BBD) was employed to run the analysis and based on the data obtained from analysis of variance (ANOVA) revealed that the model obeys quadratic model. Generally, the suitability of the model is confirmed by a higher Fisher's value (F value) with a probability value (p value) that is as low as possible. More specifically, values of "Prob > F″ lower than 0.0500 indicating the model terms are significant. In this case, the HMF conversion is a significant model term.

Additionally, the "Lack of Fit F-value" of 1.30 implies that the Lack of Fit is not significant relative to the pure error, which means the model has good predictability. Thus, the second order polynomial equation that describes the HMF conversion in terms of the actual parameters is given here:

HMF Conversion = $94.20 + 22.12A + 16.88B + 13.50C + 9.75AB + 1.50AC – 4.50BC – 19.98A^2 – 22.98B^2 – 10.72C^2$

Similarly, the result ANOVA shows that the FDCA selectivity follows quadratic model with probability value P-values less than 0.0500 which indicates that the model terms were significant. In this case A, B, C, BC, A^2, B^2 are significant model terms. The Fisher's value of 16.41 also implies that the model is significant. Moreover, the lack of fit F value of 181.03 implies the Lack of Fit is significant meaning that there is only a 0.01% chance that a Lack of Fit F-value this large could occur due to noise (Table 4.6). As a result, the polynomial equation that described the FDCA selectivity is shown below.

FDCA Selectivity = +98.40 + 21.5A + 23B + 15C – 14.5BC – 19.95 A^2 – 20.45B^2

The equation in terms of coded factors can be used to make predictions about the response for given levels of each factor. The high levels of the factors are coded as +1 and the low levels are coded as -1. The coded equation is useful for identifying the relative impact of the factors by comparing the factor coefficients.

Table 4.6 ANOVA results for the quadratic model

Source	Sum of Squares	df	Mean Square	F-value	p-value	
Model	15008.80	9	1667.64	16.41	0.0006	significant
A-Time (h)	3698.00	1	3698.00	36.40	0.0005	
B-Temperature (°C)	4232.00	1	4232.00	41.65	0.0003	
C-Catalyst amount (mg)	1800.00	1	1800.00	17.72	0.0040	
AB	0.0000	1	0.0000	0.0000	1.0000	
AC	16.00	1	16.00	0.1575	0.7033	
BC	841.00	1	841.00	8.28	0.0238	
A^2	1675.80	1	1675.80	16.49	0.0048	
B^2	1760.85	1	1760.85	17.33	0.0042	
C^2	552.01	1	552.01	5.43	0.0525	
Residual	711.20	7	101.60			
Lack of Fit	706.00	3	235.33	181.03	< 0.0001	significant
Pure Error	5.20	4	1.30			
Cor Total	15720.00	16				

As shown in Figure 4.7, the experimental results can be presented in the form of three-dimensional response-surface plots under fixed conditions for each run. These plots clearly show the integrated effects of the two random variables, wherein all plots confirmed that both the HMF conversion and FDCA selectivity increased with an increase in any individual variable. Thus, it was concluded that according to the RSM, the selectivity toward FDCA changes upon variation in the reaction factors.

From these results it can be concluded that the optimum conditions 50 mg catalyst mass, 95

°C reaction temperature and 24 h reaction time clearly favours high yield of FDCA production and is needed to fully convert HMFCA and FFCA which is crucial when attempting to selectively produce FDCA, therefore these conditions were considered the optimum conditions for oxidation of HMF in base free reaction.

4.3.3 Catalysts Modification

Having generate a set of interesting result under base and base free experiments, still two questions need to be addressed and these questions are (i) how to improve the rate of disappearance of HMF under base free experiment and controlling rate under base experiments (ii) mitigating the occurrence of side reactions noticed under base experiment. Catalyst modification by functionalizing the surface nanoparticles with amine group of an organic base was reported to be a vital option to addressed those question in hand.[4] the detailed modification recipe was outline in Chapter two under catalysts synthesis section.

Table 4.7 showing the HMF conversion and product selectivity using modified catalysts for 12 h reaction.

S/No	Catalysts	HMF Conversion (%)	Product Selectivity (%)			
			HMFCA	FFCA	FDCA	MAc
1	AuPt-$LaCrO_3$	91	76	10	11	3
2	AuPt-$LaMnO_3$	100	19	2	77	1.20
3	AuPt-$LaFeO_3$	98	32	5	63	-
4	AuPt-$LaCoO_3$	99	67	0	19	14
5	AuPt-$LaNiO_3$	94	48	0	49	3

Table 4.8 summarized the results obtained for the modified catalysts experiment after 12 h

reaction time. As reported by Mallat and Baiker[26] the negative effect of strong inorganic base (the likes of NaOH) on the HMF and its oxidative products can be addressed by substituting it with organic base (especially amines) which can be adsorbed on the metal surface and in doing so increased the chances of alcohol dehydrogenation thereby limiting the influence of the pH of the solution. With tert-butylamine as a source of amine group (to functionalise the catalysts surface) in HMF oxidation, the reaction rate was found to be slow compared to the used of NaOH addition, but the HMF and the products were stable throughout the period of the reaction, no side reaction was occurred which is in line with many finding in the literature. The conversion of HMF was in the range of 95-100% for all the catalysts after 8 h (Table 4.7). As can be seen that the oxidation of HMF is a slow process in base free experiments (Table 4.5), with FFCA rapidly oxidized with good selectivity to FDCA. The modification of the catalyst by butylamine led to an increase in HMF conversion to > 90%, but to a substantial decrease of the selectivity to FDCA with respect to catalysts without modification. An unexpected C-C cleavage has occurred forming maleic acid with the modified catalysts. This is attributed to the fact that the catalyst supports docked on amine group during the catalyst modification which is in accordance to the work of Alina and coworkers.[4] Because of the interaction of metal nanoparticle on the catalysts surface with the amine group of butylamine, a stable oxidizing species of Au(III)-bis-amine and Pt(II)-bis-amine (Scheme 4.1) was formed which is assumed to prevent the HMF ring opening to maleic acid (MAc), thereby improving FDCA selectivity.[27,28]

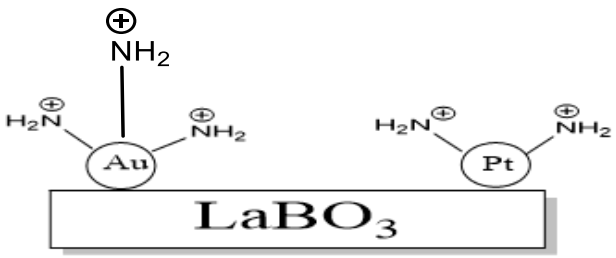

Scheme 4.1 Predicted surface metal in-situ interact with amine groups.

From the table, it can be seen that only HMFCA is the first intermediate product indicating that there is no DFF and HMFCA competitive reaction pathway in the HMF oxidation catalysed by modified catalysts. The presence of NH_2 on the Au and Pt nanoparticles facilitate the aldehyde hydration, product desorption from the active sites, and to avoid the metal leaching. The highest FDCA selectivity of 77% was recorded for $LaMnO_3$ supported catalysts and lowest recorded in $LaCrO_3$ support.

In conclusion, the catalyst modification improved the HMF conversion rate compared to catalyst without modification and improved the stability of the HMF compared to NaOH addition. However, catalyst support docked on amine group facilitates HMF ring opening.

4.4 Kinetic and thermodynamic Investigations Using Initial Rates

Understanding the specific reason why the $LaMnO_3$ perovskite support has the ability to enhance the oxidation pathway is a challenging problem, as viewing the surface of the support is virtually impossible through readily available techniques such as IR drifts and UV spectroscopy due to the support being a deep black, essentially absorbing the radiation and producing no discernible signal. The problem becomes more difficult in that the Au and Pt are indistinguishable using X-ray techniques, and therefore viewing the morphology of the nanoparticles would be extremely challenging without a computational model to support current findings. By producing a kinetic model through the initial rates method and temperature experiments, the activation barrier to the oxidation pathway can be observed and compared to the kinetic model equations in chapter 2, showing the activation energy, enthalpy, Gibbs free energy and entropy of activation for FDCA production.

Because of the complexity of this reaction system, assigning reaction orders and rate constants is difficult. It has been determined that there are at least three reactions leading to the formation FDCA proceeding simultaneously. The first step in obtaining the rate constants for the three reactions was to determine the reaction orders with respect to each reactant. This

was conducted using the initial rates methodology. Due to side reactions that occur during the process, the following assumptions helps in determining the rate of each oxidation steps.

1. FDCA is stable in the reaction mixture.
2. The supported metal nanoparticles do not actively promote the side reaction.
3. side products produced *via* the side reaction pathway is minimal when monitoring the rate of the oxidative dehydrogenation pathway.

Finally, Due to the sensitivity of the substrate to undergo degradation, the reaction rates were calculated in terms of the HMF consumption.

4.4.1 Determination of the Order of Reaction

The reaction order of each pathway was derived by monitoring the effect [O_2], [Substrate] and [NaOH] had on the reaction rate. For each reaction, short term interval sampling was used to derive reaction rates using the initial rates methodology. Figure 4.8 demonstrates how the reaction rate of each pathway is affected when the substrate concentration is varied.

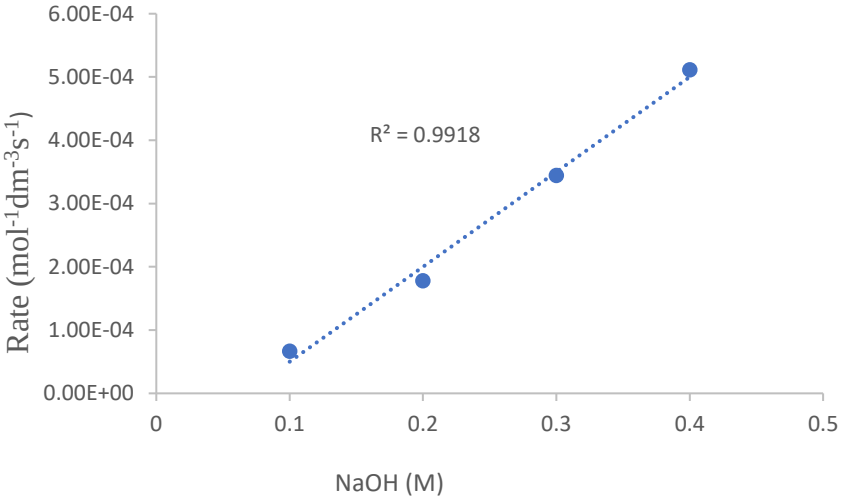

(a)

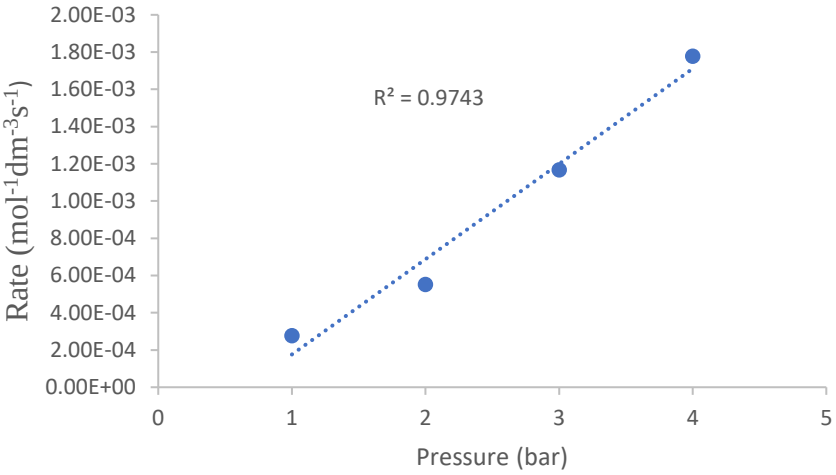

(b)

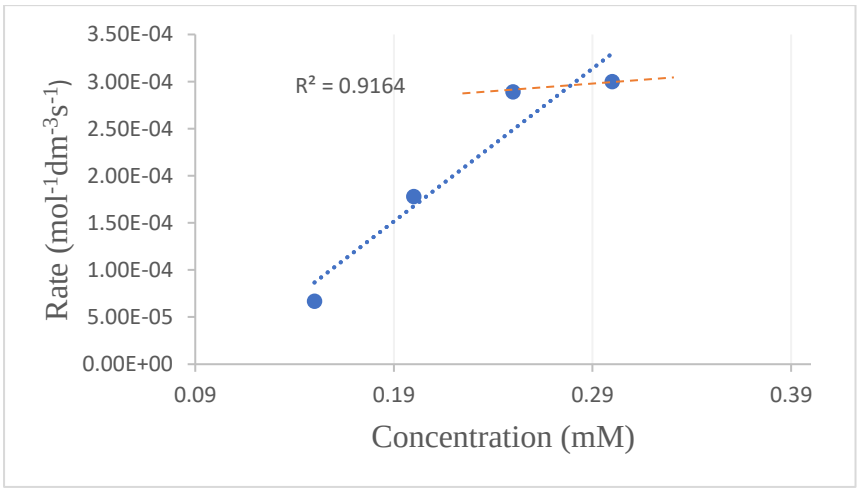

(c)

Figure 4.8 Initial rates at t = 30 mins for AuPt/$LaMnO_3$ at standard conditions altered singularly to determine rate with respect to each reactant where; (a) Base to HMF ratio (b) O_2 pressure, and (c) HMF concentration.

The catalytic oxidation of HMF appears to follow first order kinetics with respect to the HMF concentration. This suggests that concentration of HMF is crucial in the reaction mechanism. However, as the concentration reaches the standard reaction concentration (0.25M), it appears to change to follow zero order reaction kinetics. This is in good agreement with the finding of Davis *et al.*,[21] who studied the kinetics of HMF oxidation, and Vinke *et al.*,[29] also reported similar zero order kinetics in HMF concentration over Pt/Al_2O_3 catalyst. It likely this is attributed to strength of the NaOH (pKa =15.7) or possibly the surface active site of the catalyst is saturated with adsorbed substrate. Determining the reaction order of the oxidative dehydrogenation is more difficult in the presence of NaOH. The catalyst offers an alternative reaction pathway which involves the nucleophilic attack of the aldehyde by the $^-$OH species. As this transformation does not appear to take place in the absence of the catalyst, it must be assumed that the substrate must be bound to the surface of the catalyst for this to occur. It was reported that the binding of the substrate may weaken the C-H bond of the targeted carbon centre, thereby facilitating the substitution of the H with the sacrificial OH species.[1] The relationship between the reaction rate and NaOH strengthens this theory as a possible mechanistic solution.

First order trend is observed with respect to base concentration. This suggests that there is a stoichiometric relationship between NaOH and this reaction pathway, one molecule of NaOH is consumed for each conversion of HMF to FDCA. The catalyst offers an alternative reaction pathway which involves the nucleophilic attack of the aldehyde by the $^-$OH species. As this transformation does not appear to take place in the absence of the catalyst, it must be assumed that the substrate must be bound to the surface of the catalyst for this to occur. It was postulated previously in chapter one that the binding of the substrate may weaken the C-H bond of the targeted carbon centre, hereby facilitating the substitution of the H with the sacrificial OH species. The relationship between the reaction rate and NaOH strengthens this

theory as a possible mechanistic solution.

There is a clear first order relationship between the reaction rate and O_2 pressure for the catalytic oxidation of HMF to FDCA. This suggests that O_2 must play a pivotal role in the reaction mechanism. H_2O has been found to reduce O_2 in other similar catalytic reactions, leading to the formation of *OH and *OOH species.[30] It is likely that these species are responsible for the increase in reaction rate as oxygen concentration is increased.

In general, the order of HMF oxidation reaction under standard conditions has a first order rate dependence on substrate, NaOH and O_2 concentrations.

4.4.2 Determination of Reaction Rate Constant

The rate equation of HMF reaction was derived from the initial rates study. It is displayed in equation 4.3.

$$r_{OH} = k[FDCA]^1[O_2]^1[NaOH]^1 \qquad 4.3$$

From the rate equations in 3.3, it is possible to derive rate constants for each reaction. For this to be possible, the rate (r) of HMF to FDCA reaction must be determined. Figure 4.8 contain graph corresponding to the initial rates measurements of the HMF to FDCA oxidation reaction. Again, using the initial rates methodology, it is possible to extract the relative rate of this reaction. It was determined that the rate is 5.0×10^{-5} and encapsulating this rate into the rate equation along with the starting concentration of the reactant, it is possible to determine the rate constant for the reaction.

Table 4.8 The rate equation and rate constant derived for the HMF reaction pathway

Reaction Pathway	Rate equation	Rate constant
HMF to FDCA through Aldehyde group	$r_{OH} = k[HMF]^1$	2.0 x 10^{-3} (S^{-1})

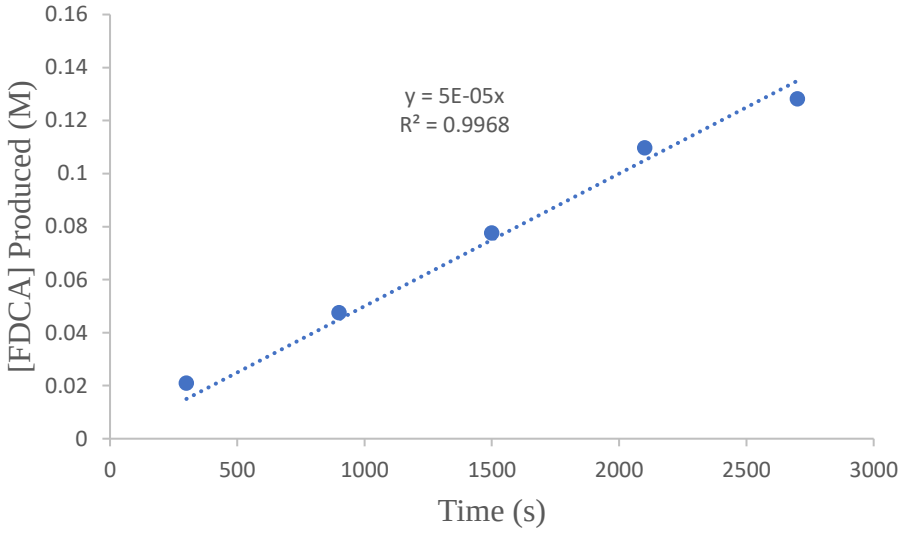

4.4.3 Determination of Activation Energy

Having systematically determined the reaction orders and rate constant of the reaction pathway, it was then necessary to determine the activation energy (Ea) of the reaction pathway to give a more complete understanding of the reaction profile. An Arrhenius plot (Figure 4.9) was then used to determine the activation energy for the oxidation pathway. To do this, additional initial rate experiments were conducted for each of the catalyst at varied temperatures. The oxidation of alcohol group pathway is not considered in this energy calculation as the breakdown of products for the 1wt% AuPt/$LaMnO_3$, show no formation of DFF. This method also assumes that the rate limiting step is the initial oxidation to the HMFCA. The activation energy can be found by rearranging the Arrhenius equation from.

$$\ln k = \ln A - \frac{E_a}{RT} \qquad 4.4$$

The slope of the Arrhenius plot is used to calculate the activation energy of the rection (Ea), R and T are ideal gas constant and temperature, respectively.

The activation energies for the disappearance of HMFCA was found to be 34.2 kJ mol^{-1} indicating that rate of HMFCA in the system is decreasing with increased temperature of the reaction (Figure3.16)

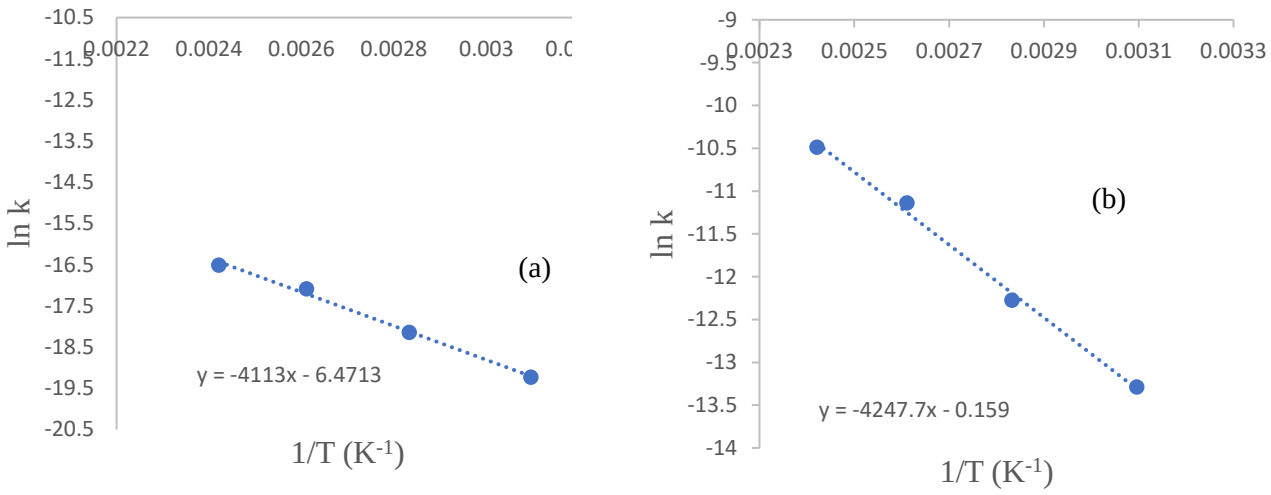

Figure 4.9 Arrhenius plot for (a) HMFCA disappearance (b) FDCA appearance, over 1 wt% AuPt/$LaCrO_3$ catalyst.

Activation energies of 18.35 kJ mol^{-1}, 35.3 kJ mol^{-1}, 28.2 kJ mol^{-1}, 20.6 kJ mol^{-1} and 18.9 kJ mol^{-1} were determined for the catalytic HMF oxidation over AuPt nanoparticles supported on LaMnO3, $LaCrO_3$, $LaFeO_3$, $LaCoO_3$ and $LaNiO_3$, respectively. From this activation energies, $LaMnO_3$, $LaNiO_3$, $LaCoO_3$ supports have lower values than $LaFeO_3$ and $LaCrO_3$ in the formation of FDCA under the same conditions. It is likely due to absorb oxygen to the surface on these catalysts over the other, as demonstrated in Figure 4.9, lowering the activation energy barrier to produce FDCA. The activation energies calculated in this study

were lower than 29 KJ mol^{-1} over Pt/C catalyst reported by Davis *et al.*,[21] except that of $LaCrO_3$ supported catalyst which is similar to 37.2 kJ mol^{-1} reported by Vinke *et al.*, over Pt/Al_2O_3 catalyst.[31]

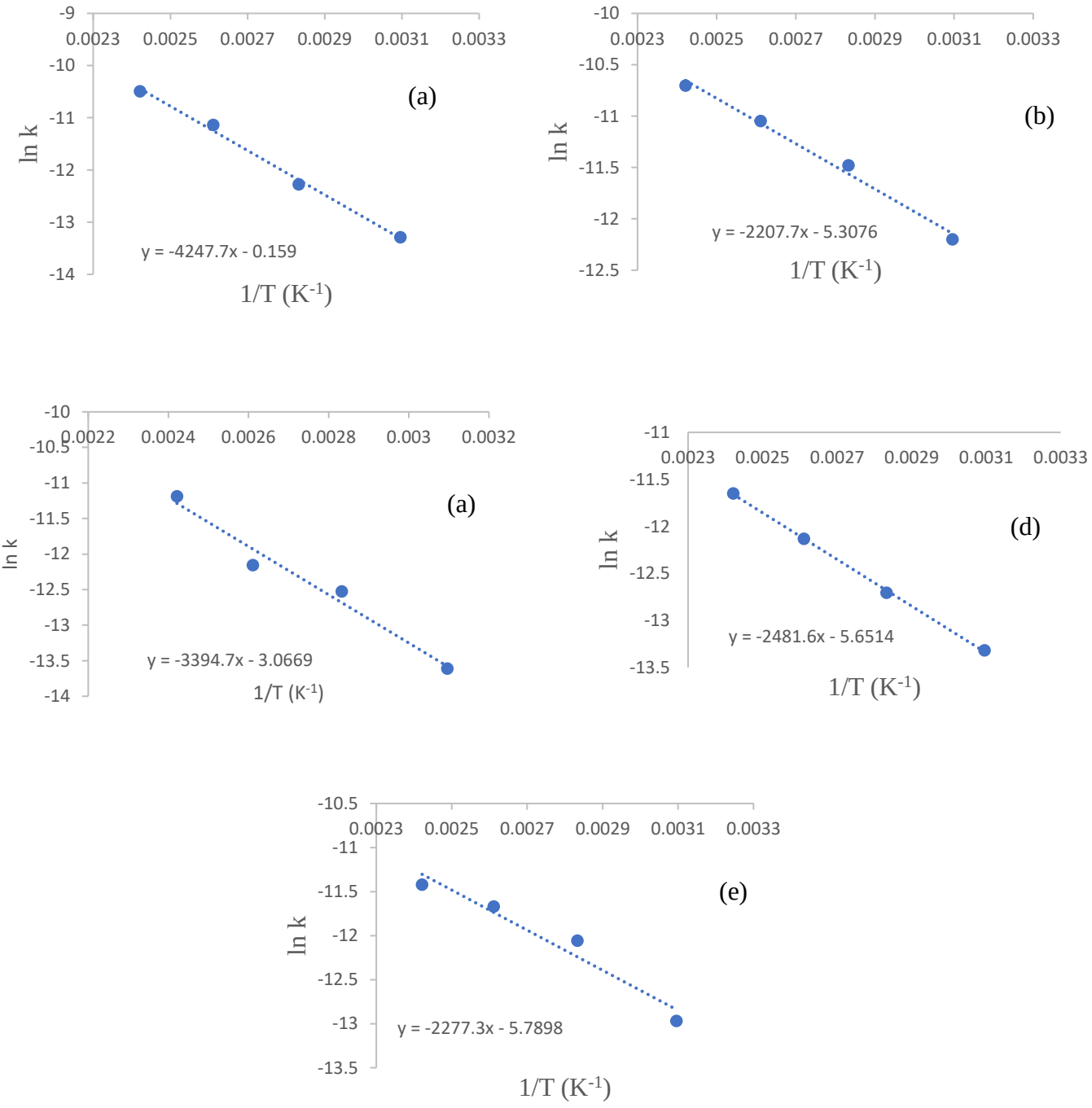

Figure 4.9 Arrhenius plot for the HMF oxidation over 1 wt% $AuPt/LaBO_3$ (a) $LaCrO_3$ (b) $LaMnO_3$ (c) $LaFeO_3$ (d) $LaCoO_3$ (e) $LaNiO_3$.

4.4.4 Determination of Thermodynamic Parameters

Having computed the activation energies for each catalyst used in the production of FDCA from HMF, it was important to know more information, such enthalpy and entropy of activation, on the reaction rate. The initial reaction rate experiment conducted at different temperatures used for Arrhenius calculations was also used in this regard. The rate constants were derived for each reaction at each temperature using the same method shown previously. Once derived, it was possible to use the rate constants to create Eyring plots for each of the catalysts by rearranged Eyring equation (eq 4.5). These are displayed in Figure 4.10. From the Eyring plots it was possible to derive enthalpy and entropy of activation for each of the catalysts by using the slope and intercept of the straight-line equation, respectively.

$$\ln\left(\frac{k}{T}\right) = -\frac{DH}{RT} + \ln\left(\frac{k_B}{h}\right) + \frac{DS}{R} \qquad 4.5$$

Table 4.10 Thermodynamic data for each AuPt supported on $LaBO_3$ catalysts for HMF oxidation.

Catalyst supports	Thermodynamic parameters		
	ΔH^* (kJmol^{-1})	ΔS^* (kJmol^{-1}K^{-1})	ΔG^* (kJmol^{-1})
$LaCrO_3$	+34.2	-0.25	+129.9
$LaMnO_3$	+13.9	-0.3	+128.8
$LaFeO_3$	+18.8	-0.26	+118.4
$LaCoO_3$	+22.3	-0.23	+110.4
$LaNiO_3$	+11.4	-0.31	+126.3

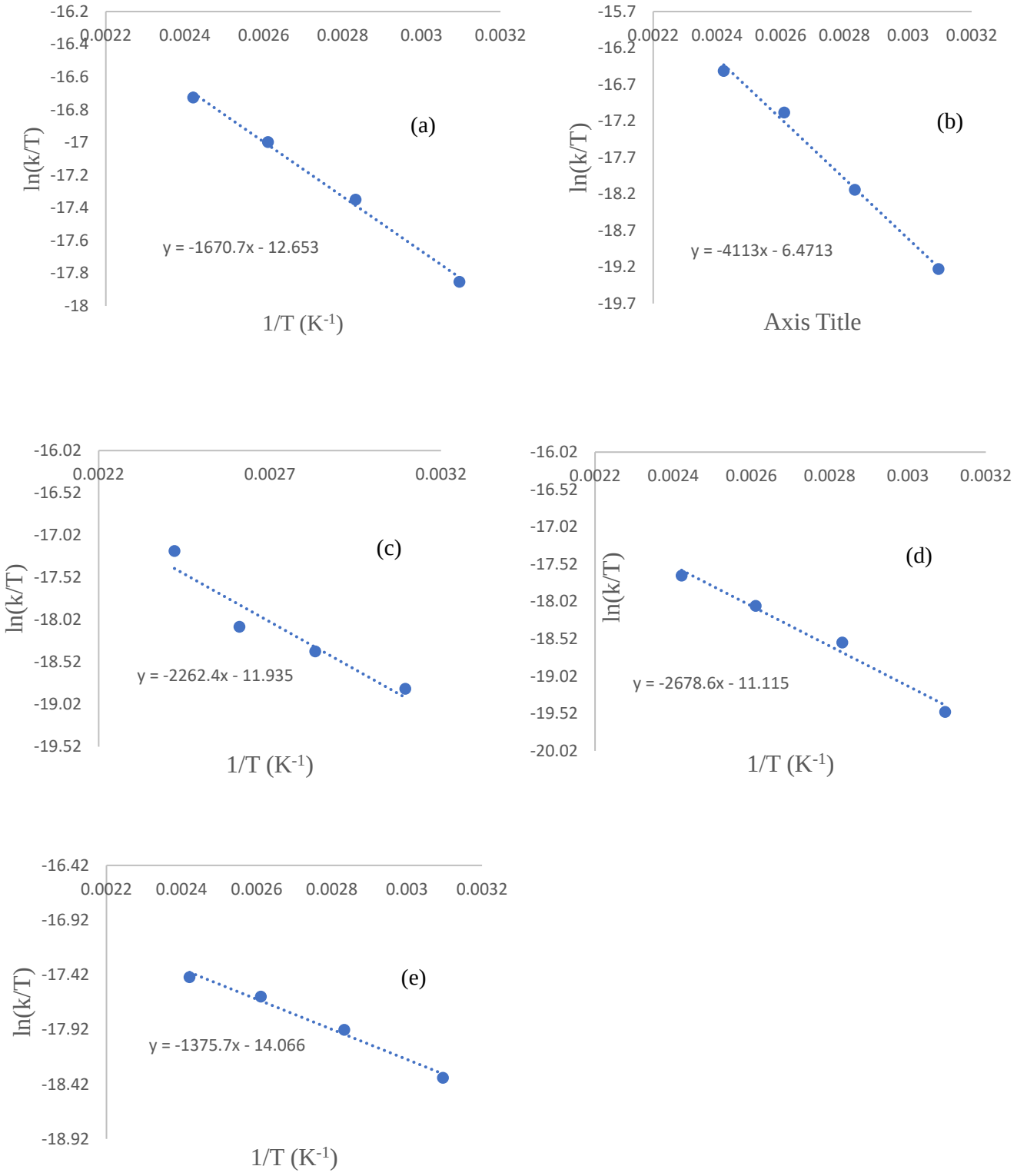

Figure 4.10 Eyring plot for the HMF oxidation over 1 wt% AuPt/$LaBO_3$ (a) $LaCrO_3$ (b) $LaMnO_3$ (c) $LaFeO_3$ (d) $LaCoO_3$ (e) $LaNiO_3$.

Table 3.14 shows the Gibb's free energy change (calculated using the optimum temperature, 383 K), enthalpy and entropy change of activation for each catalyst. The results revealed that the activation energies of these catalytic process were greatly influenced by heat of adsorption or complexation of the substrate. The corresponding entropies of activation which binding the substrate to the surface of the catalyst are negative indicating the lower activation energy for each catalyst. The more negative entropy of activation is, the lower the activation and the more HMF is converted to FDCA. The enthalpies of activation are positive, thus, representing the lower activation energies of the transition state compared to the activation energy of the substrate for each catalyst. The positive value of free energy of activation indicates that the transition state intermediates are unstable, and the activation energy is overcome for the HMF convert into FDCA.

4.5 Conclusion

The Primary objective of this area of work was to find a catalyst which could selectively oxide HMF to FDCA efficiently, under mild reaction conditions. It was quickly determined that the presence of a sacrificial base complicated the system, as it led to the activation of side reaction pathway.

Initial experiments trialled the use of a 1 wt.% AuPt/$LaMnO_3$ catalyst for this reaction to obtained optimum reaction conditions. Reasonable results were obtained but significant quantities of carbon were lost which was suggested to be a result of intermolecular polymerisation/degradation of HMF in the solution. It was subsequently discovered that increasing the reaction temperature promoted this unfavourable polymerisation, which consequentially led to the reactions being conducted at 50 ^{o}C. Pt nanoparticle leaching appeared not a problem. Catalyst leaching studies confirmed that the Pt had no effect on catalytic performance. As a result, it was hypothesised that the loss in catalytic performance

over time was a result of the irreversible binding of humins to the active sites of the catalyst.

A separate study of catalytic HMF oxidation under base free conditions to understand the role of catalyst support and the influence of switching B-site element on the reaction pathways. Lanthanum perovskite oxide with varied B-site across the first series transition metals from Cr to Ni have been previously reported to be highly active support for Au and Pt nanoparticles in the oxidation of alcohols.[31] For this reason, 1 wt% AuPt/$LaBO_3$ catalysts where B = Cr, Mn, Fe, Co and Ni were produced and tested in base free experiment. A significant improvement in terms of HMF stability was observed, however, the rate of HMF diminishing was slower in comparable with that displayed by the base addition reactions. Functionalising the catalysts with amine group significantly increase the reaction rate, which ultimately allowed for higher HMF conversion and oxidation products selectivity to be generated. Interestingly, the rate of side reaction decreased with the modified catalysts system despite the improved HMF conversion. It was speculated that the modification of the catalysts may alter the electronic properties of the active site and ultimately affected the binding strength of the substrate to the site. This is, however, purely speculation and more work would be required to confirm this hypothesis. The reusability tests determined that these catalysts did not appear to deactivate upon subsequent uses.

Because of the stability of the HMF seen under base free reactions, and higher HMF conversion and FDCA selectivity in AuPt/$LaNiO_3$, another study was carried out under base free conditions using response surface methodology to see if the interaction of the reaction variable necessarily affects this behaviour statistically. In doing so, it has been observed that all the variables were significantly involved in achieving such performance.

It is worst mentioning that $LaCrO_3$, LaMnO3 and $LaFeO_3$ catalyst supports under base free reaction, the HMF oxidation occurred through the initial oxidation of both alcohol and

aldehyde groups of the HMF leading DFF and HMFCA reaction pathways. This was hypothesised that was attributed to the amphoteric nature of these catalyst supports.

A set of experiments conducted in the absence of any catalysed confirmed that the occurrence of side reaction producing side products (humins). This confirmed a hypothesis earlier in this chapter that in the presence of strong base, degradation and Cannizzaro productions with a small quantity of the HMF oxidation products. In order to improve understanding of the catalyst supports before the HMF reaction, a separate preliminary experiment conducted using catalyst supports for the reaction with NaOH base and without base demonstrated that the catalyst supports had no catalytic activity.

Finally, kinetics was applied to the system to assess the efficiency of the catalytic reaction. The initial rates method was used to determine the rate equations for the oxidation of HMF. These rate equations were then used to calculate activation energies for each of the catalysts used in the reaction which were derived using Arrhenius plots. Activation energies of 18.35 kJ mol^{-1}, 35.3 kJ mol^{-1}, 28.2 KJ mol^{-1}, 20.6 kJ mol^{-1} and 18.9 kJ mol^{-1} were derived for the oxidation of HMF using AuPt nanoparticles supported on LaMnO3, $LaCrO_3$, $LaFeO_3$, $LaCoO_3$ and $LaNiO_3$, respectively. It is important to mention that the kinetic study was dependent on several assumption and the figures acquired can only be considered as estimates at this time. Significantly more data points must be included in the kinetic studies for the acquired figures to be consider accurate. A thermodynamic calculation was also done to acquire the information on the reaction. The values implies that the free energy of activation indicates that the activated state is unstable, and the activation energy is overcome for the HMF convert into FDCA.

4.6 Reference

1. Sajid, M., Zhao, X. & Liu, D. Production of 2,5-furandicarboxylic acid (FDCA) from 5-hydroxymethylfurfural (HMF): Recent progress focusing on the chemical-catalytic routes. *Green Chem.* **20**, 5427–5453 (2018).
2. Hu, L., Lin, L., Wu, Z., Zhou, S. & Liu, S. Recent advances in catalytic transformation of biomass-derived 5-hydroxymethylfurfural into the innovative fuels and chemicals. *Renew. Sustain. Energy Rev.* **74**, 230–257 (2017).
3. Cattaneo, S. *et al.* Continuous Flow Synthesis of Bimetallic AuPd Catalysts for the Selective Oxidation of 5-Hydroxymethylfurfural to 2,5-Furandicarboxylic Acid. *ChemNanoMat* **6**, 420–426 (2020).
4. Tirsoaga, A., El Fergani, M., Parvulescu, V. I. & Coman, S. M. Upgrade of 5-Hydroxymethylfurfural to Dicarboxylic Acids onto Multifunctional-Based Fe3O4@SiO2 Magnetic Catalysts. *ACS Sustain. Chem. Eng.* **6**, 14292–14301 (2018).
5. Yan, D. *et al.* Fe-Zr-O catalyzed base-free aerobic oxidation of 5-HMF to 2,5-FDCA as a bio-based polyester monomer. *Catal. Sci. Technol.* **8**, 164–175 (2018).
6. Li, Q. *et al.* Ruthenium supported on CoFe layered double oxide for selective hydrogenation of 5-hydroxymethylfurfural. *Mol. Catal.* **431**, 32–38 (2017).
7. Albonetti, S. *et al.* Selective oxidation of 5-hydroxymethyl-2-furfural over TiO 2 - supported gold – copper catalysts prepared from preformed nanoparticles : Effect of Au / Cu ratio. **195**, 120–126 (2012).
8. Zuo, X. *et al.* Kinetics of homogeneous 5-hydroxymethylfurfural oxidation to 2,5-furandicarboxylic acid with Co/Mn/Br catalyst. *AIChE J.* **63**, 162–171 (2017).
9. Han, X. *et al.* N-doped carbon supported Pt catalyst for base-free oxidation of 5-hydroxymethylfurfural to 2,5-furandicarboxylic acid. *Appl. Catal. A Gen.* **526**, 1–8 (2016).

10. Han, X. *et al.* Base-free aerobic oxidation of 5-hydroxymethylfurfural to 2,5-furandicarboxylic acid over a Pt/C-O-Mg catalyst. *Green Chem.* **18**, 1597–1604 (2016).

11. Gorbanev, Y. Y., Klitgaard, S. K., Woodley, J. M., Christensen, C. H. & Riisager, A. Gold-Catalyzed Aerobic Oxidation of 5-Hydroxymethyl- furfural in Water at Ambient Temperature. 672–675 (2009) doi:10.1002/cssc.200900059.

12. Bonincontro, D., Lolli, A., Villa, A. & Prati, L. base-free oxidation of HMF under mild. 4090–4099 (2019) doi:10.1039/c9gc01283d.

13. Zhang, Z. & Deng, K. Recent Advances in the Catalytic Synthesis of 2,5-Furandicarboxylic Acid and Its Derivatives. *ACS Catal.* **5**, 6529–6544 (2015).

14. Pasini, T. *et al.* Selective oxidation of 5-hydroxymethyl-2-furfural using supported gold–copper nanoparticles. *Green Chem.* **13**, 2091–2099 (2011).

15. Vuyyuru, K. R. & Strasser, P. Oxidation of biomass derived 5-hydroxymethylfurfural using heterogeneous and electrochemical catalysis. *Catal. Today* **195**, 144–154 (2012).

16. Gupta, N. K., Nishimura, S., Takagaki, A. & Ebitani, K. Hydrotalcite-supported gold-nanoparticle-catalyzed highly efficient base-free aqueous oxidation of 5-hydroxymethylfurfural into 2,5-furandicarboxylic acid under atmospheric oxygen pressure. *Green Chem.* **13**, 824–827 (2011).

17. Casanova, O., Iborra, S. & Corma, A. Biomass into Chemicals : Aerobic Oxidation of 5-Hydroxy- methyl-2-furfural into 2 , 5-Furandicarboxylic Acid with Gold Nanoparticle Catalysts. 1138–1144 (2009) doi:10.1002/cssc.200900137.

18. Jin, X. *et al.* Phase Transformed PtFe Nanocomposites Show Enhanced Catalytic Performances in Oxidation of Glycerol to Tartronic Acid. 13157–13164 (2017) doi:10.1021/acs.iecr.7b01473.

19. Ait Rass, H., Essayem, N. & Besson, M. Selective aerobic oxidation of 5-HMF into

2,5-furandicarboxylic acid with pt catalysts supported on TiO2- and ZrO2-based supports. *ChemSusChem* **8**, 1206–1217 (2015).

20. Davis, S. E., Zope, B. N. & Davis, R. J. On the mechanism of selective oxidation of 5-hydroxymethylfurfural to 2,5-furandicarboxylic acid over supported Pt and Au catalysts. *Green Chem.* **14**, 143–147 (2012).
21. Davis, S. E. *et al.* Kinetics and mechanism of 5-hydroxymethylfurfural oxidation and their implications for catalyst development. *J. Mol. Catal. A Chem.* **388**–**389**, 123–132 (2014).
22. Schade, O. R., Kalz, K. F., Neukum, D., Kleist, W. & Grunwaldt, J. D. Supported gold- and silver-based catalysts for the selective aerobic oxidation of 5-(hydroxymethyl)furfural to 2,5-furandicarboxylic acid and 5-hydroxymethyl-2-furancarboxylic acid. *Green Chem.* **20**, 3530–3541 (2018).
23. Subbiah, S., Simeonov, S. P., Esperança, J. M. S. S., Rebelo, L. P. N. & Afonso, C. A. M. Direct transformation of 5-hydroxymethylfurfural to the building blocks 2,5-dihydroxymethylfurfural (DHMF) and 5-hydroxymethyl furanoic acid (HMFA) via Cannizzaro reaction. *Green Chem.* **15**, 2849–2853 (2013).
24. Ardemani, L. *et al.* Solid base catalysed 5-HMF oxidation to 2,5-FDCA over Au/hydrotalcites: fact or fiction? *Chem. Sci.* **6**, 4940–4945 (2015).
25. Wan, X. *et al.* Base-free aerobic oxidation of 5-hydroxymethyl-furfural to 2,5-furandicarboxylic acid in water catalyzed by functionalized carbon nanotube-supported au-pd alloy nanoparticles. *ACS Catal.* **4**, 2175–2185 (2014).
26. Mallat, T. & Baiker, A. Oxidation of Alcohols with Molecular Oxygen on Solid Catalysts. (2004).
27. Li, X. & Binnemans, K. Oxidative Dissolution of Metals in Organic Solvents. *Chem. Rev.* **121**, 4506–4530 (2021).

28. Ravera, M., Gabano, E., McGlinchey, M. J. & Osella, D. A view on multi-action Pt(IV) antitumor prodrugs. *Inorganica Chim. Acta* **492**, 32–47 (2019).

29. Hibbitts, D. Reactivity of the Gold / Water Interface During Selective Oxidation Catalysis. doi:10.1126/science.1195055.

30. Bekkun, H. Van. New Developments in Selective Oxidation. *Stud. Surf. Sci. Catal.* **55**, xiv (1990).

31. Evans, C. D. *et al.* The preparation of large surface area lanthanum based perovskite supports for AuPt nanoparticles: Tuning the glycerol oxidation reaction pathway by switching the perovskite B site. *Faraday Discuss.* **188**, 427–450 (2016).

Chapter 5

The Selective Oxidation of Glycerol

5.1 Introduction

Glycerol (GLY) is a versatile multifunctional organic molecule which is produced as a by-product from the transesterification of triacylglycerols to biodiesel.[1–3] Each carbon atom in the structure is bound to a hydroxyl group which gives it great potential for exploitation as a platform chemical. For this reason, the selective oxidation of glycerol over heterogeneous catalysts has long been a subject of scientific interest.[4] It has been determined that the choice of catalyst,[5] the size of the platinum group metal (PGM)[6] and the reaction conditions[7] can all significantly influence the selectivity and the rate of the reaction.

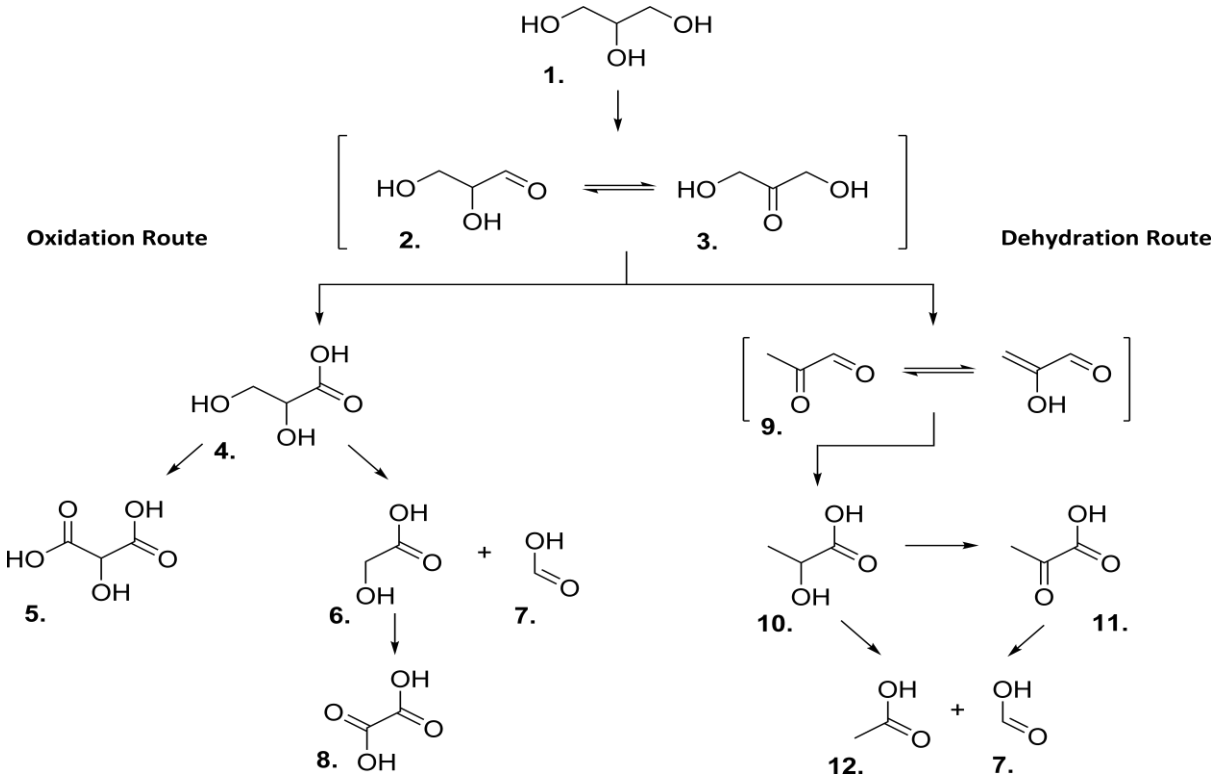

Scheme 5.1 Schematic diagram showing products of glycerol oxidation. Key: 1. Glycerol (GLY); 2. Glyceraldehyde (GLAD); 3. Dihydroxyacetone (DHA); 4. Glyceric acid (GA); 5. Tartronic acid (TA); 6. Glycolic acid (GLA); 7. Formic acid (FA); 8. Oxalic acid (OA); 9. Pyruvaldehyde (PALD); 10. Lactic acid (LA); 11. Pyruvic acid (PA); 12. Acetic acid (AA).[8]

Scheme 4.1 shows the large distribution of products which can be formed from the oxidation of glycerol. Using heterogeneous catalysts for glycerol oxidation allows for an additional avenue to control reaction selectivity. The pioneering work of Prati *et al*. demonstrated that supported Au catalysts were active for the selective oxidation of glycerol.[9] It was found that Au/C could selectively produce glyceric acid through the sequential oxidation of glycerol. Further development of the Au catalysts found that the activity of the catalysts could be significantly increased through the addition of Pd[10,11] or Pt[10]. The most desirable products that can be produced from glycerol oxidation are either the C_3 oxidation products, glyceric acid (GA) and the sequential oxidation of this product, tartronic acid (TA); or lactic acid (LA) produced through the opposing dehydration pathway. To achieve the selective production of these products, C-C scission must be hindered as much as possible. It is believed that this unfavourable C-C scission is as a result of the in-situ production of H_2O_2 from the reduction of O_2 by H_2O on the catalysts surface.[12–14] The application of hydrophobic materials as supports for the PGM has been shown to reduce this unfavourable C-C bond cleavage.[15]

It has been well documented that the catalyst support has an influence on the conversion of glycerol and product selectivity under oxidative and basic conditions.[16–18] Single metal oxides and carbon are popular supports for glycerol oxidation, with carbon shown to be more active than supports such as TiO_2 and Fe_2O_3.[10] Supports such as Al_2O_3 and NiO are highly active, but have a large distribution of product selectivity.[19] A study by Villa *et al.*[20] demonstrated the role of acid and base sites on supports used for glycerol oxidation. It was found that basic sites contributed to a higher activity with a poor selectivity breakdown of products, and supports containing acid sites had a lower activity, but higher selectivity to glyceraldehyde and dihydroxyacetone, therefore, controlling this step allows for a greater control over the product selectivity profile of the products. This research clearly shows that the support has a significant role on the activity and selectivity to products, and therefore, tailoring a support

with the desired characteristics to enhance a selected mechanistic pathway is the key to selective formation of a desired product. Depending on the synthesis methods and application, the properties of catalyst supports can be tuned to achieve the desired target.[21] Perovskite oxides are rarely used as catalyst supports due to the fact that high calcination temperatures are required to obtained a pure perovskite phase and this directly affects their surface area.[22–24] For platinum group metals (PGM) loading, a support material with surface area above 50 m^2/g is required.[25] Efforts have been made recently to synthesize perovskite oxides using different methods to improve the surface area and mitigate the poor phase purity for them to be used as catalyst supports for metal nanoparticles.[25,26] Evans *et al*. report the use of supercritical anti-solvent precipitation for the synthesis of lanthanum-based perovskite oxides to improve the low surface area reported for convention methods.[25] Although the surface area is considerably improved by this method, the phase purity remains the problem. Herein, hydrothermal and nano-casting (using carbon and silica as templates) methods were used to address these problems.

The work in this chapter is focussed toward developing high surface area of lanthanum-based perovskite using different preparation methods and see if tuning the B-site element can change reaction pathways to either Lactic acid or glyceric acid and tatronic acid.

5.2 Aim and Objectives

Aim

The aim of this chapter is to investigate the role of the catalyst support on the selectivity of the glycerol oxidation products with emphasis given on the effect of the support synthesis methods and switching the B site element in the perovskite structure.

Objectives

- Identify a catalyst support which can selectively favour the oxidation of glycerol to lactic acid.
- To investigate whether the change in synthesis method of the support influences the product selectivity.
- Response surface optimization of sensitive reaction conditions for AuPt/$LaMnO_3$ catalysts.
- Determine the catalyst performance under base free conditions.
- To elucidate the $LaMnO_3$ perovskite support prepared by hydrothermal method.

5.3. Catalyst Testing

The reaction conditions used for the glycerol oxidation testing were as follows; 60 ℃, 0.3 M glycerol, 3 bar O_2, 2:1 base: glycerol ratio (NaOH), 900 rpm stirring speed, with 1000:1 metal: substrate ratio, except for the initial catalyst screening test where 100 ℃ and 4:1 base: glycerol ratio are used. The reactions were all conducted within a colaver reactor.

5.3.1 Glycerol Oxidation Over Perovskite Oxide Prepared by Nano-casting.

Before any experiments, it is important to investigate the effect of the support and evaluate to what extent the perovskite oxide prepared by nano-casting method using SBA-15 and mesoperous carbon as templates, could have the activity on the glycerol oxidation. Each of the perovskite supports activity was evaluated under the conditions outlined in Section 4.3. As can be seen from Figure 4.2, there is no significant conversion of the glycerol over a period of 24 hours, showing that any activation of the reaction will be due to the nanoparticles deposited on to the surface.

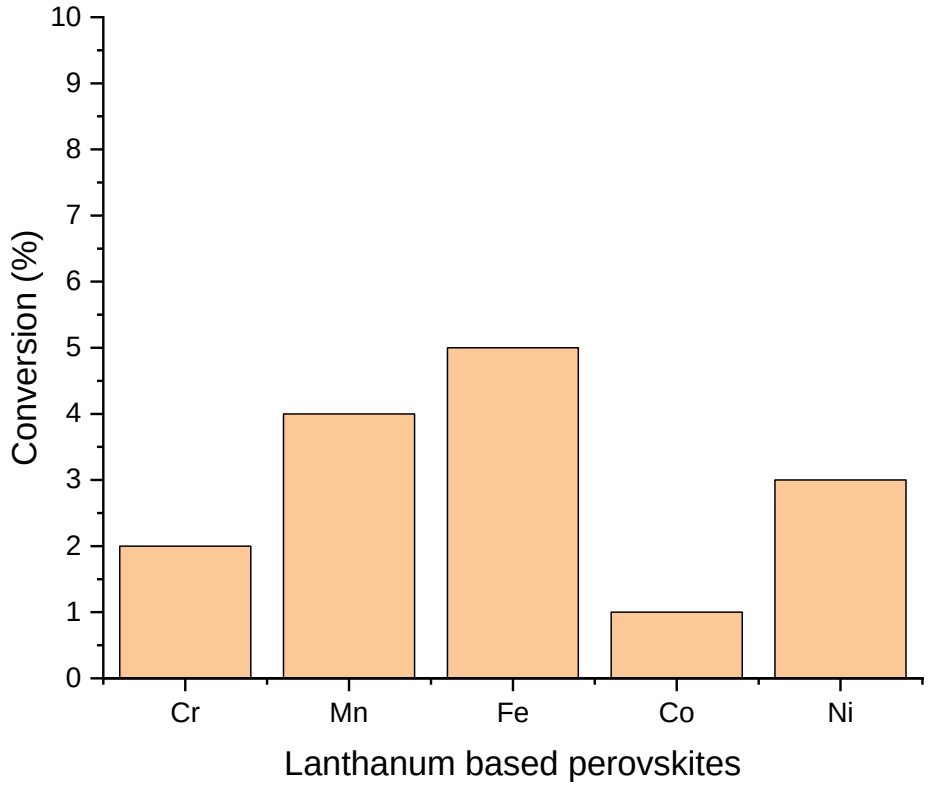

Figure 5.2 Conversion of glycerol using perovskite supports over 24 hours. Conditions: catalyst amount 50 mg, 100 °C, 0.3 M glycerol, 3 bar O_2, 4:1 NaOH - glycerol ratio, 900 rpm stirring speed.

5.3.2 Initial AuPt/$LaMO_3$ Catalysts Screening for Selective Oxidation of Glycerol

The advantage of the relatively high surface area of perovskite supports obtained through utilising the nano-casting method using SBA-15 as the template enabled the deposition of Au and Pt on to the surface of each of the supports. The choice of these high area supports is due to their ability to provide a higher availability of active sites for the reaction to proceed, potentially increasing activity. As documented, bimetallic AuPt nanoparticles have been found to be highly active for the oxidation of glycerol on a range of different supports.[27–29] For this reason, 1wt.% of 1:1 molar ratio AuPt/$LaMO_3$ catalysts (where M is Cr, Mn, Fe, Co

and Ni) were prepared by the conventional sol-immobilisation method using PVA as the stabiliser.[30] The catalysts were characterised as outlined in the characterization section 3.4 of Chapter 3, and tested under the reaction conditions detailed in Section 4.3 above and the corresponding reaction results are displayed in Table 4.1.

The conversion of glycerol appears to be influenced by the support in the AuPt/$LaMO_3$ catalysts, the rate of which appears to slow with its disappearing concentration. The $LaMnO_3$ supported catalyst was found to favour the production of C_3 products, with a high selectivity to glyceric acid over a period of 6 hours and a relatively low selectivity to the potential C-C scission products (oxalic acid, glycolic acid, formic acid, and CO_2). Interestingly, the result obtained showed that some selectivity toward lactic acid was detected that gradually disappeared as the reaction proceeds with time. This contradicted the finding of Evans *et al*.[25] where the dehydration pathway to the lactic acid was completely hindered under similar conditions. It has been reported that, under these conditions, with the use of AuPt nanoparticles supported on CeO_2 and TiO_2 produce up to 80 % of lactic acid.[8,31] It has been documented that lower reaction temperature and base ratio, 60 ℃ and 2:1 base to substrate ratio, have been shown to favour the production of glyceric acid with a selectivity of around 80%, which is similar to results found here for the $LaMnO_3$ supported catalyst. Beyond 80 ℃ reaction temperature and higher base concentration, the selectivity to LA begin to dominate with TiO_2 support material. However, Tsuji *et al*. reported that Pt/hydrotalcite (HT) catalysts under similar conditions in the absence of base, achieved 55 % glycerol conversion with high selectivity to GA. The authors noticed that dehydration route was completely hindered by these catalysts and assigned this to the basic nature of the support.[32] The effect of acid-base properties of the support on product selectivity distribution for glycerol oxidation was revisited by Xu *et al*. The authors tested different supports for the AuPt nanoparticles including acid (CeO_2), basic (MgO, $Mg(OH)_2$ and $(MgCO_3)_4Mg(OH)_2$), and amphoteric

(hydrotalcite and Al_2O_3), and concluded that the higher the basic strength of the support the tendency the selectivity to oxidation products and the higher the acidic strength, the higher the chances of producing dehydration products.[17] This observsation is the reason for AuPt/$LaMnO_3$ catalyst does not totally hindered the dehydration route to LA because of the amphoteric nature of $LaMnO_3$ support as revealed by TPD (chapter 3, section 3.4.9).

It can be seen from Table 5.1, $LaFeO_3$ supported AuPt nanoparticles had no preferable reaction pathway with lactic acid, tartronic acid and C-C scission as the main oxidation products. Glyceric acid appears in small quantity indicating it undergoes further oxidation to tartronic acid and C-C scission, and as the reaction progresses with time, the pathway to tartronic acid slightly decreases due to continuing C-C scission production. On other hand, lactic acid selectivity increases from 41 % to 55 % over the entire period of the reaction. With a total of 69 % lactic acid selectivity, the AuPt/$LaFeO_3$ has comparable activity towards previously reported catalysts under similar conditions.[33] The oxidation behaviour observed with AuPt/$LaFeO_3$ catalyst (secondary oxidation to tartronic acid) is attributed to the presence of segregated Fe_2O_3 as revealed by the XRD and XPS (Chapter 3 section 3.4.3 and section 3.4.8, respectively) on the support, suggesting that having Fe near AuPt nanoparticles weakens the binding between the metal and the C=O group in the intermediates products, that may assist oxygen transfer from nanoparticles surface to molecules, which enhances both primary and secondary oxidation rates.[34] The surface reaction mechanism of this process is displayed in scheme 5.2. Another possible explanation is that the oxidation sites on the surface of this catalyst are either blocked by reaction intermediates or have low stability.

Table 5.1. Glycerol oxidation over the AuPt/$LaMO_3$ catalyst. The effect of B-site element on catalyst performance is assessed. **Reaction conditions:** glycerol (0.3 M), NaOH: substrate ratio (4:1), O_2 (3 bar), substrate:metal ratio = 1000, 100 ºC, 6 h, and 900 rpm.

B-site Element	**Time (h)**	**Conversion (%)**	**Selectivity (%)**				**CMB* (%)**
			GA	TA	LA	C-C Sc	
Cr	0.5	32	9	4	79	8	96
	1	49	7	2	81	10	93
	2	67	7	3	80	10	87
	4	84	8	2	82	8	82
	6	100	7	1	82	10	81
Mn	0.5	22	61	5	15	19	100
	1	37	63	7	15	15	96
	2	59	65	9	14	12	98
	4	73	67	11	12	10	89
	6	94	70	14	10	6	83
Fe	0.5	21	5	31	41	23	99
	1	39	8	24	42	26	91
	2	54	5	21	47	27	89
	4	67	3	19	49	29	84
	6	76	2	12	55	31	79
Co	0.5	24	61	4	14	21	98
	1	41	62	3	15	20	99
	2	61	58	3	17	22	92
	4	79	52	4	21	23	87
	6	94	42	4	22	32	84
Ni	0.5	28	45	2	32	21	100
	1	43	43	3	35	19	96
	2	64	41	3	39	17	86
	4	89	39	4	45	12	81
	6	100	35	6	51	8	79

- CMB. means carbon mass balance.

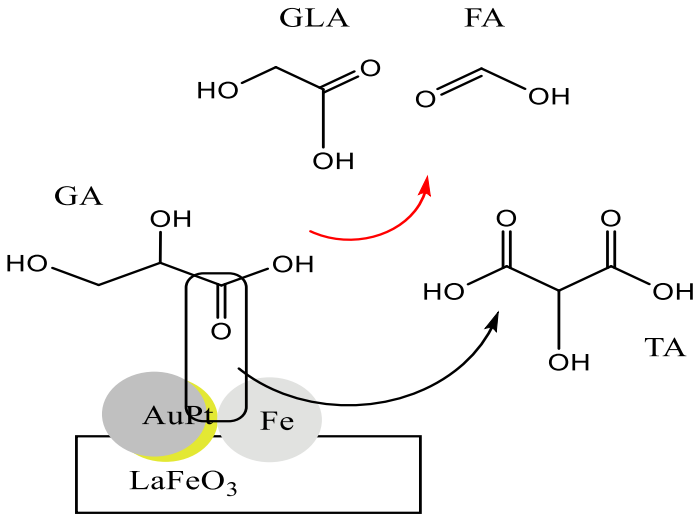

Scheme 5.2 Proposed surface reaction mechanism of secondary oxidation with Fe near AuPt nanoparticles.

The AuPt/$LaNiO_3$ catalyst (Table 4.1) shows that the selectivity towards glyceric acid and C-C scission decreases with increased conversion of glycerol from 28 % to 100 %. The decrease in glyceric acid was not attributed to further oxidation to tartronic acid or C-C scission, but rather an increase in the production of lactic acid *via* the dehydration pathway, showing an alteration in the preferred pathway from oxidation to dehydration. Although this trend is not followed by all of the supported perovskites, each of them exhibit a change in which pathway is favoured. Similar catalytic behaviour was observed for AuPt/$LaCoO_3$ with sequential oxidation of glyceric acid to C-C scission (oxalic acid, glycolic acid and formic acid).

The catalyst that presented the highest selectivity to lactic acid was the AuPt/$LaCrO_3$, producing 82 % selectivity to lactic acid and 100 % conversion of glycerol. Whereas the AuPt/$LaFeO_3$ catalyst was observed to be sensitive to conversion of glycerol, the AuPt/$LaCrO_3$ had only a slight increase in selectivity to lactic acid, ranging from 79 % - 82 % throughout the whole reaction. With the highest selectivity to lactic acid of all of the perovskite supported catalysts, and a similar selectivity to lactic acid previously observed for

SBA-15 assisted TiO_2 supported AuPt catalysts reported by Douthwaite *et al*,[8] It can be concluded the AuPt/$LaCrO_3$ is a highly effective catalyst for the production of lactic acid from glycerol. It is noted that the carbon mass balance decreases in all the catalysts to about 80%, which is signed to the associated C-C cleavage leading C-C scission products due to in situ formation of H_2O_2 in the reaction mixture under conditions of the experiment as reported in the previous literature.[35]

It is clear from these results that there is a significant variation in the selectivity profiles at similar activities for each of the perovskite supports, with the change of the B site element controlling this effect. With Mn as the B site, there is a clear suppression of the dehydration pathway to lactic acid, with glyceric acid being the dominant product formed. Even though, the dehydration pathway was not completely suppressed as reported by Evans and coworkers[25], their further study confirms a minimum amount of lactic acid can be seen at early reaction time, but usually decreases as the reaction progresses.[36] Both the Cr and Fe B site perovskite supports showed an enhanced dehydration pathway, forming the highest selectivity to lactic acid, whereas the Ni and Co B site perovskites had a lower control over the competing pathways, producing both oxidation and dehydration pathway products. As shown in the reaction scheme (Scheme 5.1), the intermediate product for both glyceric acid/tartronic acid and lactic acid is glyceraldehyde. The rate limiting step for this reaction can be the initial proton abstraction from glycerol, forming the alkoxy intermediate and, as the glyceraldehyde is only observed without a base present, this leads to significant changes in product distribution with the similar catalyst activities.

In order to better understand the effect of perovskite support behaviour on the reaction pathways observed, a separate series of experiments were carried out under base free conditions.

5.4. Selective Control of Glycerol Oxidation Products

Controlling the selectivity to a particular product during the glycerol oxidation reaction is highly desirable. Two of the perovskite oxide supports tested from the initial catalyst screening show intriguing results for their ability to selectively produce glyceric acid/tartronic acid and lactic acid ($LaMnO_3$ and $LaCrO_3$, respectively). Although there is a clear difference between the two supports, it is extremely difficult to observe exactly why this is the case, although it is probably due to a surface interaction between the support and the substrate or perhaps dependent on one of the reaction parameters. The next step of this study was to investigate the role of the experimental conditions (precisely temperature, base:glycerol ratio, oxygen pressure and Au and Pt metal ratio) have on the performance of the $AuPt/LaCrO_3$ and $AuPt/LaMnO_3$ catalysts towards lactic acid and glyceric acid/tartronic acid production respectively, to gain a greater understanding on how they affect the reaction toward these products.

5.4.1 Selective Control for Production of Lactic Acid from Glycerol.

5.4.1.1 Effect of Base to Substrate Molar Ratio

Since the conversion of glycerol is more catalytically active in the presence of base than without it, a set of experiments were conducted using a range of base to substrate molar ratio from 1 to 4 equivalent of NaOH to gain an insight of the effect of base in this reaction as it can be seen in Table 5.2.

Intriguingly, the NaOH concentration appears to have a non-linear relationship with the conversion of glycerol. An increase in the catalytic performance is observed as the NaOH concentration increases up to two molar equivalents. A decrease in conversion is subsequently observed at higher molar equivalents. This relationship between conversion and NaOH can be explained by the product distribution.

The selectivity breakdown displays a few remarkable trends as the base concentration is increased, shown in Figure 5.2. Firstly, the selectivity towards lactic acid increases dramatically, which illustrates how significant the role the hydroxide anion interaction is for the formation of lactic acid. Secondly, there is a decrease in C-C scission, and whilst the selectivity to lactic acid remains relatively constant, the selectivity towards glyceric acid decreases. This suggests that the C-C scission is occurring only from the oxidation pathway, where the glyceric acid is either sequentially oxidised to tartronic acid or split into C_1 and C_2 products. These products selectivity breakdown is apparently due to role of hydroxyl ions to subjugate either the formation of H_2O_2, or its interaction with the glycerol molecules in the reaction medium. It has been previously reported that C-C cleavage occurs because of the in-situ formation of H_2O_2.[14] It has also been reported that increasing the pH of the aqueous phase promotes the decomposition of H_2O_2.[37] Therefore it is possible to put forward that the decrease in C-C cleavage is due to the promoted decomposition of H_2O_2 by the base. The diminishing of H_2O_2 in the aqueous phase perhaps the reason why the glycerol conversion decreases at higher concentrations of NaOH. If this is true, it can be assumed that there must be a proportional relationship between H_2O_2 concentration and catalytic activity.

Table 5.2. Glycerol oxidation over the $AuPt/LaCrO_3$ catalyst. The effect of NaOH concentration on catalyst performance is assessed. **Reaction conditions:** glycerol (0.3 M), NaOH equivalents as stated, O_2 (3 bar), substrate:metal ratio = 1000, 60 ºC, 6 h.

NaOH Eq	**Time (h)**	**Con (%)**	**Selectivity (%)**				**C.B. (%)**
			GA	TA	LA	C-C Scission	
1	0.5	27	42	4	35	20	100
	1	49	41	5	36	18	99
	2	68	36	6	36	22	99
	4	80	29	8	38	25	96
	6	96	26	10	41	23	98
2	0.5	24	25	5	51	19	100
	1	45	22	7	56	15	96
	2	61	23	8	57	12	98
	4	83	21	11	58	10	95
	6	99	19	18	59	4	96
3	0.5	22	17	3	69	11	100
	1	41	14	5	70	11	98
	2	72	11	7	72	10	98
	4	92	8	9	73	9	99
	6	100	5	12	74	9	99
4	0.5	19	9	4	79	8	100
	1	37	7	3	80	9	100
	2	64	7	3	81	10	99
	4	75	8	4	81	6	98
	6	95	7	13	82	2	99

The mechanism route for the formation of lactic acid is a long-debated subject, and therefore the role of base in the formation of lactic acid is unclear and will be addressed along with the mechanism later in this chapter. A factor that has been established, however, is that base has been shown to promote the dehydration pathway of several polyol reactions. One running theory is that base promotes an initial dehydration of the terminal alcohol group on

glyceraldehyde (GLD), followed by a dehydration reaction. For the formation of lactic acid this would then require a rearrangement reaction to occur with the intermediate species. It can be seen from the base free reaction that, although the conversion is low, the selectivity to dihydroxyacetone (DHA) is high (Table 4.8). This suggests that at higher temperatures, the equilibrium that exists between GLD and DHA shifts in favour of DHA, which implies that the formation of lactic acid occurs *via* DHA rather than GLD. If this were the case, a dehydration on the terminal alcohol group would require a base promoted intra/intermolecular Cannizzaro reaction to produce lactic acid.

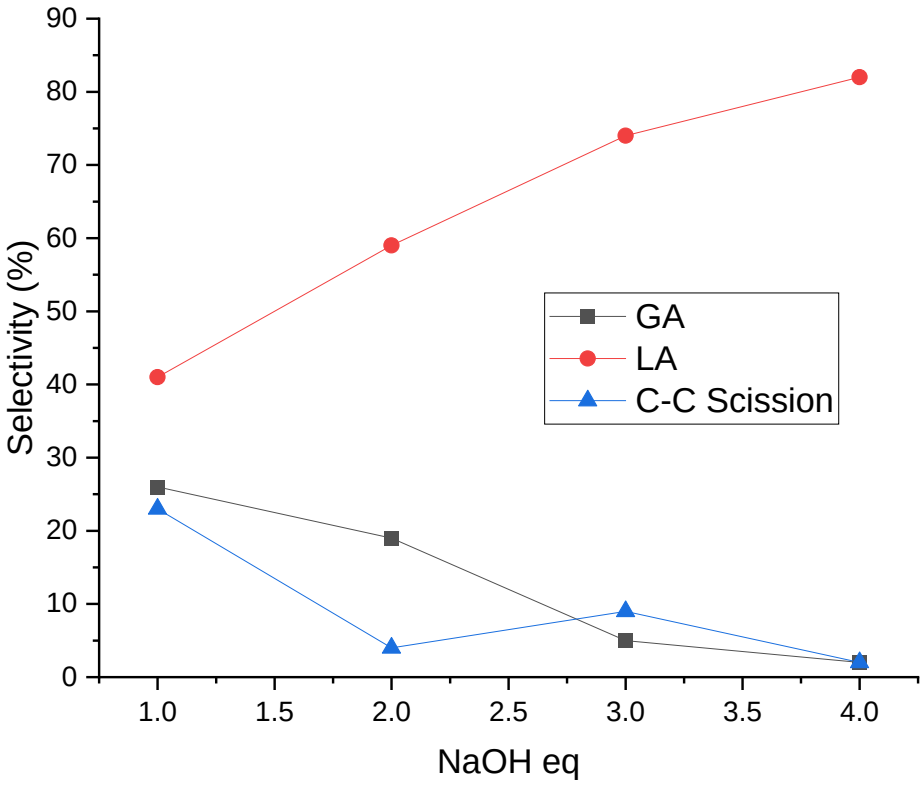

Figure 5.2 showing inverse proportional relationship between the selectivity of LA and other products at 6 h reaction time as NaOH concentration increases.

5.4.1.2 Effect of Temperature

It was previously reported that increasing the reaction temperature for the oxidation of glycerol has shown to not only promote catalytic activity, but also increase the selectivity to GA in the presence of supported Au containing catalysts at lower reaction temperature[7, 18, 19]. However, at higher temperatures of 90 °C favouring the dehydration route to lactic acid[24]. As the temperature has such a profound effect upon the reaction, it was reasoned that it should be the first parameter to be explored, with the results shown in table 5.3 here below.

As expected, there is a proportional relationship between reaction temperature and the rate at which glycerol was converted and this trend observed can be explained through fundamental collision theory. What is interesting, however, is that a substantial changes in the product selectivity was observed as the reaction temperature increased. It was found that as the temperature increased that the amount of C-C scission occurring dropped substantially. As mentioned in the introduction section, part of the C-C scission can occur through either the oxidation of glyceric acid, or the formation of H_2O_2. The excess oxidation of C_1 and C_2 products occurs at higher temperatures, however as less of the glyceric acid is formed, it is less obvious, than at lower temperatures. It is unlikely that H_2O_2 is the cause of C-C scission at higher temperatures due to the inherent instability exhibited at temperatures above 80 °C, the same point at which the C-C scission is lowered during the experiment (Table 5.3). It is also apparent that at higher temperatures there is an increase in the selective formation of lactic acid *via* the dehydration pathway of glycerol, where the rate at which the terminal alcohol group is dehydrated increases, and this is believed to be the crucial step in lactic acid formation. There is a clear switch in selectivity as the temperature approaches 100 °C. Above 100 °C the carbon balance is more difficult to maintain in the glass reactor system due to the volatility of water above its boiling point, resulting in a potentially lower yield in lactic acid, despite the increase in selectivity. From these sets of results at these conditions it can be

concluded that a higher temperature clearly favours lactic acid production and lowers C-C scission which are two of the most important factors when attempting to selectively produce lactic acid, therefore the temperature carried forward for further reactions will be set at 100 °C.

Table 5.3. Glycerol oxidation over the $AuPt/LaCrO_3$ catalyst. The effect of reaction temperature on catalyst performance is assessed. **Reaction conditions:** glycerol (0.3 M), NaOH equivalents (4:1), O_2 (3 bar), substrate:metal ratio = 1000, as stated, 6 h.

Temp (°C)	**Time (h)**	**Con (%)**	**Selectivity (%)**				**C.B. (%)**
			GA	TA	LA	C-C Scission	
40	0.5	24	61	3	14	24	100
	1	46	63	4	12	21	101
	2	81	60	4	15	21	99
	4	99	59	5	16	20	100
	6	100	58	5	17	20	99
60	0.5	31	58	5	14	23	100
	1	57	57	6	16	21	100
	2	93	57	8	16	19	98
	4	100	55	8	19	18	99
	6	100	54	9	19	18	95
80	0.5	29	40	6	43	11	99
	1	66	38	8	43	11	100
	2	81	35	11	44	10	98
	4	100	31	13	48	8	95
	6	100	29	15	50	6	94
100	0.5	45	18	9	69	4	100
	1	69	15	8	71	6	99
	2	100	13	10	71	6	101
	4	100	11	11	70	8	98
	6	100	8	13	70	9	98

5.4.1.3 Effect of Oxygen Pressure

The molecular oxygen is a variable parameter that can have a significant impact on the selectivity of the products, play crucial role in the oxidation reaction. The effect of oxygen pressure on the system involves several key mechanisms and which are complicated further by mass transfer limitations. These can limit the movement of oxygen from the gas phase to the catalyst interface, meaning there are limitations to the oxygen pressure that can be used beyond the simple boundaries of reactor parameters, as going beyond the mass transfer limitations would change the reactions rate limiting step from chemical interactions to oxygen transfer. The role of oxygen pressure in glycerol oxidation has been discussed in detail in the literature,[37,38] and as a key parameter, an investigation into how altering the oxidation pressure affects the production of lactic acid has been conducted.

The result shown in Table 5.4 illustrate that the oxygen pressure within the reaction system has a pronounced effect upon the catalyst activity. The rate of glycerol conversion significantly increases as the oxygen pressure increases, an effect that has been observed in many previous oxidation catalysis studies and illustrated more clearly in figure 5.3. As can be seen that this is not a linear trend, and by increasing the pressure further, does not increase the conversion of glycerol by a substantial amount beyond 3 bar.

Table 5.4. Glycerol oxidation over the $AuPt/LaCrO_3$ catalyst. The effect of oxygen pressure on catalyst performance is assessed. **Reaction conditions:** glycerol (0.3 M), NaOH equivalents (4:1), O_2 as stated, substrate:metal ratio = 1000, 100 ºC, 6 h.

Pressure (bar)	**Time (h)**	**Con (%)**	**Selectivity (%)**				**C.B. (%)**
			GA	TA	LA	C-C Scission	
1	0.5	11	25	1	72	2	100
	1	19	25	1	71	3	100
	2	33	23	2	71	4	98
	4	55	22	2	70	6	99
	6	67	21	3	69	7	99
2	0.5	14	23	3	70	4	100
	1	28	21	4	70	5	99
	2	49	20	4	69	7	98
	4	71	18	5	68	9	98
	6	89	16	5	68	11	99
3	0.5	23	21	3	71	5	100
	1	46	19	3	70	8	100
	2	64	15	5	70	10	99
	4	83	13	6	69	12	101
	6	100	11	7	69	13	100
4	0.5	31	15	2	72	11	100
	1	59	14	4	70	12	99
	2	72	14	4	69	15	98
	4	100	11	5	68	16	95
	6	100	5	8	67	20	94

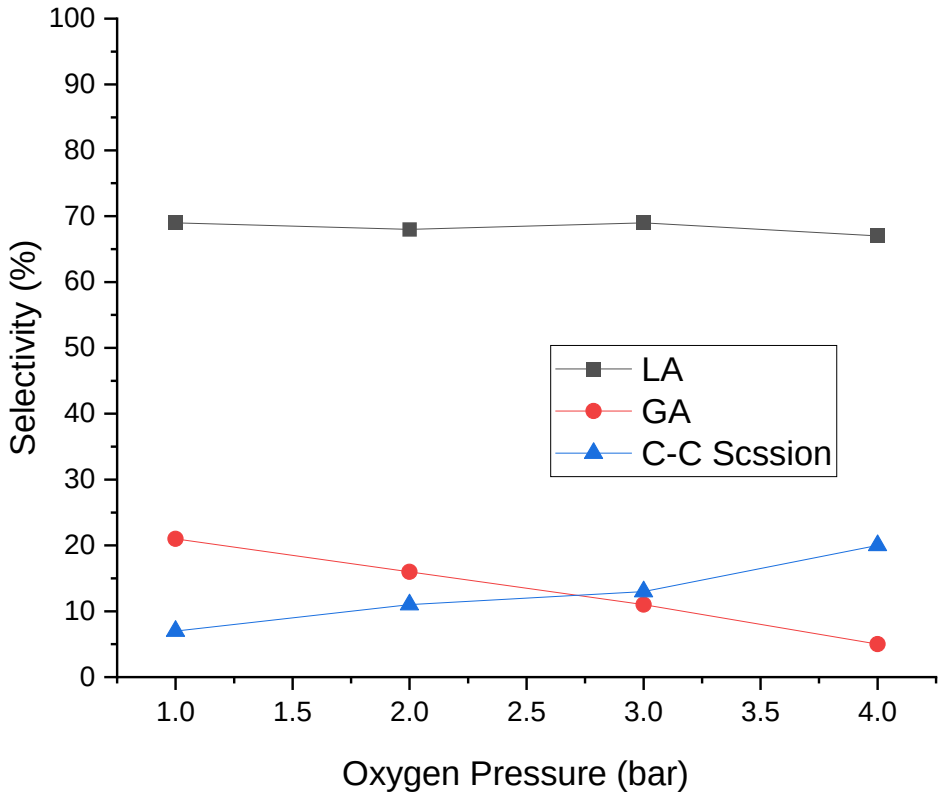

Figure 5.3 Selectivity trend towards glycerol oxidation products at 6 h as a function of O_2 pressure.

It can also be seen that increasing the oxygen pressure potential to aid C-C scission, with the C1 and C2 products increasing in selectivity as the pressure increases, with this effect becoming more pronounced when the glycerol conversion is complete. It has previously been suggested that H_2O_2 is the course of forming C-C scission products, and by increasing the pressure, the concentration of H_2O_2 would increase as more oxygen would be available, which can be reduced by H_2O thereby forming H_2O_2, and thus increasing the amount of scission conducted. This phenomenon has been observed in the work of Ketchie *et al*[14] at lower temperatures (60 – 80 °C), it is also known that H_2O_2 is unstable at elevated temperatures beyond 80 °C, meaning it is unlikely to be the cause of the increased scission in

these cases. What is more likely is that the glyceric acid produced is further oxidised into C1 and C2 products as the oxygen pressure increases, which in turn result the decrease in glyceric acid selectivity as the pressure increases, shown in Figure 5.3. Comparing the selectivity glyceric acid and lactic acid, it can be seen from the result that whilst the selectivity to glyceric acid decreases significantly at higher conversion, the selectivity to lactic acid remains relatively stable. This observation can be explained by the potential stability of the compounds at higher temperatures, whereas the glyceric acid is converted through a further oxidation, the lactic acid appears to remain stable under these conditions, despite the increased pressure, shown in Figure 5.3. This trend could partially explain why the selectivity to lactic acid remains remarkably similar throughout the reaction, as the energy required to conduct the C-C scission is likely lower than that of the production of lactic acid, as the C-C scission occurs at an accelerated rate after the glycerol is fully consumed.

Interestingly, a slight decrease in Selectivity of lactic acid as the pressure increased beyond 3 bar was observed. Looking at the selectivity of the tartronic acid, a sequential oxidation product from glyceric acid, there is no significant amount produced. Tartronic acid is a product that is rarely seen at lower temperatures due to the increased energy required to further oxidise glyceric acid, which is directly competing with the C-C scission, and therefore often only small quantities of tartronic acid are observed. With a higher oxygen content, the yield of tartronic acid production increases, therefore taking resources from the competing production of lactic acid, and thus, lowering the yield of lactic acid produced. This means that whilst the conversion of glycerol increases with pressure, the yield of lactic acid decreases above a critical pressure, which in this case is 3 bar.

5.4.2 Selective control toward Tartronic Acid and Glyceric Acid

Interestingly, from the initial catalysts screening results, it was noted that the AuPt/$LaMnO_3$ appeared to partially inhibit the dehydration route to lactic acid under the same conditions that would usually favour said reaction route. This effect gives itself by selectively promoting a more difficult oxidation pathway, allowing the further oxidation of glyceric acid to tartronic acid at relatively low selectivity over a 6 h period. These results suggest that a longer reaction time may lead to an increased conversion of glyceric acid to a higher yield of tartronic acid. Moreover, having seen the effect of oxygen pressure in the above section towards decrease formation of tartronic acid and glyceric acid, and increased formation C-C scission products as a result of the hydrogen peroxide formed in the reaction mixture from oxygen reduction by H_2O, it is worse investigating and see whether the yield of tartronic acid can be controlled by utilising response surface optimization approach in order to meet the timeframe.

As outlined in chapter two section 2.2.6, response surface methodology is tool for a systematic optimization of reaction variables through a statistical point of view. Temperature of the reaction, oxygen pressure and AuPt metal ratio were the reaction variables investigated and the setpoints were shown in Table 5.5 below. As the effect of the catalyst supports seen is purely a control for the products selectivity breakdown and not the catalyst activity itself, the ratio of the Au:Pt deposited on the surface of the $LaMnO_3$ was altered alongside temperature and pressure to established 17 runs of experiments, and to observe the effect on the selectivity profile (Figure 5.4 and Table 5.6).

Table 5.5 Experimental design of the independent variables.

Independent variables	Factors	Ranges and levels			
		−1	0	1	
Temperature (℃)	A	40	10	100	
Pressure (bar)	B	1	2	3	
Metal Ratio	C	Au	AuPt	Pt	

Table 5.6 Box-Behnken design of experiments using different nanoparticles supported on $LaMnO_3$. Condition: 0.3 M Glycerol, 6 h reaction time, 1000:1 Metal to substrate ratio at varied temperature, pressure, and metal ratio.

Entry	**Factors**			**Con (%)**	**Selectivity (%)**		
	Temperature (℃)	Pressure (bar)	Metal Ratio	GLY	GA	TA	C-C Scission
1	1	1	-1	82	51	32	17
2	0	-1	1	72	81	15	4
3	0	0	0	91	75	11	14
4	0	-1	-1	62	84	10	6
5	0	0	0	75	61	32	7
6	1	-1	1	86	76	16	8
7	-1	-1	0	69	84	12	3
8	0	1	0	100	58	21	21
9	0	0	0	96	59	34	6
10	1	0	-1	87	65	35	0
11	0	0	0	79	57	35	7
12	-1	1	0	74	72	21	7
13	1	1	0	100	52	21	24
14	1	0	-1	79	52	39	9
15	0	0	0	93	57	36	7
16	-1	0	1	67	78	17	5
17	-1	0	-1	64	81	14	5

It can be observed from the selectivity distribution (Table 5.6, entry 14) that the Au supported catalyst produces the highest selectivity towards tartronic acid of 39% at 79% glycerol conversion within 8 h reaction time. This is potentially due to the incapability of catalyst to

remove substrate from it surface a feature enabled by the addition of Pt (table 5.6, entry 13). The activity of the AuPt prepared catalyst increases with the overall conversion over an 8 h period increasing from 69 % to 100% (Table 5.6, entry 7 and 13). Two assumptions were made towards the detrimental effect of increasing the activity of the catalyst, firstly, the production of C2 and C1 C-C scission products increases, and secondly the barrier to the dehydration route becomes less pronounced, beginning to form small amounts of lactic acid. It was found that the ideal balance between the metal nanoparticles ratios tested was the 1wt% (1:1) AuPt-$LaMnO_3$, in which the conversion maintained a steady for 8 h end point (100 % conversion of glycerol), whilst still hindering the formation of lactic acid, and maintaining a low selectivity to the C-C scission products. However, C-C scission products were noted to increase at higher oxygen pressure (Table 5.6, entry 1, 7 and 13).

In the quadratic model, analysis of variance (ANOVA) was used to analyze the adequacy of the developed model, and the results are presented in Table 5.7. Generally, the suitability of the model is confirmed by a higher Fisher's value (F value) with a probability value (*p* value) that is as low as possible. More specifically, values of "Prob > F″ lower than 0.0500 indicating the model terms are significant. Looking into analysis of variance (ANOVA) towards selectivity of tartronic acid (Table 5.7), the F value of 1.18 for the statistical model implies that the model is not significant. Moreover, the lack of fit F-value of 1.03 implies that the lack of fit is not significant relative to the pure error, meaning that the model has a good predictability.

Table 5.7 Analysis of variance for the selectivity of tartronic acid.

Source	Sum of Squares	df	Mean Square	F-value	p-value	
Model	1187.49	9	131.94	1.18	0.4222	not significant
A-Temperature	276.13	1	276.13	2.47	0.1598	
B-Pressure	351.13	1	351.13	3.15	0.1194	
C-Metal ratio	12.50	1	12.50	0.1120	0.7477	
AB	4.00	1	4.00	0.0358	0.8552	
AC	0.2500	1	0.2500	0.0022	0.9636	
BC	6.25	1	6.25	0.0560	0.8197	
A^2	7.12	1	7.12	0.0637	0.8079	
B^2	491.12	1	491.12	4.40	0.0742	
C^2	17.69	1	17.69	0.1585	0.7024	
Residual	781.45	7	111.64			
Lack of Fit	340.25	3	113.42	1.03	0.4694	not significant
Pure Error	441.20	4	110.30			
Cor Total	1968.94	16				

As shown in Figure 5.4, the experimental results can be presented in the form of three-dimensional response-surface plots under fixed conditions. These plots clearly show the integrated effects of the two random variables, wherein all plots confirmed that the selectivity of glyceric acid, tartronic acid and C-C scission products increased with an increase in any individual variable. Thus, according to the RSM, the selectivity toward tartronic acid changes upon variation in the reaction factors. The model used was not significant towards the production of high tartronic acid from glycerol oxidation (Table 5.7). This assumed that high yield of tartronic acid can be achieved with improved reaction conditions (high temperature and longer reaction time). As a result, an extended reaction time study was performed to enable high tartronic acid yield under similar conditions used in RSM experiment (table 5.6, entry 13) from 8 h to 24 h.

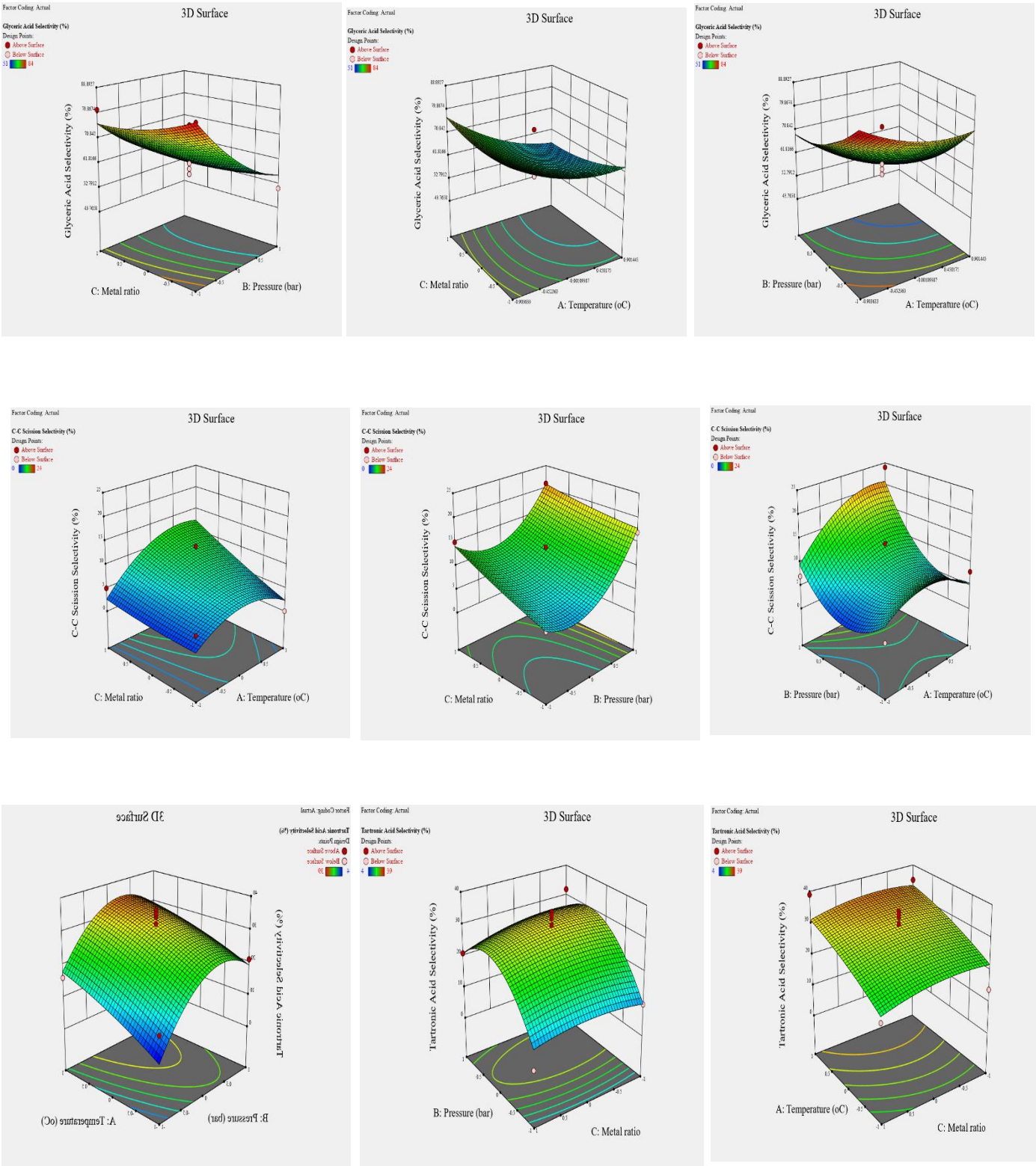

Figure 5.4 Response surface plots for the glycerol oxidation products using AuPt supported on $LaMnO_3$ (a) Glyceric acid selectivity (b) C-C scission selectivity (c) Tartronic acid selectivity; on different combination of reaction variables.

At 8 h it can be seen that the conversion of glycerol has reached 100 %, with the selectivity of glyceric acid being 66 % and the tartronic acid at 22 %. During this time there is only a marginal increase in the selectivity to tartronic acid from the 6 h point, where the total selectivity was 14%. Once the glycerol had been entirely consumed at the 8 h point, the diminishing percentage selectivity (Figure 5.4) clearly indicates the glyceric acid is being converted to tartronic acid. It can be seen that by using harsher reaction conditions than would traditionally be used for the formation of glyceric acid (60 ˚C, 2:1 base:substrate ratio) that the sequential oxidation is promoted, allowing the formation of tartronic acid.

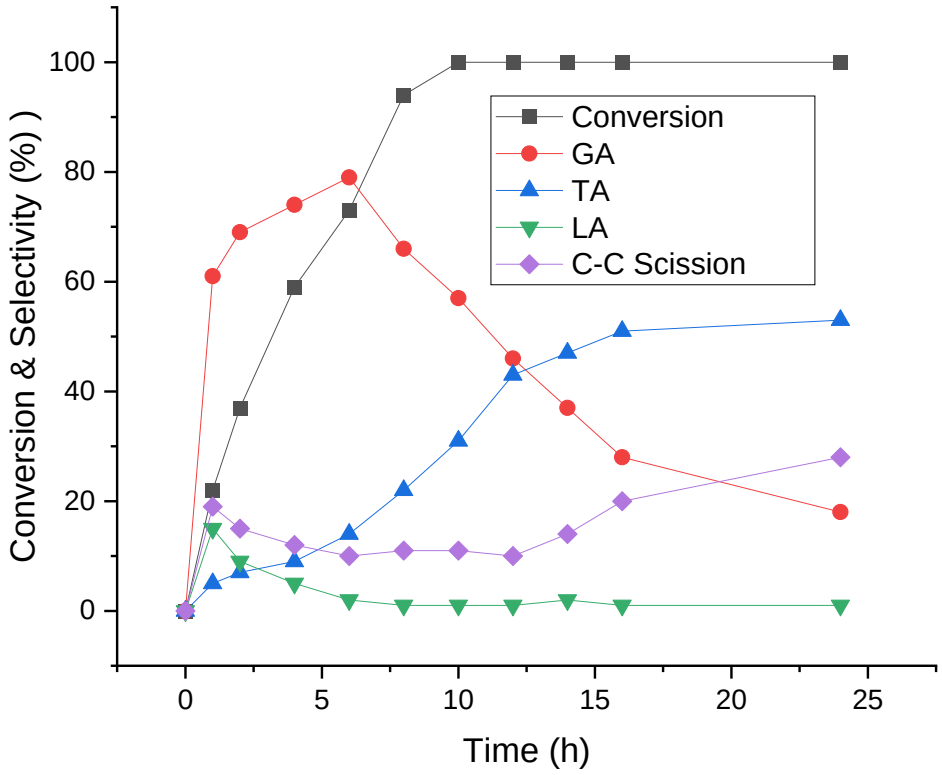

Figure 5.5 Showing conversion and selectivity profile for extended reaction up to 24 hours using 1wt% AuPt/$LaMnO_3$ Catalyst under condition outlined in Table 5.6, entry 13.

Another interesting point is that as the reaction time progressed beyond 14 h, it can be observed that the yield of C-C scission products (glycolic acid precisely) begins to increase whilst tartronic acid remains stable. Davis *et al*, have reported a similar observation when they investigated the oxidation of 0.05 M solution of glyceric acid over Au/TiO_2.[14] Davis suggested that in order to continue with the subsequent oxidation to TA, the primary alcohol group needs to be activated by an external hydroxyl group. But, as it appears that the carboxylic group is more acidic than terminal hydroxyl group, it prevents the deprotonation of the alcohol. Another potential explanation is that the working and inbuild pressure may facilitate the formation of H_2O_2, a species that causes the formation of C-C scission products. At 24 h reaction time, the selectivity of tartronic acid translates to an 53 % yield, which in good agreement with current literature using harsh conditions (100 ˚C, 4:1 base:substrate ratio).

5.5 Mechanism of Glycerol Oxidation

Theoretically, there are two competitive primary products from glycerol oxidation, lactic acid and glyceric acid and they were formed through either dihydroxyacetone (DHA) and glyceraldehyde (GLAD) intermediates under the influence of heterogeneous catalyst. However, lactic acid is the intriguing product with a complicated mechanism. As documented in the literature, two mechanisms were proposed for the formation of lactic acid, one of which is the Cannizaro reaction which would require the formation of pyruvaldehyde intermediate and would then produce pyruvic acid and hydroxyacetone (which itself would combine to dihydroxyacetone), which would then reduce to produce lactic acid. The second of which is the benzilic rearrangement reaction which would require the coupling of two species for the reaction to proceed to lactic acid.

As can be seen in O_2 pressure experiments, there is a detrimental influence on the lactic acid

selectivity when adding an excess O_2 to the reaction system. This could suggest a separation at an early stage in the reaction, with one pathway leading to lactic acid that is unharmed by oxygen content and the other leading to by-products with a rate dependent on O_2 concentration. The actual complicity of O_2 in the lactic acid pathway is therefore likely at a later point in the reaction, which could explain why the initial amount of oxidation products produced is much higher than at the latter stages of the reaction.

The possible theories for the formation of lactic acid are not simple systems, and therefore require a complex level of reaction design to identify the mechanism of formation. As a result, a series of experiments were estabished for the oxidation of glycerol. These experiments were performed to assess how they were affected by the catalyst under reaction conditions in a basic and basic free reaction medium.

Under the optimized reaction conditions (100 ˚C, 4:1 base: substrate, 3 bar O_2, 900 rpm stirring, 1000:1 metal:substrate) from catalyst screening experiments, DHA and GLAD appear to be consumed immediately, with no traces of the two compounds observed after 0.5 h of reaction. Until now, no previous studies which have studied the oxidation of glycerol in a basic reaction medium have documented observing either of these compounds. This proposed that in the presence of base, these products quickly transformed in a base catalysed reaction. These products are in equilibrium, leaving either the primary or secondary alcohol vulnerable to nucleophilic attack. Their selectivity profiles after reaction completion are similar, with the believe that DHA favoured lactic acid formation as opposed to the direct oxidation pathway.

AuPt/$LaMnO_3$ catalyst appears to neglect the said reaction pathway by favouring GA and TA instead of LA observed with AuPt/$LaCrO_3$. Having discovered such a wide difference in the selectivity profile between $LaMnO_3$ and $LaCrO_3$ under NaOH, it is crucial to investigate and see whether these can potentially be able to explain the mechanistic pathway. Table 5.8 show how the SBA-15 assisted perovskite supports can influence the AuPt/$LaBO_3$ catalyst in

glycerol oxidation reaction without base.

Table 5.8 Glycerol oxidation under base free conditions over the AuPt/$LaBO_3$ (B = Cr and Mn) catalyst. **Reaction conditions:** glycerol (0.3 M), NaOH equivalents stated, O_2 (3 bar), substrate:metal ratio = 1000, 100 ºC, 6 h.

B-site	Time (h)	Con (%)	Selectivity (%)						C.M.B. (%)
			GA	GLAD	TA	LA	DHA	C-C Scission	
Cr	0.5	5	2	51	3	20	4	20	100
	1	8	6	47	3	23	5	15	100
	2	13	8	39	5	36	0	12	100
	4	16	5	29	10	44	0	12	99
	6	21	5	19	12	53	0	11	99
Mn	0.5	3	20	1	7	0	69	4	100
	1	7	19	2	12	0	63	5	99
	2	10	16	3	11	0	52	7	102
	4	15	17	5	23	0	45	11	100
	6	19	13	3	39	0	35	11	99

As expected, the catalytic activity decreases significantly under base free conditions. Furthermore, the selectivity profile remains similar to that obtained under base addition reactions. This is a good example of how the reaction is sensitive to environmental conditions in which it occurs. Interestingly from Table 5.8 1wt% AuPt/$LaCrO_3$ produces LA through initial oxidative dehydration of the terminal alcohol group of glycerol to form GLAD. This reaction route has long been known to occur in the presence of base.[39] However, 1 wt% AuPt/$LaMnO_3$ appeared to opposed this reaction route with initial oxidative dehydration of secondary alcohol group of glycerol to DHA. It reported that oxidative dehydration of secondary alcohol group on glycerol to DHA is due to basicity of the catalyst support or co-adsorbed OH^- on the support that act as base to assist the deprotonation of secondary alcohol group.[40] Interestingly, with high selectivity to DHA with the AuPt/$LaMnO_3$ catalyst, no lactic

acid formation was detected which contrary to many findings in the literature.[12,15,41,42]

5.6 Influence of $LaMnO_3$ Support Preparation Methods

As outlined in Chapter 1, the nano-casting method using a hard template, in general, provides several advantages for the synthesis of perovskite oxides, including the access to higher surface area perovskite supports. This is because the energy barrier to form the pure phases for the perovskites is lowered when compared to other conventional methods, allowing for lower calcination temperatures. Comparison between different preparation methods that yield similar properties with the nano-casting method was necessary to observe whether the trend observed was unique to the SBA-15 assisted $LaMnO_3$ perovskite support, with hydrothermal synthesis and a citrate sol-gel method chosen as the comparative methods. Detailed experimental procedures for these methods are described in Chapter 2, section 2.2.2. The X-ray diffraction patterns of $LaMnO_3$ oxide prepared from these methods are shown in Figure 4.6, with all the prepared materials having the $LaMnO_3$ perovskite phase present. However, the hydrothermally synthesised $LaMnO_3$ perovskite comprised 30% perovskite phase with the reminder an additional shifted perovskite phase called layered Ruddlesden-Popper (La_2MnO_4) caused due to the packing height and single metal oxide Mn_2O_3 (Table 5.9).

Table 5. 9 Comparative physical properties of $LaMnO_3$ prepared through NC, CA and HT.

Methods	Phase Purity (%) *	Crystallite Size (nm)*	Surface Area (m^2/g)
Nanocasting (SBA-15)	95	12	98
Citrate Complexing	100	25	9
Hydrothermal	30	15	54

*Determined through XRD analysis using Relative Intensity Ratios of La_2MnO_4, Mn_2O_3 and $LaMnO_3$ obtained from ICDD 00-040-0002, 00-024-0508 and 00-054-1275.

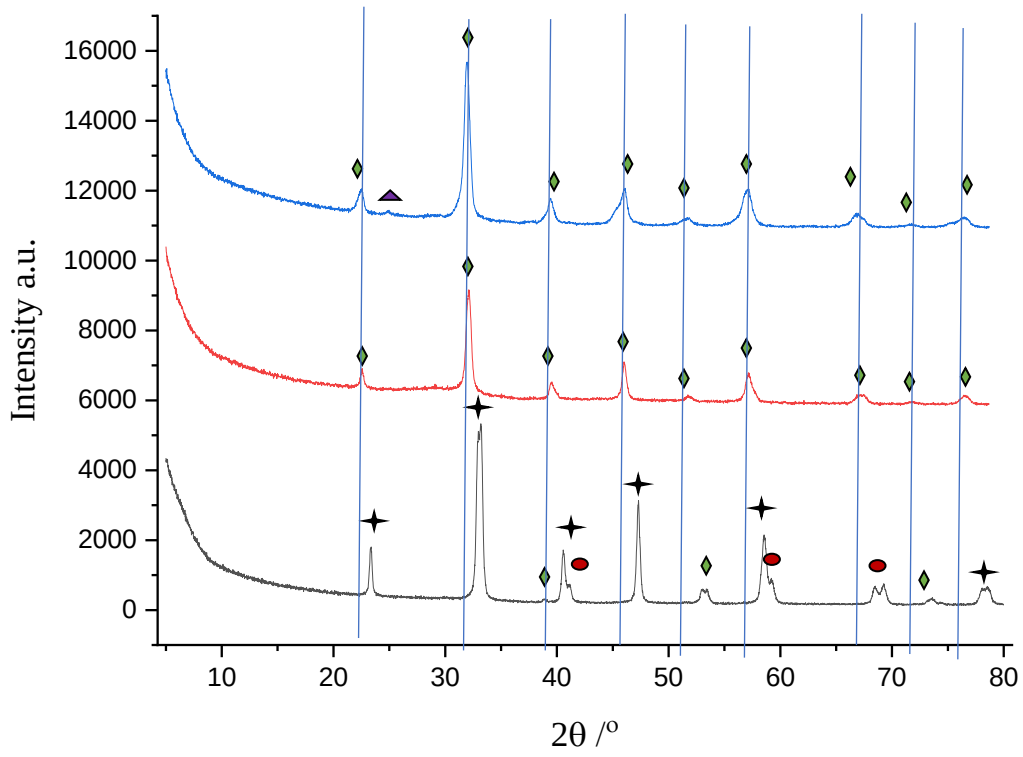

Figure 5.6 X-ray diffraction patterns of $LaMnO_3$ materials prepared by nano-casting method (blue), hydrothermal method (black) and citrate complexing method (red). $LaMnO_3$ (♦), La_2MnO_4 (✦), Mn_3O_4 (●) and La_2O_3 (▲).

Table 5.9 shows the different physical properties of the materials that were obtained by these methods, with the citrate complexing method providing a higher crystallite size and lower surface area (25 nm and 9 m^2/g, respectively), a property comparable to a typical perovskite oxide. Hydrothermally prepared support material was found to have improved surface area, much higher than citrate complexing method, although still lower than the surface area developed through nano-casting method. The $LaMnO_3$ materials prepared by these methods were individually used as a support for AuPt (50:50 wt ratio of 1wt%) by the method outlined in Chapter 2, section 2.2.3. and were tested for the oxidation of glycerol under optimum conditions (100 ˚C, 4:1 base:substrate ratio, 3 bar O_2, 900 rpm stirring, 1000:1 metal:substrate), and the results were displayed in Table 5.10.

Table 5.10 Glycerol oxidation under different preparation methods over the AuPt/$LaMnO_3$ catalyst. **Reaction conditions:** glycerol (0.3 M), 4:1 NaOH:substrate ratio, O_2 (3 bar), substrate:metal ratio = 1000, 100 ºC, 6 h.

Method	**Time (h)**	**Conversion (%)**	**Selectivity (%)**				**C.B. (%)**
			GA	TA	LA	C-C Sc	
NC	0.5	22	61	5	15	19	100
	1	37	63	7	15	15	96
	2	59	65	9	14	12	98
	4	73	67	11	12	10	89
	6	94	70	14	10	6	83
CA	0.5	7	62	3	5	24	100
	1	17	63	6	3	28	96
	2	29	64	9	0	27	98
	4	38	64	13	0	23	98
	6	47	65	15	0	20	99
HT	0.5	19	35	8	26	31	99
	1	34	35	10	25	30	98
	2	41	32	13	25	30	84
	4	55	32	14	23	31	81
	6	61	30	16	22	32	72

As expected, the nano assisted $LaMnO_3$ support catalyst offered higher glycerol conversion compared to other preparation methods. This is potentially linked to the lower surface area having fewer active sites available. However, the interesting observation is that the selectivity profile observed in hydrothermal prepared supported catalyst was significantly different to those obtained using the catalysts prepared using the other methods, with a higher selectivity to Lactic acid and scission products rather than the oxidation products. Another interesting point is that as the time progresses, the carbon mas balance decreases to 72%, a trend that was not observed in the other methods. This suggests that there may be additional unidentified products formed.

Because of the change in selectivity profile seen with the hydrothermal method, the catalyst support was further studied using Pyridine-DRIFT technique to try and understand the differences observed in the selectivity profile distribution. The DRIFT spectrum for the hydrothermal support material is displayed in Figure 5.7.

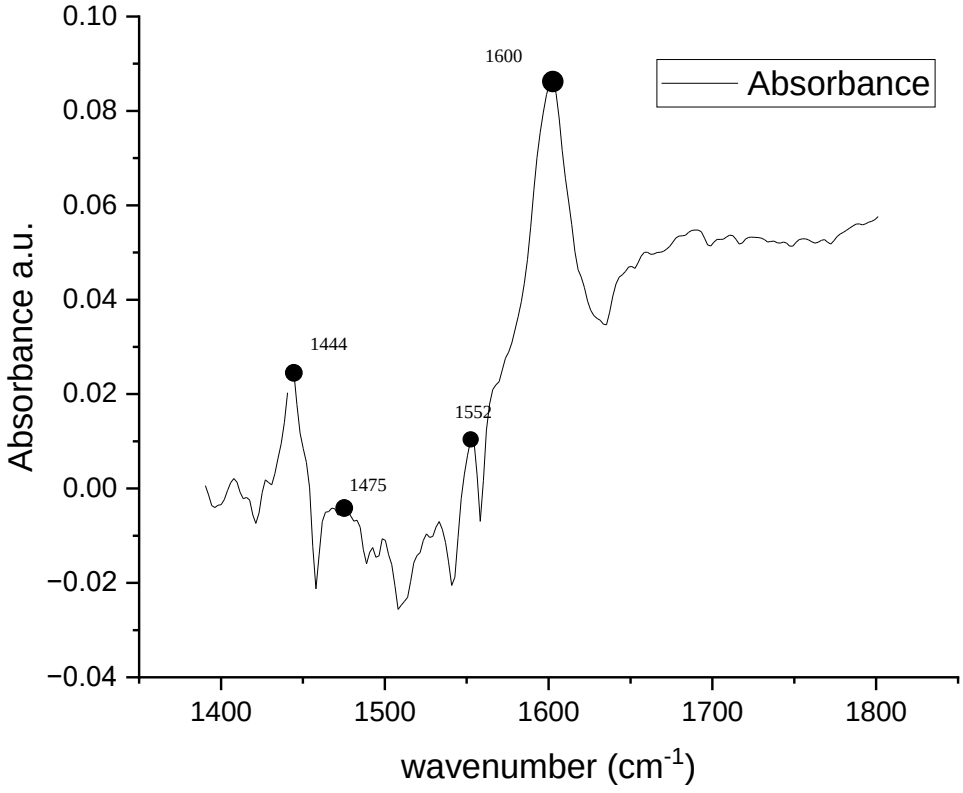

Figure 5.7 Pyridine DRIFT spectrum for hydrothermally prepared $LaMnO_3$ support. Condition: 50 ml/min N_2 flowrate, 150 °C temperature and 1 h chemisorption time.

Different number of bands were observed in the 1350–1700 cm^{-1} range, corresponding to the ring modes of C-C and C-N. The frequency and sharpness of the strong absorbance appearing at 1444 and 1600 cm^{-1} are associated with pyridine molecules chemisorbed at the Lewis acid sites. The band at 1545 cm^{-1} is attributed to the formation of pyridinium ions on the surface of the catalyst, associated with Brønsted acid sites.[43] Lastly, the low intensity band at 1475 cm^{-1}

is due to the two contributions of both Brønsted and Lewis acid sites.[44]

To provide additional insights into the interaction of substrate with Au and Pt sites, the CO chemisorption of the AuPt supported on hydrothermally prepared $LaMnO_3$ catalyst the vibrational stretching modes of CO adsorption on Au and Pt in a region 2000 – 2250 cm^{-1} as displayed in Figure 5.8. This technique has been reported previously to probe the interaction of CO and PGM supported catalysts.[45,46] Assignments of specific bands to CO adsorption on Au or Pt have been made,[47] and conducting analysis at room temperature will represents an opportunity to observe the relative population of different vibrational bands attributable to Au or Pt.

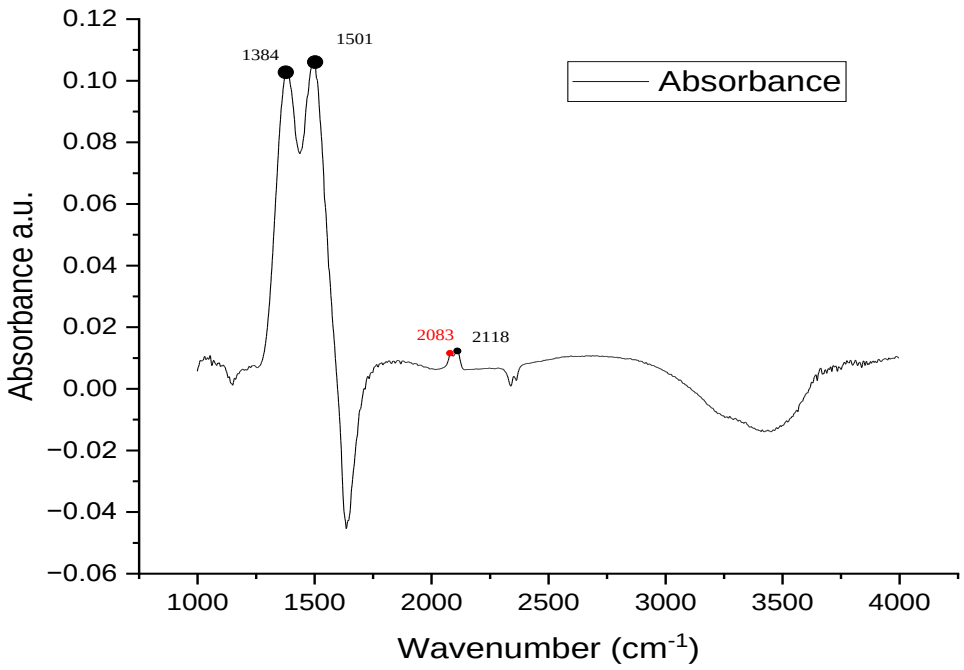

Figure 5.8. CO-DRIFTS spectrum for AuPt on hydrothermally support material. Condition; 3 ml/min flowrate of CO (2% in N_2), 30 min chemisorption time, 30 ml/min N_2 flowrate, 1 h desorption time.

The peak at 2083 cm^{-1} is assigned to C–O stretching modes, related to the CO on Au sites. The additional peak around 2118 cm^{-1} can be attributed to CO linearly adsorbed on the

surface of platinum particles (Pt).[48] The intensity of the above two peaks increase with the increased CO flow time. The intensity of these peaks remains, but, decreased after complete removal of the surface CO indicating there is adsorption of CO molecules on the gold catalysts. The absorption peaks in the range of 3600–3400 cm^{-1} are assigned to surface hydroxyl groups adsorbed on the support Additional peaks at 1501 and 1384 cm^{-1} were detected, originating from the carbonate and carboxylate species adsorbed on the $LaMnO_3$ support. In summary, the presence of Pt in one-to-one ratio Au ratio (1:1) enhances the CO adsorption and catalytic performance for glycerol oxidation (Table 5.9). The abundant hydroxyl species in the catalysts could provide more active sites and improve the catalytic ability, which might be the reason for dehydration product observed at the early stage of the reaction and increased C–C scission products, instead of tartronic acid from the sequential oxidation of glyceric acid.

5.6 Conclusion

Perovskites are typical mixed metal oxide materials with diverse physicochemical properties with almost 90 % of the metals in the periodic table can be incorporated into the perovskite structure. However, perovskite oxides normally have low surface area because of the high calcination temperature needed to form the pure perovskite phase, which in turn limits their use as supporting material for nanoparticles. As documented by Evans *el al.* the supercritical antisolvent precipitation technique enhanced the surface area of these materials, enabling them to be utilised as catalyst supports, although this technique only improved the surface area to around 50 $m^2\ g^{-1}$.[49] Here, using a nano-casting method with SBA-15 as the template, a series of similar perovskite oxides have been successfully produced with surface areas high enough to be used as supports for PGM nanoparticles for the liquid phase oxidation of

glycerol. A range of $LaBO_3$ supports with the B site substituted completely with a variety of first series transition metal cations (where B is Cr, Mn, Fe, Co and Ni), with surface areas ranging between 68 – 158 $m^2 g^{-1}$ were produced. Sol immobilisation was used to deposited 1 wt% AuPt on the perovskites, as this method allows a high dispersion of nanoparticles on the surface of the supports.

The experimental conditions obtained through the work conducted by Evans *et al.* were used for an initial catalyst screening oxidation of glycerol. The selectivity profile of the reaction was controlled, allowing the selective production of glyceric acid/tartronic acid through the oxidation pathway, or the selective production of lactic acid through the dehydration pathway by changing the B site cation of the support.

The ability to control which pathway was favoured was enabled by selecting a particular B site transition metal cation, with Co/Ni giving a broad selectivity of products, Mn providing an enhanced oxidation route with high selectivity to glyceric acid which further oxidised to tartronic acid and C-C scission products at longer reaction times, and Cr/Fe favouring the dehydration pathway enabling a high selectivity to lactic acid. A set of experiments were carried out using Cr based perovskite supported catalysts in order to obtain the optimal conditions for lactic acid yield and to study mechanistic features.

The deposition of AuPt nanoparticles was found to be necessary, as the perovskite supports themselves were almost inactive for the oxidation of glycerol, with the choice of B site in the perovskite structure having no discernible effect on the AuPt nanoparticle size which was illustrated in Chapter 3.

It appears that the oxygen vacancies in the perovskite oxides studied play a role in the selectivity distribution for glycerol oxidation with lower oxygen vacancy found to favour the glycerol oxidation pathway and those with high oxygen vacancies found to be follow dehydration pathway to lactic acid.

An extended study over 24 hours reaction for AuPt/$LaMnO_3$ catalyst were found to increase the yield of tartronic acid, however, as the time progresses beyond 16 h the selectivity of tartronic acid remained unchanged and the selectivity to C-C scission product started to increase. This was potentially due to the increased oxygen concentration which may facilitate the formation of H_2O_2, a species that causes the formation of C-C scission products.[50]

The effect of different preparation methods for the $LaMnO_3$ support was studied with hydrothermal and citrate complexing, in addition to the nano-casting method studied to see if there is a change in the performance for the oxidation of glycerol. It was found that as long the $LaMnO_3$ perovskite phase is dominant, the selectivity profile of this reaction remains the same with both nano-casting and citrate complexing method giving 95% and 100% pure perovskite phase, respectively, showing similar selectivity trend. However, the hydrothermally prepared support with 30% perovskite phase, 70% spinel phase showed a different selectivity profile and a lower carbon balance compared to other methods. This is possibly due to the presence of single metal oxide and spinal structure found in the support by the XRD.

To conclude, the study in this chapter showed the development of new supported materials with a wide range of physicochemical properties allowed the selective production of value-added chemicals from renewable feedstocks.

5.7 Reference

1. Galadima, A. & Muraza, O. Biodiesel production from algae by using heterogeneous catalysts: A critical review. *Energy* **78**, 72–83 (2014).
2. Kulkarni, M. G., Gopinath, R., Meher, L. C. & Dalai, A. K. Solid acid catalyzed biodiesel production by simultaneous esterification and transesterification. *Green Chem.* **8**, 1056–1062 (2006).
3. Sani, H. & Gaya, U. Methanolysis of Gmelina Seed Oil to Biodiesel with KNO3 Activated MgO-ZnO Composite Catalyst. *J. Turkish Chem. Soc. Sect. A Chem.* **6**, 335–348 (2019).
4. Garcia, R., Besson, M. & Gallezot, P. Chemoselective catalytic oxidation of glycerol with air on platinum metals. *Appl. Catal. A, Gen.* **127**, 165–176 (1995).
5. Villa, A. *et al.* Glycerol oxidation using gold-containing catalysts. *Acc. Chem. Res.* **48**, 1403–1412 (2015).
6. Dimitratos, N. *et al.* Effect of particle size on monometallic and bimetallic (Au,Pd)/C on the liquid phase oxidation of glycerol. *Catal. Letters* **108**, 147–153 (2006).
7. Gil, S. *et al.* Effect of the operation conditions on the selective oxidation of glycerol with catalysts based on Au supported on carbonaceous materials. *Chem. Eng. J.* **178**, 423–435 (2011).
8. Douthwaite, M., Powell, N., Taylor, A., Ford, G. & López, M. Glycerol Selective Oxidation to Lactic Acid over AuPt Nanoparticles ; Enhancing reaction selectivity and understanding by support modification. *The European Society Journal of Catalysis* 3097–3107 (2020) doi:10.1002/cctc.202000026.
9. Prati, L. & Rossi, M. Chemoselective catalytic oxidation of polyols with dioxygen on gold supported catalysts. *Stud. Surf. Sci. Catal.* **110**, 509–515 (1997).
10. Dimitratos, N. *et al.* Oxidation of glycerol using gold-palladium alloy-supported

nanocrystals. *Phys. Chem. Chem. Phys.* **11**, 4952–4961 (2009).

11. Ketchie, W. C., Murayama, M. & Davis, R. J. Selective oxidation of glycerol over carbon-supported AuPd catalysts. *J. Catal.* **250**, 264–273 (2007).
12. Ide, M. S. & Davis, R. J. The important role of hydroxyl on oxidation catalysis by gold nanoparticles. *Acc. Chem. Res.* **47**, 825–833 (2014).
13. Zope, B. N., Hibbitts, D. D., Neurock, M. & Davis, R. J. Reactivity of the Gold / Water Interface During Selective Oxidation Catalysis Reactivity of the Gold / Water Interface. *J. Colloid Interface Sci.* **330**, 74–78 (2019).
14. Ketchie, W. C., Murayama, M. & Davis, R. J. Promotional effect of hydroxyl on the aqueous phase oxidation of carbon monoxide and glycerol over supported Au catalysts. *Top. Catal.* **44**, 307–317 (2007).
15. Prati, L. *et al.* Gold catalyzed liquid phase oxidation of alcohol: The issue of selectivity. *Faraday Discuss.* **152**, 353–365 (2011).
16. Namdeo, A., Mahajani, S. M. & Suresh, A. K. Journal of Molecular Catalysis A : Chemical Palladium catalysed oxidation of glycerol — Effect of catalyst support. *"Journal Mol. Catal. A, Chem.* **421**, 45–56 (2016).
17. Xu, C., Du, Y., Li, C., Yang, J. & Yang, G. Applied Catalysis B : Environmental Insight into effect of acid / base nature of supports on selectivity of glycerol oxidation over supported Au-Pt bimetallic catalysts. *"Applied Catal. B, Environ.* **164**, 334–343 (2015).
18. Fongarland, P. & Mimura, N. Green Chemistry chemicals †. 1960–1979 (2011) doi:10.1039/c1gc15320j.
19. Liu, S., Sun, K. & Xu, B. Speci fi c Selectivity of Au-Catalyzed Oxidation of Glycerol and Other C 3 - Polyols in Water without the Presence of a Base. *ACS Catalysis* 2226–2230 (2014).

20. Villa A., Campisi S., Mohammed K. M. H, Nikolaos Dimitratos, Floriana Vindigni, Maela M., Jones W., Bowker M., Hutchings G. J. and Prati L. Tailoring the selectivity of glycerol oxidation by tuning the acid–base properties of Au catalysts. *Catalysis Science & Technology*, **2**, 1126–1132 (2015).

21. Garlisi, C. *et al.* Widely Tuneable Composition and Crystallinity of Graded Na 1 + x TaO 3 ± δ Thin Films Fabricated by Chemical Beam Vapor Deposition. 1–14 (2022).

22. Atta, N. F., Galal, A. & El-Ads, E. H. Perovskite Nanomaterials – Synthesis, Characterization, and Applications. *Perovskite Mater. - Synth. Characterisation, Prop. Appl.* (2016) doi:10.5772/61280.

23. Silva, P. R. N. & Soares, A. B. Lanthanum based high surface area perovskite-type oxide and application in CO and propane combustion. *Eclet. Quim.* **34**, 31–38 (2009).

24. Zhu, H., Zhang, P. & Dai, S. Recent Advances of Lanthanum-Based Perovskite Oxides for Catalysis. *ACS Catal.* **5**, 6370–6385 (2015).

25. Evans, C. D. *et al.* The preparation of large surface area lanthanum based perovskite supports for AuPt nanoparticles: Tuning the glycerol oxidation reaction pathway by switching the perovskite B site. *Faraday Discuss.* **188**, 427–450 (2016).

26. Deng, H., Lin, L. & Liu, S. Catalysis of Cu-doped Co-based perovskite-type oxide in wet oxidation of lignin to produce aromatic aldehydes. *Energy and Fuels* **24**, 4797–4802 (2010).

27. Bianchi, C. L., Canton, P., Dimitratos, N., Porta, F. & Prati, L. Selective oxidation of glycerol with oxygen using mono and bimetallic catalysts based on Au , Pd and Pt metals. *Catalysis Today* **103**, 203–212 (2005).

28. Prati, L., Villa, A., Campione, C. & Spontoni, P. Effect of gold addition on Pt and Pd catalysts in liquid phase oxidations. *Topic in Catalysis* **44**, (2007).

29. Pt, A. & Catalysts, T. Efficient Synthesis of Lactic Acid by Aerobic Oxidation of

Glycerol on Au–Pt/TiO 2 Catalysts. 7368–7371 (2010) doi:10.1002/chem.201000740.

30. Porta, F., Prati, L., Rossi, M., Coluccia, S. & Martra, G. Metal sols as a useful tool for heterogeneous gold catalyst preparation : reinvestigation of a liquid phase oxidation. *Catalysis Today* **61**, 165–172 (2000).

31. Lakshmanan, P., Upare, P. P., Le, N. & Kyu, Y. General Facile synthesis of CeO 2 - supported gold nanoparticle catalysts for selective oxidation of glycerol into lactic acid. *Applied Catal. A, Gen.* **468**, 260–268 (2013).

32. Tsuji, A., Rao, K. T. V., Nishimura, S., Takagaki, A. & Ebitani, K. Selective oxidation of glycerol by using a hydrotalcite-supported platinum catalyst under atmospheric oxygen pressure in water. *ChemSusChem* **4**, 542–548 (2011).

33. Zhang, C., Wang, T., Liu, X. & Ding, Y. Selective oxidation of glycerol to lactic acid over activated carbon supported Pt catalyst in alkaline solution. **37**, 502–508 (2020).

34. Jin, X. *et al.* Phase Transformed PtFe Nanocomposites Show Enhanced Catalytic Performances in Oxidation of Glycerol to Tartronic Acid. *Industrial & Engineering Chemistry Resear* 13157–13164 (2017) doi:10.1021/acs.iecr.7b01473.

35. Wang, D., Villa, A., Su, D., Prati, L. & Schlögl, R. Carbon-supported gold nanocatalysts: Shape effect in the selective glycerol oxidation. *ChemCatChem* **5**, 2717–2723 (2013).

36. Evans, C. D., Bartley, J. K., Taylor, S. H., Hutchings, G. J. & Kondrat, S. A. Perovskite Supported Catalysts for the Selective Oxidation of Glycerol to Tartronic Acid. *Catal. Letters* (2022) doi:10.1007/s10562-022-04111-2.

37. Dimitratos, N., Villa, A. & Prati, L. Liquid Phase Oxidation of Glycerol Using a Single Phase (Au – Pd) Alloy Supported on Activated Carbon : Effect of Reaction Conditions. 334–340 (2009) doi:10.1007/s10562-009-0192-8.

38. Pina, C. Della, Falletta, E. & Rossi, M. Update on selective oxidation using gold.

Chem. Soc. Rev. **41**, 350–369 (2012).

39. Shaffer, P. A. & Friedemann, T. E. Sugar Activation By Alkali. *J. Biol. Chem.* **86**, 345–374 (1930).

40. Wang, Y. *et al.* Selective Oxidation of Glycerol to Dihydroxyacetone over Au/CuxZr1- xOy Catalysts in Base-Free Conditions. *ACS Appl. Mater. Interfaces* **11**, 44058–44068 (2019).

41. Gil, S. *et al.* Effect of the operation conditions on the selective oxidation of glycerol with catalysts based on Au supported on carbonaceous materials. *Chem. Eng. J.* **178**, 423–435 (2011).

42. Hirasawa, S., Nakagawa, Y. & Tomishige, K. Selective oxidation of glycerol to dihydroxyacetone over a Pd-Ag catalyst. *Catal. Sci. Technol.* **2**, 1150–1152 (2012).

43. Hemmann, F., Agirrezabal-Telleria, I., Jaeger, C. & Kemnitz, E. Quantification of acidic sites of nanoscopic hydroxylated magnesium fluorides by FTIR and 15N MAS NMR spectroscopy. *RSC Adv.* **5**, 89659–89668 (2015).

44. Lee, B. J., Hur, Y. G., Kim, D. H., Lee, S. H. & Lee, K. Y. Non-oxidative aromatization and ethylene formation over Ga/HZSM-5 catalysts using a mixed feed of methane and ethane. *Fuel* **253**, 449–459 (2019).

45. Carter, J. H. *et al.* Synergy and Anti-Synergy between Palladium and Gold in Nanoparticles Dispersed on a Reducible Support. *ACS Catal.* **6**, 6623–6633 (2016).

46. Marx, S., Krumeich, F. & Baiker, A. Surface properties of supported, colloid-derived gold/palladium mono- and bimetallic nanoparticles. *J. Phys. Chem. C* **115**, 8195–8205 (2011).

47. Li, J., Zhu, B. & Wang, G. Catalysis Science & Technology Enhanced CO catalytic oxidation over an Au – Pt alloy supported on TiO 2 nanotubes : investigation of the hydroxyl and Au / Pt ratio influences †. 6109–6122 (2018) doi:10.1039/c8cy01642a.

48. Tanaka, K. I., Shou, M., He, H., Shi, X. & Zhang, X. Dynamic characterization of the intermediates for low-temperature pROX reaction of cO in h2-oxidation of cO with oH via hCOO intermediate. *J. Phys. Chem. C* **113**, 12427–12433 (2009).

49. Evans, C. D. *et al.* The preparation of large surface area lanthanum based perovskite supports for AuPt nanoparticles: Tuning the glycerol oxidation reaction pathway by switching the perovskite B site. *Faraday Discuss.* **188**, 427–450 (2016).

50. Evans C. D., Douthwaite M., Carter J. H., Pattisson S., Kondrat S.A., Bethell D., Knight D. W., Taylor S. H., and Hutchings G. J. Enhancing the understanding of the glycerol to lactic acid reaction mechanism over AuPt / TiO 2 under alkaline conditions. *J. Chem. Phys*. 152, 134705 (2020); doi: 10.1063/1.5128595.

Chapter 6

Conclusions and Future Work

In this dissertation, a range of heterogeneous catalysts containing supported Au and Pt nanoparticles were investigated for the selective oxidation of 5-hydroxymethyl furfural to 2,5-furandicarboxylic acid and the selective oxidation of glycerol to lactic acid. The purpose of this final chapter is to summarise the conclusions derived from each body of the work and offer suggestions of additional work which could be conducted in the future.

6.1 Selective Oxidation of 5-hydroxymethyl Furfural with Perovskite Support.

ABO_3 perovskite mixed metal oxides were formed through a nanocasting method using SBA-15 as template. This method enabled the synthesis of relatively high surface area perovskite materials, which typically have surface areas lower than 10 m^2 g^{-1}. The range of perovskites formed were La based materials with different B sites, i.e. Cr, Mn, Fe, Co and Ni. The perovskites were used as supports for gold-platinum nanoparticle catalysts and investigated for HMF oxidation, to understand how the support could affect the reaction.

Catalysts (1 wt% $AuPt/LaMO_3$, where M is a transition metal as stated above) for the HMF oxidation process were formed by the use of sol immobilization without a final acidification step in the preparation process due to the amphoteric nature of the perovskite supports. Reaction conditions from the work of Li *et al.*,[1] were used for initial catalysts screening experiments. The $AuPt/LaMnO_3$ catalyst was found to produce the highest FDCA yield with an excellent carbon balance after the reaction, indicating that additional side products were not produced. This catalyst was used for an investigation of the reaction conditions, to identify key parameters that affect the rate and selectivity of FDCA product. The aim of these experiments was twofold. Firstly, the conditions were manipulated sequentially to optimise

the highest potential yield to FDCA, and secondly, to gain an insight into how the conditions affect the selectivity and rate of the reaction. The reason for establishing a set of reaction conditions was to reduce the considerable variables for future work.

The reaction conditions were varied in a systematic way to identify the optimum conditions to produce FDCA. The first variable considered was temperature and it was found that by increasing the temperature, the rate of the reaction was also increased. This observation is expected and has been seen in many catalytic reactions. The initial oxidation step proceeded at 50 ℃ reaction temperature to HMFCA yield 61% at HMF conversion greater than 99%. As the temperature increased, the HMFCA sequentially oxidized to FFCA which is considered to be rate determining step. The selectivity to FDCA also increased with increasing temperature up to 110 ℃. Beyond this temperature, a significant decrease in carbon mass balance was observed which can be attributed to the formation of humins as by-product. It is suggested that this is a result of the limited supply of O_2 in the reaction mixture which will allow the formation of Cannizaro product, 2,5-bishydroxymethyl furan (BHMF), which reacts with HMFCA through condensation reaction to produce unit that polymerised to humins.[2] The next parameter investigated in the optimization experiments was the oxygen pressure, starting from 1 bar up to 4 bar which was the maximum operating pressure of the glass reactors used. It was found that from 1 to 2 bar oxygen pressure, HMFCA was selectively the major product. At higher pressure, the HMFCA was sequentially oxidised to FDCA with a continued selectivity increase to FDCA as the oxygen pressure increases up to 3 bar. Above this point, the FDCA selectivity remain unchanged which could be due to gold-platinum metal saturating at high oxygen pressure,[3] however, carbon mass was substantially decreased and this was accounted for the formation of by-products. This effect was more pronounced in the base:substrate ratio optimization experiments. The base:substrate ratio experiments showed that as the amount of base increases, the selectivity to FDCA also

increased. However, at higher base to substrate ratio, the carbon mass balance significantly decreases which can be explained by the formation of by-products. The effect of base in of HMF oxidation was studied in the absence of catalyst and it was observed that HMF converted to HMFCA, with the carbon mass balance of 79%, which was due to parallel degradation of HMF to humins. The scientific community continues to debate and disagree regarding the mechanism of humin formation. In fact, various mechanisms that primarily focusing on HMF suggested that poor stability of HMF in alkaline environment is the primary trigger for the formation of humins. [4–7]. It has also been documented in the literature that the formation of humins is due to the Cannizzaro disproportionation reaction that occurred between the HMF and OH^- which is initiated in the presence of NaOH.[8] The competitive route toward the formation of humins is shown in scheme 6.1.

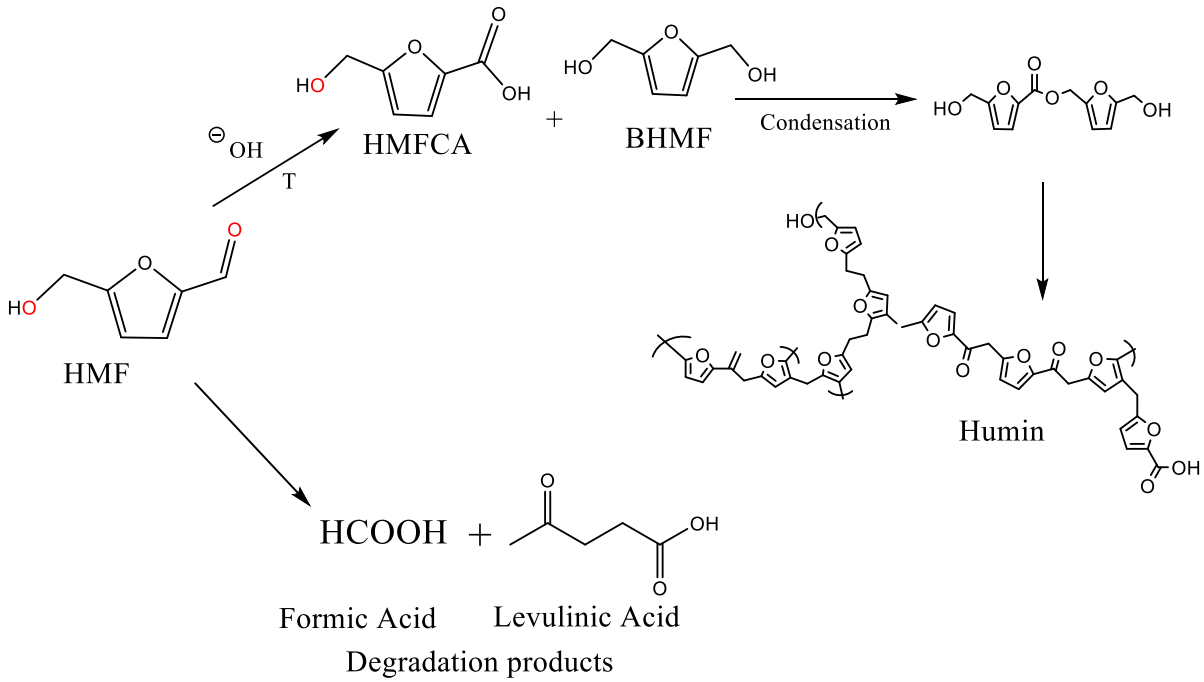

Scheme 6.1 Reaction route for the HMF oxidation in the presence of NaOH without catalyst.

The mechanism by which FDCA is produced from HMF is well discussed in the literature.[8–13] It is agreed that in the presence of base, the first two steps involve the oxidation of HMF to a

terminal diol through the nucleophilic attack of hydroxide ion of carbonyl group and the followed by dehydrogenation of the formed diol to produce HMFCA. It is possible, that increasing the reaction temperature and base amount are favouring both the oxidation and subsequent dehydrogenation step. An isotopic labelling experiment involving the use of ^{18}O as illustrated by Davis *et al.* prove this, shown in Scheme 6.2.

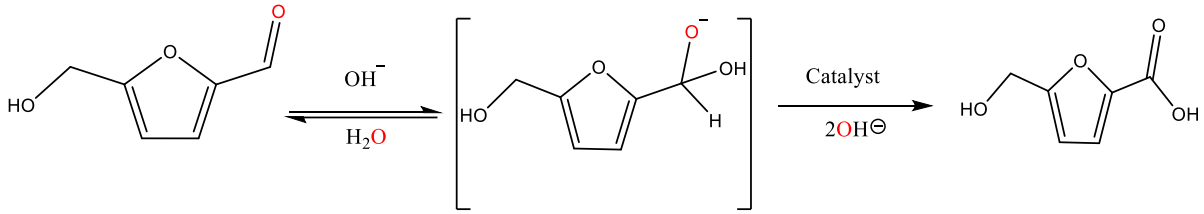

Scheme 6.2. Isotopic labelling mechanism of HMF to HMFCA.

If the reaction was conducted where the HMF consisted of terminal alcohol groups containing ^{18}O, it would be possible to determine whether temperature promotes these two steps. If this is the case, increasing the reaction temperature would lead to higher quantities of $H_2{}^{18}O$ in solution. By running reactions at different temperatures and monitoring the quantity of $H_2{}^{18}O$ in the reaction solution it would theoretically be possible to confirm this hypothesis. The next step is the abstraction of a proton from the alcohol group by the catalyst surface bound hydroxide ion to form an alkoxy intermediate and then transformed the aldehyde product to through the loss of water molecule and electrons. This step was found to be the fastest oxidation step observed in the parameter optimisation experiments (temperature, oxygen pressure and base to HMF ratio). The rehydration of aldehyde group follows, as happened in the first step, and finally abstraction of a proton from the terminal alcohol group by the hydroxide ion on the surface of the catalyst produces FDCA (Scheme 6.3). During the mechanistic steps, the six electrons liberated and deposited on the catalyst surface which were then believed to be abstracted by the oxygen and stop the catalytic oxidation process.[14]

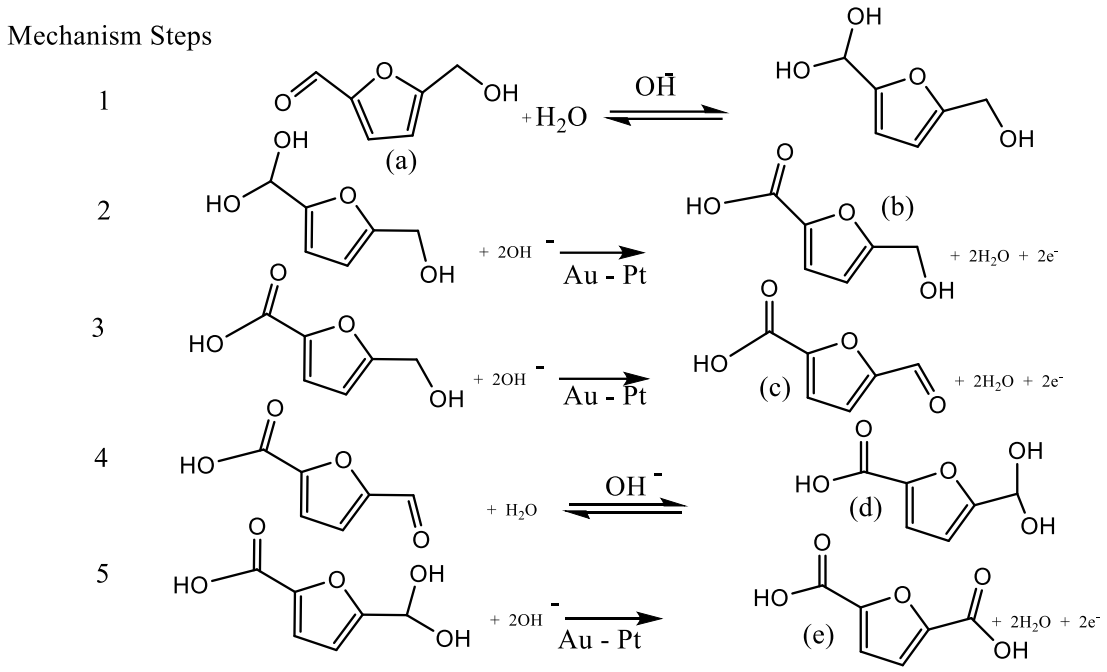

Scheme 6.3. mechanism of HMF oxidation under base condutions (a) HMF (b) HMFCA (c)FFCA (d) Alkoxy intermediate (e) FDCA.

Also noteworthy was the series of experiments showing the effect of exchanging the B-site cation of the $LaMnO_3$ perovskite catalyst support for HMF oxidation under base free conditions. Replacing the manganese with chromium (Cr) and nickel (Ni), it was observed that the reaction rate increased and that two different mechanistic oxidation routes were seen. Lanthanum based perovskite supports containing Cr, Mn and Fe initially oxidize HMF to both DFF and HMFCA intermediates. These intermediates were reported under base free HMF oxidation process with amphoteric supports.[15–18] However, the same reaction route with base added experiment was observed with $LaCoO_3$ and $LaNiO_3$ supported catalysts under base free conditions. This was attributed to the basic nature of these catalyst support, which was confirmed by the TPD data. The mechanism of HMF oxidation under base free conditions has reported in the literature,[2,10,19–21] and is thought to be dependent on the acid-base properties of the catalyst support as well as the reaction conditions.[12,22] It has previously been shown that a neutral or slightly acidic catalyst support favoured dehydrogenation of the

alcohol group in HMF to an aldehyde forming DFF, followed by the formation of a germinal diol, which then undergoes proton abstraction by a hydroxide ion on the surface of the catalyst, and free electrons which has been scavenged by the molecular oxygen to yield the FDCA as displayed in Scheme 6.4. On the other hand, basic catalyst supports favoured the dehydrogenation of carbonyl group in HMF to produce HMFCA as seen under the oxidation of HMF with base.[19]

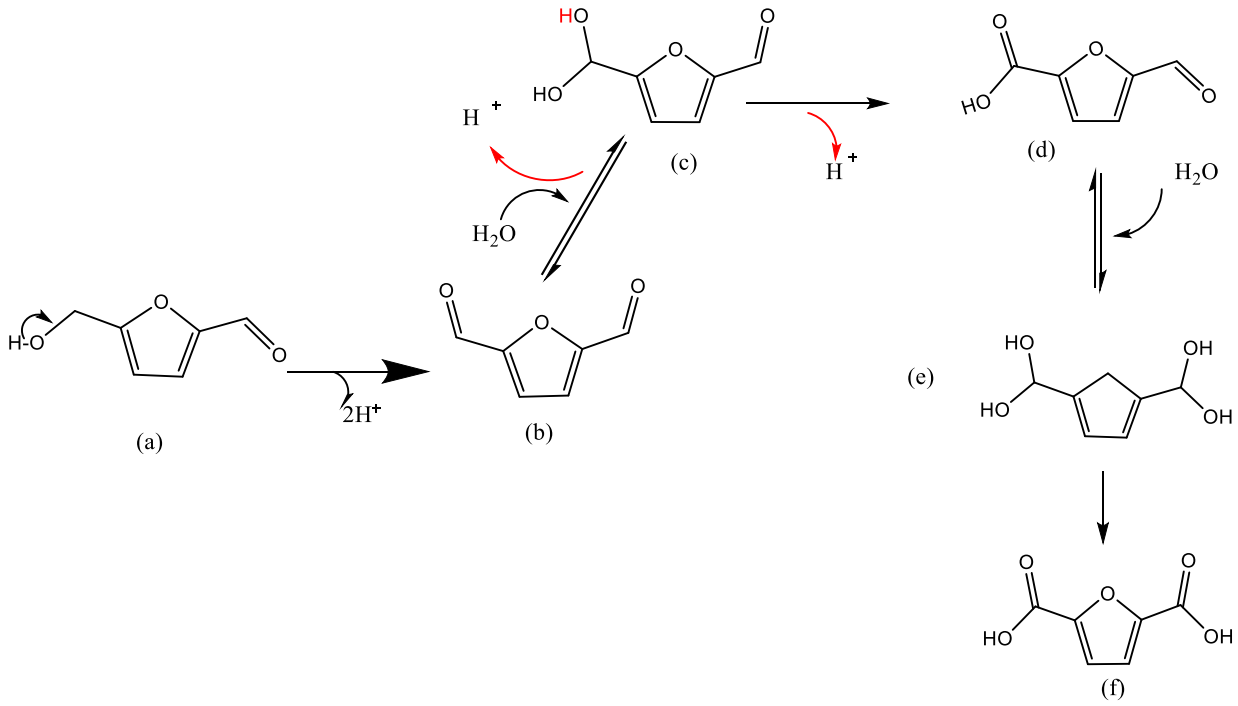

Scheme 6.4. mechanism of HMF oxidation using acid catalyst support under base free conditions (a) HMF, (b) DFF (c) Alkoxy intermediate (d) FFCA (e) Germinal diol and (f) FDCA

The catalysts were also shown to be highly reproducible. This allows the interesting results to be used as a reliable baseline for future modification of the catalysts. In particular, the area of promoter addition to functionalise these catalysts is a not well explored area in this study. Organic base promoter agents such as n-butylamine are well documented for their ability to

alter the selectivity patterns of these catalysts and minimised the HMF degradation under strong base addition.[15] Attempts should be made to elucidate the structure of the functionalized catalysts and the type of geometry between the Au and Pt nanoparticle and functional amine groups from the organic base.

Platinum group metals (PGM) exhibit remarkable catalytic activity for the oxidation of HMF to FDCA,[1,10,21–23] however due to their high cost, synthesis of non PGM catalysts have started to gain attention by researchers.[12] Another logical step for future studies would be to see whether manipulating the A or B-site of the perovskite can provide promising results for the oxidation of HMF to FDCA. Literature on this subject suggest that 85-95% of FDCA yield can be achieved with PGM free catalysts under mild reaction conditions (Table 6.1).[24–29]

Table 6.1 PGM free catalyst for the oxidation of HMF to FDCA

Catalyst	Pressure (bar)	Temp (°C)	Time (h)	FDCA Yield(%)	HMF Con(%)
Fe_3O_4-CoO_x	10	80	12	68.6	97.2
$Ce_{0.5}Zr_{0.5}O_2$	20	140	24	23.2	96.1
$Ce_{0.5}Fe_{0.15}Zr_{0.35}O_2$	20	140	24	44.2	99.9
$Fe_{0.6}Zr_{0.4}O_2$	20	160	24	60.6	99.7
MnO_x-CeO_2	20	110	15	91	98
MnO_2	10	100	24	91	100
Fe-POP	10	10	10	79	100

6.2 Selective Oxidation of Glycerol

The fundamental objective of this study was to control the selectivity profile distribution of the products. After a successful application of AuPt/$LaMO_3$ catalysts (where M = Cr, Mn, Fe, Co and Ni) for the oxidation of HMF to FDCA, their ability to alter the selectivity pattern of glycerol oxidation products was investigated.[30,31] Initial screening of the AuPt catalysts with different B-site perovskite supports was carried out under the same conditions, with two different reaction routes (oxidation and dehydration route) seen. $LaCoO_3$ and $LaNiO_3$ were found to give an even distribution across all the products, whereas $LaCrO_3$ and $LaFeO_3$ were

found to favour dehydration route as illustrate in Scheme 5.5. $LaMnO_3$ supports synthesized by supercritical antisolvent precipitation was previously reported to completely switch off the dehydration route to maximise the favoured oxidation route, initially resulting in high selectivity to glyceric acid, which was then oxidised to tartronic acid, a product that is difficult to produce.[30] However, the nanocasting assisted $LaMnO_3$ used in this work was found to produce minor dehydration product (Lactic acid) alongside oxidation products which were found to be the major products. This was attributed to the presence of small amount Lewis acid La_2O_3 as revealed by the XPS (chapter 3 section 3.4.8) that may prevent glycerol-catalyst interaction.[31]

To investigate the differences between this study and the results reported by Evans *et al*[30], the $LaMnO_3$ perovskite support was prepared by hydrothermal and citrate complexing methods to understand if the synthesis method played a role in the selectivity. It was concluded from the results obtained that as long as the 100% $LaMnO_3$ perovskite phase is used as the support for the glycerol oxidation reaction, the dehydration route to lactic acid would be completely blocked and the oxidation route would be favoured. For the $LaMnO_3$ support synthesis, it was found that the traditional complexing method produced $LaMnO_3$ with 100% perovskite phase (by XRD) and the glycerol oxidation experiment showed that the dehydration route was completely blocked as reported by Evans *et al*. However, the hydrothermally synthesised $LaMnO_3$ support with only 30% of the perovskite phase and 70% of a spinel phase found in the material, both oxidation and dehydration products were produced. Evans *et al.* suggested that this behaviour was based on the oxygen adsorption capacity of the support, suggesting that high oxygen adsorption perovskite supports favour the oxidation route whilst low oxygen adsorption supports favour the dehydration route.[30]

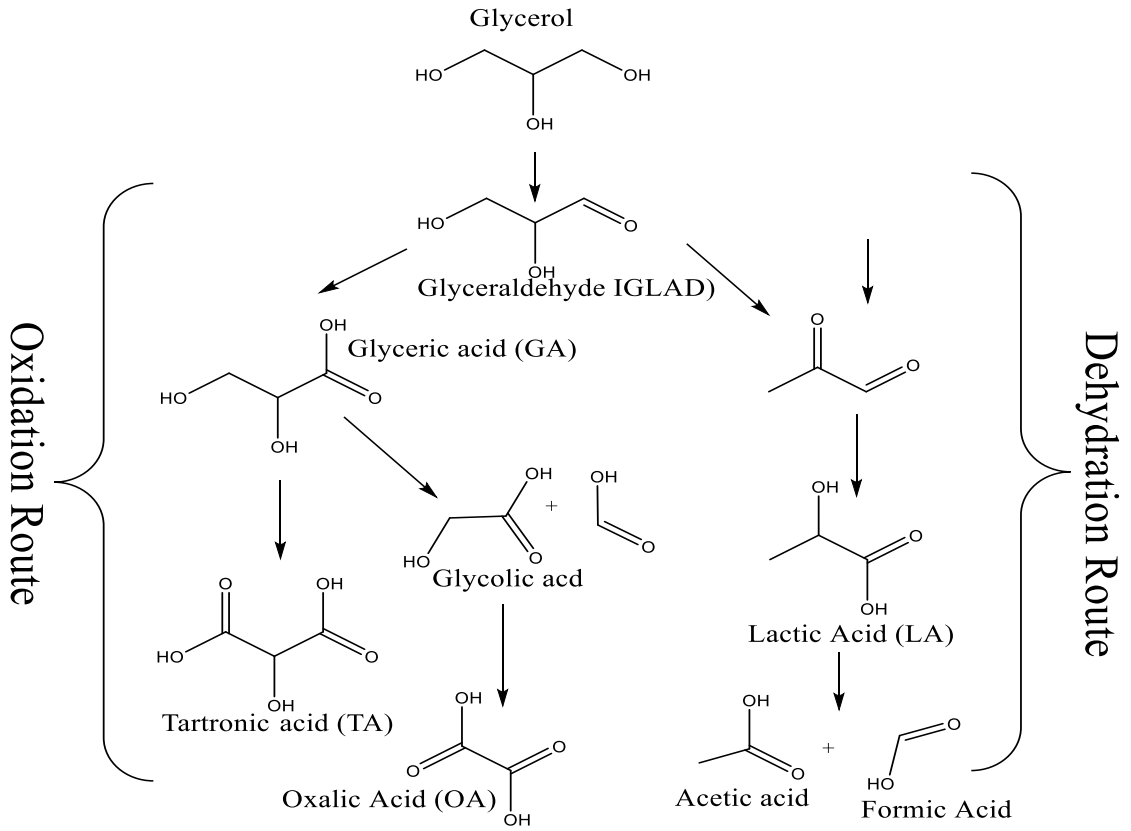

Scheme 6.5 Glycerol reaction route observed in this study with different perovskite support under alkaline conditions.

The AuPt/$LaCrO_3$ catalyst was selected for a parameter mapping study and for the purpose of understanding the mechanism of the dehydration route. it was found that by increasing temperature, the rate of reaction was also increased. This observation is expected and has been seen in many catalytic reactions. As the temperature was increased, the selectivity to lactic acid also increased up to 100 °C. Above this temperature, the carbon balance decreased substantially, indicating a loss of carbon from the system which can be explained by the production of CO_2, which lowered the yield of lactic acid produced. The second parameter to be altered was the oxygen pressure, increasing from an inert atmosphere up to 4 bar. It was found that the selectivity to lactic acid increased as the oxygen pressure increased up to 3 bar. Above this point, the oxygen pressure increases the initial rate of the reaction, causing an increase in oxidation products at lower reaction times, leading to an increase in C-C scission. The noticeable increase in C-C scission products with increasing O_2 pressure, particularly in

the final stages of the reaction was associated with the production of H_2O_2 from the reduction of O_2 by H_2O. It is therefore likely that increasing the oxygen pressure may be promoting the production of H_2O_2 in the reaction mixture. Additionally, it was observed that the selectivity to GA and LA increase and decrease respectively as the pressure was increased. This suggests that oxygen inhibiting the dehydration route through the promotion of the competitive direct oxidation pathway. The base to substrate ratio used in the reaction was also found to be important and showed that as the amount of base used increases, so too does the selectivity to lactic acid, alluding to the fact that OH^- plays an integral role in the formation of lactic acid by inhibiting either the formation of H_2O_2 or its interaction with the glycerol species. It has been suggested previously that C-C cleavage occurs as a result of the in-situ formation of H_2O_2.[32] It has also been reported that increasing the OH^- promotes the decomposition of H_2O_2.[33] This result raised an interesting question as to how this observation could be used to further the understanding of the mechanistic route to lactic acid. The mechanism has long been debated; however, it is agreed that the first two steps involve the oxidation of glycerol through either primary or secondary alcohol leading to the formation of the corresponding surface alkoxy intermediate. From the primary alkoxy intermediate, abstraction of an adjacent hydrogen leads to the desorption of glyceraldehyde which is followed by the dehydration of a terminal alcohol group to produce dihydroxyacetone. It is possible, that increasing the reaction temperature is favouring both the oxidation and subsequent dehydration steps. An isotopic labelling experiment involving the use of ^{18}O could be used to prove this, as shown in Scheme 6.5.

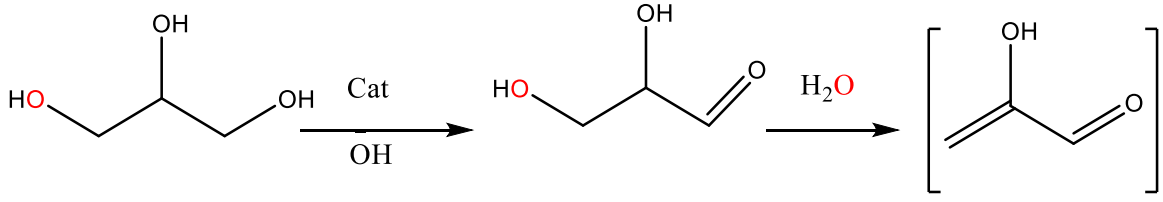

Figure 6.5. Proposed isotopic labelling experiment. ^{18}O is represented in red.

If the glycerol terminal alcohol groups were labelled with ^{18}O, it would be possible to determine whether temperature accelerates these two steps. If this hypothesis holds, increasing the reaction temperature would lead to higher quantities of $H_2{}^{18}O$ in solution. By conducting the reactions at different temperatures and monitoring the quantity of $H_2{}^{18}O$ in the reaction solution it could theoretically be possible to prove this hypothesis.

The following elementary step in the glycerol to lactic acid mechanism has been debated in the literature. It is long been reported by Shaffer and Friedemann[34] that 2- hydroxyacrylaldehyde undergoes a rearrangement to produce lactic acid. However, Crabtree *et al.*[35] proposed a different mechanistic route, suggesting that the 2- hydroxyacrylaldehyde is first oxidised to methylglyoxal, followed by an intermolecular Cannizzaro reaction to produce lactic acid via 2,1-methyl shift (Scheme 6.6). As depicted in Scheme 6.7, an additional isotopic labelling experiment that has been used to confirm Cannizzaro reactions[36,37] could be used to verify which of these mechanisms is the most likely.

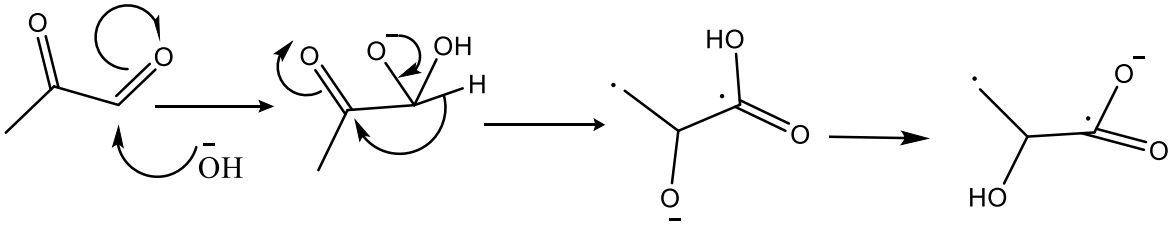

Scheme 6.6 mechanism of lactic acid from glyceraldehyde.

In the presence of deuterated base (NaOD), starting the reaction with 2-hydroxyacrylaldehyde or methylglyoxal would demonstrate that the 2- hydroxyacrylaldehyde is first oxidised to methylglyoxal, followed by an intermolecular Cannizzaro reaction to produce lactic acid. Given that hydroxide ions are known to play a crucial role in the activation of C-H bonds, it would be difficult to carry out this experiment using glycerol, which could make the analysis more complicated. The H atoms in the water could interact with the deuterated alcohol in LA to cause an additional problem.

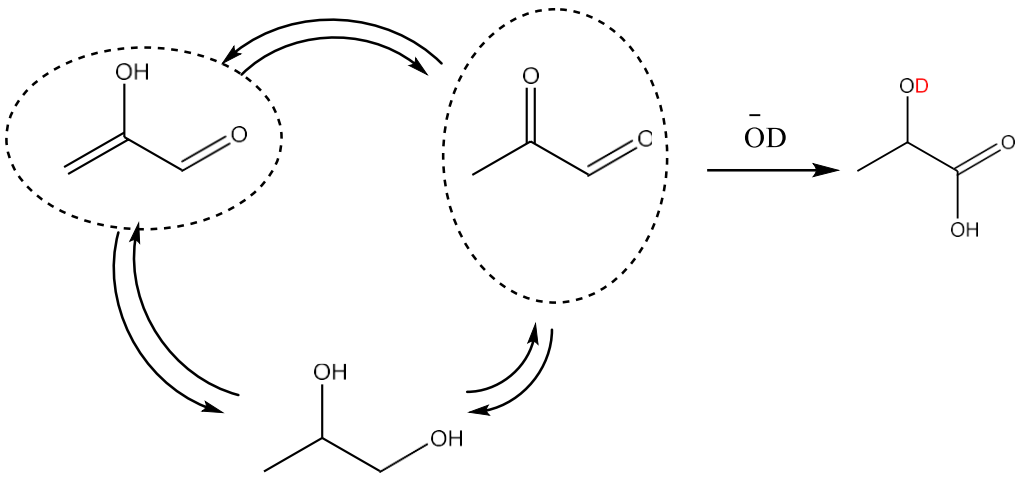

Scheme 6.7. Isotopic labelling experiment proving Cannizzaro reaction. Deuterium is represented in red

A statistical approach (response surface methodology) was applied to elucidate what would happen beyond the reaction time conducted in the initial catalyst screening experiment for the oxidation of glycerol over AuPt/$LaMnO_3$. It was found that as time progressed only oxidation products were produced with further oxidation of glyceric acid to tartronic acid. It was noted that the analysis of variance (ANOVA) of the model showed that the selectivity of tartronic acid increases with increased reaction time, temperature, gold-platinum metal ratio and base to substrate ratio.

Having stated earlier in this chapter that tartronic acid may be a primary oxidation product and is extremely difficult to produce in high yields, the basic mesoporous catalyst support material might make it possible to activate the secondary alcohol group and shorten the amount of time it takes for the catalyst and substrate to come into contact with one another. Another area to utilise these catalysts for the valorisation of glycerol is photocatalysis. It was reported that $LaMnO_3$ is an excellent photocatalyst due to its several properties like electrical, magnetic, chemical and thermal stability, and a bandgap that is in the visible spectrum. It was illustrated by Luo *et al.*[38] that glycerol oxidation products can be produced by photo-electrocatalysis. It is noteworthy to utilise the catalysts in this work as photocatalysts for the

valorisation of glycerol.

6.3 Reference

1. Li, Q. *et al.* Selective oxidation of 5-hydroxymethylfurfural to 2,5-furandicarboxylic acid over Au/CeO2 catalysts: The morphology effect of CeO2. *Catal. Sci. Technol.* **9**, 1570–1580 (2019).
2. Gorbanev, Y. Y., Klitgaard, S. K., Woodley, J. M., Christensen, C. H. & Riisager, A. Gold-Catalyzed Aerobic Oxidation of 5-Hydroxymethyl- furfural in Water at Ambient Temperature. *ChemSUSChem* 672–675 (2009) doi:10.1002/cssc.200900059.
3. Siyo, B. *et al.* Influence of support on the aerobic oxidation of HMF into FDCA over preformed Pd nanoparticle based materials. *Appl. Catal. A Gen.* **478**, 107–116 (2014).
4. Filiciotto, L., Balu, A. M., Romero, A. A., Angelici, C. & Waal, J. C. Van Der. Reconstruction of humins formation mechanism from decomposition products : A GC-MS study based on catalytic continuous flow depolymerizations. *Mol. Catal.* **479**, 110564 (2019).
5. Hoang, T. M. C., Eck, E. R. H. Van, Bula, W. P., Gardeniers, J. G. E. & Seshan, K. processing as a potential carbonaceous source for synthesis gas production . *Green Chem*. 959–972 (2015) doi:10.1039/c4gc01324g.
6. Jung, D. Kinetic study on the impact of acidity and acid concentration on the formation of 5-hydroxymethylfurfural (HMF), humins , and levulinic acid in the hydrothermal conversion of fructose. *Biomass Conversion and Biorefinery* 1155–1170 (2021).
7. Zandvoort, I. Van *et al.* Formation , Molecular Structure , and Morphology of Humins in Biomass Conversion : Influence of Feedstock and Processing Conditions. *ChemSusChem* 1745–1758 (2013) doi:10.1002/cssc.201300332.
8. Neaţu, F. *et al.* Selective oxidation of 5-hydroxymethyl furfural over non-precious metal heterogeneous catalysts. *Appl. Catal. B Environ.* **180**, 751–757 (2016).
9. Sajid, M., Zhao, X. & Liu, D. Production of 2,5-furandicarboxylic acid (FDCA) from

5-hydroxymethylfurfural (HMF): Recent progress focusing on the chemical-catalytic routes. *Green Chem.* **20**, 5427–5453 (2018).

10. Davis, S. E. *et al.* Kinetics and mechanism of 5-hydroxymethylfurfural oxidation and their implications for catalyst development. *J. Mol. Catal. A Chem.* **388**–**389**, 123–132 (2014).
11. Davis, S. E., Zope, B. N. & Davis, R. J. On the mechanism of selective oxidation of 5-hydroxymethylfurfural to 2,5-furandicarboxylic acid over supported Pt and Au catalysts. *Green Chem.* **14**, 143–147 (2012).
12. Deshan, A. D. K. *et al.* Heterogeneous Catalytic Conversion of Sugars Into 2,5-Furandicarboxylic Acid. *Front. Chem.* **8**, 1–23 (2020).
13. Miao, Z. *et al.* Aerobic oxidation of 5-hydroxymethylfurfural (HMF) effectively catalyzed by a Ce0.8Bi0.2O2-δ supported Pt catalyst at room temperature. *RSC Adv.* **5**, 19823–19829 (2015).
14. Zope, B. N., Hibbitts, D. D., Neurock, M. & Davis, R. J. Reactivity of the Gold / Water Interface During Selective Oxidation Catalysis Reactivity of the Gold / Water Interface. *J. Colloid Interface Sci.* **330**, 74–78 (2019).
15. Tirsoaga, A., El Fergani, M., Parvulescu, V. I. & Coman, S. M. Upgrade of 5-Hydroxymethylfurfural to Dicarboxylic Acids onto Multifunctional-Based Fe3O4@SiO2 Magnetic Catalysts. *ACS Sustain. Chem. Eng.* **6**, 14292–14301 (2018).
16. Han, X. *et al.* N-doped carbon supported Pt catalyst for base-free oxidation of 5-hydroxymethylfurfural to 2,5-furandicarboxylic acid. *Appl. Catal. A Gen.* **526**, 1–8 (2016).
17. Han, X. *et al.* Base-free aerobic oxidation of 5-hydroxymethylfurfural to 2,5-furandicarboxylic acid over a Pt/C-O-Mg catalyst. *Green Chem.* **18**, 1597–1604 (2016).

18. Wan, X. *et al.* Base-free aerobic oxidation of 5-hydroxymethyl-furfural to 2,5-furandicarboxylic acid in water catalyzed by functionalized carbon nanotube-supported au-pd alloy nanoparticles. *ACS Catal.* **4**, 2175–2185 (2014).

19. Gupta, N. K., Nishimura, S., Takagaki, A. & Ebitani, K. Hydrotalcite-supported gold-nanoparticle-catalyzed highly efficient base-free aqueous oxidation of 5-hydroxymethylfurfural into 2,5-furandicarboxylic acid under atmospheric oxygen pressure. *Green Chem.* **13**, 824–827 (2011).

20. Casanova, O., Iborra, S. & Corma, A. Biomass into Chemicals : Aerobic Oxidation of 5-Hydroxy- methyl-2-furfural into 2 , 5-Furandicarboxylic Acid with Gold Nanoparticle Catalysts. 1138–1144 (2009) doi:10.1002/cssc.200900137.

21. Pasini, T. *et al.* Selective oxidation of 5-hydroxymethyl-2-furfural using supported gold–copper nanoparticles. *Green Chem.* **13**, 2091–2099 (2011).

22. Siankevich, S. *et al.* A novel platinum nanocatalyst for the oxidation of 5-Hydroxymethylfurfural into 2,5-Furandicarboxylic acid under mild conditions. *J. Catal.* **315**, 67–74 (2014).

23. Ait Rass, H., Essayem, N. & Besson, M. Selective aerobic oxidation of 5-HMF into 2,5-furandicarboxylic acid with pt catalysts supported on TiO2- and ZrO2-based supports. *ChemSusChem* **8**, 1206–1217 (2015).

24. Yan, D. *et al.* Fe-Zr-O catalyzed base-free aerobic oxidation of 5-HMF to 2,5-FDCA as a bio-based polyester monomer. *Catal. Sci. Technol.* **8**, 164–175 (2018).

25. Han, X., Li, C., Liu, X., Xia, Q. & Wang, Y. Selective oxidation of 5-hydroxymethylfurfural to 2,5-furandicarboxylic acid over MnO:X-CeO2 composite catalysts. *Green Chem.* **19**, 996–1004 (2017).

26. Hayashi, E., Komanoya, T., Kamata, K. & Hara, M. Heterogeneously-Catalyzed Aerobic Oxidation of 5-Hydroxymethylfurfural to 2 , 5-Furandicarboxylic Acid.

ChemSusChem. 654–658 (2017) doi:10.1002/cssc.201601443.

27. Saha, B., Gupta, D., Abu-omar, M. M., Modak, A. & Bhaumik, A. Porphyrin-based porous organic polymer-supported iron (III) catalyst for efficient aerobic oxidation of 5-hydroxymethyl-furfural into. *J. Catal.* **299**, 316–320 (2013).
28. Si, W., Wang, Y., Peng, Y. & Li, J. Selective Dissolution of A-Site Cations in ABO3 Perovskites: A New Path to High-Performance Catalysts. *Angew. Chemie - Int. Ed.* **54**, 7954–7957 (2015).
29. Yan, D. *et al.* Base-free conversion of 5-hydroxymethylfurfural to 2 , 5-furandicarboxylic acid in ionic liquids. *Chem. Eng. J.* **323**, 473–482 (2017).
30. Evans, C. D. *et al.* The preparation of large surface area lanthanum based perovskite supports for AuPt nanoparticles: Tuning the glycerol oxidation reaction pathway by switching the perovskite B site. *Faraday Discuss.* **188**, 427–450 (2016).
31. Evans, C. D., Bartley, J. K., Taylor, S. H., Hutchings, G. J. & Kondrat, S. A. Perovskite Supported Catalysts for the Selective Oxidation of Glycerol to Tartronic Acid. *Catal. Letters* (2022) doi:10.1007/s10562-022-04111-2.
32. Ketchie, W. C., Murayama, M. & Davis, R. J. Promotional effect of hydroxyl on the aqueous phase oxidation of carbon monoxide and glycerol over supported Au catalysts. *Top. Catal.* **44**, 307–317 (2007).
33. Dimitratos, N., Villa, A. & Prati, L. Liquid Phase Oxidation of Glycerol Using a Single Phase (Au – Pd) Alloy Supported on Activated Carbon : Effect of Reaction Conditions. 334–340 (2009) doi:10.1007/s10562-009-0192-8.
34. Shaffer, P. A. & Friedemann, T. E. Sugar Activation By Alkali. *J. Biol. Chem.* **86**, 345–374 (1930).
35. Manas, M. G., Crabtree, R. H. & Sharninghausen, L. S. conversion of glycerol to lactic acid. *Nat Commun.* 1–9 (2014) doi:10.1038/ncomms6084.
36. Douthwaite, M., Powell, N., Taylor, A., Ford, G. & López, M. Glycerol Selective

Oxidation to Lactic Acid over AuPt Nanoparticles ; Enhancing Reaction Selectivity and Understanding by Support Modification. *ChemCatChem.* 3097–3107 (2020) doi:10.1002/cctc.202000026.

37. Evans CD, Douthwaite M, Carter JH, Pattisson S, Kondrat SA, Bethell D, Knight DW, Taylor SH, Hutchings GJ. Enhancing the understanding of the glycerol to lactic acid reaction mechanism over AuPt/TiO_2 under alkaline conditions. *J Chem Phys*. 2020 Apr 7;152(13):134705. doi: 10.1063/1.5128595. PMID: 32268741.

38. Luo L, Chen W, Xu SM, Yang J, Li M, Zhou H, Xu M, Shao M, Kong X, Li Z, Duan H. Selective Photoelectrocatalytic Glycerol Oxidation to Dihydroxyacetone via Enhanced Middle Hydroxyl Adsorption over a Bi_2O_3-Incorporated Catalyst. *J Am Chem Soc*. 2022 May 4;144(17):7720-7730. doi: 10.1021/jacs.2c00465